THE CONTROL OF CALCIUM AND MAGNESIUM IN A BASE METAL SULPHATE LEACH SOLUTION

by

Max Pelser

Thesis submitted in partial fulfilment
of the requirements for the degree

of

MASTER OF SCIENCE IN ENGINEERING
(EXTRACTIVE METALLURGICAL ENGINEERING)

in the Department of Chemical Engineering
at the University of Stellenbosch

Pectora roborant cultus recti

Supervised by

Mr J.J. Eksteen
Prof. L. Lorenzen
Prof. C. Aldrich

STELLENBOSCH

April 2003

Declaration

I, the undersigned, hereby declare that the work contained in this thesis is my own original work and that I have not previously in its entirety or in part submitted it at any university for a degree.

Max Pelser 30 December 2002

Acknowledgements

The work described in this thesis was carried out in the Department of Chemical Engineering at the University of Stellenbosch. This department provided the ideal support structure in terms of knowledgeable people and practical expertise. I have many people to thank for their input into this study and am grateful to all of them. There are a few I would like to acknowledge within this thesis:

- God almighty who grants wisdom.

- My study leaders: Mr J.J. Eksteen for his undying enthusiasm, continual support and above all his friendship. Prof. L. Lorenzen for his seasoned point of view for the study. Prof. C. Aldrich for his input on translating the results into words. Each of them contributed to a specific aspect of the study for which I am grateful.

- AVMIN for the initialisation of this study and financial support. In particular I would like to thank Mr A. Swarts for his input and support from the Nkomati project team and Mr F. Human for realising this study.

- The technical personnel at the Department of Chemical Engineering, in particular Ms J.E. Botha, Mr F.E. Greeff and the personnel of the workshop, Mr J.M. Barnard, Mr A.P. Cordier and Mr H. Koopman.

- Ms S.A. Kockott and Mr S.C. Barrie for their assistance in the practical work.

- My immediate family and Karin for their love, understanding and support.

Synopsis

This thesis investigates the control of calcium and magnesium in a base metal sulphate leach solution containing nickel and cobalt. The presence of calcium and magnesium in the hydrometallurgical processing of base metals, result in a number of difficulties. These problems range from the contamination of the final product, to high energy consumption and large bleed streams during electrowinning. Calcium poses a greater problem in sulphate solutions due to the low solubility of its sulphate salts.

No conventional method exists for the control of calcium and magnesium. As part of this study a review of possible control methods was conducted, which is listed within. From this list the precipitation of fluorides was selected for further investigation. The results showed that it is possible to control calcium and magnesium through the precipitation of their respective fluorides, without the co-precipitation of nickel and cobalt. For 10% stoichiometric excess of fluoride 96.5% calcium and 98.5% magnesium were removed during batch experiments.

It is known that mixing and hydrodynamics plays an important role on the characteristics of the formed precipitate, making these processes inherently difficult to scale-up. To evaluate these effects on a continuous process, the three-zone model proposed by Gösele and Kind (1991) was used. A precipitate with consistent characteristics was produced while varying the mixing on the macro, meso and micro scale.

Additionally, methods were investigated for the removal or possible recycling of the unreacted fluoride, for which activated alumina was identified. It was observed that activated alumina could adsorb fluoride to low levels in the presence of the base metal solution, after which it could be regenerated again. The activated alumina (AA) had a capacity of 8.65 gF/ℓAA at a 10 mg/ℓ fluoride breakthrough level during column tests.

Based on the experimental results a conceptual process was devised whereby only a portion of the leach stream is subjected to the fluoride precipitation process, after which it is returned to lower the overall calcium and magnesium concentrations. This method would reduce the effect of the observed dominance of magnesium precipitation, in processes where the maximum removal of both elements is not required. The fluoride precipitation process consisted of three steps being precipitation, solid-liquid separation and adsorption of the unreacted fluoride.

Sufficient information is provided on the process for a cost estimation to be carried out. Should this found to be feasible, a continuation of the project is recommended. Different reactor configurations could be evaluated for precipitation. The scaling observed during the continuous experiments should also be investigated to minimise its effect. The investigation of activated alumina was only a secondary project and more work is required on optimisation, particularly for the desorption cycle to enable the recycling of the unreacted fluoride.

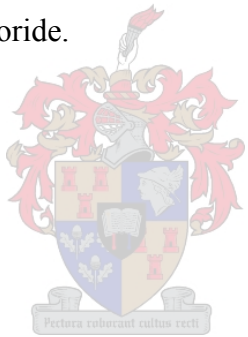

Opsomming

Saamgestel in hierdie tesis is 'n studie van die beheer van kalsium en magnesium in 'n basismetaal-sulfaatoplossing, bevattende nikkel en kobalt. Die teenwoordigheid van kalsium en magnesium in dié oplossings veroorsaak 'n verskeidenheid van probleme, wat wissel van produkkwaliteit verlaging tot hoë energieverbruik en groot bloei strome tydens platering. 'n Groter probleem word ondervind met kalsium as gevolg van die lae oplosbaarheid van sy sulfaatsoute.

Geen konvensionele metode kon gevind word vir die beheer van kalsium en magnesium gedurende die oorsig van moontlike metodes nie. Hierdie moontlike metodes is geïdentifiseer en kortliks bespreek in die tesis. Van die moontlike metodes is die presipitasie van fluoried-soute gekies vir verdere eksperimentele ondersoek. Die ondersoek het getoon dat dit moontlik is om kalsium en magnesium te beheer deur die presipitasie van fluoriede sonder om die basismetale saam te presipiteer. Vir 'n 10% oormaat fluoried toevoeging is 96.5% van die kalsium en 98.5% van die magnesium gepresipiteer gedurende die enkelladingstoetse.

Dit is bekend dat vermenging en hidrodinamika 'n groot rol speel in die kwaliteit van die presipitaat wat gevorm word. Dit bemoeilik die opskalering van presipitasie prosesse. Vir die ondersoek oor die invloed van vermenging op 'n kontinu proses is die drie-sel model van Gösele en Kind (1991) gebruik. Dit is gevind dat die karakter van presipitaat relatief konstant gebly het vir variasies van vermenging op die makro, meso en mikro skaal, wat opskaling behoort te vergemaklik.

Addisioneel is die verwydering of moontlike hersirkulasie van die ongereageerde fluoried ondersoek, en geaktiveerde alumina is geïdentifiseer as 'n moontlike adsorbeermiddel. 'n Eksperimentele ondersoek het getoon dat geaktiveerde alumina fluoried tot lae vlakke kan adsorbeer in die teenwoordigheid van die basismetale, waarna dit weer geregenereer kan word. Die kapasiteit van die geaktiveerde alumina (GA) was bereken as 8.65 gF/ℓGA by 'n 10 mg/ℓ fluoried vlak gedurende die kolom toetse.

'n Konsep-proses is opgestel na aanleiding van die eksperimentele resultate, waarvolgens slegs 'n gedeelte van die logingstroom na die fluoried presipitasie proses gestuur word, waarna dit weer teruggevoeg word om die algehele kalsium en magnesium konsentrasie te verlaag. Dié metode sal voorkom dat magnesium presipitasie domineer vir 'n toepassing waar slegs 'n gedeelte van kalsium en magnesium verwyder word. Die fluoried presipitasie proses behels drie stappe waarvolgens die fluoriede eers gepresipiteer word, waarna dit geskei word, en dan die ongereageerde fluoried geadsorbeer word.

Genoeg inligting is versamel sodat 'n kosteberaming van die proses gedoen kan word. As die koste van die proses aanvaarbaar is, word dit voorgestel dat die ondersoek voortgesit word. Verskillende reaktor konfigurasies kan vir die presipitasie stap getoets word en daar moet ook ondersoek ingestel word hoe om die korslaag wat gedurende die kontinu eksperimente geobserveer is, te verminder. Die ondersoek van geaktiveerde alumina was ondergeskik in die projek en nog werk sal gedoen moet word om dit te optimiseer, spesifiek gedurende die desorpsie siklus vir die hersirkulasie van die ongereageerde fluoried.

Pectora roborant cultus recti

Table of Contents

List of Figures

List of Tables

Chapter 1
Introduction

Objectives of Chapter 1

- Give the context of the study.
- Define the problem statement.
- Outline the objectives of the study.
- Provide an outline of the thesis.

The presence of calcium and magnesium in the hydrometallurgical processing of base metals, results in a number of process difficulties. These problems range from the contamination of the final product, where it is a precipitate (Cole, 2002), to high energy consumptions and large bleed streams during electrowinning (Booster et al., 2000). Calcium poses an additional problem in sulphate solutions due to the low solubility of its sulphate salts. A process stream could easily be supersaturated with calcium sulphate, resulting in the unwanted solids formation within the process equipment (Mayze, 2001). To have a better understanding of the mentioned problems, a short discussion of the processing of base metals ores will be presented below.

Base metal ores are characterised by their association with each other, and often more than one of these metals are of an economically recoverable grade. Of interest to this study is the processing of nickel-copper-cobalt ores with nickel being the primary metal. The conventional method of processing these ores involves pyrometallurgical treatment or a combination of pyro- and hydrometallurgical treatments. The direct hydrometallurgical treatment of these ores has only found application in recent years.

Hydrometallurgical treatments have especially excelled in the separation of base metals during the processing of complex ores. This can be directly attributed to developments in solvent extraction (SX) and ion exchange (IX), allowing for higher degrees of separations that were previously not possible with precipitation (Coussement et al., 1982).

The first step in any hydrometallurgical treatment process is the leaching of the feed material, whether it is an ore (sulphides or oxides) or an intermediate product such as matte. During leaching, the base metals are dissolved into a sulphate, chloride or an ammonia medium depending on the process. The pregnant leach solution may then be subjected to a number of separation and purification steps involving precipitation, solvent extraction, ion exchange or electrowinning. For these separation processes different problems are reported due to the presence of calcium and magnesium.

1.1 The Presence of Calcium and Magnesium in a Base Metal Sulphate Leach Solution

To discuss the behaviour of calcium and magnesium during the hydrometallurgical processing of base metal sulphate solutions, it would be easier to refer to the generic process presented in Figure 1.1. As mentioned before, the first step in the hydrometallurgical treatment process of base metals is leaching of the feed. Although a number of options exist, this discussion will be limited to the leaching into a sulphate medium. The sulphate medium may be created by the oxidative leaching of a sulphide feed or the use of sulphuric acid during leaching. This results in an acidic sulphate solution containing all of the base metals. In the diagram, this is followed by copper solvent extraction and thereafter iron precipitation.

During iron precipitation, the easily hydrolysable metals such as iron and the residual copper are precipitated. Iron precipitation is initiated by the addition of a base and oxygen to oxidise the iron to the ferric state so that it could be hydrolysed. Following iron precipitation is cobalt solvent extraction and thereafter nickel solvent extraction. Each of these steps requires additional pH adjustments. The extracted metals can either be electrowon, as indicated for copper and nickel, or precipitated as indicated for cobalt.

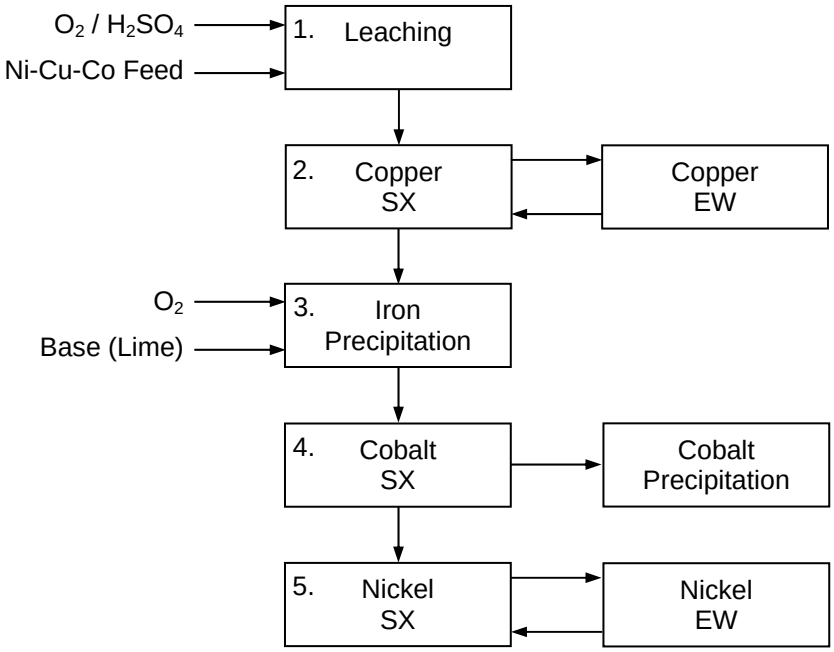

Figure 1.1 Simplified generic process for the sulphate medium treatment of nickel-copper-cobalt.

The entry points of calcium and magnesium into the process are during the leaching step, due to the mineralogy of the ore and the use of a calcium base during iron precipitation (Ritcey & Ashbrook, 1979). Magnesium concentrations in excess of 1 g/ℓ are often reported for pregnant leach solutions (Feather et al., 2002; Nagel & Feather, 2001; Preston & Du Preez, 2000).

The reason for the use of a calcium base during iron precipitation is purely economical. On an equivalent basis, a calcium base such as lime is about one sixth the cost of a sodium base (Babjak, 1986). The amount of calcium entering as lime during iron precipitation far exceeds its solubility as a sulphate. This results in the bulk of the calcium precipitating during this step, and the solution leaving iron precipitation being calcium saturated at approximately 0.6 g/ℓ. The problems reported for calcium and magnesium are associated with the latter part of the flow sheet (steps 4 and 5).

1.2 The Need for the Control of Calcium and Magnesium

During solvent extraction, a small portion of calcium and magnesium may be co-extracted. The presence of these elements in the strip liquor will result in a reduction of the quality of the final precipitated products. As an example, there is a market for

impure cobalt carbonate, but a higher price could be obtained if impurities such as manganese and magnesium were removed (Cole, 2002). The same trend is observed for cobalt oxide as shown in Table 1.1.

Table 1.1 Cobalt oxide prices during September 2002 at given purities (Chemical Market Reporter)

Cobalt oxide grade	Price (US$/kg)
72 – 73 % Co	42.17 – 89.71
71 – 72 % Co	41.62

In electrowinning circuits, the presence of calcium and magnesium is not considered to be threatening to the product quality since they will not co-deposit (Hofirek & Halton, 1990). They will, however, accumulate in the closed electrowinning circuits, resulting in higher energy consumptions (Booster et al., 2000). Bleeding is normally employed to control the concentrations of calcium and magnesium in the electrolyte, but this is also considered to be environmentally unfriendly. Calcium poses a greater problem in a sulphate medium circuit due to the low solubility of its sulphate salts, and often the calcium concentration limits the minimum bleeding ratio.

The deportment of calcium and magnesium to the electrowinning circuits can be limited to a large extent during solvent extraction. This entails counter-current solvent extraction and scrubbing of the loaded organic phase. Again, working in a sulphate medium can result in calcium sulphate precipitation as was reviewed by Mayze (2001). Bulong, one of the nickel laterite projects reviewed in the paper, uses versatic acid to extract nickel from a calcium saturated solution. Small amounts of calcium were co-extracted with the nickel, particularly in the later extraction stages, where the aqueous nickel tenor was low. The calcium was then carried up stream where the nickel scrubbed it from the organic phase. This resulted in the aqueous phase exceeding its calcium sulphate solubility. The calcium precipitated as gypsum causing scaling and blockages within the solvent extraction equipment. To minimise the gypsum precipitation, the organic flowrate was reduced to obtain maximum loading conditions and appropriate pH control was implemented. Although this reduced the amount of gypsum precipitation, it had a penalty of high nickel losses (150 mg/ℓ) to the raffinate.

A similar flowsheet to the Bulong process is planned for Anglovaal Mining's (AVMIN) Nkomati Expansion Project. Cyanex 272 and versatic acid is planned as the extractants of cobalt and nickel, respectively. The results from pilot-plant tests for the flowsheet were presented at ISEC 2002 (Feather et al., 2002). From the discussion it is apparent that gypsum precipitation was one of the main considerations in the design of the flowsheet. The cobalt scrubbing section required optimisation of the phase ratio and pH to ensure effecting scrubbing of calcium, magnesium and nickel using the minimum volume of scrub solution, while keeping the calcium concentration below saturation. Similar limitations were imposed on the nickel solvent extraction circuit and it became apparent that the solvent extraction steps could be more efficiently operated with out these limitations.

To avoid the mentioned problems, the total removal of calcium is not required. The concentration should only be controlled so that it will not precipitate. Likewise, the total removal of magnesium is also not necessary. On the contrary, the presence of magnesium helps the separation of cobalt from nickel during solvent extraction (Jones, 2000). Cyanex 272, the extractant increasingly being used for the separation of cobalt from nickel, has an intermediate selectivity for magnesium. Magnesium would therefore be preferentially extracted to nickel, minimising the amount of nickel co-extraction. It is recommended to keep the magnesium concentration equal to the cobalt concentration, although this may vary from 1:5 to 5:1.

Some consideration has to be taken when searching for methods to control calcium and magnesium. Over and above the fact that the method should successfully control the problems associated with calcium and magnesium, there are some other prerequisites that need to be considered. As seen from the above, the calcium and magnesium problem is usually associated with solvent extraction. The method should therefore have no detrimental effects on solvent extraction or any other down stream processes. It should have little or no effect on the pH of the pregnant leach solution and it should not adversely influence the concentrations of the valuable base metals. Furthermore, the concentrations of calcium and magnesium are low compared to the base metals, requiring that the method should have a high selectivity towards them

over the base metals. Finally, it should also be kept in mind that the method would operate in a sulphate medium.

There are also some limitations within which the possible method must operate. The pregnant leach solution is acidic with a high ionic strength and elevated temperatures. This might limit the materials of the equipment used for the control. It is also highly unlikely that the method would produce any valuable by-products and would only be seen as an expense. The cost of the method should therefore be at a minimum. If the calcium and magnesium is removed it is likely that it would be designated as waste products. This would require that the compounds in which they are removed be environmentally acceptable.

1.3 Fluoride Precipitation as a Method of Control

One of the possible control methods of interest to this study is the precipitation of calcium and magnesium fluoride. It was identified by a comparison of the solubilities of the base metal fluorides and the alkaline earth fluorides as indicated in Table 1.2. The alkaline earth fluorides showed very low solubilities compared to the high values of the base metals.

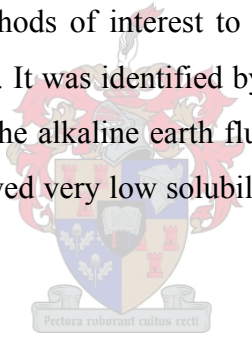

Table 1.2 Solubilties of selected fluoride compounds (adapted from CRC Handbook of Physics and Chemistry).

Fluoride Compound	Solubility (g per 100 mℓ Water at 25°C)
CaF_2	0.0016
MgF_2	0.013
NiF_2	2.6
CoF_2	1.4

The advantage of the fluoride method is that both alkaline earth fluorides are considered to be stable compounds based on their low solubility. With a good design of the precipitation reactor a crystalline product may be formed, which will require no additional processing.

The fluoride precipitation method has been proposed for controlling calcium and magnesium in a cobalt-nickel sulphate solution (Ritcey & Ashbrook, 1979); calcium in a uranium carbonate solution (Habib Jr, 1982); and magnesium in a zinc sulphate solution (Booster et al., 2000). In these references little information is given on the properties of the precipitate formed. It is known that calcium fluoride may produce a gelatinous precipitate in acid or neutral solutions that are difficult to filter (Vogel, 1961).

Shown in Figure 1.2 are the filter cakes of the fluoride precipitate formed through two different methods. The precipitate on the left was formed in a continuous process while the precipitate on the right was formed in a batch process. For both, the composition of the solutions were the same. The precipitate formed in the batch process was gelatinous with high amount of mother liquor inclusions as seen from its green colour. This precipitate has very poor filtration characteristics compared to the precipitate on the left.

Figure 1.2 Precipitate formed under different process conditions.

From this discussion it is apparent that the quality and properties of the precipitate is dependent on the processing conditions. A study would therefore be required on the effect of the process conditions, for these would have an important bearing on the feasibility of the process and the development thereof.

The fluoride precipitation process has been criticised for the excess amount of fluoride required during precipitation (Babjak, 1986). Activated alumina could possibly be used to remove or recycle the unreacted fluoride. It has been successfully

applied for the defluorination of water but would still need to be experimentally investigated as a result of the different condition to which it would be applied.

1.4 Objective of the Study

During this discussion, a number of topics has been raised that needs to be addressed. These topics could be summarised in the following objectives of the study.

The objectives are:

- A survey of the possible methods for the control of calcium and magnesium.

- Investigate the feasibility of controlling calcium and magnesium through fluoride precipitation.

- Investigate the use of activated alumina to remove or recycle the unreacted fluoride.

- Investigate the influence of hydrodynamics and mixing on the properties of the precipitated fluorides.

- Translate the experimental results into a conceptual process.

1.5 Outline of Thesis

The current study is compiled in this thesis in the form of seven chapters. Provided here is an outline of the information presented in each.

- *Chapter 2* (Background): This chapter provides the background information pertaining to the study. The Nkomati metals plant is discussed, for it is the process in which the control method will be implemented. The second part of the chapter focus on the different methods available for the control of calcium and magnesium.

- *Chapter 3* (Literature Review and Theoretical Considerations): This chapter forms the theoretical basis of the study. In it all the relevant theory of precipitation and fluoride adsorption is discussed.

- *Chapter 4* (Experimental Procedures): Described here are the experimental set-up and procedures used in this study.

- *Chapter 5* (Experimental Development of the Process): Presented herein are the results obtained for the experimental investigation into the different aspects of this project. These will be discussed in terms of their implications on the development of the process. This will serve as the results chapter.

- *Chapter 6* (The Conceptual Process): Based on the experimental result a conceptual process was developed. Given in this chapter is the insight on its development.

- *Chapter 7* (Conclusions and Recommendations): The study is concluded in this chapter and recommendations provided on the further development of the process.

Pectora roborant cultus recti

Chapter 2
Background

Objectives of Chapter 2

- Describe the Nkomati Expansion's Metals Plant flowsheet.
- Discuss the methods available for the control of calcium and magnesium.

Thus far, the problem of calcium and magnesium in base metals sulphate solutions has been described, indicating how and why it can be problematic to the hydrometallurgical processes. In this chapter the Nkomati Metals Plant for which calcium is expected to be problematic will be discussed. It was this calcium problem that initiated the current study. The latter part of this chapter would be devoted to the discussion of possible methods for the control of calcium and magnesium.

2.1 Nkomati

The Nkomati Mine is a medium-sized base metal operation situated in Mpumalanga, South Africa. The mine commenced production in January 1997 and it is currently South Africa's only primary nickel operation. It is also one of the lowest-cost producers in the world. It currently mines a high-grade *massive sulphide body* (MSB) of which the ore is beneficiated to produce a high grade platinum-group metals (PGMs) and copper concentrate, which is transported to Rustenburg for smelting; and a high grade nickel concentrate, which is transported to Botswana for smelting and Zimbabwe for refining (Avmin, 2002). Nkomati is a joint venture between Anglovaal Mining (75%) and Anglo American Operations (25%) of which Anglovaal has the management contract.

Apart form the massive sulphide body, the Uitkomst complex consists of large tonnages of low-grade disseminated ore. To exploit the full potential of the orebody, a number of feasibility studies have been conducted of which the final revision was completed in the beginning of 2002 (Creamer, 2002). An effort was made to find the optimum and environmentally acceptable method of exploiting the orebody.

2.1.1 Brief History and Mineralogy

Given here is a summary of the history and mineralogy of the Uitkomst complex. For a more detail discussion the reader is referred to Hammerbeck and Schürmann (1998) and Woolfe (1996).

History

In 1970 Anglo American Corporation (AAC) recognised the potential for a magmatic ore deposit on the farm Uitkomst 541JT. In 1972 AAC took an option on the farm and started a drilling program in a joint venture with Inco. The results from the drilling program and metallurgical testwork indicated the possibility of a high tonnage low-grade open-pit operation. This led to AAC acquiring the mineral rights on the Uitkomst farm in 1977 and later Inco's share in the joint venture. A feasibility study carried out by AAC between 1989 and 1991 showed the return on investment on the operation would be too low to motivate the development of the mine.

Meanwhile, Eastern Transvaal Consolidated Mines Limited (ETC – a subsidiary of Anglovaal Mining) started an evaluation on the nickel potential of the adjoining farm Slaaihoek 540JT in 1975. ETC already owned the mineral rights on Slaaihoek since 1929 for its gold potential. ETC started drilling work in 1989 followed up by additional drilling between 1990 and 1992. Metallurgical testwork showed favourable results and in 1993 ETC formed a joint venture called Nico with Middle Witwatersrand (Western Areas) Limited (Midwits), to carry out a major geological and metallurgical evaluation of Slaaihoek.

Since it is the same ore body extending over Uitkomst and Slaaihoek it was though best that the properties should form a single entity. This was done in 1995 when the Nkomati Joint Venture was established between Nico (75%) and AAC (25%) to exploit the Uitkomst complex and in January 1997 Nkomati Mine started production.

Mineralogy

Shown in Figure 2.1 is a cross section through the complex on Slaaihoek. The top part of the complex intruded into the shales of the Timeball Hill Formation and the bottom part into the dolomites, cherts and quartzites of the Malmani Subgroup and Black

Reef Quartzite Formation. The complex is at least 12 km long of which 8 km is exposed to the surface before dipping beneath an escarpment on Slaaihoek. The complex is between 0.5 to 1.5 km wide and the section beneath the escarpment on Slaaihoek is 760 m thick.

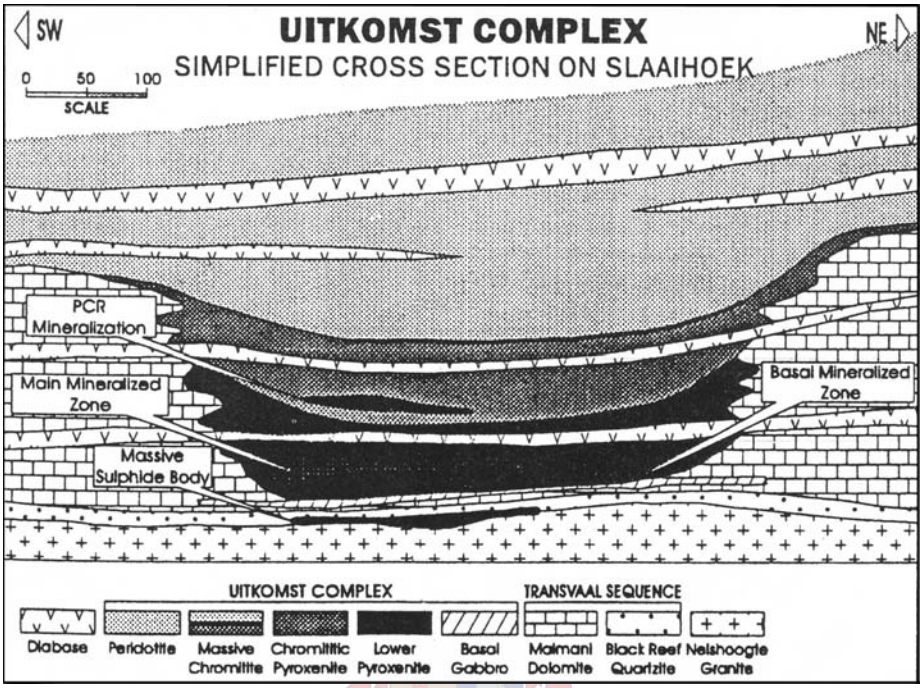

Figure 2.1 Simplified cross-section through the Uitkomst Complex on Slaaihoek (Woolfe, 1997).

Four distinct zones of sulphide mineralisation are found within the Uitkomst Complex. The first is the *chromatic pyroxenite* (PCR) mineralisation that occurs as disseminated zones of up to 20 m thick within the chromititic pyroxenite (pyroxenite is a rock consisting mainly of pyroxene with the remainder being olivine and/or hornblende; this would be a source of calcium and magnesium). The second is the *main mineralised zone* (MMZ) occurring within the *lower pyroxenite* as mainly disseminated and net-textured ore. The MMZ is fairly continuous along the length of the complex and is about 300 m wide and between 1 and 40 m thick. A simplified plan of the MMZ is given in Figure 2.2 to indicate the layout of the orebody.

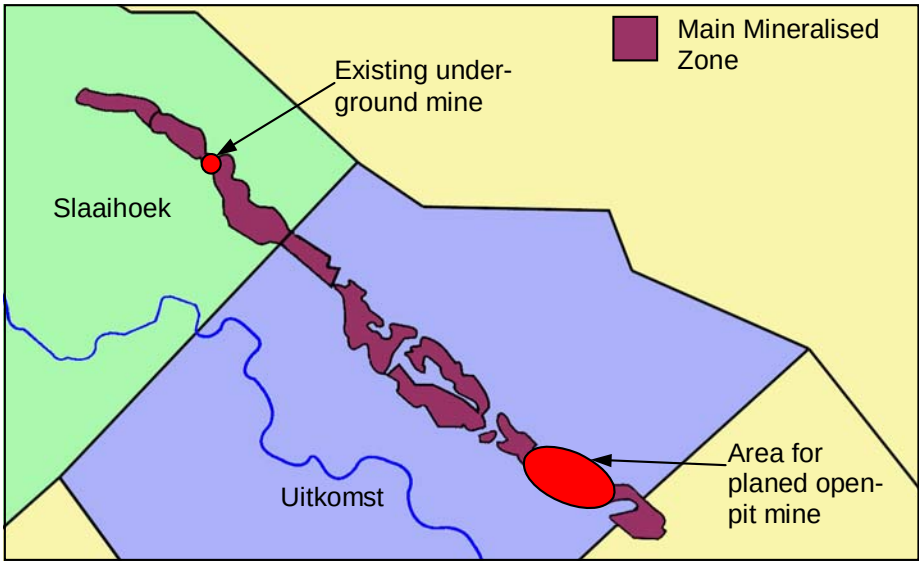

Figure 2.2 Simplified plan of MMZ over Slaaihoek and Uitkomst.

The third is the *basal mineralised zone* (BMZ) contained within the Basal Gabro as disseminated zones. It varies in thickness from 1 to 3.5 m and has a higher copper to nickel ratio than the MMZ. The last zone is the massive sulphide body (MSB) that sits below the complex mainly along the Black Reef/granite contact. The MSB is about 500 m long and 240 m across, and has a maximum thickness of 26 m. The compositions and reserves of the four mineralised zones are given in Table 2.1.

Table 2.1 Indicated Resources of the Uitkomst Complex (Hammerbeck & Schürmann, 1998).

Ore Zone	Slaaihoek					Uitkomst				
	Mt	Ni%	Cu%	Co%	PGMs +Au g/t	Mt	Ni%	Cu%	Co%	PGMs +Au g/t
PCR	6	0.5	0.1	NA	NA	2	0.53	0.12	NA	NA
MMZ	21	0.68	0.22	0.03	1.06	19	0.66	0.24	NA	1.04
BMZ	3	0.38	0.65	0.03	1.31	3	0.38	0.65	0.02	1.31
MSB	2.3	2.69	1.4	0.13	6.39	-	-	-	-	-

2.1.2 Expansion's Metals Plant Flowsheet

Described here is the flowsheet of Nkomati Expansion's Metals Plant (Figure 2.3). The Metals Plant is a new addition to the Nkomati process since the ore concentrate was toll-treated previously. It was the identification of the problematic calcium precipitation during the pilot studies that led to the initialisation of the current project. The method of calcium and magnesium control would therefore be implemented

within this flowsheet. The discussion of the flowsheet is based on personal communications with A. Swarts (various dates, 2001 – 2002).

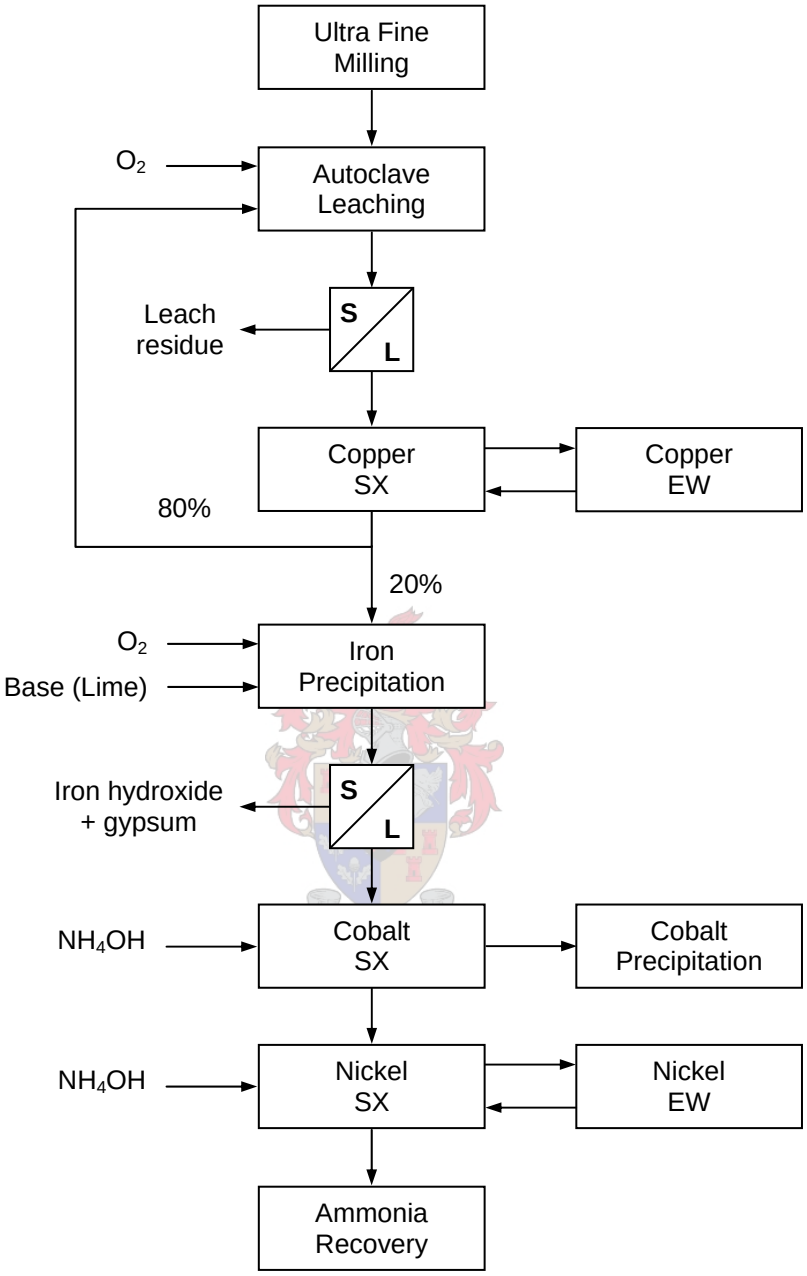

Figure 2.3 Flowsheet for the expansion's Metals Plant.

Ultra Fine Milling and Autoclave Leaching

Activox technology is a low temperature leaching process that forms the basis of the milling and leaching step. As with most nickel processes, it was originally developed for the treatment of copper concentrates. Activox leaching involves milling of the

flotation concentrate to 80% -10μm before feeding it to the autoclaves. The autoclaves are operated at 110 °C and 1000 kPa total pressure. The lower operating temperature has the advantage over higher temperature regimes that the sulphur is only partially oxidised to sulphate, decreasing the oxygen consumption considerably (Dreisinger, 2001). Acid formation in the autoclaves is therefore also decreased and the relative mild conditions allows for less expensive materials of construction to be used. The ultra fine milling is required for "enabling the leaching reactions to occur at lower temperatures" (Dreisinger, 2001).

The extractions of nickel and cobalt are both high (Table 2.2) while a significant amount of copper is left unreacted. The iron in the ore is mostly precipitated as an iron hydroxide (goethite) within the autoclaves and only a small percentage is extracted. Approximately 20% of the magnesium in the ore concentrate is extracted. The pregnant leach solution is separated from the autoclave discharge by a combination of thickening and filtration. The platinum group metals would not be leached and reports to the leach residue. After filtration the leach residue is repulped and the PGMs, unleached copper and elemental sulphur are recovered using froth flotation. The unleached copper is then toll-treated with the PGMs.

Table 2.2 Percentage metal extractions during 1999 pilot campaign.

Ni	Co	Cu	Fe	Zn	Mn	Mg
95.7	93.3	55.8	8.8	72.2	63.7	19.9

Copper Solvent Extraction

After solid-liquid separation the copper is extracted in two stages using Acorga M5640 in kerosene. The copper is then stripped in two stages from which metallic copper is recovered through electrowinning. London Metal Exchange (LME) class A copper is produced. Acid formed during electrowinning is recycled back to the autoclave with the copper raffinate. Twenty percent of the copper raffinate is bled to the downstream processes involving iron precipitation, cobalt solvent extraction and nickel solvent extraction. The recycling of the leach solution has a number of advantages including a higher nickel tenor for down stream processes and a reduction in oxygen and lime consumption. An additional copper solvent extraction stage is placed in the bleed stream to increase the copper recovery.

Iron Precipitation

Iron can be co-extracted with cobalt and nickel in the downstream processes and therefore needs to be controlled. It is precipitated from the bleed stream at a pH of 4 – 4.5 in a dedicated process step. The ferrous ions (Fe^{2+}) is oxidised to the ferric state (Fe^{3+}) by the introduction of oxygen. By adjusting the pH the ferric ions are hydrolysed to form an iron oxy-hydroxide precipitate. Three iron oxy-hydroxides are normally encountered:

- ferric hydroxide ($Fe(OH)_3$),
- goethite ($FeO(OH)$),
- hematite (Fe_2O_3).

Although not confirmed, based on the conditions during iron precipitation (~50 °C), goethite is thermodynamically the most likely precipitate to form. The overall reaction is given in Equation 2.1.

$$4Fe^{2+} + O_2 + 6H_2O \rightarrow 4FeO(OH) + 8H^+ \qquad \textbf{Equation 2.1}$$

The lime added during iron precipitation has a dual purpose. It is firstly used to adjust the pH to 4 for the iron hydrolysis and thereafter needs to neutralise the acid formed during the hydrolysis. The total lime addition was indicated as 30 kg CaO per m^3 of solution. This equates to approximately 21 g/ℓ calcium, which is 36 times the solubility of calcium as calcium sulphate. The bulk of the calcium precipitates as gypsum ($CaSO_4.2H_2O$) during iron precipitation, resulting in a calcium-saturated solution at a concentration of 0.5 to 0.6 g/ℓ.

More than 99% of the iron is precipitated along with most of the remaining copper. After thickening and filtration the leach solution contains less than 2 mg/ℓ iron and 7 mg/ℓ copper.

Cobalt Solvent Extraction

Caynex 272, a phosphinic acid, is used as the cobalt extractant based on is selectivity over nickel. Most of the minor impurities like copper, zinc and manganese are co-extracted with cobalt, which is seen as an advantage for the downstream recovery of

nickel. Bateman pulsed columns were selected as the contacting devices during extraction and stripping. Ammonia is used to control the pH during extraction and sulphuric acid during stripping. A conventional mixer-settler is used to scrub any calcium or nickel that is loaded before the cobalt is stripped. The final form of the cobalt is still uncertain although cobalt carbonate has previously been considered. The uncertainty seems to be surrounded by some impurity problems such as with magnesium. Additional purification would therefore be required.

Nickel Solvent Extraction

An inexpensive extractant, Versatic 10, was selected for the solvent extraction of nickel. Versatic acid has the disadvantages of a high solubility in aqueous solutions (150 mg/ℓ) and poor selectivity over some impurities. A particular problem is the co-extraction of calcium. Bateman pulsed columns were selected for nickel solvent extraction and mixer settlers to scrub calcium from the loaded organic. Ammonia and sulphuric acid is again used for pH control during the solvent extraction. The extracted nickel is recovered as nickel cathode during electrowinning. Anode bags are used during electrowinning. Special organic compound removal steps are placed in the electrowinning circuit and the nickel raffinate stream to recover the dissolved versatic acid.

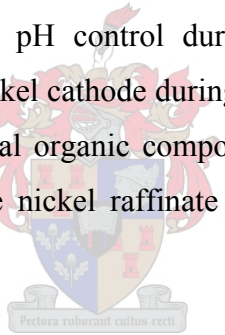

Ammonia Recovery

Ammonia is used throughout the process for pH control of the leach solution and ends up in the cobalt raffinate. The formed ammonium sulphate cannot be discharged into unlined tailings dams and therefore needs to be recovered. The concentration of the ammonium sulphate is too low to be crystallised but the “lime boil process” can be used to recover it. This process involves mixing quicklime (CaO) with the raffinate and heating it to 95 – 100 °C using steam. The ammonium reacts with the quick lime to form ammonia that can be recovered from the off gas as a diluted solution. The calcium precipitates as calcium sulphate (likely to be the anhydrite form), which is then stored in a dedicated disposal facility. The barren leachate is finally disposed in the tailings dams.

Behaviour of Calcium and Magnesium

From the above discussion it was seen that magnesium enters during the leaching step owing to the mineralogy of the gangue minerals and calcium enters mainly during the iron precipitation step. There is no information on how much, if any, calcium enters during the leaching step, but this amount is irrelevant since the amount of calcium entering during iron precipitation would overshadow this. Given below is a list of problems experienced during the pilot campaigns owing to calcium and magnesium.

Nkomati Pilot Plant:

- Blockages of strip column inlet and internals (nickel).
- Gypsum precipitation within both the cobalt and nickel extraction columns.

Yakabindie Pilot Plant:

- Gypsum precipitation in the scrub and strip mixers.

Identified potential problems:

- Gypsum precipitation on cloth of anode bags.
- Magnesium concentration too high during electrowinning.

It is considered possible to control magnesium in the electrowinning circuits through bleeding but it would not be practical for calcium, since a too large bleed stream would be required. Another important problem is the precipitation of gypsum within the solvent extraction equipment for which there is no conventional solution.

2.2 Methods for the Control of Calcium and Magnesium

The search for methods for controlling calcium and magnesium has been slow and the information found was scattered. It appears that calcium and magnesium has not been considered problematic, since their concentration encountered previously was probably to low. It is only in the recent flowsheets, developed for the direct hydrometallurgical treatment of ores, that the concentrations of calcium and magnesium are sufficient to be problematic. This was concluded from the review of the processing of nickel ores given in Appendix A.

Provided here are a discussion of the methods found which in the authors opinion may be used to control calcium and magnesium. In the search the conventional separation technologies such as precipitation, ion exchange and solvent extraction were first looked at. For each of these at least one option was identified. Additionally some methods were also found for evading the precipitation of gypsum during solvent extraction.

2.2.1 Precipitation

Precipitation, also some times referred to as reactive crystallisation, is the process whereby a sparingly soluble compound is forced to exceed its solubility. This results in the compound forming a solid phase that could be separated from the liquid. The crossing of the solubility of a compound is effected by either adding a specie into the solution which will form the insoluble compound with one of the other species in the solution or by changing the process condition resulting in one of the already present compounds exceeding its solubility. The most important criteria during the initial screening for precipitation methods were the selectivity over the base metals.

The opposite of precipitation is also possible, for admixtures exist that would inhibit precipitation. Rather than using precipitation to remove calcium, an inhibitor could be used to evade the precipitation of calcium.

Fluoride Precipitation

For precipitation, an initial scan was carried out looking at the solubilities of the metals ions in the system with respect to different anions. The key species looked at was fluorides, oxalates, carbonates, phosphates, sulphates and sulphides. From this list, the fluorides appeared to be the most promising for the removal of calcium and magnesium based on the difference between the solubilities of the alkaline earth elements compared to the base metals. The precipitation of fluorides has been proposed for controlling calcium and magnesium in a cobalt-nickel solution (Ritcey & Ashbrook, 1979); calcium in a uranium solution (Habib Jr, 1982); and magnesium in a zinc solution (Booster et al., 2000).

The solubilities of the fluorides of calcium and magnesium are low compared to the high solubilities of the cobalt and nickel (Table 2.3).

Table 2.3 Solubilities of Fluoride Compounds (Adapted from CRC Handbook of Physics and Chemistry).

FluorideCompound	Solubility (g per 100 mℓ Water at 25°C)
CaF_2	0.0016
MgF_2	0.013
CuF_2	0.075
CoF_2	1.4
NiF_2	2.6

Another strong point of the process is the fact that the fluorides of both calcium and magnesium are environmentally innocuous. The product is stable and safe even though a potentially dangerous and environmentally unfriendly reagent (the fluoride) is used in the process. This will minimise the cost in disposing the waste product. In the Metals Plant flowsheet the unreacted fluoride from the precipitation step will precipitate as calcium fluoride during the lime boil process. Thus, no harmful fluoride would leave the plant. The process would only consist of the precipitation step followed by solid-liquid separation. The process does need to be operated at elevated pressures and temperatures; and with a well-designed precipitation reactor, an easily filterable precipitate could be produced.

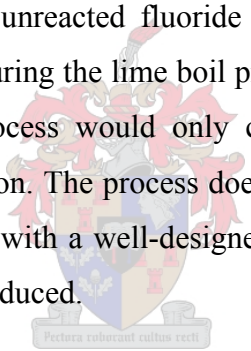

Calcium Sulphate Precipitation

The solubility of calcium sulphate is one of the more interesting systems and has been studied by many researchers. The following is a summary of a discussion provided by Zemaitis et al. (1986) on the modelling of calcium sulphate's solubility. It is known that the solubility of gypsum ($CaSO_4.2H_2O$) in pure water increases with temperature up to ~30°C, after which it starts decreasing again. The solubility of anhydrite ($CaSO_4$) is also known to have a negative dependence on temperature, crossing the solubility curve of gypsum to be the least soluble at temperatures higher then approximately 50°C. This is indicated on Figure 2.4.

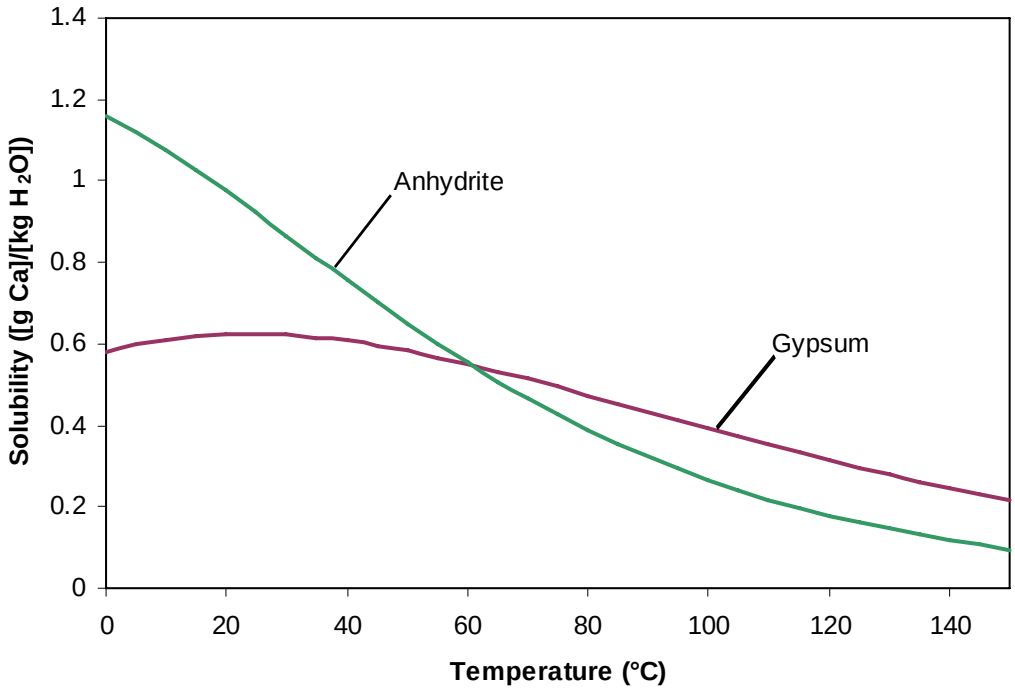

Figure 2.4 Solubility of calcium sulphate in pure water.

There is general disagreement over the actual transition point from gypsum to anhydrite in pure water, with values reported from 38 to 97°C. A temperature of 42°C appears to be the more accepted transition point based on the intersection of the solubility curves, thermodynamic calculations and vapour pressure measurements. Zemaitis et al. (1986) suggested that the reason for the inconsistency in experimental results is the slow transformation from the gypsum phase to the anhydrite phase. Some researchers reported that equilibrium has only been reached after days or even months, depending on the temperature.

In the region that anhydrite is the most stable it appears that calcium sulphate follows Ostwald's law of stages, stating that a thermodynamically less stable phase could be formed before the more stable phase, provided that the formation of the less stable (metastable) phase proceeds sufficiently fast. It is therefore, possible that gypsum is formed at temperatures higher than the transition point and would then slowly transform into the more stable anhydrite phase.

Dutrizac (2002) has observed that the negative temperature dependence of gypsum solubility disappears in high sulphate solution as encountered in hydrometallurgical processes. Experimental results showed that the solubility of gypsum increases monotonically with temperature under these circumstances. Elevated temperatures in the region of 50°C are normal for pregnant leach solutions and under these conditions the solubility behaviour of calcium sulphate could be used in two ways to remove calcium from the solution. The solution can either be cooled to precipitate gypsum ($CaSO_4.2H_2O$) or it can be heated to temperatures in excess of 100°C to precipitate anhydrite ($CaSO_4$).

Dreisinger (2001) presented a method of precipitating gypsum from pregnant zinc leach solution using cooling towers to decrease the temperature. The process is illustrated in Figure 2.5. This system operates at a low supersaturation level, necessitating the need of the recycle of seed crystals and long residence times. A residence time of six hours was quoted during the presentation.

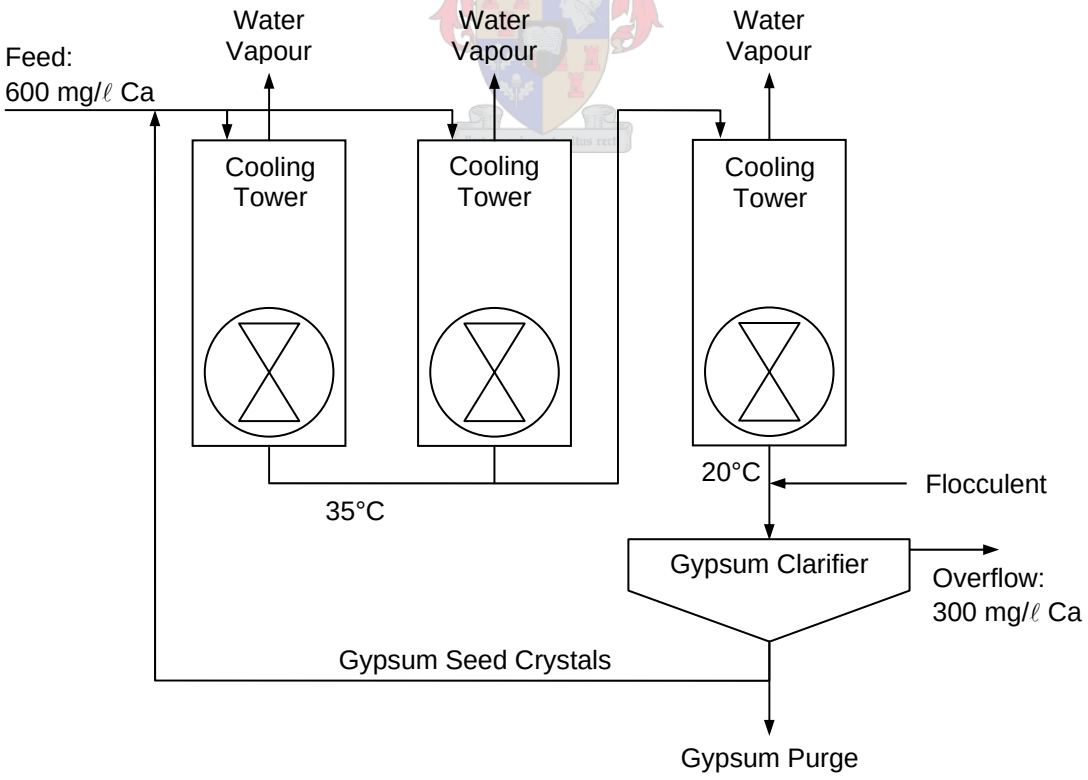

Figure 2.5 Gypsum precipitation for the control of calcium (Dreisinger, 2001).

Higher supersaturation levels could be reached by heating the solution for the precipitation of anhydrite. The process illustrated in Figure 2.6 was originally intended for the control of sulphate in acid mine drainage (AMD) and was developed by a South African company called the WREN Group. They presented the process at the Controlling Precipitation Processes Workshop in March 2001. This process has not been tested on pregnant leach solutions but in principle it should work to remove calcium sulphate. The solution is heated using steam in two stages to 100°C and then 150°C. In both stages anhydrite is precipitated and allowed to settle to the bottom of the reactors from where it could be removed. The reactors are operated at a pressure sufficient to prevent the solution from boiling.

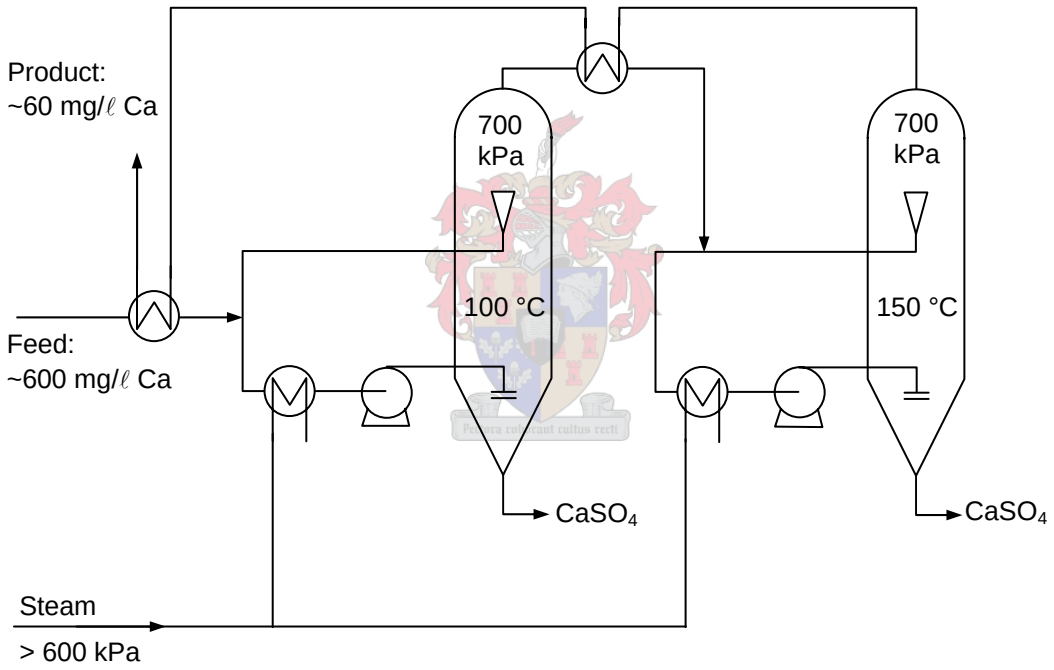

Figure 2.6 Anhydrite precipitation process developed by the WREN Group.

Two concerns of this process is the scaling of the heat exchanger surfaces and the energy consumption. The WREN Group admitted that scaling has been one of the major challenges in the design, but they claim that they have managed to eliminate it. They also claimed that 95% of the energy leaving the reactors in the heated solution, is recovered through the heat exchanger network (WREN, 2002). The formation of anhydrite is an exothermic reaction at 240 kJ/kg. Relating this to the amount of steam

(600 kPa(abs)) required for the reaction only comes to a value of 0.115 kg steam per kg of anhydrite formed.

Special consideration should be taken regarding the materials of construction for implementing this process to a pregnant leach solution. The high temperatures and pressures would require the reactors to be autoclaves and although the pH of the leach solution after iron precipitation is only slightly acidic, the solution would still be very corrosive compared to AMD for which the process was designed.

For both the gypsum and anhydrite precipitation methods, the solution leaving the precipitation reactor would still be saturated with calcium sulphate, although at a lower concentration. To eliminate the saturation, the solution needs to be brought back to its inlet temperature, which presents a higher solubility. In the anhydrite process the saturation is effectively removed by cooling the reactor discharge using the heat exchanger network.

Sulphide Precipitation (Precipitation-and-Releach)

This option derives from the low solubility of base metal sulphides compared to other impurities. It should be possible to precipitate all of the valuable metals and separate them to be re-leached separately without the impurities. This option is a more expensive route since the cobalt and nickel, which is present in relative high quantities, is precipitated as apposed to precipitating some of the impurities. For this option it would be important, if possible, to regenerate and recycle the sulphide used in the precipitation. To eliminate the possibility of gypsum precipitation after the second leaching step, a different base to lime should be used. This will affect the economics of the process.

A precipitation-and-releach step has been considered for the Nkomati Metals Plant but it was decided in favour of the direct solvent extraction route due to the lower operating cost. Two circuits that do implement a precipitation-and-releach step are the Australian laterite operations, Murrin-Murrin and Cawse (Mayze, 2001). In the Murrin-Murrin circuit, the base metals are precipitated as sulphides followed by oxidative leaching, where as in the Cawse circuit the base metals are precipitated with some impurities as hydroxides. The hydroxide precipitate is then leached with

ammonia-ammonium carbonate solution. For the Murrin-Murrin circuit the sulphide precipitation is the purification step while the ammonia leaching step is for the Cawse circuit.

Precipitation Inhibitors

Precipitation inhibitors, in the context of this study, are classified as a special group of admixtures that adsorb onto crystal surfaces, particularly in the active sites or along the growth step, to disrupt crystal growth. They may be present in low concentrations, far below the concentration of the compound it is inhibiting, and still be effective. A number of chemicals has been identified for exhibiting this property on calcium salts (Axelrad et al., 1964) and has been used in the control of scale formation in circulating aqueous systems such as cooling water systems.

In most applications precipitation is stopped irreversibly, but examples exist of admixtures that would inhibit crystal growth only for a certain period of time, after which the growth is continued at a rate corresponding to the growth rate in the absence of the admixture. This behaviour has been observed for gypsum owing to the influence of triethyl-diamine-tetramethylene phophonic acid (Söhnel & Garside, 1992).

Pectora roborant cultus recti

Espencheid et al. (1978) took advantage of the similar behaviour for calcite under the influence of sodium hexameta-phosphate for the control of scaling in an uranium in situ leaching operation. The controlled addition of the inhibitor to the lixiviant prevents calcite precipitation for the time it is in the critical parts of the circuit after which it is allowed to precipitate. It is important that the calcite do precipitate in the non-critical parts to avoid the accumulation of calcium in the circuit.

Precipitation inhibitors are being looked at for the control of gypsum precipitation in the Australian laterite operation, Bulong (Mayze, 2001). The Nkomati Project Team has also indicated interest in precipitation inhibitors and has looked at a locally manufactured inhibitor under the trade name Chematron 672. This product is a blend of organic phosphonates and phosphenocarboxylic acid and it is claimed that it could effectively increase the solubility of calcium sulphate from 2.1 g/ℓ to 10 g/ℓ.

Precipitation inhibitor could work in a once through circuit provided it does not have any adverse effects on solvent extraction. There is some concern at Bulong since the long-term effects of inhibitors on solvent extraction have not been studied yet. In a closed circuit the calcium would quickly accumulate. The amount of calcium entering as lime during iron precipitation is far higher than what could be accommodated by the increased solubility provided by the inhibitors.

In the Metals Plant Circuit the inhibitors might influence the lime boil process where the precipitation of calcium sulphate is wanted. The calcium sulphate precipitation could be seen as a method of reducing the calcium and sulphate concentrations of solution before it is disposed in the tailings dams. If this does prove to be a problem an inhibitor such as triethyl-diamine-tetramethylene phophonic acid of which the inhibiting effect could be localised to the solvent extraction section, should be looked at.

2.2.2 Ion Exchange

No suitable ion exchange resin with a high enough selectivity for calcium and magnesium could be identified. Instead a process was found that calcium and magnesium is removed form cobalt using ion exchange where the selectivity is owed to the oxidative state of the base metal and the medium. Although this method would not be practical in the current application it is still included for the completeness of this study.

The process described by Gray et al. (1996) was developed by Queensland Nickel to refine an impure cobalt sulphide feed to produce cobalt oxide hydroxide (CoOOH). The process consisted of six steps:

- Oxidative leaching.
- Zinc and iron removal using solvent extraction (Cyanex 272).
- Cobalt transfer from a sulphate medium to an ammonical medium using solvent extraction (D2EHPA).
- Nickel removal using Ammoniacal Solvent Extraction (ASX) with LIX87QN.
- Calcium and magnesium removal using ion exchange.
- Cobalt precipitation.

The calcium and magnesium ion exchange step are dependent on the two proceeding steps. The transfer from the sulphate medium to the ammoniacal medium results in the formation of the base metal ammine complexes. During the nickel ASX step the cobalt is oxidised to cobaltic state (Co^{3+}) using a combination of aeration and hydrogen peroxide, after which the nickel is extracted using LIX87QN. The unoxidised cobalt (Co^{2+}) is co-extracted with nickel and it is therefore, important to keep its concentration as low as possible.

Several different ion exchange resins has been tested for the removal of calcium and magnesium from the cobalt(III) ammoniacal solution. All of the resins were macroreticular cation resins bonded to a styrene/divinylbenzene support, which was designed for selectivity of heavy metal cations over alkali and alkaline earth elements. The selectivity appears to be contradictory to the described application but it was confirmed in the product specifications for one of the resins used, Purolite S-930. In the specifications the selectivity is given as: Cu > **Ni** > Zn > **Co** > Cd > Fe(II) > Mn > **Ca**. Either the cobaltic oxidation state, or the ammine complexation, serves to mask the cobalt from the resin so that only calcium and magnesium would be removed.

This method is not applicable to the separation of calcium and magnesium from nickel. Whereas Co^{3+} is a stable ion in an aqueous solution, Ni^{3+} would be hydrolysed immediately (Kerfoot, 1991). In the Metals Plant this may be looked at as a method of purifying cobalt after solvent extraction but it will not help for the control of calcium and magnesium in the presence of nickel.

2.2.3 Solvent Extraction

Most solvent extraction steps for base metals already provide a degree of separation from calcium and magnesium. Recent research focussed on improving this separation. Methods being looked at are the optimisation of the pH and organic-aqueous phase ratio for increased separation and the addition of synergistic compounds to the extractant. Solvent extraction steps also exist for the separation of calcium and magnesium from the base metals. All of these methods will be discussed below.

Solvent Extraction of Calcium and Magnesium

Based on the selectivity of some common extractants it would be possible to remove calcium and magnesium from the base metals using solvent extraction. Provided below is the selectivity of D2EPHA, PC 88A and Cyanex 272 (Burkin, 1987) used for the extraction of calcium and magnesium:

D2EHPA	$Fe^{3+} > Zn > Ca > Cu > Mg > Co > Ni$
PC 88A	$Fe^{3+} > Zn > Cu > Ca > Co > Mg > Ni$
Cyanex 272	$Fe^{3+} > Zn > Cu > Co > Mg > Ca > Ni$

The first approach would be to use D2EPHA to extract calcium. This would serve as a general impurity removal step since zinc and manganese would be co-extracted. This is the approach reported by Cole (2002) for the refining of cobalt. In the reported process, D2EPHA is used to extract zinc, manganese and calcium at a pH decreasing from 2.37 to 2.26 in three extraction stages. A scrub stage is still required to minimise the deportment of cobalt. Hydrochloric acid was used to strip the impurities, avoiding the limitations of gypsum precipitation. The difference in selectivity between magnesium and cobalt was not sufficient to remove magnesium. In the particular process, the impurities solvent extraction step was followed by cobalt solvent extraction using Cyanex 272. The purpose of the cobalt solvent extraction step was to separate it from magnesium and any nickel present as impurities.

D2EPHA is also used in the HIKO direct hydrometallurgical process (Dreisinger, 2001) for the removal of calcium, followed by magnesium removal using IONQUEST 801. IONQUEST 801 is the same extractant as PC 88A, only it is produced by a different company. In the HIKO process the aim is to generate a high purity nickel stream suitable for the production of nickel chemicals. Cobalt is not recovered and is extracted with the magnesium and other impurities. Hydrochloric acid is also used in the HIKO process for the stripping of calcium and magnesium during the impurities solvent extraction steps.

Cominco has developed a process for the direct hydrometallurgical treatment of sulphide concentrates (Jones, 2000). In their process, after copper solvent extraction and iron precipitation, the leach solution is subjected to a precipitation-and-releach

step. Cobalt and nickel is precipitated as hydroxides at a pH of 7 to 8 after which it is leached in an ammonia-ammonium carbonate solution. The precipitation-and-releach step seemingly controls the calcium, while magnesium enters the ammonia leach solution. The solvent extraction section involves three steps beginning with cobalt extraction followed by magnesium and then nickel extraction. Cobalt is extracted with Cyanex 272 in the presence of magnesium where it is advantageous for the separation of cobalt from nickel owing to its intermediate selectivity. Magnesium would occupy the sites not loaded by cobalt, thereby limiting the amount of nickel that is co-extracted. After cobalt solvent extraction, magnesium is extracted also with Cyanex 272 at a higher pH. Nickel is finally extracted using LIX 84 in the absence of magnesium.

The cost of solvent extraction makes it unattractive for the extraction of worthless elements such as calcium and magnesium. Another problem would be that after solvent extraction the calcium and magnesium would still be in a solution, which needs to be dealt with. The introduction of a new extractant to a circuit can adversely affect solvent extraction steps already present. When the solvent extraction steps are used in series, the upstream extractants tend to contaminate the downstream organic phases over a period of time. The contamination is owed to the solubility (although very low) of the extractant in the aqueous phase and the entrainment of the upstream organic phase in the raffinate. If the upstream extractant is different to that used downstream, the cross contamination would result in the co-extraction of impurities. This is cited as one of the reasons for gypsum precipitation in the Bulong process. Versatic 10 was contaminated with Cyanex 272, which load calcium at the conditions used for nickel solvent extraction (Mayze, 2001). Although the cross contamination of extractants can be controlled using equipment such as after settlers and carbon columns, it would still be best if the number of different extractants used in a circuit could be minimised.

Optimisation of Solvent Extraction

This is a method that has already been discussed in Chapter 1 and has been applied for cobalt extraction using Cyanex 272 (Babjak, 1986) and nickel extraction using Versatic 10 (Feather et al., 2002). The additional limitations imposed by the low solubility of gypsum sets this type of optimisation apart from the normal optimisation.

The pH profile of the extraction stages needed to be optimised to limit the amount of calcium that is co-extracted and the phase ratio for scrubbing and stripping is limited by gypsum precipitation. Using a different solution to sulphate such as a chloride can eliminate the problem of the minimum phase ratio during scrubbing and stripping, but this may not be compatible with the overall process.

Bajak (1986) first described a method of controlling calcium during the counter-current extraction of cobalt involving Cyanex 272 through the adjustment of the pH in the individual extraction stages. The pH of the aqueous phase was adjusted during the initial stages maximising the extraction of cobalt. In the later stages, where the depleted aqueous phase was contacted with the unloaded organic, the pH was adjusted to permit the extraction of cobalt while minimising the co-extraction of calcium. The pH was controlled using automatic titrators loaded with a base solution such as ammonium hydroxide. For cobalt extraction using Cyanex 272, the pH was adjusted to 5.0 during the initial stages. In the later stages, where the cobalt was depleted, the pH was adjusted to 4.5. Although a pH of 4.5 was less favourable for the loading of cobalt, it is more favourable for the loading of cobalt in preference to calcium. The co-extraction of calcium was therefore minimised, avoiding gypsum precipitation.

Feather et al. (2002) simulated the Nkomati Metals Plant's extraction circuits, shown in Figure 2.7, on laboratory scale to optimise the process. The Bateman Pulsed Columns were represented by a number of individual mixer-settler units.

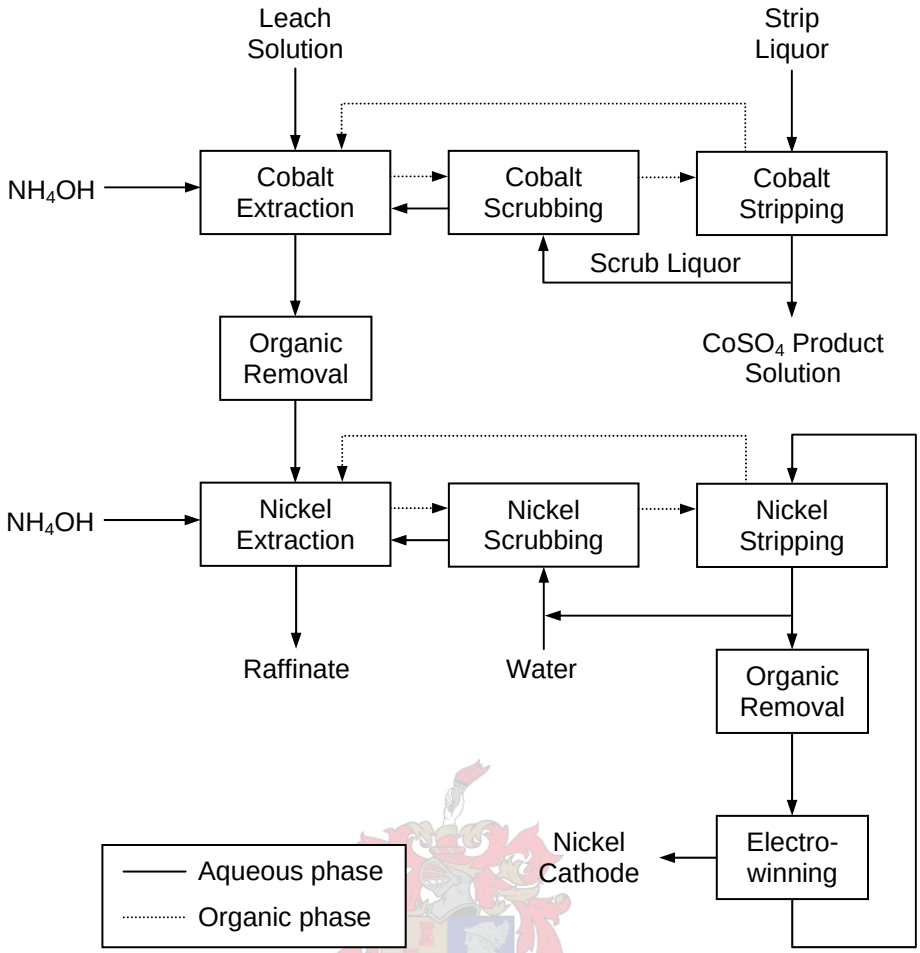

Figure 2.7 Flowsheet for Nkomati's cobalt and nickel solvent extraction circuit (adapted from Feather et al., 2002).

The scrubbing section was the area in the cobalt solvent extraction circuit for which the optimisation was limited by gypsum solubility. The pH and advance phase ratio had to be optimised to ensure that the magnesium, calcium and nickel are scrubbed from the organic phase to meet the cobalt product specifications. The scrub solution volume had to be minimised to ensure that at least 50% of cobalt is loaded onto the organic whilst ensuring that the scrubbed calcium would not exceed its solubility.

In the nickel solvent extraction section both the extraction step and scrubbing step had to be optimised within the limitations imposed by calcium solubility. The objective of the extraction step was to achieve 99% extraction of nickel while minimising calcium co-extraction. This was achieved by controlling the pH profile. An additional extraction stage had to be included to reach the 99% extraction target.

In the scrubbing section the calcium concentration on the organic had to be scrubbed below 9 mg/ℓ to ensure that the calcium concentration in the electrowinning circuit was below the gypsum solubility with a bleed stream less than 5%. This was again achieved by controlling the pH profile over the scrubbing stages. Although it is possible to optimise the solvent extraction to operate within the limitations of gypsum solubility, the circuit would not operated at its most efficient level with respect to the extraction of the valuable metals.

Synergists

Preston (1984) reported that Versatic 10, the extractant planned for nickel solvent extraction in the Nkomati Metals Plant, has poor selectivity over impurities such as manganese, calcium and ferrous iron. In an effort to improve selectivity, Preston and Du Preez (2000) have extensively researched the effects of organic compounds such as pyridinecarboxylate esters on the extraction of nickel. Their previous research indicated a synergistic effect of *n*-octyl 3-pyridinecarboxilate towards the extraction of nickel, increasing its selectivity over other base metals such as manganese and other impurities such as calcium and magnesium. In their more recent research they looked at the effects of alkylpyridines, in view of possible commercialisation.

Pectora roborant cultus recti

Figure 2.8 illustrates the effect of an alkylpyridine on the extraction of nickel and calcium. It has a synergistic effect on nickel by shifting the extraction curve to lower pH values and an antagonistic effect on calcium by shifting the extraction curve to higher pH values. The shifts in the pH values are quantified by the ΔpH_{50} value. This is defined as the shift in the pH value at which 50% of the metal ion is extracted at the given conditions. The ΔpH_{50} is calculated from Equation 2.2. The pH value at which 50% of the metal ion is extracted, pH_{50}, can also be used to indicate the selectivity between nickel and other impurities using Equation 2.3.

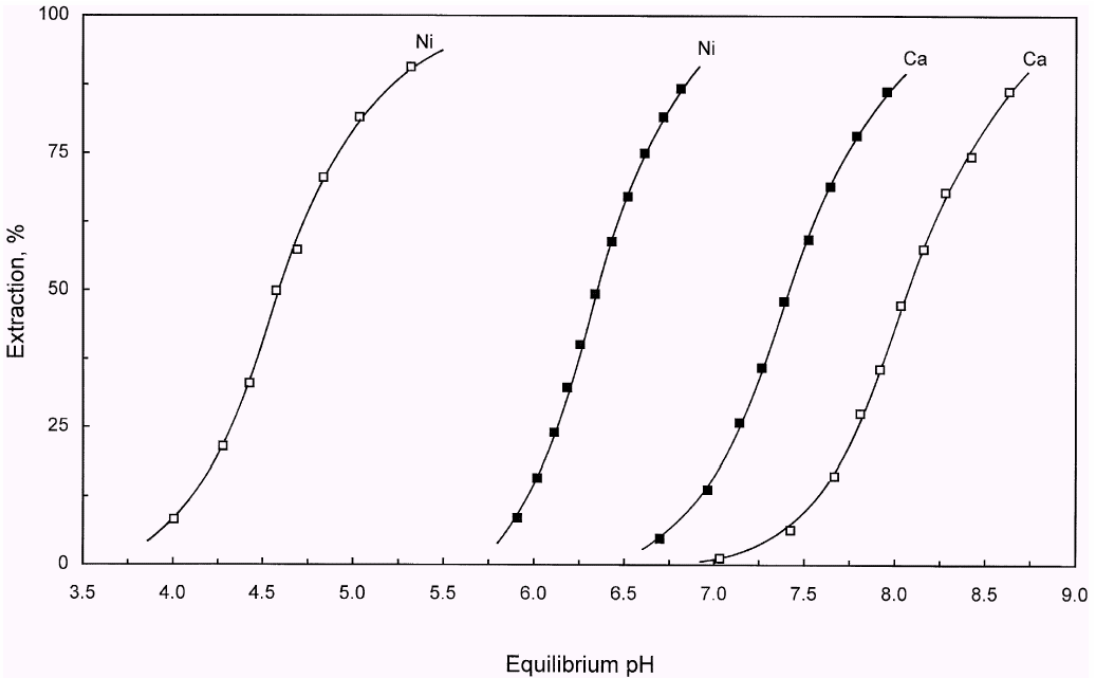

Figure 2.8 The effect of an alkylpyridine on the extraction of 0.05 M Nickel and Calcium by 0.50 M Versatic 10; ■ Versatic 10 alone; □ Versatic 10 with 0.50 M 4-(5-nonyl)pyridine (Preston & Du Preez, 2000).

$$\Delta pH_{50} = pH_{50}\ (Versatic\ alone) - pH_{50}\ (Versatic\ \&\ alkylpyridine) \qquad \textbf{Equation 2.2}$$

$$pH_{50}^{Me-Ni} = pH_{50}^{Me} - pH_{50}^{Ni} \qquad \textbf{Equation 2.3}$$

Preston and Du Preez (2000) used a nitrate medium for their tests to minimise the effect of complexation of the metal ions with the anions at a temperature of 20°C. Under these conditions they reported a synergistic shift for nickel of ΔpH_{50} = 1.72 and antagonistic effect for calcium of ΔpH_{50} = 0.65. Overall the selectivity increased from pH_{50}^{Ca-Ni} = 1.04 without the alkylpyridine to pH_{50}^{Ca-Ni} = 3.48 with the alkylpidine. A test was performed in a sulphate medium with the same ionic strength as the nitrate solution for which pH_{50}^{Ca-Ni} = 3.23.

The increase in selectivity from the alkylpyridine would reduce or even eliminate the precipitation of gypsum during nickel solvent extraction. The extraction at lower pH values would also be beneficial for Versatic acid since it suffers from a relative high

solubility in an aqueous solution, which increases with an increasing pH value. It would be interesting to follow the commercialisation of synergists. One of the major determining factors for the use of alkylpiridines would be the cost of it since an equimolar addition of the alkylpiridines was used with Versatic 10.

2.3 Summary of Methods

A number of methods have been discussed this far without comparing them. The different methods are tabulated below, pointing out the advantages and disadvantages of them.

Table 2.4 Summary of methods for the control of calcium and magnesium.

Method of Control	Advantages	Disadvantages
Fluoride Precipitation	- High selectivity for calcium and magnesium over base metals. - Single step to control both calcium and magnesium. - Environmentally stable precipitate produced.	- Potential dangerous reagent (fluoride), which need to be removed after precipitation. - Possible introduction of unwanted cation accompanying the fluoride. - Possible gel formation.
Gypsum Precipitation	- No extra chemicals needed for precipitation. - Selective for calcium.	- Although at a lower concentration the solution is still saturated unless it is heated again. - Low removal of calcium at only ~50%. - The process requires long residence times (6 hours). - Cooling duty required/cooling towers (significant capital investment). - Cannot control magnesium.

Table 2.4 (Continued)

Method of Control	Advantages	Disadvantages
Anhydrite Precipitation	- No extra chemicals needed for precipitation. - Selective for calcium. - Higher removal of calcium than gypsum precipitation at ~90%.	- Process at elevated temperatures and pressures with possible corrosion problems. - Medium pressure (>600 kPa) steam plant required. - Cannot control magnesium. - Large capital investment and running costs (energy).
Sulphide Precipitation	- General impurity removal step. - Can separate base metals to a limited extent.	- High reagent consumption to precipitate all the base metals. - Requires an additional leaching step. - A lime base can still not be used after the releach step. - Possible introduction of unwanted cation accompanying the sulphide.
Precipitation Inhibitors	- Would avoid gypsum precipitation by effectively increasing its solubility. - Compounds available that would only temporarily inhibit precipitation.	- Can only be applied to once through systems to avoid the build up of calcium. - Long term effects on solvent extraction not studied yet. - Possible negative effect on down stream process steps such as the lime boil process where the precipitation of calcium is wanted. - Cannot control magnesium.

Table 2.4 (Continued)

Method of Control	Advantages	Disadvantages
Ion Exchange	- Selective for Calcium and magnesium. - Single process step to control both calcium and magnesium.	- The presented process requires an ammoniacal medium and the oxidation of the base metals to 3+ state. - Can only applied to solutions without nickel. - Suitable resin with selectivity for calcium and magnesium over base metals not found.
Solvent Extraction of Calcium and Magnesium	- Can be a general impurity removal step.	- Different extractants needed for calcium and magnesium. - Introduction of a new extractant into the circuit that can contaminate the other extractants. - Introduction of a solvent extraction step to remove valueless elements.
Optimisation of Solvent Extraction	- Can control calcium and magnesium within limits.	- Inefficient operation with respect to the extraction of the valuable elements. - Limited by the solubility of gypsum. - May require additional stages to achieve the desired recovery.
Solvent Extraction Synergist	- Limits the co-extraction of impurities, allowing the solvent extraction to be operated more efficiently.	- Not commercialised yet. - Equimolar amounts of the synergist required for the extractant.

Fluoride precipitation has been selected from the list of possible methods based on its high selectivity to be developed into a process for the control of calcium and magnesium in the Nkomati Metals Plant. The two disadvantages can be overcome by the lime boil process, which would remove the unreacted fluoride, and the selection of

an appropriate soluble fluoride compound that would not introduce any foreign cations into the system. Two possibilities would be hydrofloric acid (HF) and ammonium fluoride (NH_4F). It is of key importance that the fluorides are recovered in easily filterable form during the continuous process. Additionally methods of removing or possibly recycling the unreacted fluoride should also be looked at.

Chapter 3

Literature Review and Theoretical Considerations

Objectives of Chapter 3

- Provide the theoretical basis for this study.
- Discuss the relevant precipitation theory.
- Discuss the relevant adsorption theory.

In the preceding chapters the background to this study was provided. Insight was given to the problems associated with calcium and magnesium. In this chapter two distinct topics would be looked at. The first topic that would be explored is the theory of precipitation. This will be followed by theory of adsorption. The discussions in this chapter would form the theoretical basis for all of the proceeding chapters.

3.1 Precipitation Theory

Precipitation has found many applications in the field of hydrometallurgy ranging from impurity control (e.g. iron precipitation and the proposed fluoride precipitation of calcium and magnesium), separation of valuable metals (e.g. sulphide precipitation of base metals) to the reduction of metals (e.g. hydrogen reduction of nickel). There are not many hydrometallurgical processes that do not employ precipitation and it is more widely applied than classical crystallisation. It is no wonder that Habashi (1999), from a metallurgist point of view, classified crystallisation as subclass of precipitation in his book: "A Textbook of Hydrometallurgy."

Precipitation is generally seen as a subclass of crystallisation, but there is no precise definition to distinct it. Söhnel and Garside (1992) prefer to define precipitation as embodying fast crystallisation, where the rapidity of the process is a consequence of the high super saturation at which it takes place. Of more importance are the consequences of this definition, as set out by them.

A compound that is precipitated is relatively insoluble and a high supersaturation can be generated for it. Under these high supersaturations the rates of primary nucleation are very high and plays as an important role as crystal growth in precipitation. The high rates of nucleation results in the generation of a high number of small crystals typically with sizes of 0.1 to 10 μm at particle concentrations between 10^{11} to 10^{16} particles per mℓ. Secondary processes such as ripening, ageing, agglomeration and coagulation are also more pronounced in precipitation and would have a major influence of the precipitate size distribution. Precipitation, as it is intended in the fluoride precipitation process, would involve the reaction between ions in two liquids that is mixed to generate the supersaturation. Under these conditions the precipitation reactions are generally fast enough that the role of mixing have an important bearing on the properties of the precipitate formed.

A number of topics relating to precipitation have been referred to in the preceding discussion ranging from the driving force of precipitation being supersaturation, to the mechanisms involved in precipitation. In the following section the different topics are discussed in more detail to give a better understanding of precipitation.

3.1.1 Precipitate Characterisation

The characteristics of the precipitate formed is often more important than just thermodynamic feasibility of the reaction. Accordingly it is found that the largest portion of precipitation theory is focussed on mechanisms involved in the formation of the precipitate and the influence of it on the characteristics. Listed below are some of the more important characteristics:

- The size distribution of the precipitate.
- The shape of the individual crystals.
- Polymorphism.
- The inclusion of volumes of the mother liquor with in the precipitate.
- The uptake of impurities within the crystal lattice.
- The degree to which the precipitate particles tend to agglomerate.
- The surface roughness of the crystals.

The characteristics and the inherent quality of the precipitate are dependent on the reaction conditions under which it was formed. The design of a precipitation reactor should therefore focus around controlling the reaction conditions to produce a precipitate that meets the product requirements. Properties such as filterability, which is dependent on one or a combination of the above listed characteristics, can also be of importance. The product requirements of the precipitate might vary depending on the aplication of the precipitation step. In the case of using precipitation for impurity control, the focus would be to produce a filterable precipitate with the minimum amount of mother liquor inclusions. The latter requirement will minimise the loss of the valuable components during the precipitation step. In the case of the precipitate being the valuable product, the minimisation of the inclusion of mother liquor will still be of importance, but the particle size distribution rather than filterability would be concentrated on. Each of the above mentioned characteristics will now the discussed to highlight their implications.

Size Distribution

The size distribution is considered the most important characteristic for any crystallising system. It is not only important for the quality of the product but also has an important bearing on the performance of the process, the separation of the product and the subsequent handling properties of the product. In crystallisation (as apposed to precipitation) the solid phase is formed as individual crystals and the measured size distribution would be of the crystals. The size distribution is therefore referred to as the *crystal size distribution*, CSD. In precipitation, secondary processes such as agglomeration are unavoidable resulting in the individual crystals clustering together and forming bonds. It would therefore not be possible to measure the individual crystals. For this case, the size distribution would be of the agglomerated particles and is sometimes referred to as the *particle size distribution*, PSD.

There are different definitions for the size of a particle and the resulting size distributions from these definitions would not necessarily correspond. A size distribution is therefore meaningless without the definition of the particle size. Given in Table 3.1 are the definitions most often found.

Table 3.1 Definitions of particle size (Van Rosmalen et al., 2001)

Name	Definition
Length	Maximum visible length.
Sieve diameter	Width of minimum square aperture through which the particle will pass.
Volume diameter	Diameter of a sphere having the same volume as the particle.
Surface diameter	Diameter of a sphere having the same area as the particle.
Projected area diameter	Diameter of a sphere having the same projected area as the particle viewed from a fixed direction.

With the length of the particle, L, the following two shape factors, k_a and k_v, can be defined:

$$\text{Particle Surface Area} = k_a L^2 \qquad \textbf{Equation 3.1}$$

$$\text{Particle volume} = k_v L^3 \qquad \textbf{Equation 3.2}$$

A distribution of the particle size can be obtained by analysing a representative sample of the particles. This distribution can be represented in four ways. It can either be represented as a cumulative number distribution, N(L) [#/m^3], indicating the number of particles per unit volume smaller than a given size, L, or it can be represented as a mass distribution, M(L) [kg/m^3], indicating the mass of particles smaller than a given size, L. The derivatives of the above two representations results in two more representations of the size distribution. The derivative of the cumulative number distribution is called the number density distribution, n(L) [#/m.m^3], and the derivative of the mass distribution the mass density distribution, m(L) [kg/m.m^3]. The relationship between the four representations is given by Equation 3.1 to Equation 3.5 and is illustrated in Figure 3.1.

$$N(L) = \int_0^L n(L)dL \qquad \textbf{Equation 3.3}$$

$$M(L) = \int_0^L m(L)dL$$ **Equation 3.4**

$$M(L) = \rho k_v \int_0^L L^3 n(L)dL$$ **Equation 3.5**

A lot of information is contained in a size distribution, but the raw distribution is not in a format that facilitates quantitative comparisons. To allow comparison a number of statistical properties can be extracted based on the moments of the number density distribution. The j^{th} moment of the distribution is defined in Equation 3.6 and has the units of m^j/m^3.

$$m_j = \int_0^\infty L^j n(L)dL$$ **Equation 3.6**

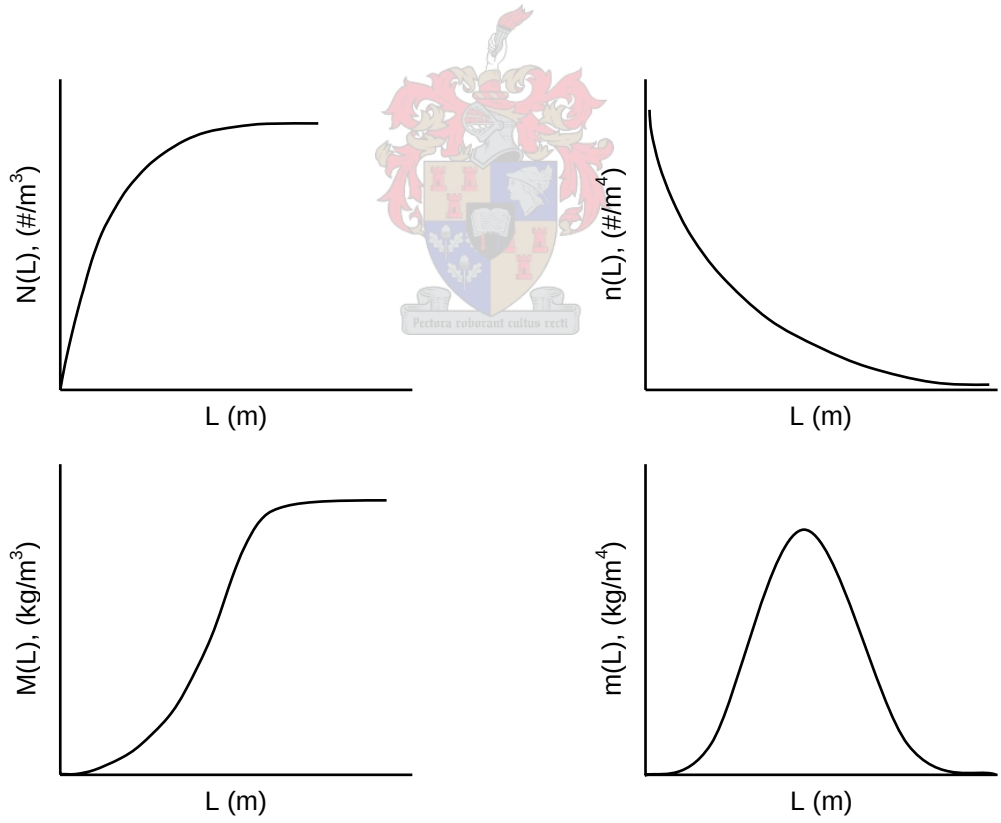

Figure 3.1 Relationship between different distributions (Van Rosmalen et al., 2001).

From the moments of the number density distribution the following properties can be calculated:

- Total number: $N_T = m_0$
- Total Length: $L_T = m_1$
- Total surface area: $A_T = k_a m_2$
- Total volume: $V_T = k_v m_3$
- Total Mass: $M_T = \rho k_v m_3$
- Number based mean size: $L_{1,0} = m_1/m_0$
- Surface area based mean size: $L_{3,2} = m_3/m_2$
- Mass based mean size: $L_{4,3} = m_4/m_3$
- Coefficient of Variation $CV = \left[\frac{m_3 m_5}{m_4^2} - 1\right]^{0.5}$

Other properties that can be extracted from the mass density distribution is the mode, L_D, which is the size at the maximum of the distribution and the median size, $L_{50,}$ the size at which the relative mass distribution is 50%.

Shape of Crystals

The unit cell of a crystal is the subdivision of the lattice that retains the overall characteristic of the crystal lattice. Crystal grown under mild conditions (low supersaturation levels) tends to retain the shape imposed by the unit cells. Fourteen types of unit cells exist which is also referred to as the Bravais lattices. The different types of unit cells may again be divided into seven symmetry classes being:

- Cubic
- Tetragonal
- Orthorhombic
- Hexagonal
- Rhombohedral
- Monoclinic
- Triclinic

Each symmetry class has a defined geometry which confines the shape of the crystal to specific flat faces. The different faces of the geometry are identified according to

the Miller indices system. The faces of a crystal may grow at different rates resulting in the slower growing faces becoming more predominant while the faster growing faces becomes smaller in area. The resulting shape is referred to as the crystal habit. The rate of growth is determined by both the crystallising system itself, and the conditions under which it is grown.

Some crystal shapes are more desirable than others. Anisotropic crystals, crystals that have different properties in different directions, may form needle like crystals. Needle shaped crystals are undesirable owing to their tendency to break easily and their poor filterability. Some measures can be taken if an undesirable shaped crystals are formed. The process conditions can be manipulated to reduce the growth of the offending crystal face or even to produce a more suitable polymorph if it exist. Lower supersaturations reduces the anisotropy of the crystal and admixtures can be used to control the growth of some of the crystal faces.

Mother Liquor Inclusions

The uptake of volumes of mother liquor within the crystals is dependent on the mechanism and rate of crystal growth (Section 3.1.4, p.60). It is therefore, strongly dependent on the level of supersaturation, with the inclusions increasing with increasing supersaturation. Mother liquor inclusion can also be the result of attrition of the crystals. Beyond a certain size the crystals become susceptible to attrition resulting in the corners of the crystals being fractured. During the healing process the crystal faces may not align, resulting in volumes of the mother liquor being captured within the crystal.

Mother liquor inclusions invariably result in a reduction of the purity and the strength of the crystals. Another negative effect is that the liquor can be liberated during transport and storage resulting in caking by the formation of salt bridges between crystals. Mother liquor inclusions should therefore be avoided if possible.

Impurities in Crystal Lattice

Crystallisation processes has always been seen as a superior separation technique owing to the rigid crystal structure that is formed. Impurities can only be accommodated within the crystal lattice if it has a similar size as the growth units,

which limits the uptake of impurities. The uptake of impurities within the lattice is quantified by the effective distribution coefficient, k_{eff}, as defined in Equation 3.7 where c_c is the concentration of the impurity within the crystal and c_b is the concentration in the bulk liquid.

$$k_{eff} = \frac{c_c}{c_b} \qquad \textbf{Equation 3.7}$$

Degree of Agglomeration

Agglomeration is the process whereby individual crystals collide and adhere to each other. In time the crystals are cemented to from a single particle. This process is practically unavoidable during precipitation. Agglomeration has the negative effect that the mother liquor can be captured between the agglomerated particles. As with mother liquor inclusions within the crystal, this will lead to a reduction in the purity of the precipitate. The agglomerates also tend to break more easily than the individual crystals, reducing the strength of the particles and releasing mother liquor that can lead to caking during storage and transport. Agglomeration does have the advantage during precipitation that it increases the particles size, aiding in the separation of it.

Agglomeration, as most other properties of the precipitate, is dependent on the reaction conditions under which it was formed. The mechanism of it will be discussed in Section 3.1.6, p.71.

Surface Roughness

A rough crystal surface is the result of unordered growth occurring at high supersaturations. The rough growth results in an increase in mother liquor inclusions within the crystals. A rough surface also has the disadvantage that it breeds more secondary nuclei during attrition, increasing the number of smaller particles.

Rough growth is a supersaturation dependent process and can be limited by reducing the supersaturation ratio. Rough growth can only be identified by the inspection of the crystal surfaces.

Filterability of Precipitate

The filterability of a precipitate can be characterised by its mass filtration resistance, α_F, which is based on the Carman-Kozeny equation for flow through particle beds. For constant pressure filtration the equation can be rearranged into the following form where V_F is the volume of filtrate at time t (Söhnel & Garside, 1992):

$$\frac{t}{V_F} = A + BV_F \qquad \textbf{Equation 3.8}$$

The constant A is directly related to the resistance of the filter media, R_m, and the coefficient B to the filtration resistance, α_F. Equation 3.9 and Equation 3.10 give these relationships.

$$A = \frac{\mu_F R_m}{\Delta P} \qquad \textbf{Equation 3.9}$$

$$B = \frac{\alpha_F \mu_F G_F}{2\Delta P A_F^2} \qquad \textbf{Equation 3.10}$$

Where:

μ_F : Viscosity of the filtrate,

G_F : Mass of precipitate per volume of filtrate,

A_F : Filtration area.

The mass filtration resistance can be determined experimentally by measuring the volume filtrate against time during filtration. Plotting the data of t/V_F against time should give a straight line with the gradient B and the intersection with the y-axis A. The other parameters in Equation 3.10 can either be estimated or measured, allowing the mass filtration resistance to be calculated.

For the case where the filterability of the precipitate is more important than the particle size, the design of the precipitation system would be a trade-off between the volume of the precipitation reactor and the area of the filter. A larger reactor would have a longer residence time and would produce larger particles with a lower mass filtration resistance, decreasing the area of the filter needed. In contrast, a smaller

reactor would produce smaller particles with a higher mass filtration resistance, increasing the area of the filter needed.

3.1.2 The Driving Force of Precipitation: Supersaturation

The term "supersaturation" has often been used and the reader should have an idea that it is a measure of how far the concentration of a compound in solution exceeds its solubility. In this section supersaturation is quantified by deducing it, using thermodynamic principles. This deduction would only be done for molar concentrations and is based on the deduction provided by Söhnel and Garside (1992).

The thermodynamic driving force for crystallisation, $\Delta\mu$, is the difference between the *chemical potential* of the compound in the supersaturated solution, μ_1, and that of the crystal, μ_2:

$$\Delta\mu = \mu_2 - \mu_1 \qquad \textbf{Equation 3.11}$$

For a compound to spontaneously crystallise the difference in the chemical potential should be negative ($\Delta\mu < 0$). It is preferred to state the driving force as a positive value and therefore *reaction affinity*, ϕ, is introduced:

$$\phi = -\Delta\mu \qquad \textbf{Equation 3.12}$$

The chemical potential of a compound is defined as:

$$\mu = \mu_c^0 + RT \ln a_c \qquad \textbf{Equation 3.13}$$

The subscript c indicates the activities to be measured in terms of molar concentrations. Combining reaction affinity with the chemical potential into Equation 3.11, results in:

$$\frac{\phi}{RT} = \ln \frac{a_c}{a_{c,eq}} \qquad \textbf{Equation 3.14}$$

The activity of a compound that dissolves and dissociates into ν_+ cations and ν_- anions is related to the molar concentration of its ions through:

$$a_c = a_{\pm,c}^{\nu} = c_+^{\nu_+}\ c_-^{\nu_-}\ \gamma_{\pm,c}^{\nu} \qquad \textbf{Equation 3.15}$$

Where $\nu = \nu_+ + \nu_-$ and $\gamma_{\pm,c}^{\nu}$ is the mean ionic activity coefficient. Substituting Equation 3.15 into Equation 3.14 results in Equation 3.16 in which supersaturation is quantified:

$$\frac{\phi}{RT} = \nu \ln\left(\frac{c_+^{\nu_+}\ c_-^{\nu_-}\ \gamma_{\pm,c}^{\nu}}{c_{+,eq}^{\nu_+}\ c_{-,eq}^{\nu_-}\ \gamma_{\pm,c,eq}^{\nu}}\right)^{\frac{1}{\nu}} \qquad \textbf{Equation 3.16}$$

For this the *supersaturation ratio*, S_c, may be defined as:

$$S_c = \left(\frac{c_+^{\nu_+}\ c_-^{\nu_-}}{c_{+,eq}^{\nu_+}\ c_{-,eq}^{\nu_-}}\right)^{\frac{1}{\nu}} \qquad \textbf{Equation 3.17}$$

and the *activity coefficient ratio* as:

$$\xi_c = \left(\frac{\gamma_{\pm,c}}{\gamma_{\pm,c,eq}}\right) \qquad \textbf{Equation 3.18}$$

Using these two definitions Equation 3.16 is simplified to a more manageable form:

$$\frac{\phi}{RT} = \nu \ln S_c \xi_c \qquad \textbf{Equation 3.19}$$

The supersaturation ratio in this instance has been deduced for ionic molar concentrations, but it should be clear that it could also be deduced for any concentration unit such as molalities or mole fractions. The supersaturation ratios calculated with these different concentration units would be related but not equal.

If the ionic concentrations are stoichiometric, the compound concentrations, c, rather than the ionic concentrations can be used, so that the supersaturation ratio reduces to:

$$S_c = \left(\frac{c_+^{\nu_+} \, c_-^{\nu_-}}{c_{+,eq}^{\nu_+} \, c_{-,eq}^{\nu_-}} \right)^{\frac{1}{\nu}} = \frac{c}{c_{eq}} \qquad \textbf{Equation 3.20}$$

The *relative supersaturation ratio*, σ_c, is also used at times in literature and is related to the super saturation ratio by:

$$\sigma_c = S_c - 1 \qquad \textbf{Equation 3.21}$$

If the reaction affinity (Equation 3.12) is negative, the solution is undersaturated and no solid phase is formed. A reaction affinity of zero indicates the solution to be in equilibrium with the solid phase and a positive value indicates the solution to be supersaturated resulting in the precipitation of the solid phase. For an ideal solution the activity coefficients would be unity and the value of the reaction affinity at constant temperature (according to Equation 3.19) would only depend on the supersaturation ratio. For this ideal solution the following would hold:

- $S_c < 1$: undersaturated,
- $S_c = 1$: saturated,
- $S_c > 1$: supersaturated.

To use Equation 3.17, the equilibrium composition of a solution needs to be known. The equilibrium compositions can either be determined experimentally or the solubility product of the compound may be used from literature. The thermodynamic solubility product, K_{sp}, for an anhydrous compound is defined as:

$$K_{sp,c} = c_{+,eq}^{\nu_+} \, c_{-,eq}^{\nu-} \, \gamma_{\pm,c,eq}^{\nu} \qquad \textbf{Equation 3.22}$$

The definition of the thermodynamic solubility product is the same as the denominator in Equation 3.16. The thermodynamic solubility product is independent

of the solution composition and is determined for specific temperature and pressure conditions. In some literature sources the solubility product, K_s, rather than K_{sp} is given. This solubility product would only hold for the conditions and composition under which it was determined. The published thermodynamic solubility products can be used in Equation 3.16 as follows:

$$\frac{\phi}{RT} = \nu \ln\left(\frac{c_+^{\nu_+}\ c_-^{\nu_-}\ \gamma_{\pm,c}^{\nu}}{K_{sp,c}}\right)^{\frac{1}{\nu}} \qquad \textbf{Equation 3.23}$$

It can also be used to calculate the supersaturation ratio as follows:

$$S_c = \left(\frac{c_+^{\nu_+}\ c_-^{\nu_-}}{\left(K_{sp,c} \middle/ \gamma_{\pm,c,eq}^{\nu}\right)}\right)^{\frac{1}{\nu}} \qquad \textbf{Equation 3.24}$$

Now that super saturation has been quantified the influence of it will be evaluated. Supersaturation is considered to be the single most important variable for any precipitation system as indicated in Figure 3.2. Supersaturation governs the kinetics of nucleation, growth and aging at both the rate of the processes and dominating mechanism. These three precipitation processes have an important bearing on the size distribution of the formed precipitate and would be discussed in more detail in the proceeding sections. Additionally, the growth rate influences the purity of the precipitate whereby a high supersaturation may result in the formation of inclusions of the mother liquor into the precipitate. The growth kinetics would also influence the tendency of the crystals to grow on solid surfaces and hence form scale.

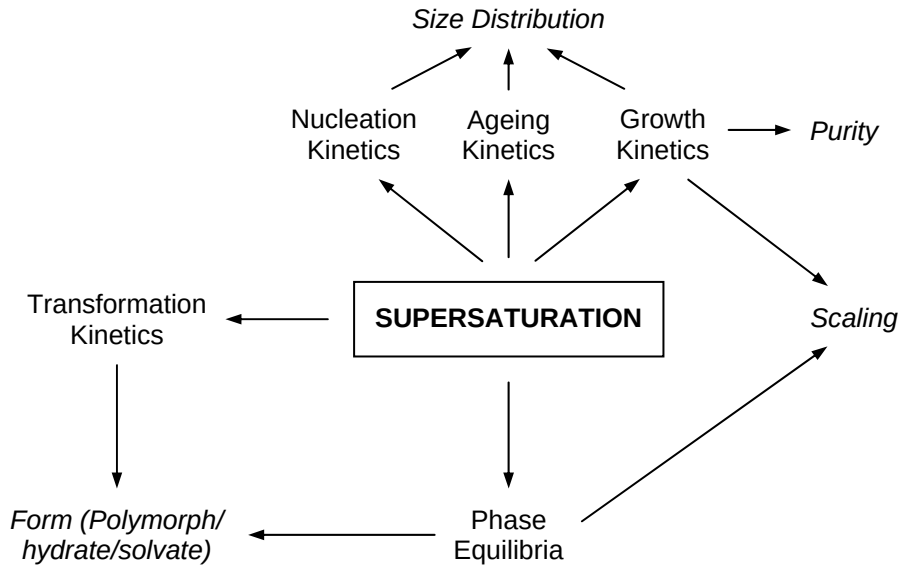

Figure 3.2 The role of supersaturation in precipitation (Söhnel & Garside, 1992).

The supersaturation level would determine the position of the system in the appropriate phase diagrams and the kinetics of the transformation reactions. Combined they would influence the form of the precipitate in terms of the polymorph and the hydration/solvation of the crystal. A compound displaying polymorphism is able to form more than one crystal structure. It is also possible for a compound to include different numbers of water or solute molecules into its crystal structure and is referred to as pseudo-polymorphism.

It is therefore seen that supersaturation is the central variable controlling all of the physical and chemical properties of the precipitate. It indirectly controls the size distribution, purity and form of the precipitate.

3.1.3 Nucleation

Nucleation is the formation or birth of new crystals from a solution. For the formation of these crystals it is a prerequisite that the solution need to be supersaturated although it is not a guarantee that nucleation would commence as soon as supersaturation is established. There are a critical number of solute entities that need to combine before the crystal is formed and hence nucleation occurs. In precipitation different mechanisms have been identified for nucleation and they are presented in Figure 3.3.

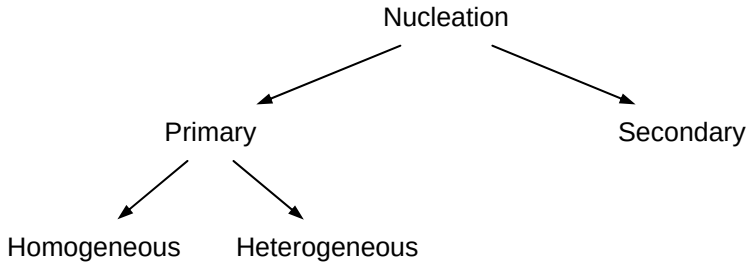

Figure 3.3 Nucleation mechanisms (Söhnel & Garside, 1992).

Primary nucleation is subdivided into homogeneous nucleation and heterogeneous nucleation. Heterogeneous nucleation takes place on foreign substrates such as dust or dirt particles present in the solutions, where as homogeneous nucleation takes place independently from these particles. In homogeneous nucleation the clustering of solute entities forms the nuclei. Secondary nucleation on the other side is dependent on the prior presence of crystals of the same material as the crystallising compound.

Primary Homogeneous Nucleation

The classical model for homogeneous nucleation is the attachment and detachment of single solute entities, A, represented by Equation 3.25:

$$A_N + A \leftrightarrow A_{N+1} \qquad \textbf{Equation 3.25}$$

The change in Gibbs free energy for the attachment of each solute entity to a cluster has two apposing terms. The attachment of each solute entity would decrease the free energy by a value of ϕ, while the increment of the cluster's surface area would have a positive contribution. In Equation 3.26 the free energy function is divided into a volume term and a surface term:

$$\Delta G = \Delta G_{volume} + \Delta G_{surface} \qquad \textbf{Equation 3.26}$$

Assuming the clusters to be spherical, Equation 3.26 becomes (Van Rosmalen et al., 2001):

$$\Delta G = -\frac{4\pi r^3}{3V_m}\phi + 4\pi r^2\gamma$$ **Equation 3.27**

Where :

r : Radius of the cluster,

V_m : Molecular volume,

γ : Interfacial free energy.

The first term of the free energy equation will always be negative while the second term would always be positive. Initially the magnitude of the latter term would be greater than the first term resulting in the free energy increasing with an increase in size. Eventually the higher order of the first term would start outweighing the latter term and the free energy would start decreasing with an increase in size. While the free energy of the cluster is increasing with an increase in size it would be unstable and would rather decay than grow. The cluster would only become stable as soon as the free energy decrease with increasing size. There therefore exist a *critical cluster radius*, r^*, at which the growth and decay would be equal. This critical radius has an associated amount of *critical free energy*, ΔG^*, which needs to be overcome before a stable nucleus could be formed. This is illustrated in Figure 3.4. The critical cluster radius can be calculated differentiating Equation 3.27 and finding the maxima. In doing this, it may be shown that the critical radius is:

$$r^* = \frac{2\gamma V_m}{\phi}$$ **Equation 3.28**

Substituting the critical radius into Equation 3.27, the critical amount of free energy may be calculated:

$$\Delta G^* = \frac{16\pi\gamma^3 V_m^2}{3\phi^2}$$ **Equation 3.29**

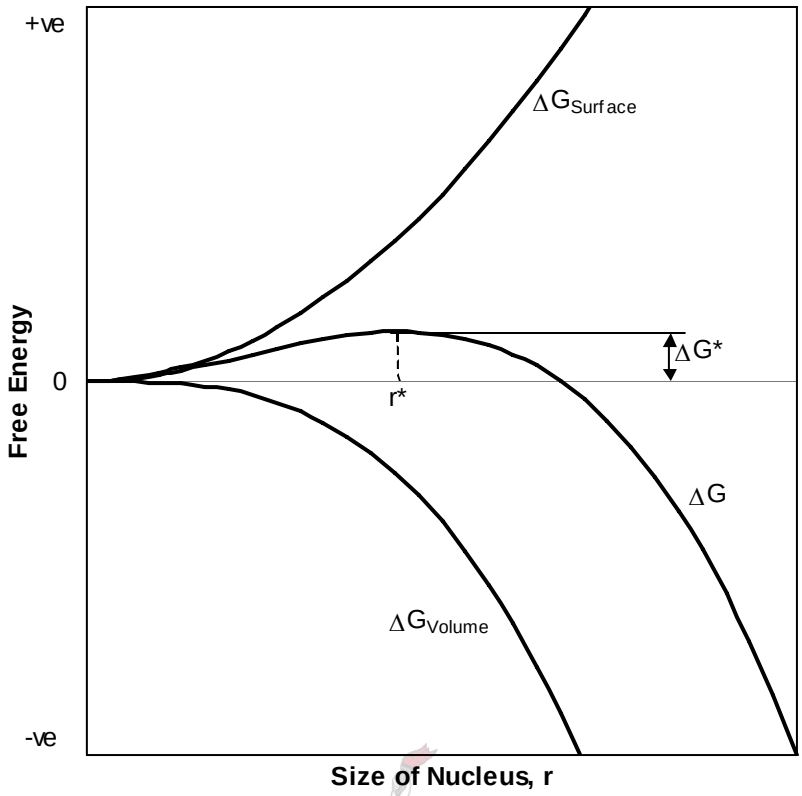

Figure 3.4 Change of Gibbs free energy as a function of the nucleus size (Van Rosmalen et al., 2001).

The change in free energy of the attachment of a solute entity can be calculated using a similar equation to Equation 3.19, expressed for an unit of solute using the Boltzmann Constant:

$$\phi = kT \ln S \qquad \textbf{Equation 3.30}$$

The supersaturation ratio is given in terms of activities, but other ratios may also be used if the appropriate activity coefficient ratio is included.

More importantly, the above results may be used to calculate the number of solute entities, N^*, needed to form a stable cluster. If the supersaturation were known this would be the first check to see if primary nucleation takes place ($N^* < 10$). Equation 3.31 gives the number of solute entities:

$$N* = \frac{4}{3}\frac{\pi r*^3}{V_m}$$ **Equation 3.31**

Moving on to the rate of nucleation. The nucleation rate is measured of the number of super critical nucleus formed per unit time in a defined volume. Based on the classical model of homogeneous nucleation, involving attachment and detachment of solute entities, it may be shown that the rate of nucleation*, J,* follows an Arrhenius type of expression (Van Rosmalen et al., 2001):

$$J = \Omega e^{-\frac{\Delta G*}{kT}}$$ **Equation 3.32**

Primary Heterogeneous Nucleation

Process liquors, unless specially cleaned, contains vast amounts of insoluble particles. Heterogeneous nucleation is therefore found more frequently than homogeneous nucleation (Söhnel & Garside, 1992). The particles are seen as having a catalytic effect on the formation of the solid phase by reducing the critical amount of free energy. This reduction is taken into account by the introduction of the wetting angle, Θ, as a measure of the wetting characteristics of the particles. The critical free energy for heterogeneous nucleation, ΔG^*_{hetero}, is calculated as follows:

$$\Delta G^*_{hetero} = \Delta G^*_{homo} f(\Theta)$$ **Equation 3.33**

Where:

$$0 \le f(\Theta) \le 1 \text{ for } 0° \le \Theta \le 180°.$$

Although the wetting angle has no physical meaning for the formation of the precipitate, it can be interpreted as follows. If the liquid does not wet the solid phase, the wetting angle would be 180° and $f(\Theta)$ would be 1. The critical free energy would therefore be the same as for homogeneous nucleation and would not be influenced by foreign particles. If, however, the wetting angle were less than 180°, $f(\Theta)$ would be less than 1 and the critical free energy for heterogeneous nucleation would be smaller

than homogeneous nucleation. The foreign particles would then act as nucleation catalysts.

The rate of heterogeneous nucleation is evaluated using a similar expression to Equation 3.32:

$$J_{hetero} = \Omega_{hetero} e^{-\frac{\Delta G^*_{hetero}}{kT}} \qquad \textbf{Equation 3.34}$$

The pre-exponential term, Ω_{hetero}, would be smaller than for homogeneous nucleation as would the exponential term. The influence of this is seen in Figure 3.5 where the different nucleation mechanism are compared as a function of supersaturation. It is seen that the rate of heterogeneous nucleation exceeds that of homogeneous nucleation. The gradient of the rate of homogeneous nucleation is greater then that of heterogeneous nucleation and provided a sufficiently high supersaturation, it would exceed the rate of heterogeneous nucleation. Shown also on the figure is the rate of secondary nucleation, B_0. This would be described next.

Secondary Nucleation

Secondary nucleation was already defined as nucleation dependent on the prior presence of crystals of the same material. The definition might be ambiguous if considered as such, but it is so defined to encompass a large number of different types of secondary nucleation. The definition only becomes clear when looking at these different types of secondary nucleation from the list provided by Van Rosmalen et al. (2001):

- *Initial breeding*, also known as *dust breeding*, occurs when seed crystals are introduced into a crystalliser. A small fraction of the crystals tend to break during the dry handling of the seed crystals and become suspended in the solution as new nuclei.
- *Dendrite breeding* occurs at extreme high supersaturations allowing dendrites to be formed along the edges of the crystals. At such high supersaturations

surface roughening can also occur that may lead to *needle breeding*. These crystals break off and act as secondary nuclei.

- *Attrition breeding* results from the collisions of the crystals with the impeller blades or vessel walls. It can also result from the collisions between the crystals resulting in the formation of secondary nuclei. Attrition breeding is considered to be the most important source of secondary nuclei in a reactor.
- *Fluid sheer breeding* occurs when the shear forces exerted on a crystal by the fluid exceeds the yield stress of the crystal, resulting in its fragmentation. Rather high shear forces are needed for this type of secondary nucleation and is therefore considered of less importance.

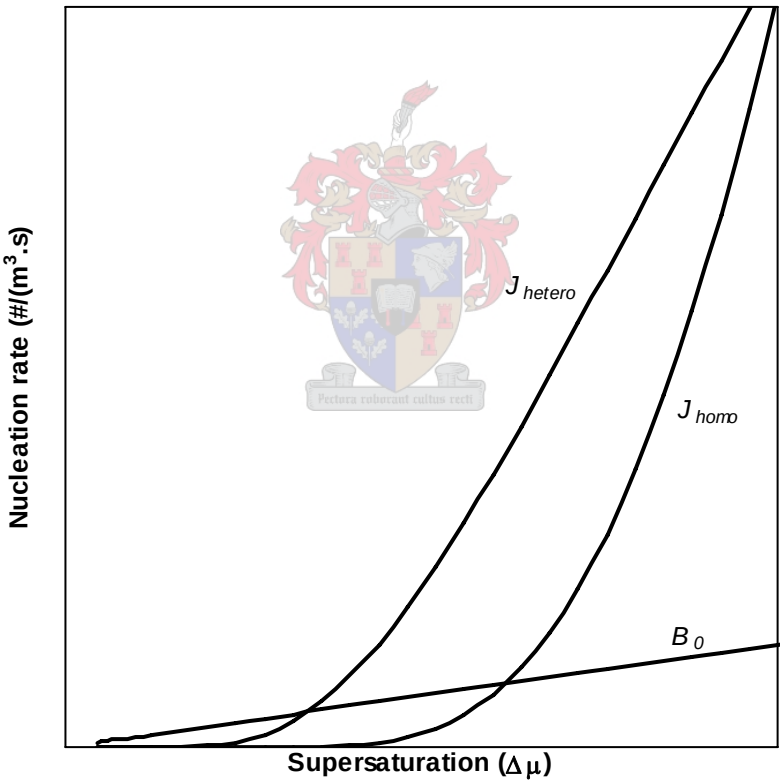

Figure 3.5 Comparisons between different nucleation mechanisms as a function of super-saturation (Van Rosmalen et al., 1992).

The rate of attrition breeding, being the most regular mechanism of secondary nucleation, is modelled empirically with the power law:

$$B_0 = k_N^1 \sigma^l \varepsilon^m M_T^n$$ **Equation 3.35**

Where:

B_0 : secondary nucleation rate, #/(m^3.s),

k_N^1 : constant dependent on reactor geometry,

ε : power input from impeller,

M_T : crystal mass of slurry.

Values often encountered for the *l*, *m* and *n* are $1 < l < 3$; $0.6 < m < 0.7$ and $n = 1$ or 2.

Söhnel and Garside (1992) is of the opinion that although secondary nucleation is of great importance to crystallisation of readily soluble compounds and to a lesser extent to intermediate soluble compounds, it does not occur, or only to a small extent, during the precipitation of sparingly soluble compounds. The reason provided is that the particles formed during precipitation is too small for the secondary nucleation mechanisms, and the number of secondary nuclei that does form, is overshadowed by primary nucleation. Nevertheless it does form part of precipitation theory and may be used to explain some of the phenomena encountered in precipitation. A method for identifying secondary nucleation in *mixed suspension mixed product removal* (MSMPR) precipitator is to study a plot of ln(n(L)) versus crystal length L, as shown in Figure 3.6. Secondary nucleation as a result of attrition breeding is marked by an increase in the number of smaller particles at the cost of the large particles.

Induction Period

The final topic that needs to be discussed with regard to the nucleation is the induction period. It is defined as the time-lapse between the establishment of supersaturation to the first change in the systems physical properties due to the formation of the precipitate. The value of the induction time would vary depending on the specific physical property that was observed in its determination. The induction period can be determined visual by the first appearances of crystals, an increase in the turbidity, a decrease in concentration or a change in conductivity. For all of these different methods the following equation can be applied:

$$t_{ind} = t_i + t_g$$ **Equation 3.36**

The induction period consist of the time required to form the critical nucleus, t_i, and the time required for the critical nucleus to grow to a size that it may be detected, t_g. For instances where $t_i >> t_g$ it can be shown (Söhnel & Garside, 1992):

$$t_{ind} = \frac{1}{J}$$ **Equation 3.37**

In this equation, 1 has the dimensions of reciprocal volume corresponding to the volume units used for J. For this instance the induction time can be used to estimate nucleation rates as seen from Equation 3.37.

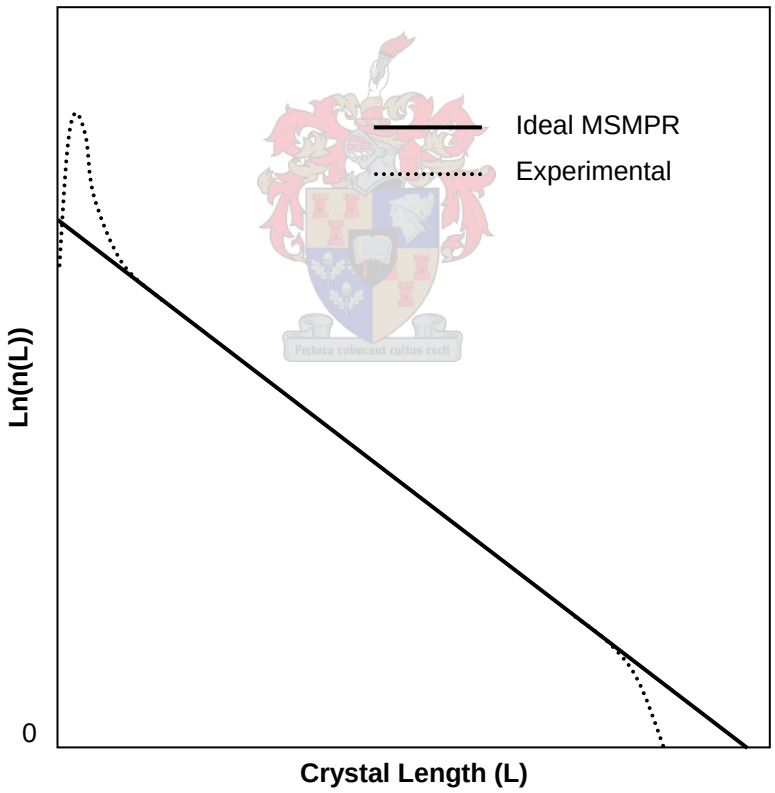

Figure 3.6, Deviation of the experimental line from an ideal MSMPR precipitator as a result of secondary nucleation.

3.1.4 Crystal Growth

After the formation of the nucleus, new growth units are incorporated into the crystal lattice for it to grow in size. The growth tends to obey the crystallographic system specific for the compound. For these systems the growth rate can be defined as the rate of displacement of the crystallographic face in the direction perpendicular to the face. This rate would vary for the different faces and can be measured if the crystal is sufficiently large enough to be observed. The crystals normally produced during precipitation are too small to be observed for the visual measurement of the growth rate and must rely on the perceived flux based on concentration measurements. For these crystals an overall linear growth rate, $\dot{r}$, is defined by Equation 3.38 where r is half the size of the crystal (Van Rosmalen et al., 2001). More often it is found that the size of the crystals are defined in terms of a sphere having the same volume as the crystal and r would therefore be the radius.

$$\frac{1}{A}\frac{dm}{dt} = \frac{\rho k_v}{k_a L^2}\frac{dL^3}{dt} = 6\frac{k_v}{k_a}\rho\dot{r} \qquad \textbf{Equation 3.38}$$

Two consecutive processes control crystal growth, the first being the mass transfer from the bulk solution to the crystal surface, followed by the process of integration of material into the crystal lattice. Any of these two processes can be limiting and would therefore determine the rate of crystal growth. In some instances the rate of the two processes may be comparable and both would contribute to the rate of crystal growth. Different mechanisms have been experimentally observed and will be discussed in this section.

Diffusion Controlled Growth

Around each crystal a boundary layer is established through which the growth units must be transported to be incorporated into the crystal lattice. For instances where diffusion is the rate-limiting step, the concentration close to the adsorption boundary would be equal to the equilibrium concentration determined by the solubility. The driving force for diffusion across the boundary layer would therefore be the difference between the bulk and the equilibrium concentration, c - c_{eq}. Fick's law can be used to

describe the rate of mass transfer across the boundary layer. The increase in the mass of a crystal equals:

$$\frac{dm}{dt} = k_D A_T \left(c - c_{eq}\right) \qquad \textbf{Equation 3.39}$$

The mass transfer coefficient, k_D, is related to the diffusion coefficient, D, and the boundary thickness, δ, by:

$$k_D = \frac{D}{\delta} \qquad \textbf{Equation 3.40}$$

Using Equation 3.38 the rate equation can be transformed into the overall linear growth rate equation:

$$\dot{r}_D = \frac{k_a k_D}{6 k_v \rho}\left(c - c_{eq}\right) \qquad \textbf{Equation 3.41}$$

Or:

$$\dot{r}_D = \frac{k_a k_D}{6 k_v \rho} c_{eq}\left(S_c - 1\right) \qquad \textbf{Equation 3.42}$$

For electrolyte systems the growth rate equation becomes more complicated since the transfer of both the cation and anion must be taken into account. This is also true for systems where the average distance between the crystals is less than 20 particle diameters. For these situations the reader is referred to Söhnel and Garside (1992) for more information regarding the form of the correlation and the conditions it applies to.

Surface Integration: Two-Dimensional Nucleation Mechanism

Surface integration follows the mass transport of the crystallising material and involves a number of steps for the incorporation of the growth units into the lattice. The first step involves the adsorption of the growth units onto the crystal surface during which part of the growth unit's solvation shell is released. From this point the growth unit can either desorb again or it can diffuse in the adsorption layer to specific

points where in may be incorporated into the crystal lattice. Before it is incorporated it looses the rest of its solvation shell. These specific points at which the growth units are incorporated in is referred to as *kink* sites and occurs along the growth steps. A growth step is the step formed by the boundary of the new growth layer on the crystal surface.

Different mechanism exist for surface integration with respect to how the growth layer is initially formed. The process of adsorption and diffusion in the adsorption layer is dynamic involving more than one growth unit. These growth units collide to form two-dimensional nucleuses and as for their three-dimensional counterparts, there exists a critical 2-D nucleus size that must be overcome for the nucleus to be stable. If the 2-D nucleus were stable it would provide the kink sites for the new crystal layer to grow. Thereby a new crystal layer with a thickness of one growth unit is formed. If the 2-D nucleus grows to form a complete new crystal layer before the next 2-D nucleus is formed on top of it, the growth is described as *mononuclear*. The mechanism of mononuclear growth is rarely observed and only on very small crystals or for very low 2-D nucleation rates. The formation of more than one 2-D nucleuses with some of the nucleuses forming on top of each other is more often observed. This mechanism is referred to as *polynuclear* growth and is illustrated in Figure 3.7.

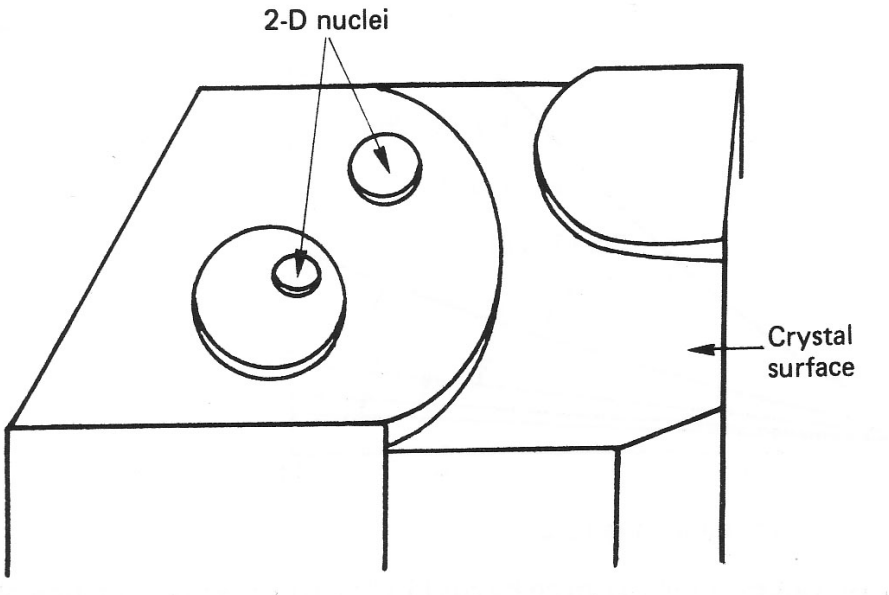

Figure 3.7 Crystal growth by polynuclear mechanism (Söhnel & Garside, 1992).

For the polynuclear mechanism the following growth rate equation has been deduced (Söhnel & Garside, 1992):

$$\dot{r}_P = k_P f(S) \exp\left(-\frac{\beta \gamma^2 V_m^{4/3}}{3(kT)^2 \nu \ln S} \right) \qquad \textbf{Equation 3.43}$$

Where

k_P : Pre-exponential constant,

β : Shape factor for relating the perimeter shape factor with the area shape factor,

$f(S)$: Predefined function of supersaturation.

All of the constants in the equation are related to physical parameters of the system and the reader may again refer to Söhnel and Garside (1992) for the meaning of each and how to calculate them. When fitting experimental data to the equation it would be easier to work with the equation in the following form (Nielsen & Toft, 1984):

$$\dot{r}_P = k_P f(S) \exp\left(-\frac{K_p}{\ln S} \right) \qquad \textbf{Equation 3.44}$$

The suggested form of the function $f(S)$ is (Nielsen, 1984):

$$f(S) = S^{7/6} (S-1)^{2/3} (\ln S)^{1/6} \qquad \textbf{Equation 3.45}$$

Many variations have been proposed for this equation, which only differs in the power to which the first term is raised. According to Møller and Madsen (1984) the form of $f(S)$ provided in Equation 3.45 is the most appropriate.

Surface Integration: Screw Dislocation Mechanism

At low supersaturations, where 2-D nucleation does not yet occur, the growth units are dependent on crystal defects such as screw dislocations to provide the kink sites for growth. A screw dislocation as shown in Figure 3.8, is formed during the normal

growth of a crystal and would remain even after a new crystal layer has grown on top of it. It would therefore, continue to provide new kink sites for the next layers and it is expected to develop as a spiral that rotates about its axis during growth.

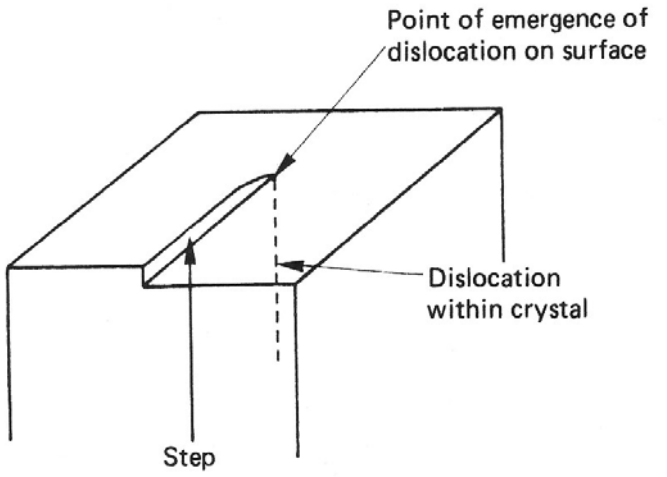

Figure 3.8 Screw dislocation as a source of kink sites for growth (Söhnel & Garside, 1992).

The growth rate equation for the screw dislocation takes on the following form:

$$\dot{r}_S = C_s\left((S-1)^2/B_S\right)\tanh\left(B_S/(S-1)\right) \qquad \textbf{Equation 3.46}$$

The *screw dislocation mechanism* is also referred to as the *BCF mechanism* after the three authors, Burton, Cabrera and Frank, who first provided the theoretical treatment of screw dislocations. The two constants, C_S and B_S, are dependent on the system parameters and can both be calculated theoretically (Söhnel & Garside, 1992). Of more interest are the two limiting conditions to which the rate equation reduces. For high supersaturation ratios $B_S/(S-1) << 1$ and therefore $\tanh\left(B_S/(S-1)\right) \approx B_S/(S-1)$. Equation 3.46 reduces to:

$$\dot{r}_S = C_S(S-1) \qquad \text{(high supersaturation ratios)} \qquad \textbf{Equation 3.47}$$

On the other side, for low supersaturation ratios $B_S/(S-1) >> 1$ and therefore $\tanh(B_S/(S-1)) \approx 1$. For this instance Equation 3.46 reduces to:

$$\dot{r}_S = C_S(S-1)^2/B_S \quad \text{(Low supersaturation ratios)} \qquad \textbf{Equation 3.48}$$

Using the two limiting conditions the rate equation reduces to two equations that can easily be applied to experimental data. Especially the latter equation (Equation 3.48) has found many applications in describing the growth rate of different crystallising compounds. The two constants in the equation are lumped together for easier treatment and the resulting equation, Equation 3.49, is referred to as the *parabolic growth law*. According to Söhnel and Garside (1992) the parabolic rate law is valid for supersaturation ratios less or equal to 20.

$$\dot{r}_S = k_S(S-1)^2 \qquad \textbf{Equation 3.49}$$

Surface Integration: Rough Growth

The last surface integration method to be discussed is *rough growth*. This occurs at "too high" supersaturations where the size of the critical nucleus is in the order of one growth unit. The growth units arriving at the crystal surface can attach to any random site without the need to diffuse to the kink sites. The growth is unordered and the resulting crystal surface is described as rough on a molecular scale. The rate of growth depends on difference between the flux of new growth units reaching the crystal surface and the flux of growth units leaving the surface. It can therefore be shown that the rate of growth is linearly dependant on supersaturation (Van Rosmalen et al., 2001):

$$\dot{r}_R = k_R(S-1) \qquad \textbf{Equation 3.50}$$

The above is based on a discussion provided by Van Rosmalen et al. (2001). Söhnel and Garside (1992) briefly mention it, but they do not acknowledge it as an independent integration mechanism. It appears that they interpret instances of this mechanism as an embodiment of mass transport controlled growth.

Application of Growth Rate Equations

A number of crystal growth mechanism have been discussed thus far and any of these can be the rate limiting step during crystal growth. Surface integration mechanisms are normally the rate limiting step at low supersaturation levels. It is possible for the different integration mechanisms to proceed in parallel, resulting in the mechanism with the fastest rate to be dominating. As seen from Figure 3.9, screw dislocation is the initial rate controlling mechanism and is thereafter exceeded by polynuclear growth. The rates of the surface integration mechanisms continue to increase until the rate of integration starts to equal the rate of mass transfer. The rate of integration cannot exceed the rate of mass transfer since the two steps occur in series. From this point onward the growth rate is limited by diffusion. Although it is not clear from literature reviewed, this also appears to be the region where the surface integration mechanism switches to rough growth.

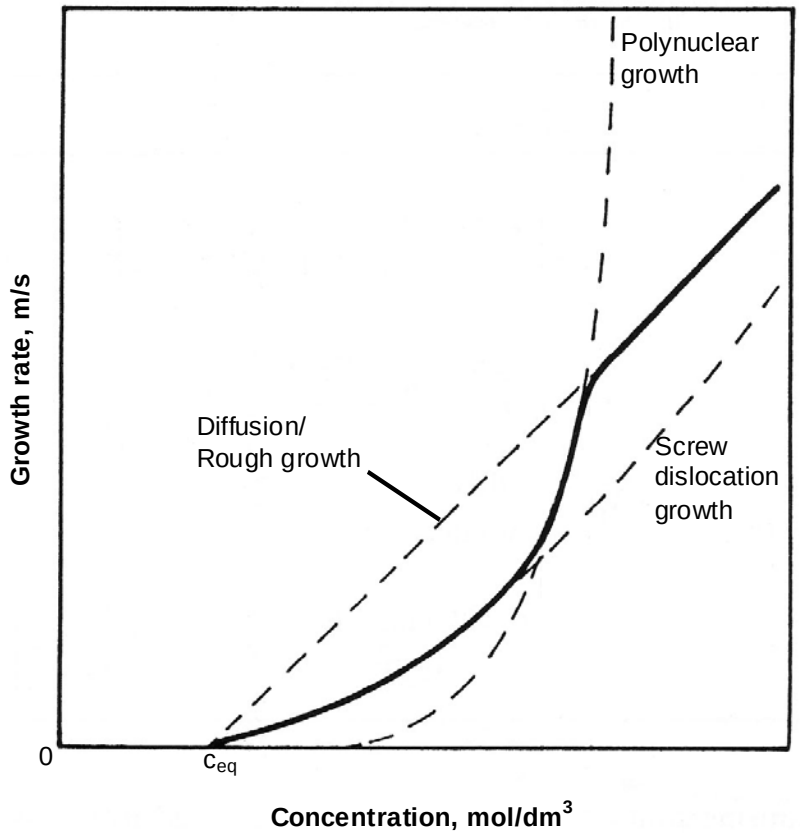

Figure 3.9 Growth rate of a crystal with increasing supersaturation (Söhnel & Garside, 1992).

It should be clear for a constant temperature, that the growth rate of the crystals is only dependent on the supersaturation ratio. For engineering calculations the growth rate expressions can be simplified to:

$$\dot{r} = k_G (S-1)^g \qquad \textbf{Equation 3.51}$$

With

$g = 1$: Rough growth or diffusion controlled growth,

$g = 2$: Screw dislocation growth,

$g > 2$: Polynuclear growth.

This function can easily be fitted to experimental data and the value of the exponent, g, would give an indication of the controlling mechanism. Equation 3.51 can be used for rough growth, diffusion controlled growth and screw dislocation growth, and to a limited extend for polynuclear growth.

3.1.5 Kinetics for a MSMPR Precipitation Reactor

Nucleation and crystal growth has been treated as two independent processes in previous two sections. In any precipitation reactor these two processes occur concurrently and it is the aim of this section to combine the two processes for the interpretation of the particle size distributions.

The discussion will be limited to continuously operated precipitation reactors. The ideal continuous precipitation reactor is known as the *mixed suspension mixed product removal* (MSMPR) reactor and is based on many of the same assumptions as for the *continuous stirred tank reactor* (CSTR). For the ideal reactor the following assumptions are made:

- The reactor operates at steady state,
- The reactor is perfectly mixed,
- The composition of the suspension leaving the reactor is the same as any point within the reactor volume.

The treatment will be further limited to only primary nucleation and crystal growth. Secondary processes such as secondary nucleation and aggregation will be ignored. It will also be assumed that the growth of the particles are size independent and therefore follows McCabe's ΔL law. A schematic representation of an MSMPR reactor is given in Figure 3.10. Since the reactor is operated at steady state it would imply that the concentrations within the reactor stays constant and therefore also the rate of nucleation and the rate of crystal growth.

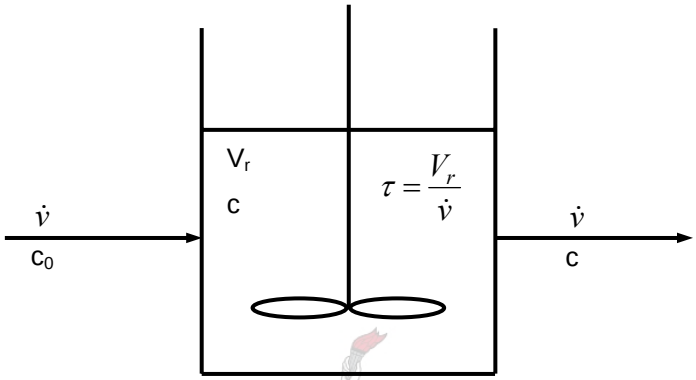

Figure 3.10 Schematic of an MSMPR precipitation reactor with a volume V_r and a volumetric feedrate $\dot{v}$.

Based on the above-mentioned assumptions the number density distribution of an MSMPR precipitation reactor can shown to be (Söhnel & Garside, 1992):

$$n(L) = \frac{J}{2\dot{r}} \exp\left(-\frac{r}{2\dot{r}\tau}\right) \qquad \textbf{Equation 3.52}$$

Or:

$$\ln n(L) = -\frac{1}{2\dot{r}\tau} r + \ln\left(\frac{J}{2\dot{r}}\right) \qquad \textbf{Equation 3.53}$$

In order to evaluate experimental size distribution results for an MSMPR precipitation reactor it would be easier to use Equation 3.53. A plot of ln *n(r)* versus particle radius should yield a straight line as indicated in Figure 3.11 with the gradient of $-1/\dot{r}\tau$ and an intercept of $\ln(J/\dot{r})$ on the ordinate. The nucleation rate and the crystal growth rate can therefore be determined. It should be kept in mind when applying Equation 3.53 that the particle size distribution measured is of the particle diameter, thus 2*r*.

Deviations that can be expected for the MSMPR plot would be the result of secondary nucleation, agglomeration, *size dependent growth* or *growth rate dispersion*. Size dependent growth is a phenomenon whereby the growth rate of the crystal particles is dependent on its size. Growth rate dispersion is where the crystals in the population grow at different constant rates.

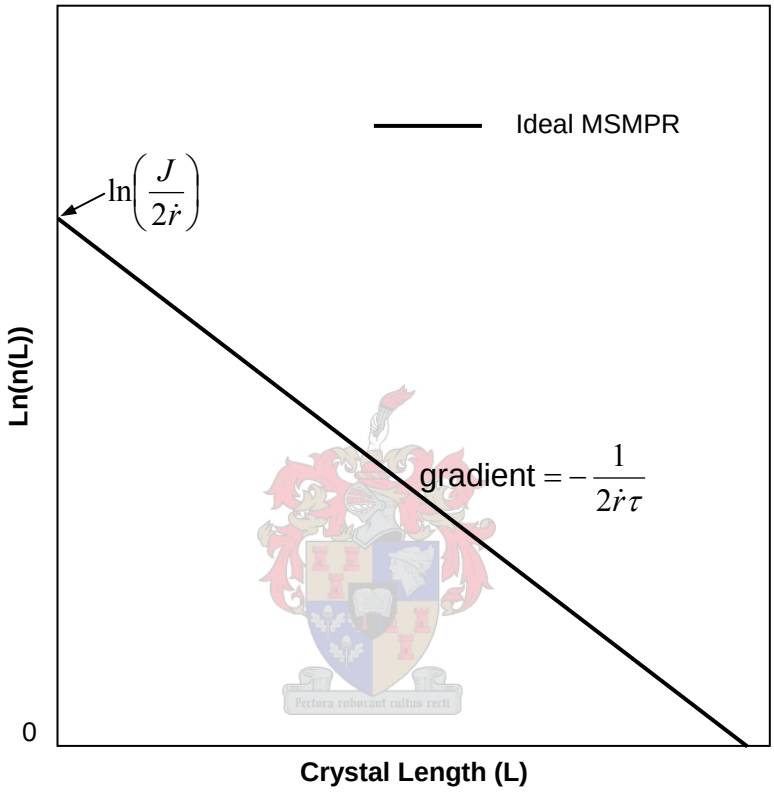

Figure 3.11 Size distribution for a theoretical MSMPR precipitation reactor.

The effect of secondary nucleation as a result of attrition has already been indicated in Figure 3.6. The number density of the particles would drop where the size of the particles become susceptible to attrition. This would result in an increase in the number density of the small particle (Van Rosmalen et al., 2001). Upward curvature in the range of the small particles could be expected if the crystal growth is size dependent with the smaller crystals growing slower.

The changes in the MSMPR plot can be very subtle and hard to detect. Van Peborgh Gooch et al. (1996) provides a discussion on how to discriminate between the

different mechanisms responsible for the form of the MSMPR plot. They developed a system whereby agglomeration, size dependent growth and growth rate desperation could be identified through an experimental investigation. When analysing experimental data it would be best to interpret the growth rate as the overall growth rate that incorporates all the size enlargement mechanisms such as crystal growth and agglomeration.

3.1.6 Secondary Processes

Precipitation is a dynamic process for which a number of secondary processes exists. These processes influence the physical and chemical properties of the precipitate formed. One of the following processes can occur while the precipitate is still in contact with the mother liquor:

- Recrystallisation,
- Ostwald ripening,
- Ageing,
- Aggregation,
- Agglometation,
- Coagulation.

Recrystallisation

This is the process whereby the size and sometimes the shape of the crystals changes through the mechanism of surface integration and mass transfer through the solution. The recrystallisation can be affected by a change in temperature or concentration. A special condition of recrystallisation is *Ostwald ripening*. This occurs at constant temperature and concentration. The Gibbs energy of the system is related to the surface area of the precipitate particles and the system would strive to minimise it by minimising the surface area. The smaller particles would therefore redissolve to allow the larger particles to grow and decrease the surface area. A shift to a larger mean particle size is observed as the result of this process. Recrystallisation is seen as a relatively quick process.

Ageing

Ageing is termed as the process in which the contact of the precipitate with the mother liquor leads to a change in the chemical and physical properties of the precipitate. It is found that non-equilibrium particle shapes such as dendrites and needles would recrystallise into more compact shapes. Where polymorphism exists, the meta-stable polymorph would transform into the more stable form, and an amorphous phase would transform into a crystalline phase. The rate of these processes is relatively slow and depends on the precipitation conditions.

Aggregation, Agglomeration, Coagulation

Aggregation is the process whereby smaller particles cluster together and may be bonded, to form a larger particle. This results in a decrease in the total number of individual particles. Aggregation can be subdivided into *agglomeration* and *coagulation*. The definition of aggregation, agglomeration and coagulation differs from literature sources and hence for this study the definitions would be used as set out by Söhnel and Garside (1992). Agglomeration is the clustering of particles to form strong secondary particles held together primarily by crystalline bridges formed between the particles and sometimes by physical forces. Coagulation is classified as a special case of agglomeration occurring at very small particle sizes (in the nanometer particle size range) where physical forces solely holds the particles together. In precipitation the process of agglomeration is considered the most important since it forms large particles that are relatively strongly bonded, whereas aggregates can consist of loosely bounded agglomerates and coalesced particles that can be broken down.

Van Rosmalen et al. (2001) distinguish four sub-processes during the formation of agglomerates:

1. Transport and collision,
2. Interaction between forces,
3. Disrupture and
4. Cementing.

For the initial cluster to form, the particles need to be brought into close approximation of each other. This is dependent on the transport and the collision of the particles. There are distinguished between three mechanisms through which this occurs. The first is the collision of particles owing to the Brownian motion and is called the *perikinetic collision mechanism*. This mechanism is dominant for small particles of a size less than 0.5 μm. For larger particles, movement is forced by the flow regime and is known as the *orthokinetic collision mechanism*. This mechanism is dominant for particles smaller than $6\lambda_k$, where λ_k is the *Kolmogoroff length scale of turbulence* as defined by Equation 3.54. The Kolmogoroff length scale is normally of the order of a few tenths of micrometers in a stirred tank (Söhnel & Garside, 1992). The final mechanism of importance is *inertial collision mechanism* dominant for particles larger than $25\lambda_k$. Gravitational and inertial forces influence the motion of these particles.

$$\lambda_K = \left(\frac{\eta^3}{\bar{\varepsilon}} \right)^{\frac{1}{4}}$$ **Equation 3.54**

Where:

η : Kinematic viscosity,

$\bar{\varepsilon}$: Mean energy dissipation.

For each of these mechanisms a frequency of collisions could be associated (Van Rosmalen et al., 2001). The higher this frequency, the higher the likelihood of particles coming close enough to each other to form a cluster. The frequency of collisions is dependent on the size of both the particles colliding. The collision frequency of both the orthokinetic and the inertial mechanism is directly related to the square root of the *mean energy dissipation* ($\sim\sqrt{\bar{\varepsilon}}$) in the solution. Therefore, the higher the intensity of mixing, the higher the likelihood of agglomerates forming.

The different collision mechanisms would bring the particles close together for the inter-particle forces to become decisive. Around each particle a so-called electrical double layer is formed as the result of the selective adsorption of ions onto the surface

of the particle. This results in the build up of a charged layer surrounding the particles that would repel each other. The charge of the outer layer surrounding the particle is measured in terms of the zeta potential. The strength and sign of this charge is dependent on the chemical conditions of the surrounding solution such as the ionic strength. The attractive forces between the particles such as the Van der Waals forces need to overcome the repulsive force of the double layer before a cluster can be formed.

Other than the inter-particle forces, there is also the external force imposed on the particle by the surrounding flow pattern. This force is similar to the forces that originally resulted in the collision of the particles and can disrupt the formed cluster. It is expected that this disruptive force is directly proportional to the mean energy dissipation rate ($\sim\bar{\varepsilon}$) for particles smaller than 10 λ_k and directly proportional to the square of the mean energy dissipation ($\sim\bar{\varepsilon}^2$) for particles larger than 25 λ_k. These disruptive forces would limit the size of the agglomerates to the size range of the Kolmogoroff length scale (Söhnel & Garside, 1992).

The final step in the formation of the agglomerates is the cementing of the particles. This step is directly related to the crystal growth rate at the corners and the spaces between the particles and can be the rate-limiting step in the overall agglomeration process. The supersaturation level would have a determining influence on the rate of cementation.

From the above it can be deduced that the main process variables that influences the four sub-processes and thereby the rate of agglomeration is:

- The energy dissipation,
- The supersaturation of the fluid phase,
- The number and size distribution of the particles.

3.1.7 Influence of Hydrodynamics and Mixing

A topic of particular interest to this study is the influence of hydrodynamics and mixing on the precipitation process. The link between mixing and the characteristics

of the formed precipitate is well established (Söhnel & Garside, 1992). The kinetics of both nucleation and crystal growth has been observed to be influenced by mixing. With increasing mixing intensity the induction period decreases, the number of crystals increases and in some cases the rate of crystal growth increases (Söhnel & Garside, 1992). The morphology of the crystals formed can also depend on the prevailing mixing conditions. An example of this is the calcium carbonate system for which Roques and Girou in 1974 (cited Söhnel & Garside, 1992) observed that calcite, vaterite and aragonite could be simultaneously formed, but at an increased stirring intensity only aragonite would form.

Söhnel and Garside (1992) made the following summary on the influence of mixing from a review of studies. The manner and the rate at which the reacting solutions are mixed influence the rate of precipitation, the average size of particles being formed and the width of the size distribution. The faster the mixing of the solutions the faster the precipitation rate, the smaller the mean particle size and the narrower the size distribution. Fitchett and Tarbell (1990) made an apparent contradictory conclusion from their studies on the precipitation of barium sulphate ($BaSO_4$) in an MSMPR precipitation reactor. From their results they observed that the mean particle size increases with increasing stirring speed (increasing mixing intensity). They concluded that turbulent diffusion limited the particle growth and that this can dominate the influence of micromixing. According to this an increase in mixing intensity would always increase the mean particle size.

Bałdyga (1999) does not agree that such a simple explanation exits for the influence of mixing on the mean particle size. From Pohorecki and Bałdyga's studies in 1983, 1988 and 1990 (cited Bałdyga 1999) of $BaSO_4$ precipitation, they also observed the increase in particle size with increasing mixing intensity in an MSMPR reactor. For batch precipitation they observed an opposing trend of a decrease in the mean particle size with increasing mixing intensity, and for semi-batch precipitation they observed a minimum in the curve of mean particle size against mixing intensity. They managed to explain the different trends using an engulfment micromixing model. It is Bałdyga's opinion that no simple intuitive rules exist with which the influence of mixing can be predicted.

Scales of Mixing

The influence of mixing on precipitation can be better understood if the progression of mixing is compared to the progression of the precipitation reaction. Villermaux and David in 1983 (cited Söhnel & Garside, 1992) divided the mixing of two liquids in three consecutive (sometimes parallel) stages:

1. The two liquids are dispersed into each other to achieve a uniform average composition. On a microscale, however, the mixture consist of entirely segregated parts of the two liquids and the local concentrations in the different segregated regions still corresponds to the concentrations of the non-mixed liquids.
2. The segregated regions of uniform composition spread resulting in the contact area between the two liquids increasing.
3. Mixing by molecular diffusion occurs across the boundaries of the segregated liquids, resulting in the segregated regions disappearing and the mixture attaining homogeneity on a molecular level.

The first stage represents *macromixing* whereas the latter two represents *micromixing*. Bałdyga and Pohorecki (1995) recognises a third scale of mixing known as *mesomixing*, which fits in between macromixing and micromixing. Mesomixing reflects the coarse-scale turbulent exchange between the fresh feed and its surroundings.

Marcomixing is the dispersion of the segregated liquids throughout the reactor volume and is achieved through the pumping action of the impeller (Figure 3.12(a)). Macromixing reduces the scale of the size of the segregated liquid volumes from the order of the reactor vessel diameter to the Kolmogoroff length scale, λ_k (Söhnel & Garside, 1992). Macromixing would determine the local conditions under which meso- and micromixing would proceed. The characteristic time of macromixing, τ_C, is the volume of the reactor divided by the volumetric pumping capacity of the impeller. It can be loosely defined as the time required for the liquid to circulate once through the reactor volume.

During the feeding of fresh reagent, a volume of liquid will be formed around the feed inlets having concentrations higher than the bulk concentration. Fast chemical reactions would be localised in this volume. The volume around the feed inlet would evolve into a plume shape as a result of the radial dispersion of the feed (Figure 3.12(b)). The dispersion is dependent on the process of turbulent diffusion and inertial-convective disintegration of large eddies (Bałdyga & Pohorecki, 1995). For mesomixing, two mixing times can be calculated, one for the turbulent diffusion process, τ_D, and one for the inertial-convective disintegration process, τ_S.

Micromixing is the last step in the progression of mixing and can take place trough two mechanisms: laminar stretching of the segregated regions, and their turbulent erosion (Söhnel & Garside, 1992). With laminar stretching, the contact area between the segregated liquids increases, while the volume of the individual segregated liquids stays constant. This results in the formation of thin lamellas of the segregated liquids. In turbulent erosion, turbulent forces within the liquids and mass transfer between the different regions reduce the volumes of the segregated liquids. The final step in micromixing is laminar convection and molecular diffusion over length scales smaller than the Kolmogoroff length scale, λ_k. The final step becomes rapid at the scales of the order of the Batchelor concentration microscale, λ_B (Equation 3.55). Typical values for λ_k and λ_B in an aqueous liquid are 30μm and 1μm, respectively. Micromixing is represented in Figure 3.12(c).

$$\lambda_B = \lambda_K Sc^{-1/2} \qquad \textbf{Equation 3.55}$$

According to Bałdyga (1999) the limiting step in micromixing that needs to be considered during precipitation is the turbulent erosions mechanism, called by him the micromixing by engulfment. For this mechanism a mixing time, τ_E, could be estimated which would represent the micromixing time. The micromixing time is inversely proportional to the square root of the local energy dissipation.

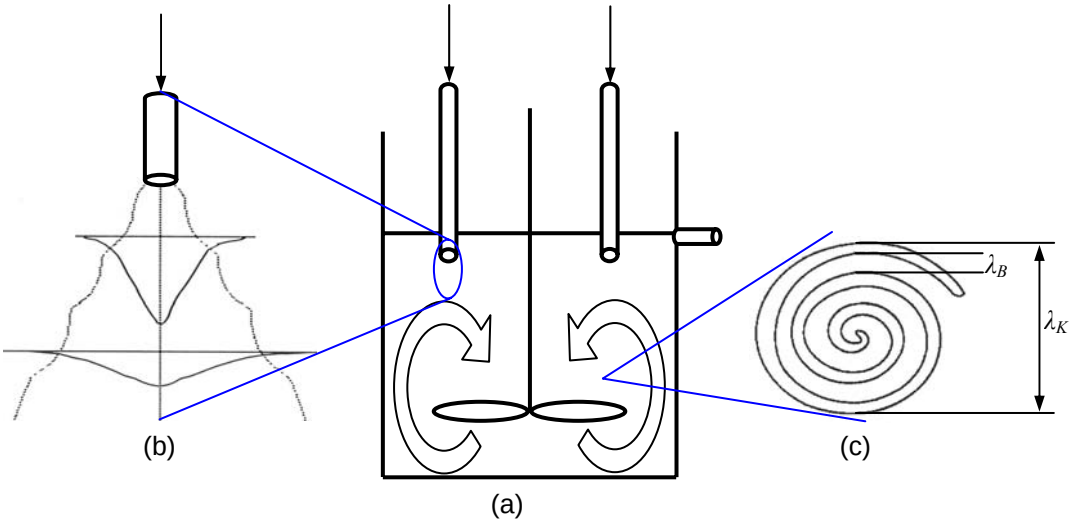

Figure 3.12 Diagrammatically representation of an MSMPR with macromixing (a), mesomixing (b), and micromixing (c) indicated (adapted from Van Rosmalen et al., 2001).

The reactants are first brought into contact with each other through mixing followed by the chemical reaction to form the precipitate compound. After the compound has been formed the processes of nucleation and crystal growth can proceed to produce the precipitate particles.

For each of the above mentioned steps a characteristic time could be estimated where τ_R is the time for the chemical reaction; τ_N, the time for nucleation and τ_{Gcr} the time for crystal growth. The reader may refer to Bałdyga (1999) on how to estimate these characteristic times. A comparison between the characteristic times for the precipitation reaction with the mixing times would give an indication of the possible influence of mixing. Bałdyga (1999) carried out this comparison and his results are summarised in Figure 3.13.

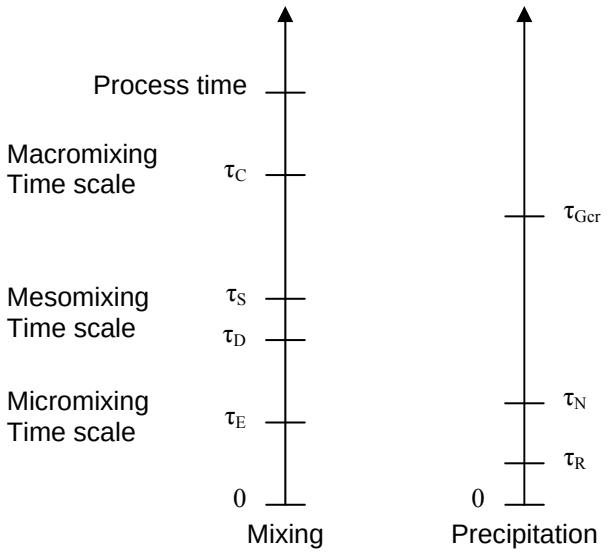

Figure 3.13, Comparison of characteristic times of mixing and precipitation (Baldyga, 1999).

Chemical reaction, nucleation and crystal growth are all molecular-level processes and can therefore only be directly influenced by mixing on a molecular scale. The characteristic precipitation times therefore need to be compared to the micromixing time to see if their rates would be limited. The chemical reaction has the smallest time and is considered instantaneous. It would be limited by micromixing since its characteristic time, τ_R, is smaller than the micromixing time, τ_E. As for nucleation, $\tau_N \approx \tau_E$ and the influence would depend on the local micromixing. For a high local energy dissipation the micromixing would be more intense and τ_E would become shorter. Nucleation will then not be limited by micromixing and would proceed at the rate as determined by the local supersaturation. For a lower local energy dissipation, τ_E would become longer and micromixing would limit the nucleation rate. The nucleation rate would then be slower than that determined by the local supersaturation. The characteristic time for crystal growth, τ_{Gcr}, is much longer than τ_E and would therefore not be limited by micromixing. It would proceed at the rate as determined by the local supersaturation.

The fact that only micromixing can directly influence the rates of the precipitation reactions is not to say that macro- and mesomixing has no influence on it. The macro and meso mixing times are longer than the characteristic nucleation time. If any spatial variations exist, the nucleation rate is fast enough to proceed at a rate according to the local supersaturation. Macro- and mesomixing would determine the

local supersaturation and thereby influence the rates. This effect is better illustrated in Figure 3.14 based on a discussion provided by Gösele and Kind (1991).

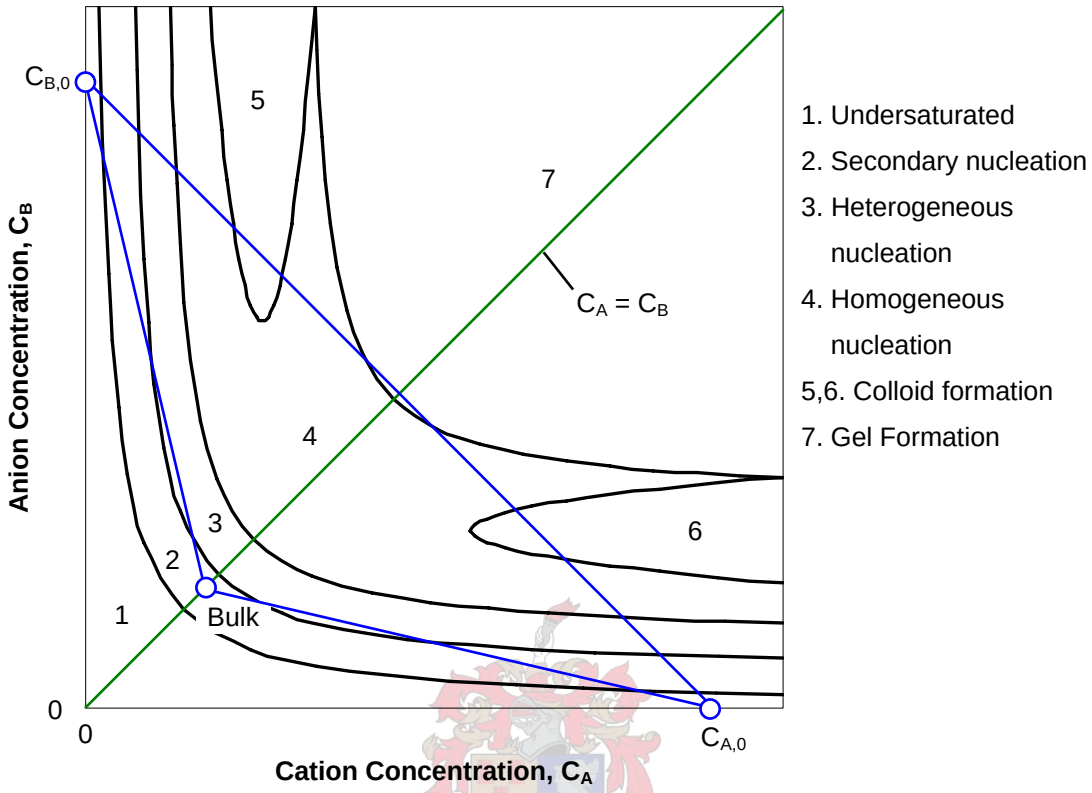

Figure 3.14 Different nucleation regions as a function of anion and cation concentration (Gösele & Kind, 1991).

Indicated in Figure 3.14 is the different nucleation region as a function of the cation and anion concentrations. The diagram was constructed for an ideal system where the solubility line is a hyperbole according to the solubility product. The regions numbered from 1 to 7 are the different nucleation mechanisms. Included are regions 5 and 6 where colloids are formed and region 7 where gels are formed. Colloids are unwanted since they are very small particles with electrical charged surfaces that are difficult to remove from the solution and gels are unwanted since they form an amorphous structure that captures large volumes of the mother liquor within it. Gels are also very difficult to separate and have a high filtration resistance. As shown in the introduction, the formation of gels and colloids are very probable for calcium and magnesium fluorides.

This discussion would be based on the hypothetical reaction of a cation, A^+, and an anion, B^-, which react to form the precipitate, AB, as indicated in Equation 3.56.

$$A^+ + B^- \rightarrow AB\downarrow \qquad \textbf{Equation 3.56}$$

Line $C_A = C_B$ is the stoichiometric line at which the reactants are at a ratio of 1:1. Line $C_{A,0} - C_{B,0}$ represents the mixing line between volumes of liquid from the two reactant inlets. Lines $C_{A,0}$ – "Bulk" and $C_{B,0}$ – "Bulk" represents the mixing lines of the liquids from the two respective reactants inlets with the reactor's bulk liquid. The concentrations formed between the mixing of two liquids can be anywhere along the mixing line depending on the volume ratio. For the case of the MSMPR where three liquids are mixed (two reactant liquids and the bulk liquid), the resulting concentrations can be anywhere with in the triangle $C_{A,0} - C_{B,0}$ – "Bulk". It is therefore possible that there exists spatial variations within the reactor for which the concentration would be within regions of unwanted nucleation mechanisms. The existence of these volumes would depend on the macro- and mesomixing conditions and the reactor configuration. The rate of nucleation is fast enough to react according to the local conditions.

It is therefore seen that micromixing can directly influence the rate of precipitation reaction, whereas macro- and mesomixing can indirectly influence the rate by determining the local supersaturations.

The Scale-up Predicament

A problem common to any system that is sensitive to mixing is scaling it up. It is highly unlikely that the same hydrodynamic conditions would prevail in a large-scale reactor as on a laboratory scale, even if it were geometrically scaled-up. The simple reason for this is illustrated in Figure 3.15. The mixing system is based on the Rushton geometry. Indicated on the x-axes is the diameter of a stirrer and on the left y-axes the rotation speed. Indicated on the right y-axes is the macromixing time, which is inversely proportional to the rotation speed. Plotted on the diagram are the contours for constant average energy dissipation, which for the argument would result in a constant micromixing time.

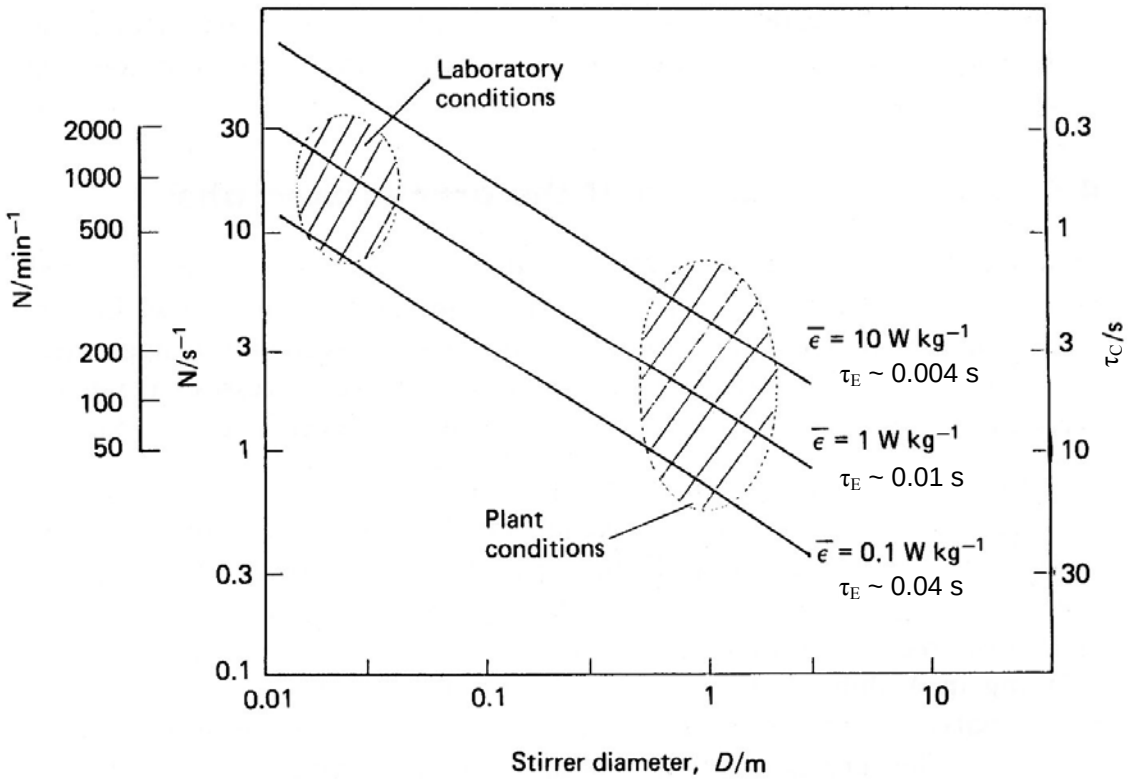

Figure 3.15 Variation of the macromixing time, τ_C, and the micromixing time, τ_E, in the Rushton geometry stirred tank (Söhnel & Garside, 1992).

For the laboratory conditions stirrers with small diameters at high rotation speed are used. The rotation speed has to decrease when scaling-up at constant energy dissipation (constant micromixing, τ_E). This decrease in rotation speed would result in an increase in the macromixing time in the order of magnitude. Scaling-up at constant macromixing time would result in the average energy dissipation increasing drastically. This would reduce the macromixing time, but at the cost of a high energy consumption which might not be feasible. It is therefore impossible to scale-up a reactor geometrically while still keeping the macro and micro mixing times constant. A study of the individual influences of the different scales of mixing is therefore required before a reactor can be scaled-up with any certainty.

Three-zone Experiment

There are no simple rules for scaling-up. The mixing conditions on laboratory scale and plant scale will differ extensively and can influence the quality of the precipitate produced. A method is therefore required to evaluate the effect of the different scales

of mixing on a small scale. This would allow better judgement for the large-scale reactor equipment and layout, to control the different scales of mixing.

One approach often taken is to model reactor configurations using *Computational Fluid Dynamics*, CFD. This involves building a computer model of the physical system and subdividing it into a large number of finite elements. For each of these elements the *partial differential equations* (PDE) of mass and moment conservation (Navier-Stokes equations), thermal energy and chemical species is solved. This can then be coupled to a model of the precipitation process to predict the characteristics of the precipitate formed. Although CFD is a very powerful modelling tool, there are still a number of simplifying assumptions that need to be made. The CFD would give varying results depending on the models and assumptions used. It would therefore still require experimental verification. The time required building a predictive CFD model and verifying it does not fit within the limitations imposed by the current study. An experimental method would therefore be more suited.

Torbacke and Rasmuson (2001) used a loop reactor as indicated in Figure 3.16 to investigate the different scales of mixing. The reactor is operated in semi-batch mode. The circulation induced by the marine propeller represents macromixing, the diameter and volumetric feedrate varies mesomixing and the mixing intensity from the turbine varies micromixing. The system that was studied in the reactor was the precipitation of benzoic acid. For this system and the conditions it was evaluated, it was found that the mean particle size increases with increasing circulation rate in the loop, with increasing mixing intensity at the feed point, with decreasing feeding rate and decreasing feeding pipe diameter. Torbacke end Rasmuson (2001) concluded from the results that the mean particle size increases with an increase in mixing intensity for all the scales of mixing of which mesomixing was found to be most important.

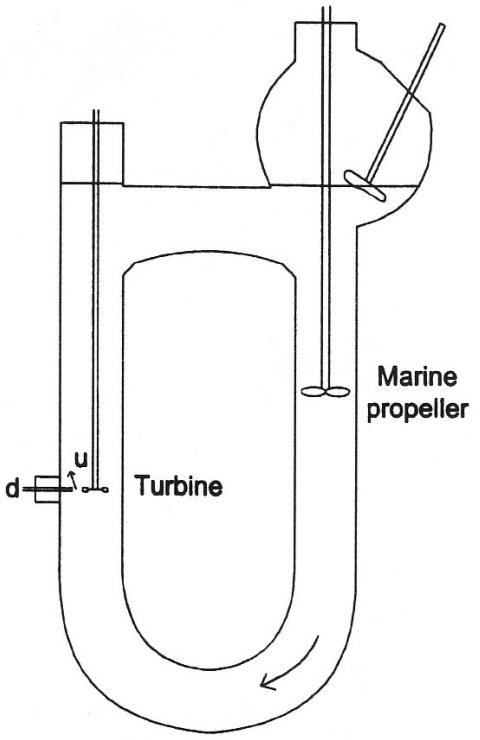

Figure 3.16 Loop reactor for the investigation of mixing (Torbacke & Rasmuson, 2001).

Gösele and Kind (1991) introduced the *three-zone experiment* for continuous systems. Faced with the problem of the differences in the mixing conditions between laboratory scale experiments and plant scale they decided to divide an MSMPR reactor into three zones. Two smaller zones would represent the volume around the two feed inlets and a larger zone that would represent the bulk of the reactor. The three zones in a reactor is represented by three smaller reactors (Figure 3.17). Gösele and Kind (1991) claimed that the set-up would be able to simulate the macro- and micromixing times experienced on a plant scale. Macromixing is represented by the circulation between the reactors, and micromixing by the energy dissipation in the in the individual zones. Macromixing can therefore be controlled through the circulating pumps and micromixing through the stirring rate.

Gösele and Kind (1991) used the set-up to investigate the precipitation of copper carbonate. They reported the characteristics of the precipitate in terms of the specific filter resistance. They presented the results of the experiments in terms of two parameters: the macromixing time and the ratio of exchange flowrates between the

zones. The macromixing time, t_{mixing}, is quantified in Equation 3.57 and the ratio of exchange rates, Ψ_{AC}, in Equation 3.58.

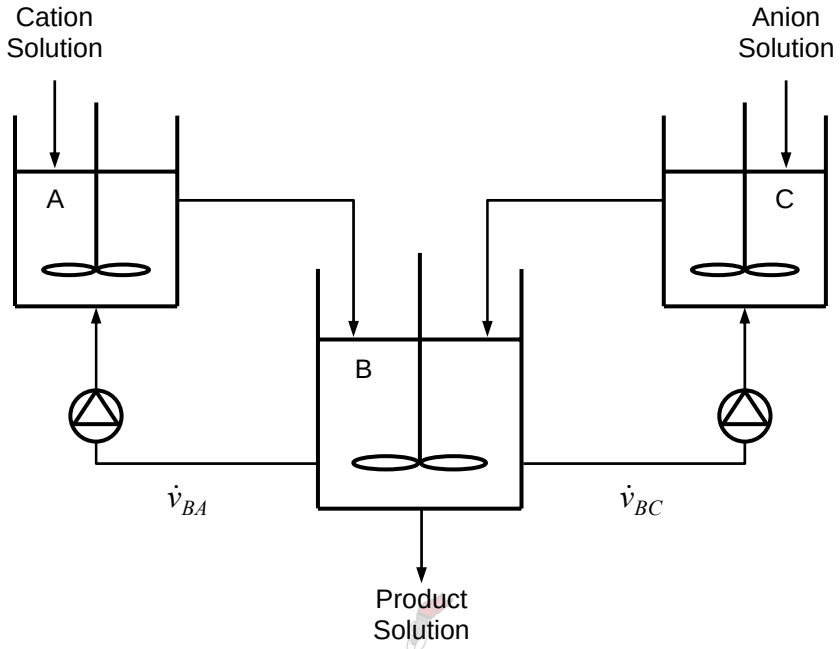

Figure 3.17 Three-zone experimental set-up (Gösele & Kind, 1991).

$$t_{mixing} = V_{total} / (\dot{v}_{BA} + \dot{v}_{BC}) \qquad \textbf{Equation 3.57}$$

$$\Psi_{AC} = \dot{v}_{BA} / (\dot{v}_{BC} + \dot{v}_{BA}) \qquad \textbf{Equation 3.58}$$

They observed that for the system and the parameters investigated, the filter resistance decreased for increasing macromixing time, t_{mixing}. They also observed large increases in the filter resistance at the limiting values of Ψ_{AC} (0,1). They ascribed it to an excess of carbonate or copper ions in the bulk reactor for which copper had the largest negative effect. They remarked that they were able to produce a precipitate on laboratory scale that had the same characteristic as on a plant scale. Although they recognised the potential of the set-up to investigate micromixing, they presented no results to that end.

Van Leeuwen et al. (1996) also recognised the potential of the three-zone experiment for the investigation of mixing. Their interpretation of the system is slightly different to that of Gösele and Kind (1991). They also interpret the exchange between the three zones as macromixing and the stirring rate as micromixing. The difference is that they saw the two inlet reactors as the mesomixing zones. According to this interpretation the volume of the inlet reactor would represent the result of mesomixing. The stronger the mesomixing, the quicker the inlet liquids mixed with the bulk solution, and the smaller the volume of the inlet zones would be.

Van Leeuwen et al. (1996) selected the barium sulphate system for the evaluation of the three-zone model for its well-known kinetics. In their experiments the exchange flowrates where kept equal as well as the volumes of the inlet zones. The parameters investigated where the exchange flowrates, $\dot{v}_{BA}, \dot{v}_{BC}$ ($\dot{v}_{BA} = \dot{v}_{BC}$); the inlet concentrations and the volumes of the three zones, V_A, V_B and V_C ($V_A = V_C$). The residence time and total volume of the system where kept constant. Two ratio where defined for presenting the data:

$$\psi_F = v_{in} / \left(v_{in} + v_{BA,BC}\right) \qquad \textbf{Equation 3.59}$$

$$\psi_V = V_B / V_{A,C} \qquad \textbf{Equation 3.60}$$

The results showed the surface mean particle size to increase with decreasing Ψ_F (increasing macromixing) and increase with increasing Ψ_V (increasing mesomixing). The latter effect was found to level off, which was the same observation made by Torbacke and Rasmuson (2001) for mesomixing in their system. Van Leeuwen et al. (1996) found that the inlet concentration had the strongest influence on the particle size but they also remarked that the influences of all the parameters rather small. The results were compared to particle sizes obtained form a single reactor with an equivalent total volume. An estimation of the circulation parameter for the single laboratory scale reactor showed $\Psi_F < 0.1$, which is far below the range obtainable with the set-up. They concluded that the range obtainable in the set-up would be more representative of reactors on an industrial scale.

3.1.8 Experimental Studies of CaF_2 and MgF_2

Magnesium fluoride and particularly calcium fluoride have been studied by a number of authors in their investigation of the mechanisms and kinetics of precipitation systems. Presented here is a review of some of the findings published by them. The studies on the hydrometallurgical applications of fluoride precipitation are excluded from this section since their focus was more process orientated and it had little or no information on the kinetics or characteristics of the precipitate.

Nucleation

Nielsen (1955) provided a review of the experimental data of Tovborg Jensen (1937 cited Nielsen, 1955) who measured the induction period of calcium fluoride by a change in the visible turbidity. The parameters investigated were temperature, ionic strength and initial concentration. The induction period varied from 2 minutes (23°C, only the salt at 0.004 mol/dm^3 CaF_2) to 140 minutes (18°C, 0.1 ionic strength and 0.0023 mol/dm^3 CaF_2). The data showed a negative salt effect and a decrease in the induction period with increasing temperature.

Growth Mechanism

Shyu and Nancollas (1980) introduced the *constant composition seeded growth technique* for the experimental evaluation of calcium fluoride's crystal growth rate. *Seeded growth experiments* involve the addition of well-characterised seed crystals to a metastable supersaturated solution. The addition of the seed crystal would initiate crystal growth, which could be followed by monitoring the concentration of the species in solution. The constant composition seeded growth technique is similar except that the activities of the precipitating species are kept constant throughout the experiment. This is achieved for calcium fluoride by continuously measuring the fluoride activity with a fluoride specific ion electrode connected to two mechanical burettes. The burettes contain stock solutions of calcium and fluoride ions. The set point for the fluoride activity is maintained by the intermittent addition of the stock solutions. The rate of crystal growth can then be determined by the rate of addition from the burettes. The results obtained for this method is claimed to be more repeatable.

Shyu and Nancollas (1980) investigated growth rates of calcium fluoride at activity based supersaturation ratios, S_a, from 1.2 to 2.66 and 37°C. The activities where calculated with the Debye-Hückel equation. A fitting of an equation similar to Equation 3.51 (p. 67) has shown $g = 2 \pm 0.1$ for supersaturation ratios between 1.75 and 2.66. For lower supersaturation ratios g was found to be 3. From the results they concluded the growth to be surface integration controlled in terms of the parabolic rate law. They also investigated the effect of phosphates on crystal growth. The phosphate were found to inhibit the growth of calcium fluoride for a set period after which the crystal growth continued at a rate that would be expected in the absence of the phosphates.

Nancollas et al. (1982) extended the constant composition seeded growth technique to other Group II fluorides (calcium, magnesium, strontium and barium). The growth rates were studied at 25°C. For calcium g were 1.9 ± 0.1 ($S_a = 1.4 - 3.0$), for magnesium 1.8 ± 0.1 ($S_a = 1.4 - 1.8$) and 5.0 ± 0.1 ($S_a = 2.0 - 2.6$). The growth mechanism was interpreted to be the screw dislocation mechanism for calcium and low supersaturations ratios of magnesium, and polynuclear growth for higher supersaturarion ratios of magnesium. The inhibiting effect of phosphates were also investigated and it was found that the growth of magnesium fluoride was also inhibited, but to a much lesser extend compared to calcium fluoride

Yoshikawa and Nancollas (1984) used the kinetic data obtained from the their previous work on Group II fluorides to further investigate the mechanism of surface integration. They observed a relationship between the dehydration rates of the cations and the rate of crystal growth. It was concluded that the dehydration rate of the cations are rate-limiting step during the surface integration of the growth units. The rate constants estimated based on cation dehydration was on average three orders faster than what is experimentally observed. The slower experimental rate was attributed to higher activation energy for the dehydration owing to the simultaneous loss of more than one water molecule from the cation.

Møller and Madsen (1985) studied the spontaneous precipitation of calcium fluoride at 25 and 37°C. The supersaturation ratios in their investigation were higher than used by the previous authors. They found the polynuclear mechanism of surface integration

to best describe their results, although deviations were noted at lower supersaturation levels. The deviations were seen as the change in mechanism from polynuclear growth to growth by the screw dislocation mechanism. They were unsuccessful to fit the screw dislocation model to their data but they still assumed it to be so. The increase of growth rate at the higher temperature was worked back to be a decrease in the interfacial free energy (γ in Equation 3.43, p. 63).

Nielsen and Toft (1984) studied a range of different electrolytes, which included calcium fluoride, in their investigation into the theory of electrolyte crystal growth. The experiments were conducted at 25°C. For calcium fluoride the screw dislocation mechanism was observed for supersaturation ratios (S_a) between 1 and 3. This is at variance with the observations of Nancollas et al. (1982). Polynuclear kinetics best described the growth rate at higher supersaturation ratios of between 4 and 40.

Growth Rates

Only Møller and Madsen (1985) and Nielsen and Toft (1984) used their results to calculate linear growth rates. Nielsen and Toft defined the growth rate as for a volume equivalent sphere, while Møller and Madsen defined the growth rate of the cubic crystal face. The latter results where converted to the volume equivalent sphere growth rate and is compared to the rate of Nielsen and Toft in Figure 3.18. There is not a good agreement between them as was noted by Møller and Madsen. The discontinuity in the plot of Nielsen and Toft's data is the region where the crystal growth mechanism changes from screw dislocation to polynuclear growth.

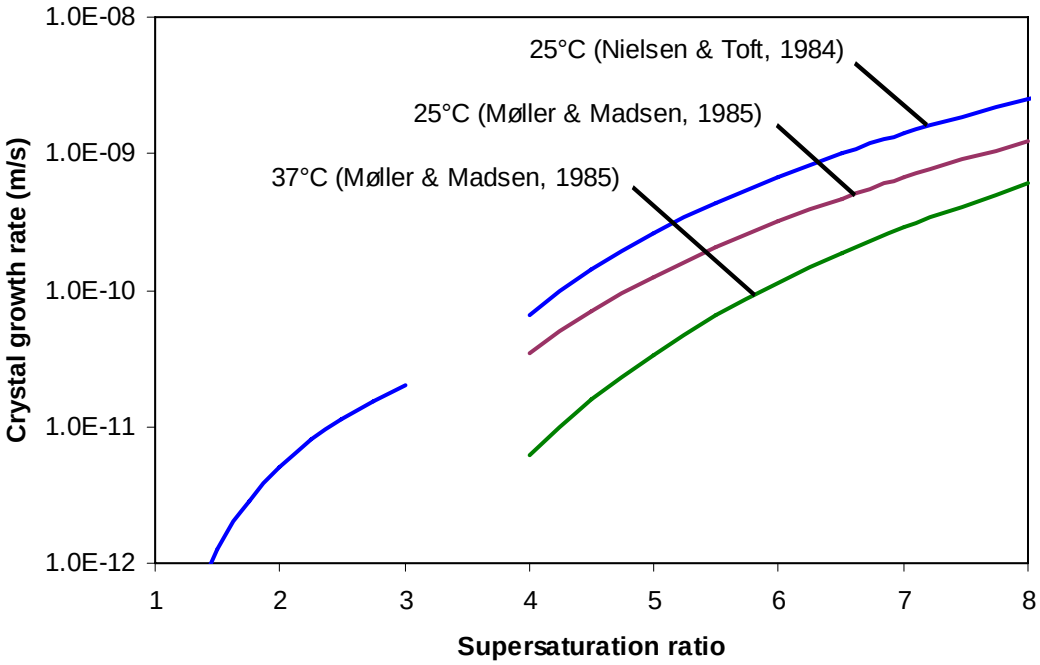

Figure 3.18 Crystal growth rates reported in literature.

3.2 Fluoride removal

There would be a residual amount of fluoride left in the solution after the fluoride precipitation process. For the Nkomati application this could be up to 1000 mg/ℓ if a 10% excess of fluoride is used. The effect of the fluoride would depend on the position of the fluoride precipitation process. The fluoride would adversely affect electrowinning if it enters the electrowinning circuit. In the zinc industry the presence of fluoride during electrowinning result in the firm sticking of the zinc to the aluminium starting sheets. The acceptable levels of fluoride in the purified zinc sulphate solutions are below 10 mg/ℓ (Booster et al., 2000). It can be expected that fluoride would also adversely affect nickel electrowinning. The removal of fluoride would be important if the precipitation process is implemented within the electrowinning circuit.

The implementation of the fluoride precipitation process envisaged for the Nkomati would be after iron precipitation. The cobalt and nickel solvent extraction steps will provide a barrier between the fluoride containing leach solution and the strip liquor.

The residual fluoride would then be precipitated during the lime boil process. In this instance the fluoride would not have any detrimental effects on the process. A fluoride removal process would be beneficial in this case if it were possible to recycle the unreacted fluoride. This would reduce the reagent consumption.

A number of processes were reviewed for their application of fluoride removal. The selectivity of the process towards fluoride, automatically eliminated a large number of these potential processes such as reverse osmosis. The selective processes, all of which were adsorption processes, are summarised in Table 3.2. Making a direct comparison of the values in the table will be misleading due to the different conditions under which the adsorbents were evaluated. Some of the authors do provide a comparison of their adsorbent with activated alumina. It was found that activated alumina has a higher capacity than aluminium-impregnated carbon (Leyva Ramos et al., 1998) and the soil sorbent (Wang & Reardon, 2001).

Table 3.2 Possible adsorption materials for fluoride removal.

Adsorption Material	Capacity [g F]/[kg material] (Initial conditions)	Reference
Activated Alumina	3.8 (pH 5.0, 10 mg F/ℓ)	Lounici et al., 1997
La(III)- Loaded Chelating Resin	14 (pH 5.0)	Kanesato et al., 1988
Fired clay chips	0.2 (pH 5.8, 20 mg F/ℓ)	Moges et al., 1996
Aluminium-impregnated carbon	0.55 (pH 5.0, 7 mg F/ℓ)	Leyva Ramos et al., 1998
Rare earth oxides	15 (pH 6.5, 150 mg F/ℓ)	Raichur and Jyoti Basu, 2001
Soil sorbent	0.15 (pH 7.0, 4 mg F/ℓ)	Wang and Reardon, 2001

Activated alumina appears the most promising of these adsorbents because it is fairly specific for fluoride, has a relatively high fluoride exchange capacity, is not affected by the normal concentrations of chlorides and sulphates in a water, and can be regenerated. Its capability has been known for a long time (Boruff, 1934) and is used for the removal of fluoride and arsenic from drinking water.

No documented evidence was found of the application of activated alumina to hydrometallurgical processes, although according to J.R. Harlamovs (personal comunications, September 25, 2002) Cominco has evaluated it for the control of fluoride in zinc electrowinning circuits. They dismissed it based on financial rather than technical reasons. The activated alumina needs to be experimentally evaluated for the current application since it is unique to any of its previous applications. The activated alumina would be subjected to higher fluoride concentrations and will be operated at elevated temperatures. Under these conditions the activated alumina should still show high selectivity and capacity to make it applicable.

3.2.1 Adsorption

A review of the appropriate adsorption theory is necessary for the evaluation of activated alumina. Adsorption in the current context can be defined as the preferential distribution of molecules between the liquid phase and the surface of a solid phase known as the adsorbent. The molecules are held onto the surface by physical forces such as Van der Waals forces or chemical bonds. The latter is referred to as *chemisorption* and is less easily reversed than physical adsorption. The application of adsorption requires it to be a reversible process where the regeneration of the adsorbent is known as desorption.

Pectora roborant cultus recti

Isotherms

An equilibrium state is established after a sufficient time has elapsed between the concentration of a solute in a liquid and the loading of an adsorbent. This state can be described in terms of so-called *adsorption isotherms*. Equilibrium isotherms are theoretical or empirical models, which establish a relationship between a fixed absorbed mass and the solution concentration, c_E, at the equilibrium state.

Two isotherms that found application in the description of the adsorption equilibrium in solid-liquid systems are the *Langmuir* and the *Freundlich isotherms*. The Langmuir isotherm was one of the first attempts to develop an isotherm equation and is based on the assumption of monolayer adsorption. Mathematically the Langmuir adsorption isotherm has the following form:

$$X = X_m \frac{c_b}{b_L + c_b}$$ **Equation 3.61**

Where:

X : Equilibrium loading,

X_m : Loading for monolayer coverage,

c_b : Bulk concentration of the component,

b_L : Constant for the isotherm.

The Langmuir isotherm can be fitted to experimental data by transforming it into the following linear form:

$$\frac{c_b}{X} = \frac{1}{X_m} c_b + \frac{b_L}{X_m}$$ **Equation 3.62**

The Freundlich isotherm was empirically developed for adsorption from aqueous solutions and was later shown to have some thermodynamic justification. The isotherm equation takes on the following form:

$$X = b_F (c_b)^{n_F}$$ **Equation 3.63**

Where:

b_F : Empirical factor for the isotherm,

n_F : Exponential factor for the isotherm.

This isotherm can also be transformed to a linear form to be fitted to experimental data:

$$Log(X) = n_F Log(c_b) + Log(b_F)$$ **Equation 3.64**

The isotherms would indicate the upper limit to which an adsorbent can be loaded. In practical application the adsorbent may never be fully loaded owing to kinetic effects.

Adsorption Kinetics

The progression of a molecule during the adsorption process is as follows. The molecule diffuses from the bulk solution through the boundary layer surrounding the adsorbent particle. The driving force would be the concentration gradient over the boundary layer. At the external surface of the particle the molecule diffuses through the pores until it reaches an adsorption site where it is held. The desorption process would be the reverse of this. The diffusion of the molecule through the boundary layer is considered to be rapid. The rate-limiting step is the diffusion into the adsorbent's pores and in the case of chemisorption, possibly the surface reaction.

During the loading process a fixed bed adsorber can be divided into three zones as a result of the kinetics of adsorption. The three zones are indicated in Figure 3.19. Starting with a free bed the molecules will first load onto the bed close to the inlet. As the adsorption sites become less at the inlet, the adsorbing molecules would penetrate deeper into the bed before it is adsorbed. Some of the sites in the bed would load the molecules more readily and would be the first to be occupied, while some others would require a higher concentration of the molecules in the surrounding solution. This would result in the formation of the *mass-transfer zone* where the bed is loaded to varying degrees. The mass-transfer zone would be bounded by the *saturated adsorbent*, which is fully loaded, and the *free adsorbent*, which has not been in contact with the adsorbing molecules.

As the bed becomes loaded, the mass-transfer zone would progress downwards. A condition would be reached, referred to as the *breakthrough point*, when the mass-transfer zone reaches the outlet. The concentration of the adsorbing molecules would increase in the outlet as the mass-transfer zone passes through. When the concentration in the outlet equals the inlet concentration the bed would be completely loaded and this point would be referred to as the *saturation point*. These would be discussed in the next section.

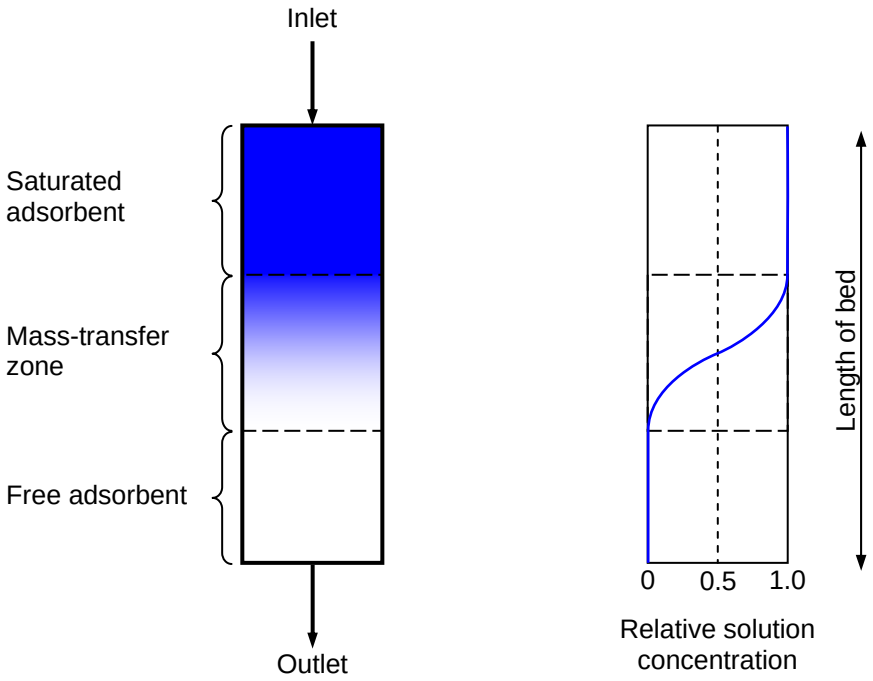

Figure 3.19 Zones in a fixed bed adsorber.

Breakthrough Point, Capacity and Regeneration Ratio

A *breakthrough curve* could be constructed of a fixed bed adsorber by monitoring the outlet concentration. Indicated on Figure 3.20 is a typical breakthrough curve with the breakthrough point and the saturation point indicated.

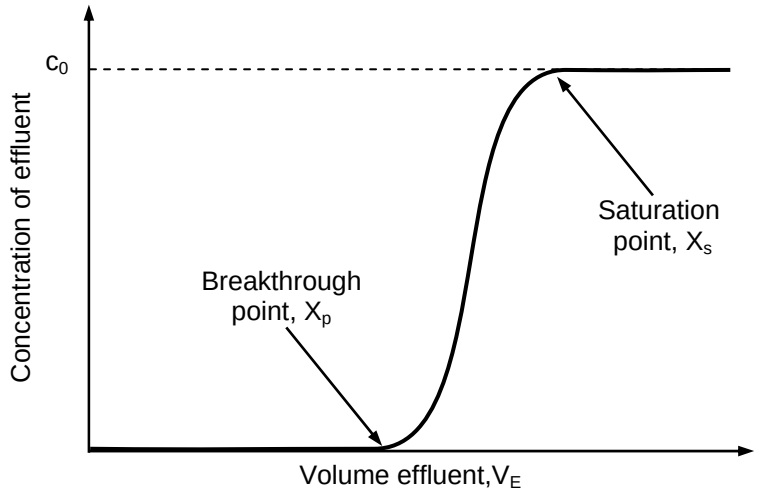

Figure 3.20 Breakthrough curve for a fixed bed adsorber.

Using the difference between the inlet concentration, c_0, and the outlet concentration, c, the capacity of the bed can be calculated. Two capacities can be defined for a bed, the capacity at the breakthrough point, X_p, and the capacity at saturation, X_s (Lounici et al., 1997). These two can be calculated by integrating Equation 3.65 to the volume of effluent (V_E) at the breakthrough point (X_p) and the saturation point (X_s). The parameter m is the mass of the adsorbent.

$$X = \int_0^{V_E} \frac{c_0 - c}{m} dV \qquad \textbf{Equation 3.65}$$

After the loading the bed needs to be regenerated. This is normally done by changing the pH of the solution in contact with the adsorbent resulting in desorption. The efficiency of the regeneration process can be measured by the ratio of the amount of molecules desorped (m_d) compared to the amount originally adsorbed (m_a). This ratio is given by (Lounici et al., 2001):

$$R_{d:a} = \frac{m_d}{m_a} \qquad \textbf{Equation 3.66}$$

Pectora roborant cultus recti

3.2.2 Activated Alumina

Activated alumina included a series of partially hydroxylated alumina oxides (Al_2O_3). The composition of the aluminas could be described by the general formula $Al_2O_{(3-x)}(OH)_{2x}$ where x range from 0 to 0.8. The term "activated" referrers to the large specific surface areas resulting from the process by which aluninas were manufactured from its precursor, aluminium hydroxide. The process involves the calcination of the aluminium hydroxide during which the hydroxide groups are driven off, leaving a porous structure.

The different activated alumina forms have found many applications ranging from the drying of gasses and liquids, catalyst supports, chromatography applications and the adsorption of fluoride and arsenic from water. The specific activated alumina used for the latter application of interest is a mixture of amorphous and gamma alumina (γ-Al_2O_3) produced by low temperature calcination (300 – 600 °C). This activated alumina has a specific surface area ranging from 50 to 300 m^2/g. The activated

alumina is loaded into a column in the form of particles having a size between 0.3 to 0.6 mm. It is operated as a fixed bed and is subjected to cycles adsorption and regeneration. The mechanism involved in the cycle is analogous to ion exchange (Clifford, 1990) and will be discussed in the next section.

The Defluorination Process

Describe here is the cycle used in the defluorination of drinking water. The mechanisms involved for each step is given in terms of the reaction equations. Starting out with neutral activated alumina (Alumina·HOH):

1. The first step is the acidification of the activated alumina using sulphuric or hydrochloric acid. This is required for the proceeding step where the activated alumina surface needs to be protonated for the exchange reaction. The surface reaction proceeds as follows:

$$\text{Alumina·HOH} + H_2SO_4 \rightarrow \text{Alumina·}H_2SO_4 + H_2O \qquad \textbf{Equation 3.67}$$

2. After acidification, the activated alumina is ready to adsorb the fluoride. The adsorption proceeds by the displacement of the sulphate ions with the fluoride. This reaction is analogous to ion exchange where the activated alumina acts as an anion exchanger. The exchange reaction requires solution to be slightly acidic at a pH of between 5 and 6. The optimum is reported to be a pH of 5.6 (Lounici et al., 1997).

$$\text{Alumina·}H_2SO_4 + 2\ HF \rightarrow \text{Alumina·}2HF + H_2SO_4 \qquad \textbf{Equation 3.68}$$

3. Between the loading and the regeneration step a backwashing step is included to redistribute the activated alumina and remove suspended solids. This would eliminate wall effects and channelling.

4. The activated alumina is regenerated with a dilute sodium hydroxide (NaOH) solution. A 1% - 2% mass solution is normally employed but lower concentration (0.1%) has been suggested, Lounici et al. (2001). In the basic

region the activated alumina acts as a cation exchanger and the sodium is adsorbed onto the surface:

$$\text{Alumina}\cdot 2HF + 4\ NaOH \rightarrow \text{Alumina}\cdot 2NaOH + 2NaF + 2\ H_2O \quad \textbf{Equation 3.69}$$

5. The regeneration is followed by a rinsing step to wash excess reagent and remove any entrapped material such as precipitates that could have formed.

6. The fluoride capacity can now be restored by acidifying the activated alumina:

$$\text{Alumina}\cdot 2NaOH + 2H_2SO_4 \rightarrow \text{Alumina}\cdot H_2SO_4 + Na_2SO_4 + 2H_2O \quad \textbf{Equation 3.70}$$

3.3 Summary from Literature Review

The purpose of this chapter was to provide the theoretical basis for this study. Two distinct topics were covered, starting with a discussion of the theory of precipitation necessary for the fluoride precipitation process. The chapter was ended with the theory of adsorption for a fixed bed system.

The bulk of this chapter was devoted to precipitation. A broad review on the theory of precipitation was given which can be referred to beyond its application in the current study. The characterisation of the precipitate was first discussed indicating the measures of its quality. The characteristic of importance would depend on the application of the precipitation step and its quality on the process of its manufacture.

The thermodynamic driving force for precipitation is supersaturation. This is the central parameter that influences all of the processes involved in precipitation and hence the characteristics of the formed precipitate. The two primary processes that occur during precipitation is nucleation and crystal growth. These two processes proceed in parallel according to a number of different mechanisms.

The combined effects of nucleation and crystal growth in a continuous reactor were discussed for the mixed suspension mixed product removal MSMPR precipitation

reactor. It was shown that the apparent nucleation and crystal growth rate could be estimated for a continuous reactor by plotting Ln(n(L)) as a function of particle size. The plot should form a straight line with the gradient related to the linear growth rate ($\dot{r}$) of the precipitate particles and the intercept to the nucleation rate.

Other than the two primary processes there are a number of secondary processes that occur in precipitation. All of these processes are dependent on the level of supersaturation. Of these the most important in precipitation is agglomeration. It influences both the quality and the size of the precipitate. The formation of agglomerates result in the capture of mother liquor between the particles, which reduces its quality. It also results in an increase in the size of the particles that aid in the separation of the precipitate from the solution.

A topic of particular interest to this study is the influence of hydrodynamics and mixing on the precipitation process. Three scales of mixing were defined:

- Macromixing,
- Mesomixing,
- Micromixing.

Only micromixing can directly influence the rate of precipitation reactions since it is the only scale of mixing that occurs at a molecular scale. Macro- and mesomixing can indirectly influence the precipitation process by the resulting spatial variations in the reactor. The rates of the precipitation reactions are fast enough to react to these spatial variations. An experimental method is therefore required to investigate the influence of mixing. For this the three-zone method introduced by Gösele and Kind (1991) was identified for it ability independently simulate the effect of the three scales of mixing.

The discussion on precipitation was ended by a review of experimental studies found in literature on calcium and magnesium fluoride. The screw dislocation mechanism was observed for calcium and magnesium fluoride at supersaturation ratios between 1.4 – 3.0 and 1.4 – 1.8, respectively. Polynuclear growth was observed at higher supersaturations for calcium (4.0 - 40) and magnesium (2.0 – 2.6). It was also found that phosphates have an inhibiting effect on the crystal growth rate of both calcium

and magnesium but to a lesser extend for the latter. The experimental studies found in literature were for simple systems at low ionic strengths and temperatures. This makes the current study unique for it investigates the characteristics of the precipitate formed at high temperatures and complex systems at high ionic strengths.

The final topic that was looked at was the removal of the unreacted fluoride after precipitation. Adsorption of fluoride using activated alumina was identified as a possible method for the removal of it. The experimental studies found in literature on fluoride adsorption are limited to simple systems at low temperatures and fluoride concentrations. The application of it in the current study would be at higher concentrations and temperatures. The theory provided in the adsorption section of this chapter would enable the experimental evaluation of activated alumina in a fixed bed column. It would be evaluate in terms of its saturation and breakthrough capacity. The regeneration process would be evaluated by the regeneration ratio.

Chapter 4

Experimental Procedures

Objectives of Chapter 4

- Describe the experimental set-up and procedures used.
- Discuss the experimental parameters to be investigated.
- Describe the analytical methods used.

Described here are the experimental set-up and procedures used in this study. The experiments will be discussed from the preparation of the solutions, the procedure of the experiments to the analytical methods used.

From an early stage in this investigation, it was decided that the best position for implementing a fluoride precipitation step within the Nkomati circuit would be after iron precipitation. Iron precipitation is the last entry point for calcium into the circuit and the next processing step, cobalt solvent extraction, would benefit from the reduction of the calcium and magnesium. The composition of the solutions used in the experiments would be required to represent the solution leaving iron precipitation. The composition and conditions of the solution was obtained from A. Swarts (personal communications, 13 March 2001) and is given in Table 4.2, P.106.

The three-zone technique was identified in the literature review as a method of investigating the effects of mixing on precipitation. An experimental set-up had to be constructed to carry out the three zone experiments. Considerations that needed to be taken into account for its design were, the elevated temperature that needed to be maintained and the corrosion resistance of the materials used. The use of fluoride imposed the largest limitation on the materials to be used in the experimental set-up, thus making glassware unsuitable. The experimental set-up was designed and constructed in-house to meet all of the requirements.

4.1 Experimental Set-up

An overview of the experimental set-up will now be presented. The reader may refer to Appendix D for photos of the experimental set-up.

4.1.1 Overview

Presented in Figure 4.1 is a schematic of the experimental set-up designed according to Gösele and Kind's (1991) three-zone model. The current implementation could be divided into two cycles, of which the primary cycle was the reactor cycle and the secondary cycle was the water cycle. The latter was used to maintain the temperature of the set-up. The two cycles operated independently and do not come into contact.

Reactor Cycle

The reactor cycle consisted of the two inlet reactors (Reactor A and C) and the bulk reactor (Reactor B). The solution was circulated between the reactors using a dual head peristaltic pump, *Pump B* (Watson Marlow 313S with an 313X extension pumphead). As a result the circulation rate to the inlet reactors was equal. Marprene tubing with an inside diameter of 8 mm was used for the interconnections between the reactors. The selection of Marprene tubing was based on its fluoride resistance and long life. This allows a maximum flow rate of 1000 mℓ/min to each inlet reactor. The circulation between the reactors represents macromixing and is therefore adjusted with Pump B.

Peristaltic pumps (P*ump A*: Watson Marlow 501U and *Pump C*: Watson Marlow 503S) controlled the feeding rates of the two solutions to the inlet reactors. The tube inside diameter (Marprene) was selected to be in the range of a maximum residence time of 2 hours. For the feeding of the fluoride solution a 0.5 mm tube was used (0.4 – 7.1 mℓ/min) and for the sulphate a 1.6 mm tube (4.2 – 73 mℓ/min). The sulphate solution was preheated and maintained at the operating temperature in the water bath, whereas the fluoride solution was fed to the reactor at room temperature. This was done to be representative of the expected implementation, although the long residence times used in the experiments would have made the system insensitive to the feeding temperatures. Mesomixing was simulated by the adjustment of the volumes of the three reactors while maintaining the total volume.

Micromixing was controlled by the stirring rate of the three marine impellers in the individual reactors. The stirrer material was Teflon. Bench drilling machines were used to drive the stirrers of which the rate was selected and controlled by belt settings.

An outlet was provided to the bulk reactor. The flow resistance provided by the outlet tube controlled the flow rate. This could be adjusted to a limited extent by the height of the outlet tube relative to the level of the solution in the bulk reactor. The product from the reactor was collected in a beaker where it was stirred for an additional time until sufficient sample was collected.

Water Cycle

The main volume of the water was held in a 70ℓ water bath maintained at a constant temperature (±0.1°C) using an PID controlled thermostat (Haake DC3). The water bath was elevated above the experimental set-up allowing the water to circulate under hydrostatic pressure. Connected to the water bath were five water lines, three of which was used for the reactors and two auxiliaries. The lines used for the reactors were connected to the outer shell of the reactor, allowing the water to flow in the volume in between the outer shell and the outside wall of the reactor. Two plates extending from the outer shell to the outer wall ensured that the water circulated underneath the reactors. The water from the outlets was collected in a reservoir, which had a maximum capacity of 5ℓ. A level controller connected to a centrifugal pump maintained the level in the reservoir. The water was intermittently pumped back to the water bath. Not shown on the diagram was an overflow that was located above the upper level of the controller. Should the centrifugal pump have failed for any reason, the water would have overflow into the drain. The thermostat would have automatically switched off if the level in the water bath became to low.

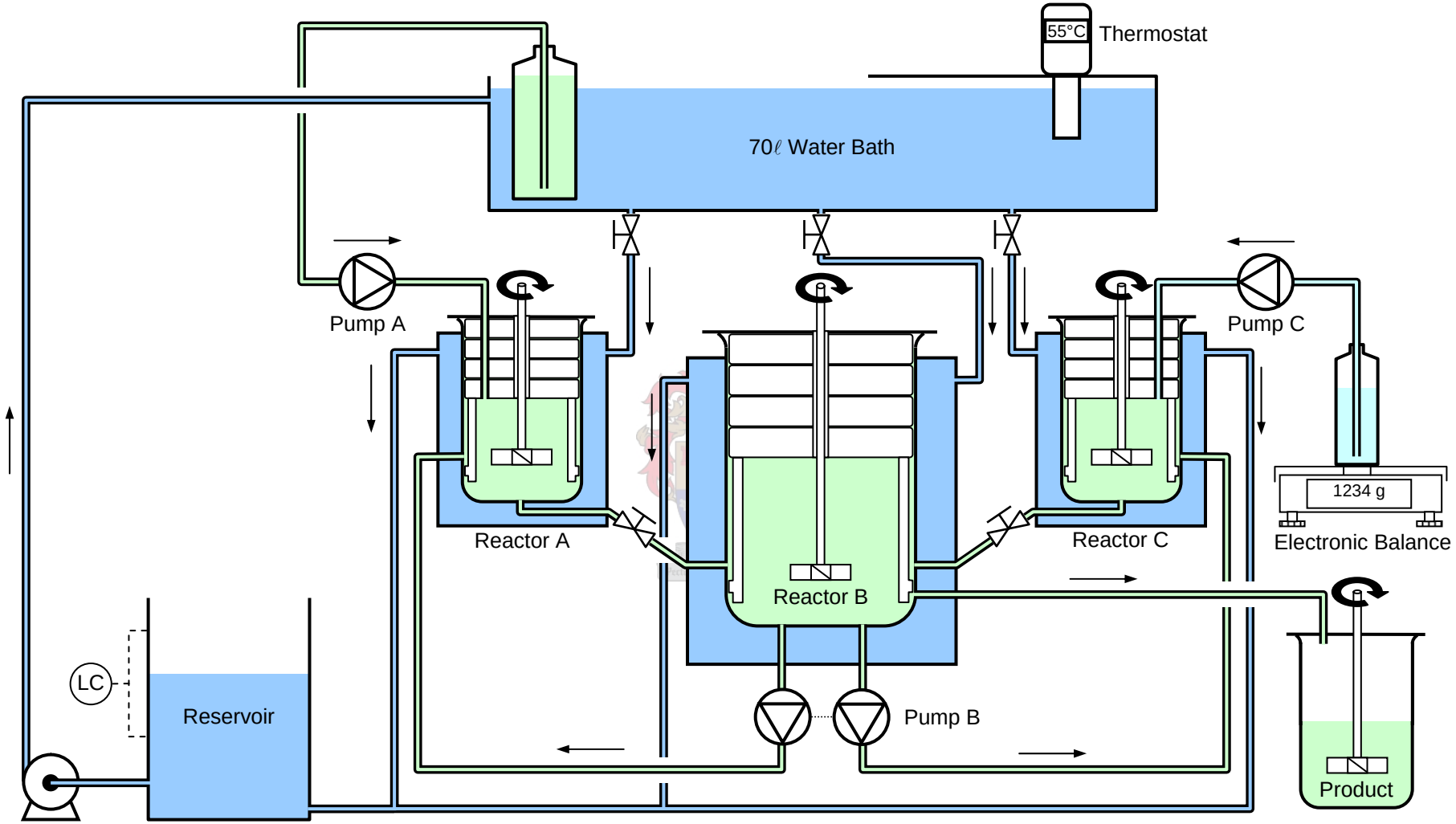

Figure 4.1 Schematic representation of the experimental set-up.

4.1.2 Reactors

The dimensions of the reactors are summarised in Table 4.1. Polypropylene beakers were used as the basis for the reactors owing to its fluoride resistance. The volume of the inlet reactors was 1ℓ and the bulk reactor 2ℓ. The volumes of the reactors could be limited by the addition of polypropylene discs of which each represented approximately 100 mℓ. The discs were manufactured to a tight tolerance. Each of the reactors also had six baffles designed according to the guidelines provided by Garrison (1983). A spacing of 1 mm was provided between the reactor wall and the baffle to ensure that the precipitate would not get entrained in between. The reactors were assumed to be well mixed on a macro and meso scale with no large spatial variations. This is the inherent assumption of the three-zone model.

Table 4.1 Dimensions of the reactors.

Dimension	Reactor A & C	Reactor B
Volume	1ℓ	2ℓ
Diameter	105 mm	130 mm
Material of construction	Polypropylene	Polypropylene
Width of baffles	10 mm	10 mm
Number of baffles	6	6
Type of impeller	Teflon Marine propeller	Teflon Marine propeller
Diameter of impeller	60 mm	60 mm

Presented in Figure 4.2 is a photograph of the internals used in the reactors. From the photograph the baffles, stirrer and polypropylene discs could be seen. The two bolts extending from the top held the discs together. The internals shown are for one of the inlet reactors. Two shafts are provided in the discs extending throughout the length. The first is in the centre for the impeller shaft and the second is off-centre for the feeding tube. This tube can also be seen extending from the top. A photograph of the whole experimental set-up is also provided in Figure 4.3. The three reactors and Pump B are identified on the photograph.

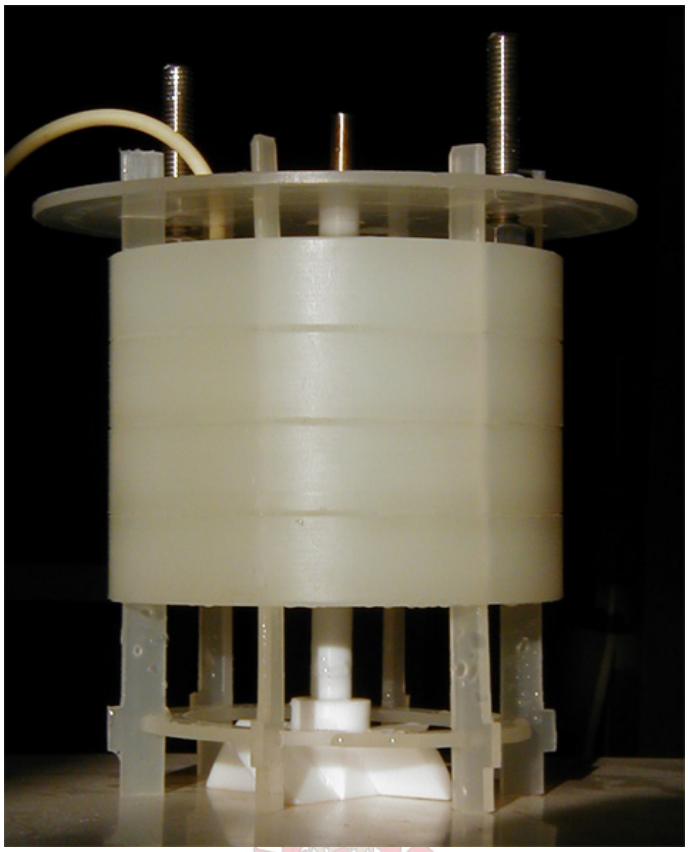

Figure 4.2 Photo of the reactor internals.

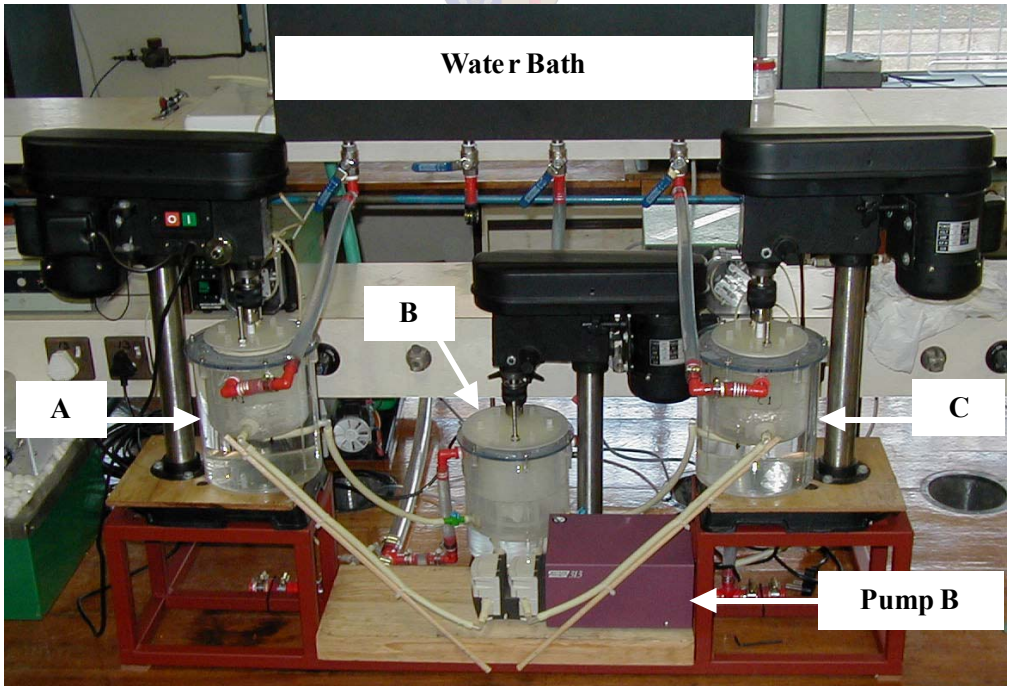

Figure 4.3 View of the complete experimental set-up.

4.2 Solution Preparation

The indicated composition of the solution leaving iron precipitation is given in Table 4.2. The solution used in the experiments should be representative of this. The ideal would have been to obtain a sample of the actual solution, but there was none available from the Nkomati pilot runs. A synthetic solution therefore needed to be made up.

Table 4.2 Composition of solution leaving iron precipitation (A. Swarts, personal communications, 13 March 2001).

Metal ion	Concentration (g/ℓ)
Nickel (Ni)	32.7
Cobalt (Co)	1.87
Copper (Cu)	0.007
Manganese (Mn)	0.305
Aluminium (Al)	< 0.001
Iron (Fe)	< 0.002
Zinc (Zn)	0.121
Silicon (Si)	0.042
Calcium (Ca)	0.576
Magnesium (Mg)	3.58
pH	5.2
Temperature	55°C

Pectora roborant cultus recti

The concentrations of some of the minor elements falls into the impurity range of the analytical reagents of the high concentration elements. It would therefore, be difficult to reproduce the solution exactly and as a result some of the minor elements could be left out. From the above a reduced list of elements was compiled which is summarised in Table 4.3.

The synthetic solution was made up from analytical grade sulphate salts obtained from Merck and Sigma-Aldrich. The salts were weighed and dissolved in distilled water using 2ℓ volumetric flasks. Distilled water was found to be the purest water available at high quantities, based on conductivity measurements. The solution was heated to 55°C while dissolving the salts and made up to the 2ℓ mark at this

temperature. This was found to give the most consistent solution since deviations were experienced in the calcium concentration when dissolving the salts at room temperature. This is believed to be the result of the incomplete dissolution of the calcium sulphate. After all the salts were dissolved, the pH of the solution was found to be close to 5.2 (5.0 – 5.4), which required no additional pH adjustments.

Table 4.3 Composition of the synthetic solution.

Metal ion	Concentration (g/ℓ)
Nickel (Ni)	32.7
Cobalt (Co)	1.87
Calcium (Ca)	0.576
Magnesium (Mg)	3.58
Manganese (Mn)	0.305
Zinc (Zn)	0.121

Large quantities of solution were required for the continuous three-zone experiments to ensure that steady state was reached. Twenty litre of solution was required for one run and at the cost of the base metal chemicals of ~R100/ℓ these experiments were too expensive. This forced us to use ammonium sulphate ($(NH_4)_2SO4$) at a cost of ~R 2.50/ℓ to replace the base metal sulphates. The solution was made up to the same ionic strength as with the base metals.

The fluoride solutions were made up in a 100 mℓ or a 1ℓ polypropylene volumetric flask by diluting hydrogen fluoride (HF) or dissolving ammonium fluoride (NH_4F) in distilled water. The concentrations were made up so that the volume of the fluoride solution would be 5% of the volume of the solution treated (the sulphate solution). This value was selected to be representative of what could be expected for the large-scale implementation of the process.

4.3 Batch Precipitation Experiments

The intention of the batch experiments is to evaluate parameters such as the fluoride addition and the effects of temperature. This could be seen as the equilibrium study of the system. A reactor of the three-zone experimental set-up could be easily isolated to be used in the batch experiments.

4.3.1 Procedure

The two 1ℓ reactors was used for the batch experiments. One litre of solution (composition as in Table 4.3) was loaded into the reactor and heated to the required temperature. At the desired temperature the fluoride solution was slowly fed to the reactor with a peristaltic pump. The volume of the fluoride solution was 50 mℓ (5% of the treated solution volume). The rate of the addition was selected so that the fluoride was fed over a period of an hour. After one hour, the solution was stirred for an additional hour. After the total time of two hours, the precipitate slurry was filtered using a Millipore 0.45 μm membrane filter.

The procedure was based on preliminary experiments. In these experiments it was observed that a too fast addition of the fluoride results in the formation of a gelatinous precipitate. Some of the initial experiments were seeded with calcium fluoride crystals. The seeded and unseeded experiments were found to give the same results with the difference between them falling within the variance of the analysis methods ±1%). The final set of experiments was unseeded.

4.3.2 Parameters Investigated

The parameters selected for investigation with their values indicated in brackets where the following:

- Level of fluoride addition (10%, 25%, 50%, 75%, 100% and 110% of stoichiometric addition required for calcium and magnesium combined).
- Molar ratio of calcium to magnesium (0:1, 1:1, 1:2, 1:3, 1:4, 1:10 and 0:1).
- Identity of the soluble fluoride used (NH_4F and HF).
- Effects of temperature (45, 55 and 65°C).

4.4 Continuous Precipitation Experiments

The intention of the continuous experiments was two-fold. First the effect of residence time had to be evaluated. For an initial value the maximum residence time was guessed to be two hours. Much can be gained in terms of a reduction reactor size and capital cost if this value could be reduced, as long as it does not adversely effect the quality of the precipitate. The second intention is to investigate the effects of the

different scales of mixing. The results would provide a guide for the scale-up of the process.

4.4.1 Procedure

A single reactor was used for the residence time tests. The procedure will only be described for the three-zone experiments of which the single reactor experiments could be seen as a simplification.

The internals of the reactor were assembled beforehand, where the volumes of the reactor were determined by the addition of the polypropylene discs. The total volume of the system was kept constant at 2ℓ. The internals were then placed inside reactor and sealed with silicone sealant. It was found advantageous to seal the reactor airtight, which helped to maintain the levels in the reactors. The circulation in between the reactors could be forced allowing for higher circulation rates to be obtained and more stable operation.

The reactors was first filled with distilled water and brought to the operating temperature. During this the distilled water was circulated and stirred at the rate as intended for the experiment. After the operating temperature was reached, the feeding of the solutions was initiated. The flowrates was monitored with an electronic balance for the fluoride solution and the addition rate of the solution to the holding flask for the sulphate solution. The duration of the firsts residence time was used to adjust the flowrate to the desired value, after which it was monitored. The length of the experiment was ten durations of the residence time, as suggested by Söhnel and Garside (1992), to ensure that steady state was obtained.

One litre samples were collected in the product beaker, which was then subjected to filtration tests using a 0.45 μm Millipore filter. Samples were taken of the filtrate for analysis and the filter cake was washed with distilled water. The precipitate was then dried and stored for later analysis.

4.4.2 Parameters Investigated

The parameters selected for the single reactor experiments with their values indicated in brackets where the following:

- Residencetime (½, 1 and 2 hours)
- Type of sulphate solution [$(NH_4)_2SO_4$ and base metals sulphates]

For the continuous experiments a high level and low level was selected for each scale of mixing (see Table 4.4). Both macro- and micromixing were treated as a single parameter for the experimental runs, whereas the mesomixing of the sulphate and fluoride solution was treated as two separate parameters. This amounted to four factors for which a full factorial design would require 16 experimental runs. For the initial screening it was decided to select an arbitrary base case and vary each parameter individually. This amounted to five experiments. If required, the results could have been used in the extension of the experimental runs to the full factorial design.

Table 4.4 High and low levels selected for the experimental parameters.

Scale of mixing	Represented by	High level	Low level
Macro	Circulation between reactors	1080 mℓ/min	300 mℓ/min
Meso	Volume of inlet reactors	~0 mℓ	400 mℓ
Micro	Stirrer rate	900 rpm	520 rpm

The awarding of the values to the high and low levels of macro and micromixing were intuitive. The reasoning behind the awarding of the values to mesomixing was as follows: the volumes of the inlet reactor represent the result of mesomixing. The higher the level of mesomixing the better the inlet solution is dispersed in the bulk solution and the smaller the volume becomes. The high level of mesomixing was obtained in the experimental set-up by bypassing the specific reactor.

4.5 Adsorption Experiments

The intention of the adsorption experiments was to investigate the feasibility of using activated alumina to remove or even possibly recycle the unreacted fluoride after

precipitation. The fluoride should be adsorbed to low levels during the loading phase and desorbed again to a high concentration during regeneration.

4.5.1 Batch Procedure

As with precipitation, some batch experiments were carried out for the activated alumina to investigate the equilibrium conditions of the system. It also served as the initial screening of the option.

For these experiments, the activated alumina was soaked in distilled water overnight to ensure complete wetting. One litre of sulphate solution was prepared similar as the composition in Table 4.3, but with the calcium and magnesium excluded. Ammonium fluoride was added to provide the desired fluoride concentration. The experiment was carried out in an isolated inlet reactor of the three-zone set-up. To this the alumina slurry was added after the bulk of the water was decanted. The solution was allowed a predefined period to equilibrate before samples of the solution was taken. The pH of the solution was adjusted using sulphuric acid (H_2SO_4) or sodium hydroxide (NaOH).

4.5.2 Column Experiment Set-up and Procedure

The column experiments were used to simulate the defluorination cycle discussed in the literature review (Section 3.2.2, p.96). It would therefore give an indication of the kinetics of the adsorption process. This would be reported in terms of the breakthrough capacity and the saturation capacity for the adsorption cycle, and the regeneration ratio for the desorption cycle.

The experimental set-up that was used is presented in Figure 4.4. Two column sizes were used during the evaluation, a 32 mm (inside diameter) column and a smaller 11 mm (inside diameter) column. The activated alumina was retained in the column by a sinter glass disc. A jacket through which water from the waterbath was circulated maintained the temperature of the column.

Presented in Figure 4.4 is the smaller column during the adsorption cycle. The preheated base metal sulphate solution containing fluoride was fed from the top of the column under gravity for which the flow rate was controlled by the two valves. 100

mℓ samples were collected at the bottom to determine of the fluoride concentration. Water from the water bath was circulated upwards trough the jacket from where it was returned to the reservoir.

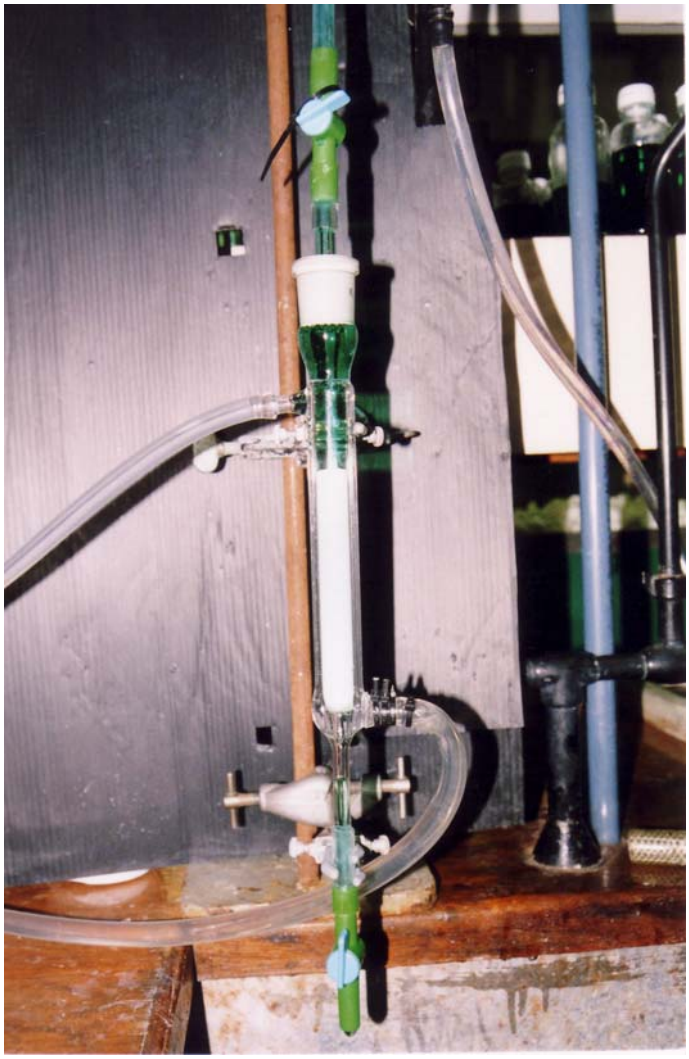

Figure 4.4 Column loaded with activated alumina during the adsorption cycle.

The fluoride containing base metal sulphate solution was prepared using the same method as for the batch experiments. For each experimental run, fresh activated alumina was used after it was soaked overnight in distilled water. After the activated alumina was loaded in the column, the following cycle was used:

1. *Acidification*: 20 bedvolumes of 0.2N sulphuric acid was washed through the bed.

2. *Loading*: The fluoride containing base metal solution was passed through the column at the desired flowrate, which was measured with a measuring cylinder. Samples of the effluent were taken for the determination of the fluoride concentration afterwards.

3. *Rinse and fluidisation*: Five bedvolumes of distilled water was passed trough the column to wash out the free sulphate solution. This proved an important step, for failing to do so would have brought the base metal solution into contact with alkaline solution used for regeneration. This would have resulted in the hydrolysis of the base metals to form a precipitate within the column and thus block it. After rinsing, the bed was briefly fluidised by passing distilled water from the bottom and allowing it to settle again.

4. *Regeneration*: Sodium hydroxide at a concentration of either 0.1% or 1.0% was passed trough the column. The regeneration process was also carried out at the operating temperature, although it would have been more representative of the large-scale implementation if this step were carried out at ambient temperature. Samples were collected for the determination of the fluoride concentration.

Pectora roborant cultus recti

4.5.3 Parameters Investigated

The parameters selected for investigation with their values indicated in brackets where the following:

- Initial fluoride concentration (400, 600 and 800 mg/ℓ)
- Adsorption temperature (45, 55 and 65 °C)
- Flowrate (1000 and 4500 ℓ/m^2.min)
- Sodium hydroxide concentration (0.1 and 1% by weight)

4.6 Analytical Methods

A number of different analytical methods were used for the analysis of the products from the experiments. Given here is a short list of the methods.

4.6.1 Solution Analysis

The analysis carried out on the solutions were the following:

- Atomic absorption spectrometry (AA) for the cations (Ni, Co, Ca, Mg, Mn, Zn).
- Liquid chromatography (LC) for the anions (F, SO_4).
- Fluoride ion-selective electrode for fluoride analysis in the presence of high sulphate concentrations.
- pH measurements.

For more information on the method used for the AA and the fluoride ion-selective electrode the reader may refer to Appendix B.

4.6.2 Solid Phase Characterisation

The solid phase characterisation needed to be done for the precipitate and the activated alumina. The following analysis were carried out:

- BET specific surface area for the activated alumina.
- Filtration resistance of the precipitate.
- Particle size analysis of the precipitate.
- Scanning Electron Microscope (SEM) photographs of precipitate.
- Thermo gravimetric analysis (TGA) of precipitate.
- X-ray fluorescence (XRF) for the composition of the precipitate.
- X-ray diffraction (XRD) for the phases present in the precipitate and activated alumina.

For more information on the method used to measure the filtration resistance the reader may refer to Appendix B.

4.7 Summary

The discussion on the experimental procedures can be summarised as follows.

4.7.1 Experimental Set-up

First, the experimental set-up was described. The set-up consisted of two separate cycles, a reactor cycle and a water cycle. The function of the water cycle was to maintain the temperature of the set-up. This was achieved by circulating water from a waterbath through jackets of the experimental equipment.

The primary cycle of the set-up was the reactor cycle, which consisted of three interconnected reactors. The set-up was built according to the three-zone model of Gösele and Kind (1991). Macromixing was simulated in the set-up by the exchange flowrates between the reactors, which was controlled by the circulation pump (Pump B). Mesomixing was simulated by the volumes of the inlet reactors, and micromixing by the stirring rate in each reactor. The reactor could also be isolated for the various batch experiments.

Pectora roborant cultus recti

4.7.2 Solution Preparation

The solution used in the experiments needed to be representative of the solution leaving iron precipitation. The minor cations present in the solution were left out reducing the list to six (Ni, Co, Ca, Mg, Mn, Zn). This synthetic solution was used in most of the experiments. For the continuous experiments the use of the base metal solution would have been too expensive, forcing the replacement of the base metals with ammonium sulphate. The preparation of the solutions was described in full.

4.7.3 Batch Experiments

The batch experiments were used to study the equilibrium conditions with varying parameters. The procedure consisted of adding a small volume of fluoride solution to the base metal solution over a period of time. Some of the parameters were fluoride addition, temperature and the molar ratio of calcium to magnesium.

4.7.4 Continuous Experiments

The continuous experiments could be divided into the single reactor experiments and the three-zone experiments. With the single reactor experiments the effect of residence time was evaluated and with the three-zone experiments the effect of the different scales of mixing. For each scale of mixing, a high level and a low level was selected and the mesomixing of the two feeding streams was treated as two separate parameters. The full factorial design would require 16 experimental runs. This list was reduced to five experiments of which one serves as the control experiment and a single parameter was varied at a time. If the preliminary results invited a more detailed investigation, the other runs in the factorial design could have been completed.

4.7.5 Adsorption Experiments

The adsorption experiments also consisted of batch experiments for the investigation of equilibrium of the system. The second part of the experiments was the column experiments with which the different cycles of an adsorption column were simulated. The procedure followed for each of the experiments was described.

4.7.6 Analysis

The analytical methods used were briefly listed, stating the methods used for the characterisation of the solutions and the methods used for the characterisation of the solid phases.

Chapter 5
Experimental Development of the Process

Objectives of Chapter 5

- Discuss the results obtained during the experimental investigation and their implications.
- Relate the results to the theory of precipitation and adsorption.

Presented here are the results obtained for the experimental investigation into the different aspects of this project. The experiments were carried out according to the methods described in Chapter 4 and the results will be interpreted according to the theory discussed in Chapter 3.

5.1 Batch Precipitation Study

The batch experiments were intended as an investigation into the thermodynamic feasibility of the system. The thermodynamic feasibility was based on reagent consumption, selectivity between the base metals and the alkaline earth elements, selectivity between calcium and magnesium, and the influences of environmental parameters such as temperature. The results presented are from the last of three sets, for which the experimental and analytical techniques were progressively improved. The same trends in selectivity were observed in all three sets of which the final set was more quantitative. From the initial experiments it appeared that equilibrium was attained quickly and the calcium and magnesium concentrations varied little after the addition of the fluoride has ended. The observations were made for another two hours after the feeding. These initial experiments will not be discussed, but their results are provided in Appendix E. It may be possible that given a longer equilibrium time, the observed concentrations might have been lower, but it is doubtful if these decreases would have been larger than the inherent experimental error.

The results presented are based on the analysis of the metal ion concentrations. A factor was used to adjust the analysis so that the concentrations of the non-reacting

species would match their initial concentrations. These factors would encompass any errors made during the dilution of the samples. In all of the batch experiments the precipitation of the base metals was not detected. This was confirmed by XRF analysis for which the base metal concentrations were less than 1% by weight and in the same ratio as for the mother liquor, indicating that they are only present as mother liquor inclusions. Some computer thermodynamic simulations were also carried out to explain the observed trends. More information on the simulations will be subsequently given.

5.1.1 Computer Thermodynamic Calculations

The thermodynamic calculations were performed with Outokumpu HSC Chemistry Ver. 4.1, using its Equilibrium module. The module employs a Gibbs energy minimisation routine to calculate the equilibrium composition. The program does not provide any models for calculating the activity coefficients; although simple user defined models may be entered. For the calculated values given here, activity coefficients of unity were used. The other options selected in the program were the use of the Criss-Cobble extrapolation for species with missing heat capacity data and the "Invariant phases" option for expected precipitated phases. The latter option would treat the precipitate as separate phases, assigning an activity of unity to them.

Pectora roborant cultus recti

A number of species were excluded after the initial simulations. Most of the species excluded was based on a low equilibrium presence of it. Of the solid phases, gypsum ($CaSO_4.2H_2O$), anhydrite ($CaSO_4$) and cobalt fluoride (CoF_2) were excluded. The calcium sulphate salts were excluded since HSC calculated a too low solubility for them. The typical calcium concentration predicted was ~0.2 g/ℓ for which the experimental concentration was ~0.6 g/ℓ. Cobalt fluoride was excluded since the simulations predicted large amounts of CoF_2 precipitating, which was not observed.

It can be expected that the computer-simulated values would not compare well with the experimental data owning to the assumption of ideality for a high ionic strength system. The aim of the simulation was not to predict the experimental data, but to use it to explain some of the phenomena observed. The simulated values will be compared where necessary.

5.1.2 Fluoride Addition

In solvent extractions circuits such as in Nkomati much higher magnesium concentrations can be tolerated than calcium. It is more important to control calcium to avoid gypsum precipitation than it is to control magnesium. For this instance the fluoride consumption would be lower if calcium could be precipitated in preference to magnesium. It was the aim of the initial set of experiments to evaluate the behaviour of the system at fluoride additions lower than the total stoichiometric demand for both. Presented in Figure 5.1 are the results of the experiments in terms of the percentage of calcium and magnesium precipitated.

It is seen that magnesium precipitation dominated for all the sub-stoichiometric additions of fluoride. Calcium precipitation was always below 20% up to an addition of 75%. Between the 75% and the 100% fluoride addition, the percentage of calcium precipitated increase more than fourfold to 85%. The percentage calcium and magnesium precipitated continued to increase for the 10% excess addition, with calcium gaining more compared to magnesium. Therefore, for the solution under investigation, the removal of calcium requires an excess addition of fluoride in terms of the stoichiometric demand for both calcium and magnesium.

Included in the results are two sets for the 100% addition. The second set for the experiment was carried out to have an indication of the repeatability of the results. From the percentage precipitated the two sets of results appear to compare well. The difference in the percentage precipitated was only 0.2% for both the calcium and the magnesium.

Compared in Figure 5.2 is the simulated percentage precipitated to the experimental results. The experimental results for magnesium are all below the simulated values indicating that the activity of magnesium in solution is lower than predicted. For calcium, the simulated results also show the dominance by magnesium, but the point at which calcium increases is at a much lower fluoride addition. For the calculated results the percentage of calcium precipitated increases monotonically after the 40% addition, while the experimental results increases slowly up to 75% after which a marked increase is seen. The fact that the experimental results for calcium does not show such a distinct point of increase, can be seen as a manifestation of the kinetic

nature of precipitation processes. Although magnesium was thermodynamically favoured at the low additions, both calcium and magnesium were supersaturated and the precipitation reactions proceeded in parallel.

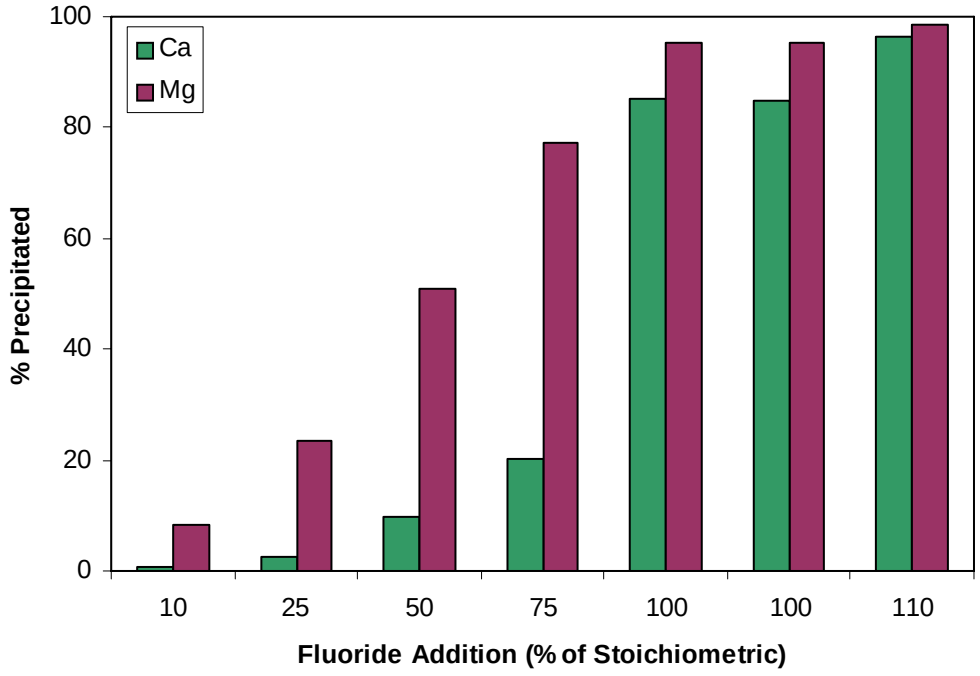

Figure 5.1 The percentage of calcium and magnesium precipitated at different fluoride additions.

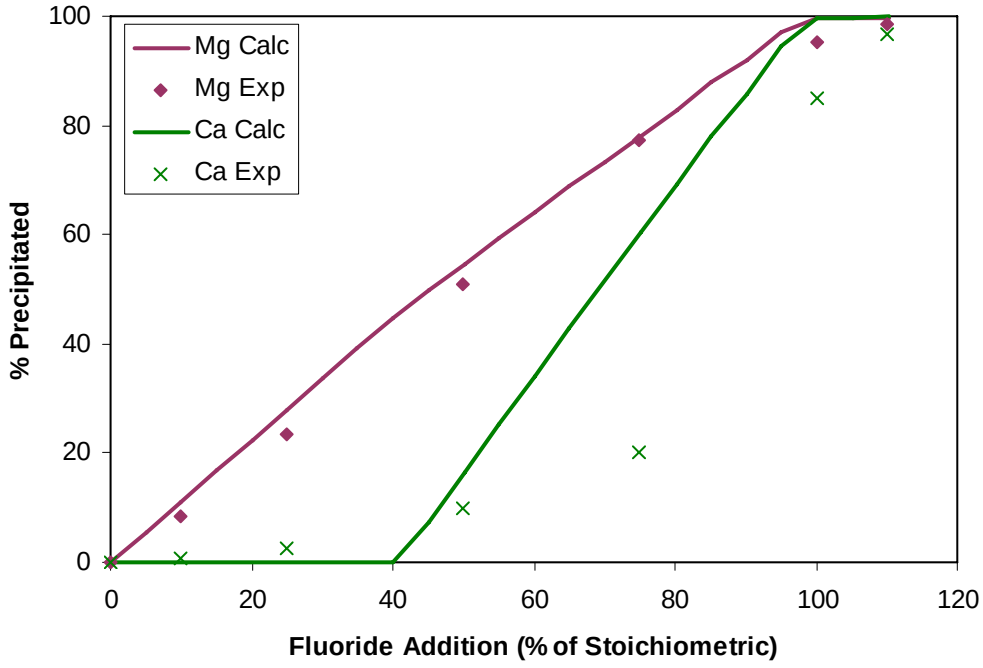

Figure 5.2 Comparison between experimental data and the thermodynamic simulations.

For the control of gypsum, the concentration of the calcium rather than its removal is of more importance. In the preceding results the dilution effect of the added fluoride solution was not evident. Presented in Figure 5.3 are the concentrations of calcium and magnesium after precipitation for the different fluoride additions.

The same trend was predicted from the thermodynamic simulations as was observed in the experimental data. The calcium only started to decrease at high fluoride additions and to remove the calcium to low concentrations the fluoride addition should be in excess of the stoichiometric value.

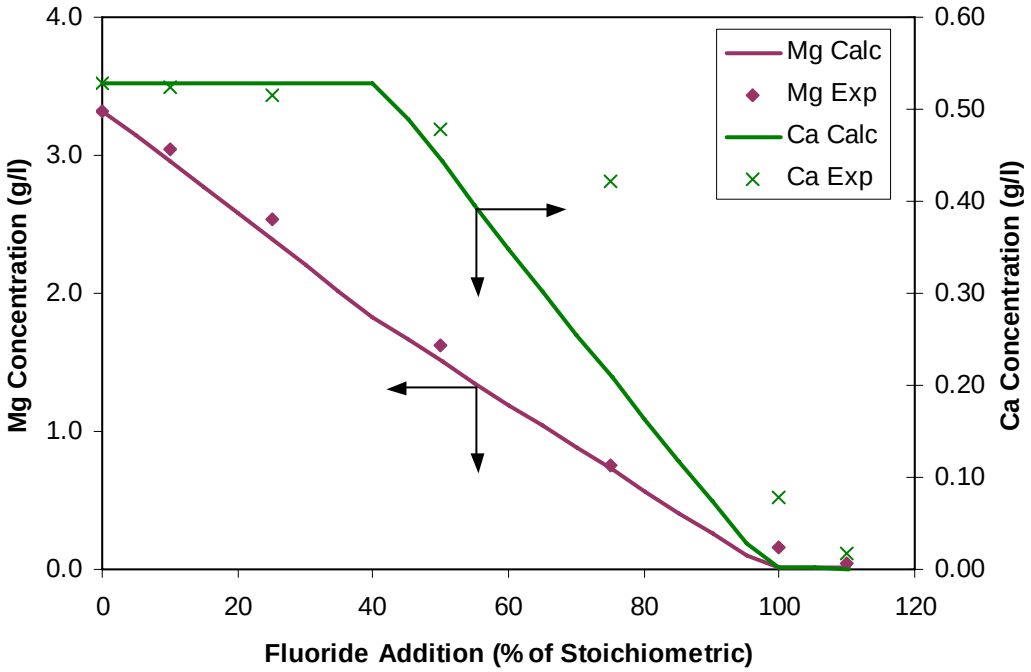

Figure 5.3 Final concentrations of calcium and magnesium at different fluoride additions.

As an example, for the 100% addition 0.473 g calcium was removed per litre of solution treated. As a result of the dilution from the addition of the 5% volume of fluoride solution the solution can accommodate 0.477 g calcium per litre before reaching is initial concentration. This effect would increase with an increase in the volume of the fluoride solution. For the application of the fluoride precipitation process, the advantage of the dilution effect is outweighed by its implications on the downstream processes. The size of the downstream equipment would need to increase

to accommodate the extra volume of solution. The concentration of the valuable metals would also decrease, resulting in a lower driving force during solvent extraction. The volume of effluent that needs to be treated from the plant would also increase. It was for these reasons that the volume of the fluoride solution was selected at a low value of 5% of the solution treated.

The reason for the dominance of magnesium precipitation is the result of its high concentration and therefore, high thermodynamic activity. On a molar scale, the initial concentration of magnesium is approximately tenfold the concentration of calcium. Therefore, in the preceding graphs a 1% change in the amount of magnesium precipitated would consume the equivalent amount of fluoride as for a 10% change in the calcium precipitated. The high consumption for magnesium precipitation can be better seen in Figure 5.4.

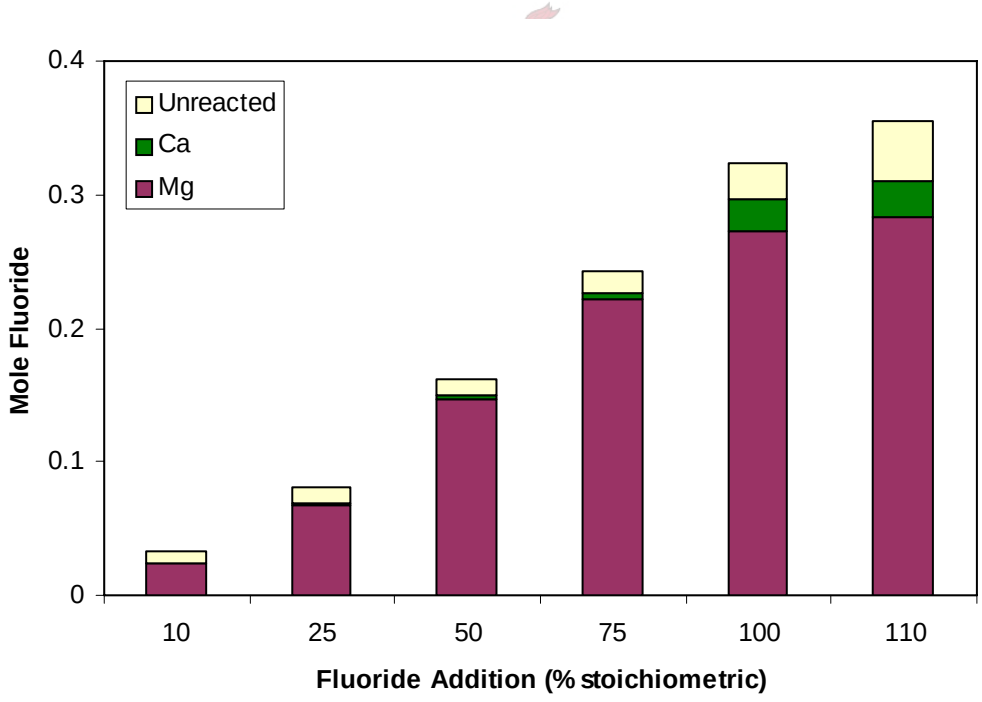

Figure 5.4 Fluoride consumption during precipitation.

It is seen that the bulk of the fluoride is consumed in the magnesium precipitation reaction and it is only at high fluoride additions that the consumption for the calcium reaction becomes noticeable. The amount of unreacted fluoride also increases with an

increasing addition. This is a result of the solubility product forcing more fluoride to react at the lower addition as a result of the higher concentrations of calcium and magnesium.

5.1.3 Identity of Soluble Fluoride

For this study ammonium fluoride (NH_4F) and hydrogen fluoride (HF) were selected based on their accompanying cation. The results obtained for the 100% addition of the fluoride are summarised in Table 5.1.

Table 5.1 Comparison between the 100% addition of ammonium and hydrogen fluoride.

	NH_4F	HF
% Magnesium Precipitated	95.20	63.05
% Calcium Precipitated	85.10	29.55
pH of resulting solution	5.17	2.50

A much higher completion of the reaction is obtained for ammonium fluoride compared to hydrogen fluoride for both calcium and magnesium. It was initially assumed that this is the effect of the complexation of fluoride to form the hydrogen and hydrogen bi-fluoride complexes, reducing the concentration of the free fluoride. The same trend was predicted during the simulations. Given in Figure 5.5 is the speciation of the fluoride predicted from the simulations.

This confirmed the complexation of the free fluoride to form the hydrogen fluoride complex. This would reduce the supersaturation resulting in the lower completion of the reactions. The other complexes that are formed with the fluoride are the base metals mono-fluoride complexes.

The resulting pH from the addition of hydrogen fluoride would also be problematic. In the application, the pH would need to be adjusted after precipitation to 5.2 for the solvent extraction steps. This would require the addition of a base other than a calcium base. The acidic fluoride solution would also be more corrosive. In comparison to this, the addition of ammonium fluoride would have almost no effect on the pH.

In summary, the use of hydrogen fluoride results in the lower completion of the reactions as a result of the complexation of the fluoride ions. To maintain a high level of precipitation, a much higher addition of fluoride will be required. The resulting acidic solution would be more corrosive and the pH would need to be adjusted again, using a base other than a calcium base.

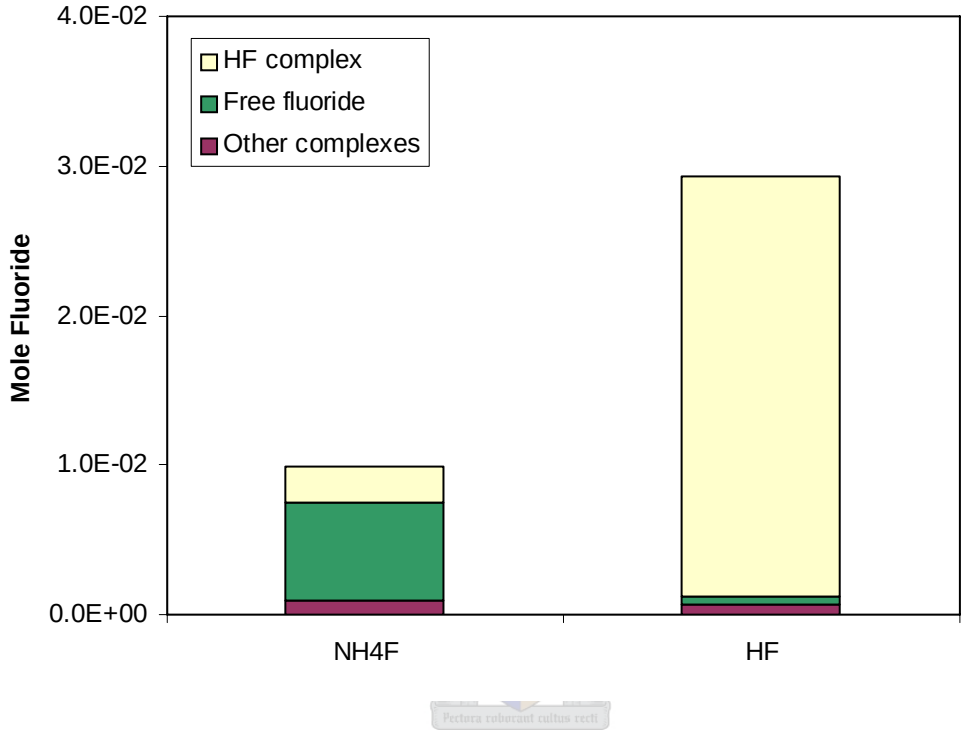

Figure 5.5 Fluoride speciation predicted from simulations.

5.1.4 Magnesium : Calcium Molar Ratio

It could be reasoned from the lower solubility of calcium fluoride compared to magnesium fluoride, that it would be thermodynamically favoured. In the preceding results it was seen that magnesium dominated as a result of its high concentration. It is therefore possible that there exist a set of conditions for which the dominance would change from magnesium to calcium. This was investigated in terms of the calcium to magnesium molar ratio. The calcium concentration would always be constant at saturation coming from the iron precipitation step, whereas the magnesium concentration might vary depending on the mineralogy of the ore concentrate and the leaching conditions. For the experiments, the calcium concentration was kept constant at 0.57 g/ℓ while the molar ratio of magnesium to calcium was varied. To this, a

constant amount of fluoride was added, equivalent of the stoichiometric value required for calcium alone. Presented in Figure 5.6 are the results obtained for these experiments.

Calcium dominated at low ratios, after which there was a transition to magnesium dominance. From the simulations, the transition was calculated at a ratio of 3. Experimentally the transition was observed between the molar ratio of 3 and 4. The final experimental point represents the solution encountered in the proposed application at a magnesium to calcium molar ratio of 10.3. At these conditions the precipitation of magnesium dominated completely with almost no calcium precipitated. In Figure 5.7 the consumption of fluoride is presented.

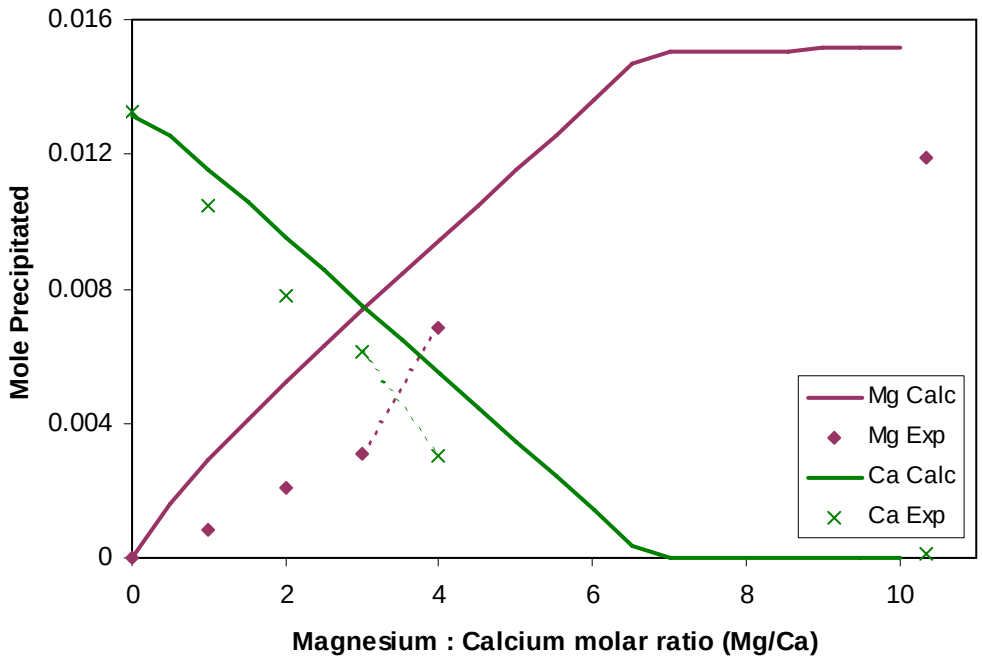

Figure 5.6 Effect of the calcium : magnesium molar ratio.

The fraction of unreacted fluoride increases with an increasing ratio until the dominance changes to magnesium, from where it decreases again. This behaviour was not reflected in the simulations for which the free fluoride only decreased with an increasing magnesium ratio, as would be expected from the solubility product. The

presence of magnesium appear to have an inhibiting effect on calcium fluoride precipitation. This is can be seen in Figure 5.8.

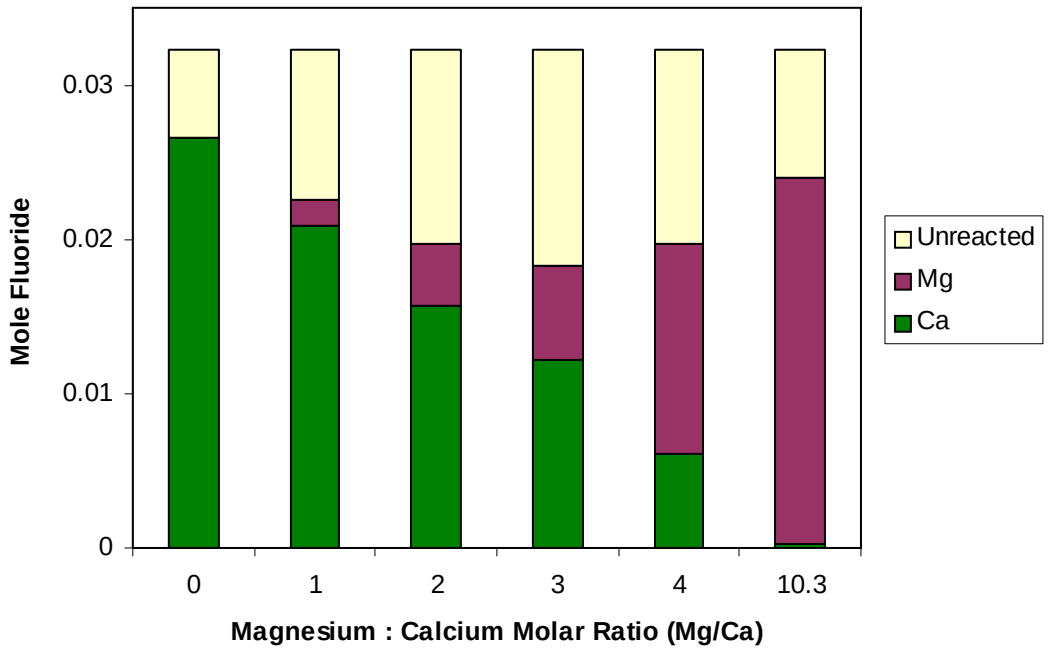

Figure 5.7 Fluoride consumption at the different magnesium : calcium molar ratios.

Given in Figure 5.8 are the results for experiments where calcium and magnesium was precipitated in the absence of each other, with a stoichiometric amount of fluoride added. The experiments where conducted with the full background of the base metal solution. The percentage calcium precipitated individually is higher than in the presence of magnesium, while no real difference is observed for magnesium. From this it appears that magnesium inhibits calcium fluoride precipitation to a small extent, but this would require further research to proof it.

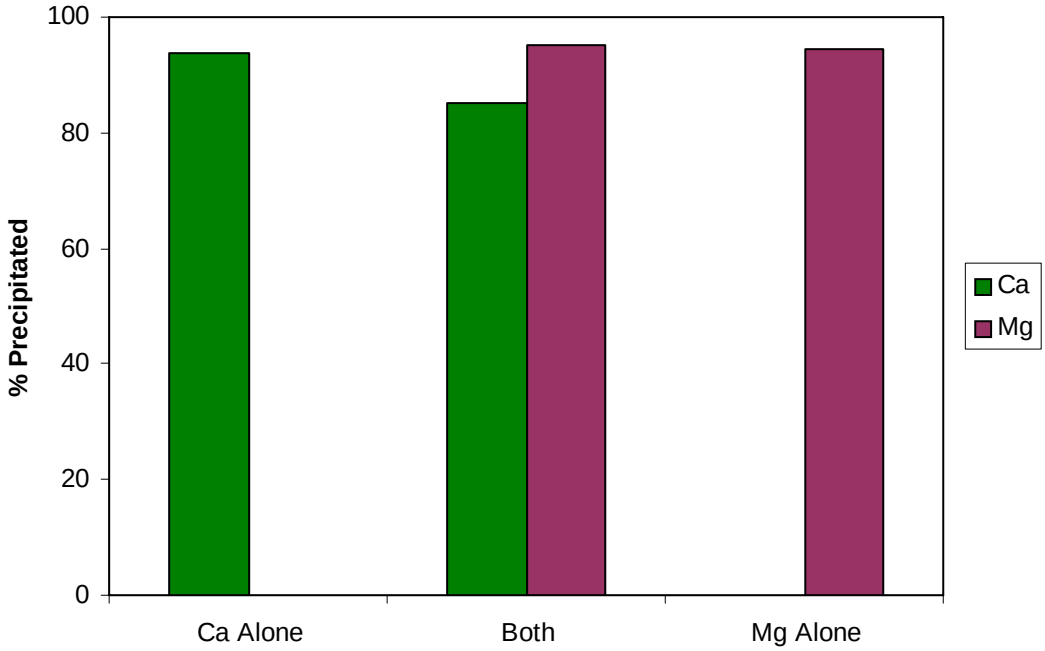

Figure 5.8 The precipitation of calcium and magnesium in the absence of each other and together.

5.1.5 Fluctuations of Temperature and Fluoride Addition

Temperature was selected to be investigated as external variable on the system. It was decided to investigate its influence relative to the fluoride addition in the form of a factorial design experiments. A low and high level of 45°C and 65°C were selected for the temperature and 90% and 110% for the fluoride addition. A centre run at 55°C and 100% addition was included. Presented in Figure 5.9 are the results obtained for calcium and in Figure 5.10 for magnesium.

The percentage of calcium and magnesium precipitated showed both a positive correlation with temperature and fluoride addition. For the selected levels it is seen that the fluoride additions has a larger effect relative to temperature. The centre runs are above the linear surface for both calcium and magnesium. This indicated the amount of precipitate formed is more sensitive for a variation of fluoride addition at sub-stiochiometric levels. This is expected as a result of the solubility product. Below the stoichiometric addition, the calcium and magnesium are present in excess and would readily react with any of the fluoride. Above the stoichiometric addition the

calcium and magnesium are depleted and much higher fluoride concentrations are needed to have the same ionic product as for below the stoichiometric addition.

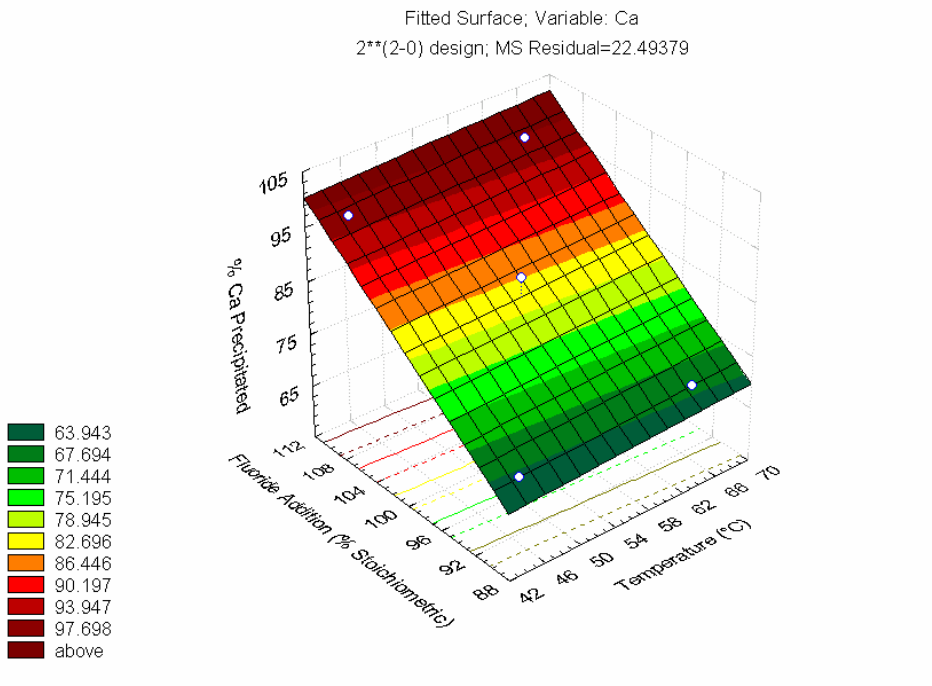

Figure 5.9 Response of calcium removal as a function of fluoride addition and temperature.

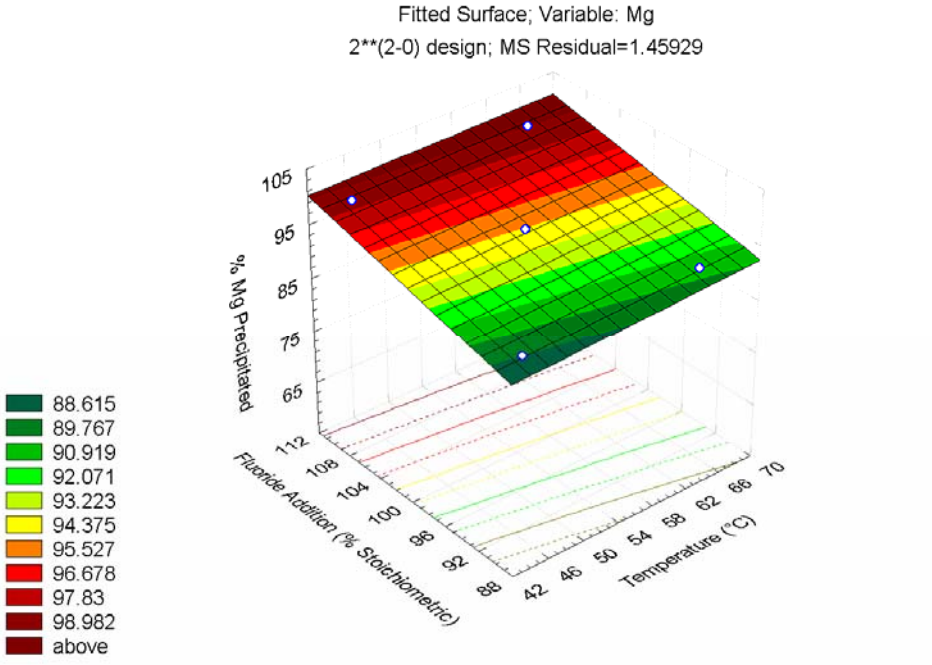

Figure 5.10 Response of magnesium removal as a function of fluoride addition and temperature.

The relative effects of temperature and fluoride addition can better be seen in the interaction plot (Figure 5.11). Similar results are obtained for the same addition at the different temperatures. With an increase in temperature from 45°C to 65°C the percentage of calcium or magnesium precipitated increased by less than 2%. For the same temperature the percentage calcium and magnesium precipitated increased by approximately 32% and 9%, respectively, as a result of the fluoride addition. For the selected values of the temperature and fluoride addition, the latter had the largest effect on the precipitation of calcium and magnesium.

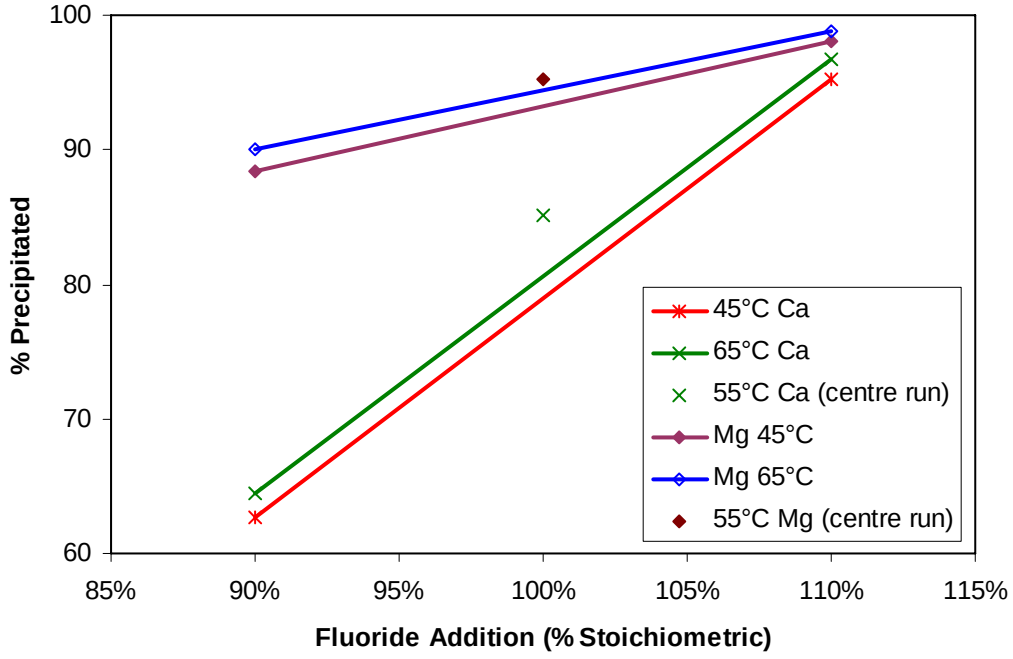

Figure 5.11 Comparison of the effect of temperature and fluoride addition on calcium and magnesium.

5.1.6 Solubility Product

The solubility product for calcium and magnesium is defined by Equation 5.1 where *M* represents Ca or Mg.

$$K_{s,c} = \left(M_{eq}^{2+}\right)\left(F_{eq}^{-}\right)^2 \qquad \textbf{Equation 5.1}$$

The solubility product is required to evaluate the supersaturation ratio, which for the current application is calculated by:

$$S_c = \left(\frac{[M][F]^2}{K_{s,c}} \right)^{\frac{1}{3}} \qquad \textbf{Equation 5.2}$$

The approach normally taken is to use the thermodynamic solubility product (K_{sp}) and calculate the activities of the species with a model such as the Debye-Hückel equation. In the current study the ionic strength is too high for the application of the Debye-Hückel and although there does exist models for higher ionic strengths such as the Pitzer model, the parameters are not readily available at the temperatures and compositions of this study. An experimental solubility product is therefore required.

For the estimation of the experimental solubility product the free calcium, magnesium and fluoride ion concentrations are required. Only the total concentrations are available from the measurements. The solubility product could be based on this if it is assumed that the complexation of the ions is minimal compared to the free ion concentration. It was observed that this is not necessarily true. Provided in Table 5.2 are the solubility products calculated from the total ion concentrations for different experiments. It is seen that a lower solubility product is obtained for calcium when it is precipitated in the absence of magnesium while such a large difference is not seen for the solubility product of magnesium.

Table 5.2 Experimental solubility product based on the total concentrations.

	Calcium solubility product	Magnesium solubility product
Published K_{sp} (Söhnel & Garside, 1992)	3.55×10^{-11}	8.51×10^{-9}
Calcium Alone	3.19×10^{-8}	-
Magnesium Alone	-	1.69×10^{-6}
Combined	4.64×10^{-7}	1.50×10^{-6}

In the absence of a better value the solubility product calculated in the combined experiments will be used to estimate the super saturation ratio.

5.2 Continuous Precipitation Study

With the continuous experiments the behaviour in an MSMPR reactor was investigated, as this is the type of system envisaged for the application of the precipitation process. This part of the study is focussed on the characteristics of the formed precipitate and how it is affected by parameters such as residence time and mixing. The discussion of the results would be more descriptive, for the aim of the investigation was only to observe the effects rather than to explain it.

5.2.1 Characterisation of Precipitate

The characteristics of the precipitate formed during the different experiments were relatively consistent with most of the variations being less than the deviations encountered of a single sample for the particular measure. The characteristics of the precipitate would therefore only be discussed once, after which the particle size distribution would be used as a measure to compare the results obtained for the different parameters. The particular experiment that will be used for the discussion of the precipitate characteristics was conducted with a 30 minutes residence time in a single reactor.

General

For the continuous experiments a 10% excess addition of fluoride was used. The percentage of the calcium and magnesium precipitated were in excess of 94% for both. As a result the magnesium to calcium molar ratio of the precipitate was in the order of 10:1. The precipitate was not retained in the reactors and operated at a solids volume concentration of 3.0×10^{-6} m^3/m^3 (volume precipitate/volume solution). The dry mass of precipitate formed per volume solution was 9.6 kg/m^3.

The supersaturation for the reactor was calculated using the experimental solubility product from the batch experiments. The supersaturation ratio for calcium fluoride was in the region of 1.5 and for magnesium fluoride 2. Using this and interfacial free energies found in literature, the critical nucleus radius (r^*) was calculated at 2.84×10^{-9} m and 5.85×10^{-10} m for calcium and magnesium fluoride, respectively. This amounts to 4500 (CaF_2) and 65 (MgF_2) solute entities required to form the

critical nucleus. From these high values it would appear that primary nucleation would not be dominating in the system.

Particle Size Distribution

The particle size distribution obtained from the Malvern analysis reported the size of the particles as a % volume density distribution. This is related to the mass density distribution (m(L)) by the density of the particles. The typical distribution obtained is indicated in Figure 5.12. The size is given for a volume equivalent sphere. A bimodal distribution was observed to varying extents for all of the experiments, for which the smaller peak represented approximately 13% of the volume. A simple explanation for this behaviour did not present itself, for this is not normal for an MSMPR reactor. Initially it was thought to be the calcium and magnesium fluoride having two separate particle size distributions, but later analysis proofed this wrong. No correlation to the experimental conditions could be detected. This could be the result of secondary processes during precipitation or it might be the result of the handling of the precipitate afterwards.

The Malvern analysis automatically provide the surface based mean size ($L_{3,2}$) and the volume based mean size ($L_{4,3}$). The latter would be the same as for the mass based mean size for a constant density of the particles. The analysis also presents the span of the distribution, which would be the equivalent to the coefficient of variance of the distribution.

For the size distribution given below the results were:

$L_{3,2}$: 10.35 μm

$L_{4,3}$: 18.75 μm

Span : 1.421

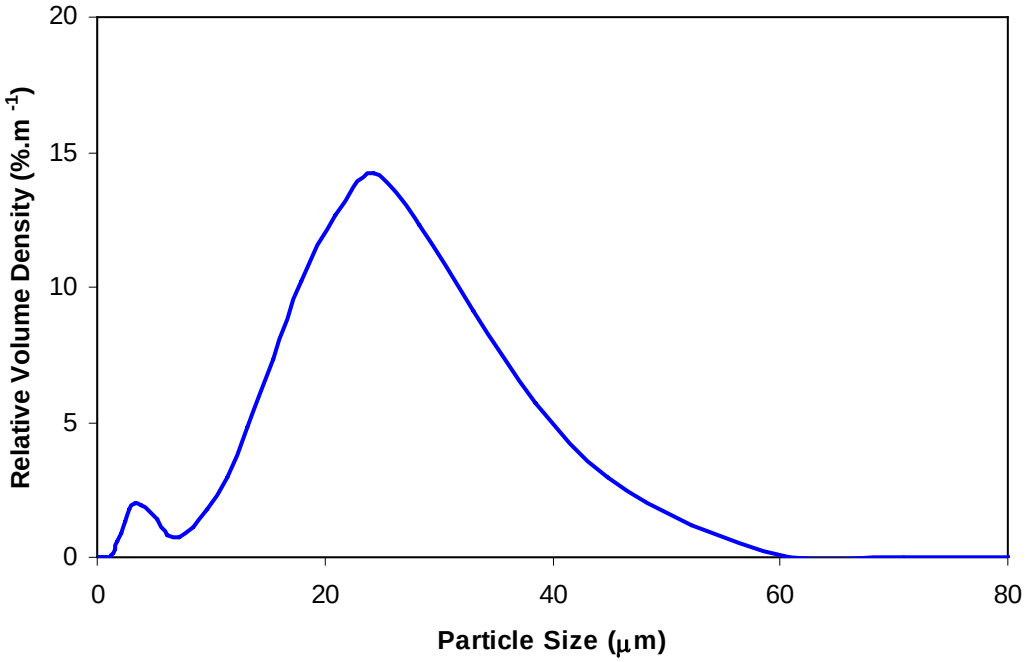

Figure 5.12 Typical size distribution observed for the experiments.

The number density distribution was calculated from the volume density distribution to be used in the MSMPR plot. Provided in Figure 5.13 are the MSMPR plot for the particular experiment with a straight line fitted to the data. The data is observed to deviate from the straight line at the smaller particle sizes. This could be attributed to the smaller peak of the volume density distribution. The straight line does not present good fit, but it would still give an indication of the apparent nucleation and growth rates.

Using the method as described in the literature review (Section 3.1.5, p.67), the crystal growth rate can be deduced from the gradient of the plot and the nucleation rate from the intercept. For the data, the apparent nucleation and crystal growth rate were 1.58×10^{7} nuclei/m^3.s and 1.43×10^{-9} m/s, respectively. These were the highest nucleation and crystal growth rates observed during the experiments.

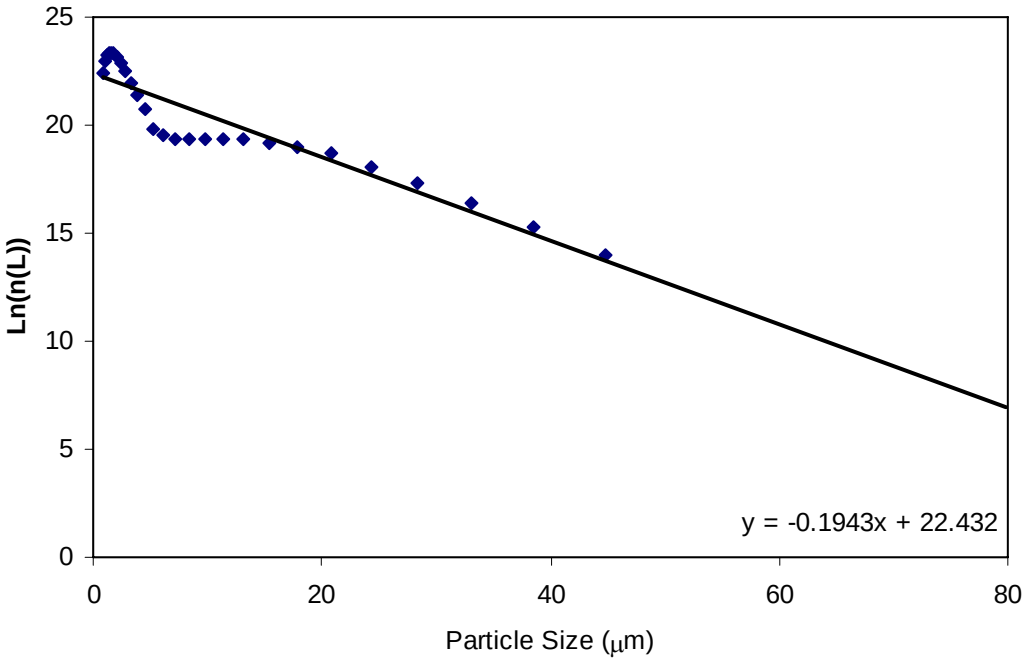

Figure 5.13 MSMPR plot for the data presented above.

Crystal Habit

Presented in Figure 5.14 is a SEM photo of the precipitate. Distinct clusters of the size ~20 μm are seen which appears to be made up of a large number of smaller particles. Provided in Figure 5.15 is an enlargement of a single particle. No distinct crystal faces could be seen for which a cubic shape is expected for the calcium fluoride crystals and a tetragonal shape for the magnesium fluoride. This brought into doubt the crystallinity of the precipitate. The clustered particles appear to be highly agglomerated with a rough surface.

The X-Ray diffraction pattern of the precipitate was determine to ascertain whether the precipitate has crystalline phase or is amorphous. Presented in Figure 5.16 is the XRD pattern of the precipitate. The pattern was characterised by very low counts, although faint peaks could be distinguished from the background noise. These peaks appeared to correspond to the theoretical lines of magnesium fluoride. The distinct patterns for calcium and magnesium fluoride would have been expected if they where present as well defined crystals. The pattern for calcium fluoride was not detected and only the faint peaks for magnesium fluoride. This contributes to the impression that

the precipitate is an amorphous phase. Another possible explanation for the absence of the well defined peaks is the crystals being too small resulting in the broadening of the peaks.

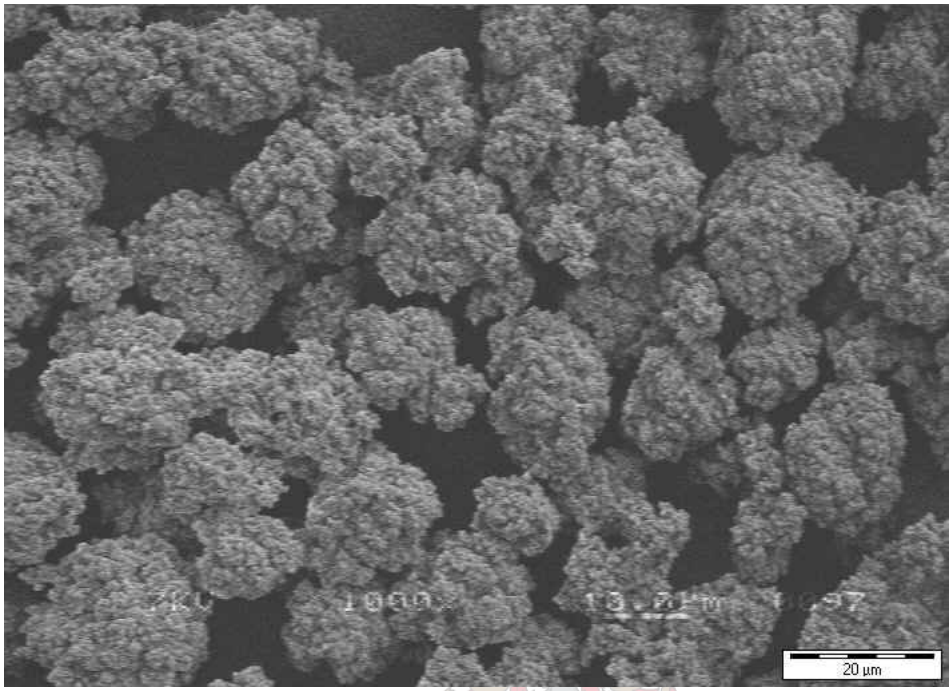

Figure 5.14 SEM photo indicating the habit of the precipitate (1000x enlargement).

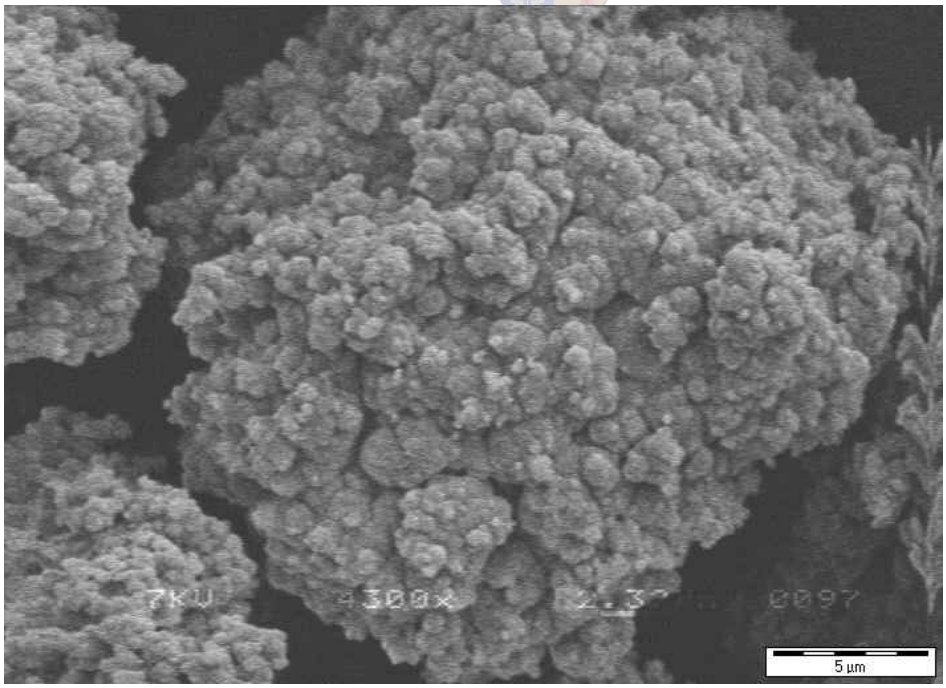

Figure 5.15 Enlargement of a single particle (4300x enlargement).

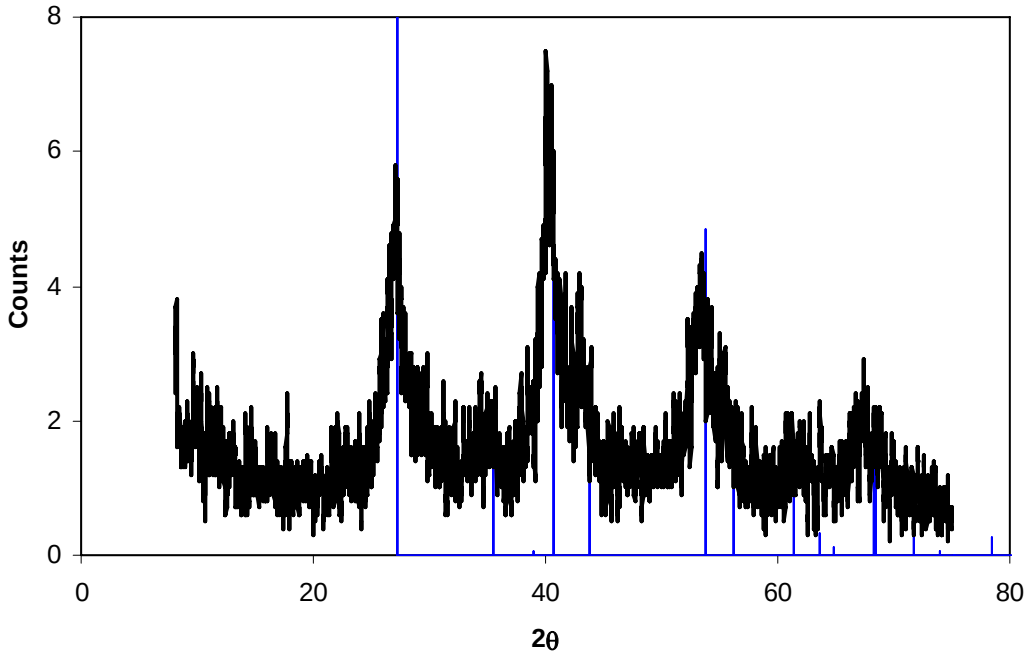

Figure 5.16 XRD pattern of the precipitate.

The system also had the tendency to form a flaky translucent scale layer in the reactors. Presented in Figure 5.17 is a photograph taken from the top of the bulk reactor. The scale layer is observed on the sides of the reactor with some of the loose flakes lying at the bottom of the reactor. During the runs some of the flakes became dislodged from the walls resulting in the blockages of the in- and outlets of the reactors. This may be a serious problem for the large scale implementation of the process.

Figure 5.17 Example of scaling observed in the bulk reactor.

Mother Liquor Inclusions

XRF analysis of the trace elements revealed the precipitate to contain 7400 ppm Ni and 440 ppm cobalt, which equates to an 0.23% loss of the valuable base metals. The ratio of nickel to cobalt was therefore 17:1, which is similar to the ratio of nickel to cobalt in the mother solution (18.5:1). From this result it appears that the nickel and cobalt were present as mother liquor inclusions within the precipitate. Using the concentration of nickel, the mass of mother liquor captured per mass of precipitate was 0.25 kg/kg. This amounted to 25%, which is of the same order as the TGA results that indicated the precipitate to contain 9% mother liquor. The lower result for the TGA could be due to the evaporation of the water during the drying of the precipitate before analyses.

As a result of the mother liquor inclusions within the precipitate it may not be environmentally innocuous as was initially thought. Further investigation is required into this to ascertain the potential risk and it may be required to that the precipitate be dispose of in a lined pond to avoid the potential release of the base metals into the environment.

Filterability of the Precipitate

The filterability of the precipitate will be discussed in terms of the cake filtration resistance (α_F). Initially intended as the characteristic for comparison, it was observed that the variance of the filtration resistance for a single experiment where comparable with the variance observed for the different experiments. This made filtration resistance an insensitive measure of comparison. It also indicated, as was observed for the other properties, that the quality of the precipitate was not adversely affected in the range of parameters investigated. The typical filtration resistance observed where 4.0×10^9 $m^3/kg.m^2$.

5.2.2 Residence Time

Provided in Figure 5.18 are the relative volume density distributions of the precipitate at various residence times. The ammonium sulphate solution was used for the 120 minute residence time and the base metal solution for the 30 minute residence time. The 60 minute residence time was evaluated using both solutions and would serve as a comparison between the two. The size distribution of the 120 minute residence time appear to have a larger mode whereas for the other it appears to be the same. The two 60 minute distributions appear to have a larger span compared to the 30 minute distribution. These values are quantified in Table 5.3 for comparison.

For the 30 and 60 min residence times no large variations in the mean particle size was observed. It is seen for the two 60 minute experiments that a larger surface area mean size was obtained for the ammonium sulphate solution whereas a larger volume mean size for the base metal solution. The span was expected to stay constant since the residence time should not have an influence on the coefficient of variance (Van Rosmalen et al., 2001). The variance observed may be the result of the bimodal distribution.

Using the size distribution to estimate the apparent nucleation and growth rates it is observed that both decrease with an increasing residence time. The nucleation rates and the growth rates of the base metal solution and ammonium sulphate solution

compare well and therefore the results obtained for ammonium sulphate are regarded as representative of the base metal solution.

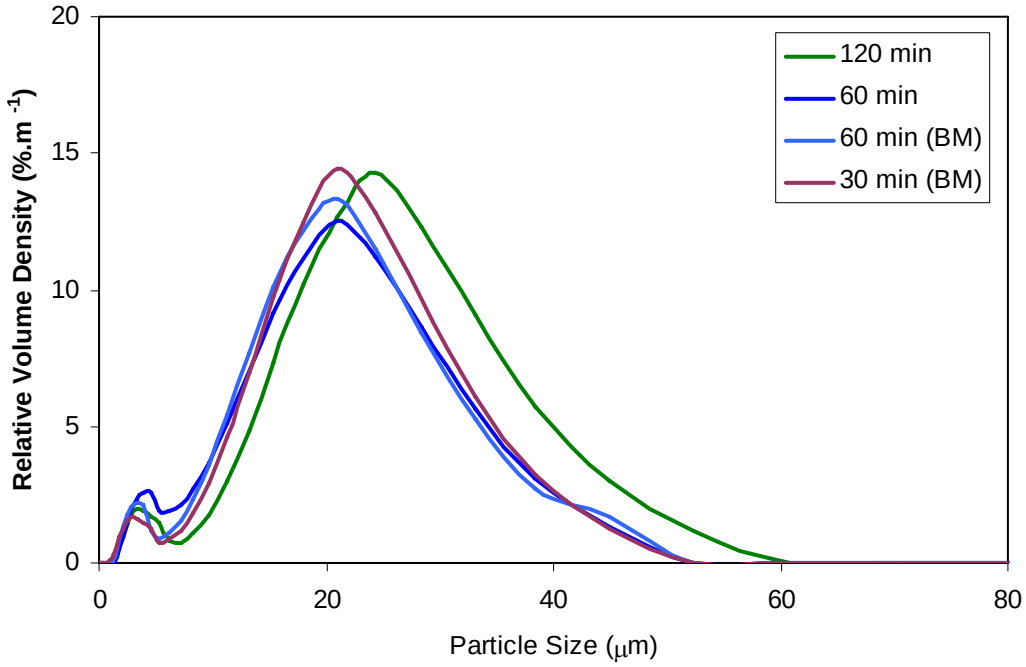

Figure 5.18 Size distributions for the different residence times.

Table 5.3 Results for the different residence times.

Residence Time (min)	$L_{3,2}$ μm	$L_{4,3}$ μm	Span	Nucleation #/m^3.s	Growth Rate m/s
30 (BM)	10.35	18.75	1.421	1.58×10^{7}	1.43×10^{-9}
60 (BM)	10.05	17.80	1.482	6.93×10^{6}	7.44×10^{-10}
60	10.27	17.69	1.514	6.83×10^{6}	7.47×10^{-10}
120	12.00	21.41	1.443	2.49×10^{6}	4.30×10^{-10}

The residence time stated was for the reactor and does not include the extra time spent in the product beaker. To quantify the effect of the product beaker a sample was taken at the reactor outlet to be analysed. The largest deviation was observed for the 30 minute experiment for which the amount of calcium and magnesium precipitated increased by 0.2% and 2.5% in the product beaker. The bulk of the solid formation occurred within the reactor and the results should therefore reflect the conditions

inside the reactors. It is still possible that some secondary changes could have taken place, but these could not be quantified.

5.2.3 Effects of Mixing

The parameter field used in the experiments with their representative values are presented in Table 5.4. The average energy dissipation was calculated from the electrical energy consumption of a stirrer. A comparison of these values to what is expected on a plant scale (Figure 3.15, p.81) revealed the micromixing to be in the correct range and the macromixing to be in the lower than on a plant scale.

Table 5.4 The experimental parameters and their representative values.

Level of mixing	Experimental Parameter	Representative Values
Macromixing	Circulation Pump Flowrate	Circulation Time
	300 ml/min	200 s
	1080 ml/min	55 s
Mesomixing	Inlet Volumes	
	400 ml	
	~0 ml	
Micromixing	Stirring Rate	Average Energy Dissipation
	520 rpm	2.2 W/kg
	900 rpm	4.6 W/kg

The control experiment used for comparison was carried out at the high levels of macro- and micromixing and the low level of mesomixing for both inlets. The effects of the different scales of mixing will now be discussed separately.

Macromixing

Illustrated in Figure 5.19 are particle size distributions obtained at the two levels of macromixing. It is seen that an increase in macromixing results in a decrease in the mode and the span of the distribution. The volume based mean size decreased from 22.29 μm to 16.40 μm with an increase in macromixing. This is contradictory to the results of Torbacke and Rasmuson (2001) and Van Leeuwen et al. (1996) for which the mean particle size increased with increasing circulation rate.

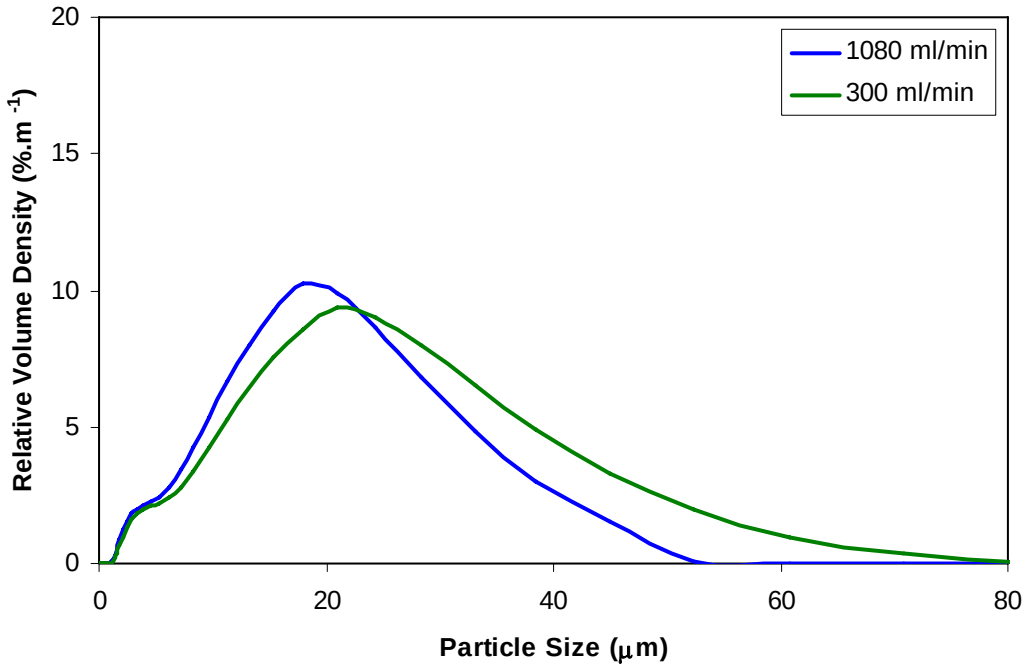

Figure 5.19 Effect of macromixing of the particle size distribution.

Mesomixing

An inherent flaw in the three-zone experiment is that the mean energy dissipation rate, and therefore the micromixing, in the reactors would change, if the volume of the reactor were changed at constant stirrer rate. In the current implementation, where one of the inlet reactors were bypassed for mesomixing, the total energy dissipated would also be lower owing to a decrease in stirrers. The results for the two mesomixing experiments could therefore only be compared to one another since their micromixing would be similar.

The size distributions for the two mesomixing experiments appear to fit each other (Figure 5.20), with the high level mesomixing (small inlet volume) of the sulphate stream shifted to a larger particle size. The volume based mean size obtained where 18.11 μm at the high level of sulphate mesomixing and 16.67 μm at the high level of fluoride mesomixing.

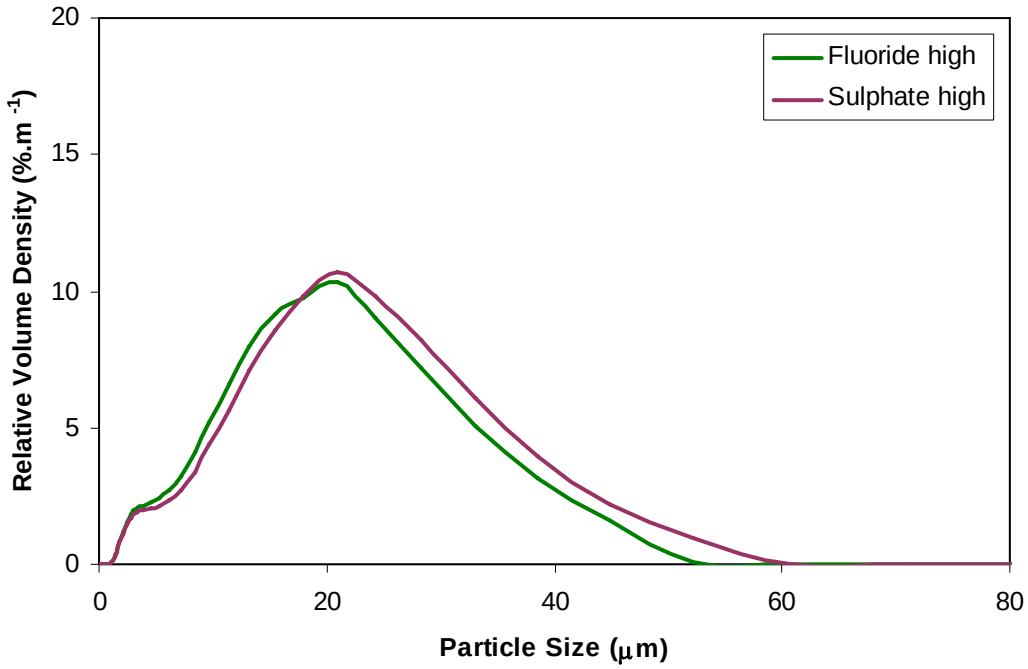

Figure 5.20 Effect of mesomixing on the particle size distribution.

Micromixing

It is observed that the volume density size distribution is shifted to smaller particle sizes with an increase in stirring rate (Figure 5.21). Accordingly, the volume based mean size shifted from 21.12 μm to 16.40 μm with an increase in stirring rate (micromixing). The decrease of particle size with increasing micromixing was also observed by Torbacke and Rasmuson (2001) in their studies.

5.2.4 Overview

For the parameters investigated some variation in the characteristics of the precipitate were observed but these were relatively small. In terms of the volume based mean particle size, it varied from 17.69 μm to 21.41 μm during the residence time experiments and 16.40 μm to 22.29 μm during the mixing experiments. From this, it appears that the process could easily be scaled-up to produce a precipitate of the same quality as observed on a laboratory scale. From the investigation it was also observed that the precipitate tends to form scale and have a high fraction of mother liquor inclusions. These are two areas that may be improved upon.

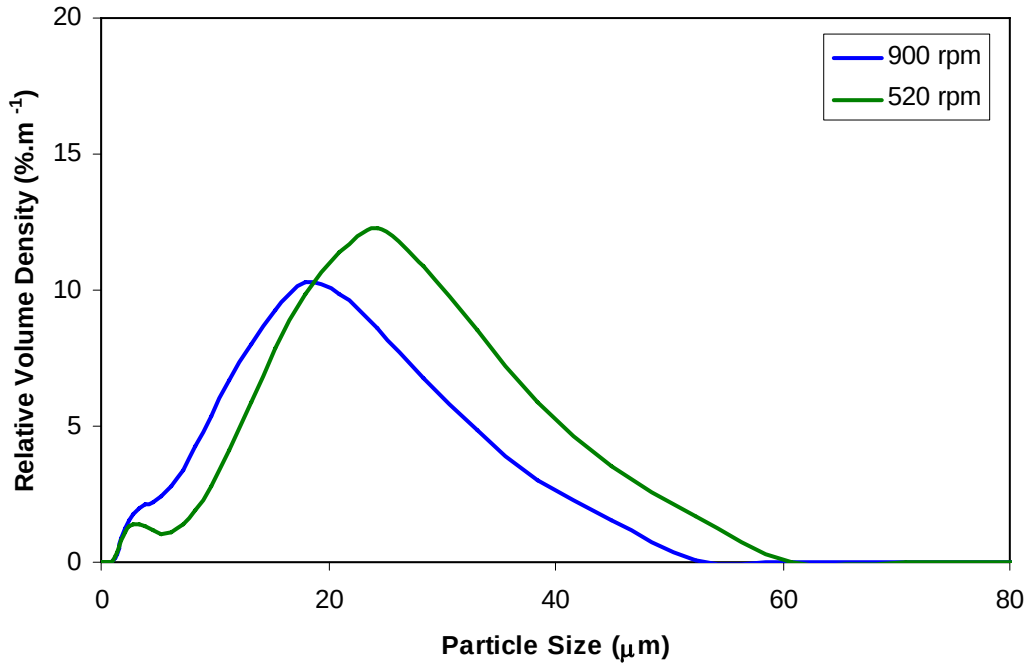

Figure 5.21 Effect of micromixing on the particle size distribution.

5.3 Activated Alumina Adsorption

Discussed here are the results obtained from the experimental study on the feasibility of the use of activated alumina to adsorb the unreacted fluoride. The investigation may be divided into equilibrium studies through batch experiments and continuous studies through the column experiments.

For the evaluation, two samples of activated alumina where sourced from Fluka and Unilab. The two samples had similar XRD patterns of which the exact phase of the alumina could not be determined, although both had strong similarities to γ-alumina. The BET specific surface area of the samples where also measured and where in the same range typically found for activated alumina used in water defluorination. The specific areas are provided in Table 5.5.

The experiments done where not sensitive enough to distinguish between the two samples for they preformed equally well in the batch and the column tests. The Unilab sample was finally selected for the bulk of the column work since it had a coarser

particle size. The activated alumina bed of the Unilab sample provided less flow resistance and was completely retained by the sinter glass disc.

Table 5.5 BET specific surface areas of the two activated alumina samples evaluated.

Activated Alumina	BET specific surface area (m^2/g)
Unilab	136
Fluka	186

5.3.1 Batch Adsorption

The initial batch experiment was aimed at an initial investigation of the activated alumina system. A 100 g sample of activated alumina was brought into contact with a 600 mg/ℓ fluoride in water solution at ambient temperature. The fluoride concentration was measured at different pH values for the solution. The results obtained are illustrated in Figure 5.22.

The fluoride is adsorbed to low concentrations at a pH below 8 and desorbs at higher pH values. This corresponds to the pH value of 8.2 given by Clifford (1990) as the zero point of charge. Above this value the activated alumina acts as a cation exchanger and below as an anion exchanger. According to the model discussed in the literature review, the fluoride is adsorbed in the region where the alumina acts as an anion exchanger and desorbed where it acts as a cation exchanger.

It was attempted to construct the isotherm for the adsorption of the fluoride at higher concentrations. To this end batch experiments were carried out where different quantities of activated alumina were contacted with the base metal solution containing different initial concentrations of fluoride. The fluoride concentration was measured after a period of 24 hours and based on the initial fluoride concentration; the amount of fluoride adsorbed was calculated. Other than the initial pH, no other adjustment was made.

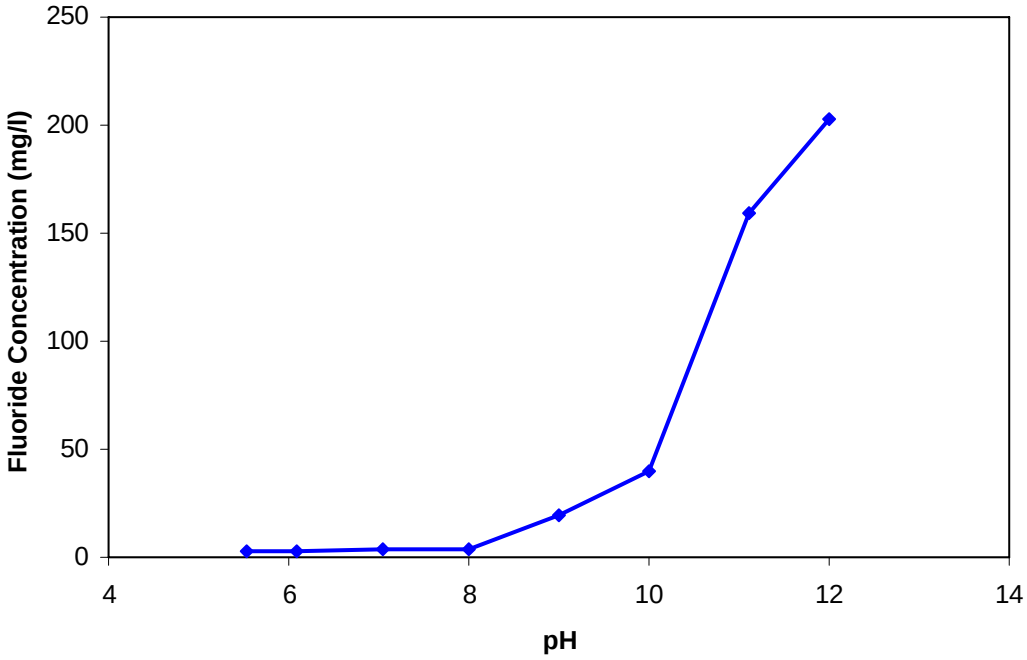

Figure 5.22 Fluoride concentration as a function of pH (initial: 600 mg/l)

Indicated in Figure 5.23 are the results obtained with the capacity specified as gram fluoride adsorbed per litre of activated alumina (using an observed bulk density of 1000g AA/ℓ). The Freundlich and the Langmuir isotherms were fitted to the data for the 24 hour contact time. The fit was not good for both. The reason appears to be the system not reaching equilibrium in the allocated contact time. Grouped on the graph are experiments with the same initial conditions, but different contact times. It can be seen with increasing contact time there is a corresponding increase in fluoride adsorbed. The value obtained for the 42 hour contact time is a manifestation that equilibrium was not obtained in the 24 hour period (data points used for the fitting of the adsorption isotherms). The results for the isotherm will therefore not be discussed further.

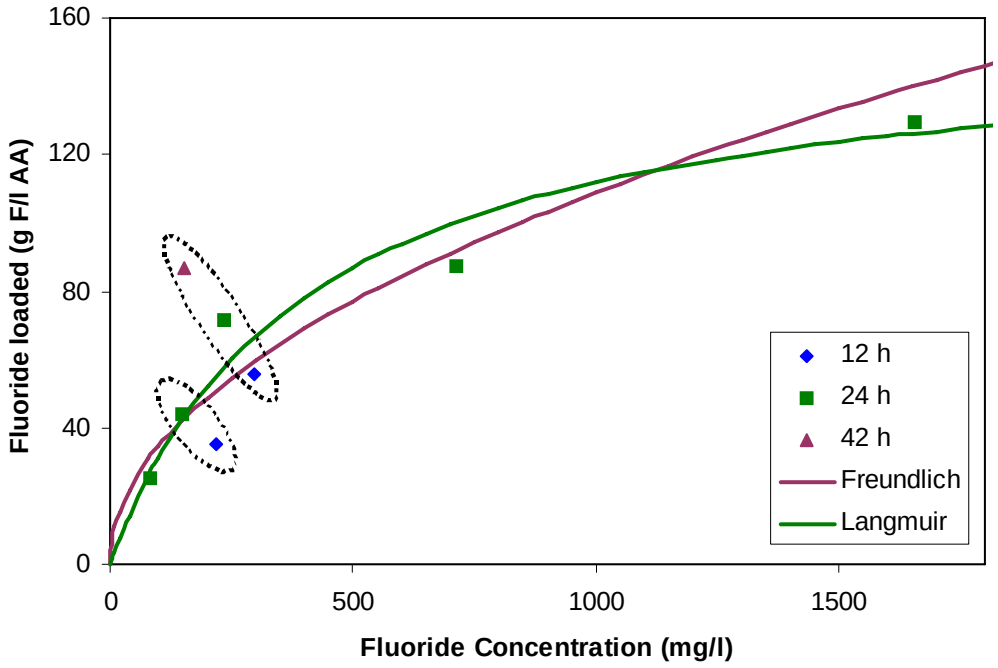

Figure 5.23 Fluoride adsorption onto activated alumina as a function of fluoride concentration.

Two more important conclusions can be drawn from the results above. The activated alumina had significantly higher apparent saturation capacity compared to the results obtained in literature. A typical saturation capacity reported was 3.8 g/ℓ AA (Lounici et al., 1997). This can be attributed to the higher fluoride concentrations used in the current study.

The solution was stirred at a rate of 520 rpm during the batch experiments. The experiments were considered to be well mixed at these conditions and not mass transfer limited. It appears from the slow rate of adsorption, that the process is limited by the chemisorption reaction. The capacities observed in the batch experiments were never reached in the column experiments which is to be expected as a result of the impractically long contact times required.

5.3.2 Column Experiments

It was never sure if the breakthrough point or the saturation point was attained during the experimental run as a result of the fluoride concentrations only being analysed after completion of the experiments. This required a fair amount of initial experiments

to make sure that enough solution is passed through the column so that at least the breakthrough point was reached. The breakthrough point was selected as 10 mg/ℓ fluoride which corresponds to the maximum allowed in zinc electrowinning circuits. The results for the adsorption and desorption cycles will be discussed separately.

Adsorption

Temperature and the inlet fluoride concentration were selected as external variables to be investigated. It was decided to investigate them relative to each other in the form of a factorial designed experiment. A centre run was included which was considered to be the standard conditions (600 mg/ℓ fluoride, 55 °C). The high and a low level for temperature were selected at 45 and 65°C and a fluoride inlet concentration at 400 and 800 mg/ℓ, respectively. All of the factorial experiments were carried out on a 50 g activated alumina bed at a constant flowrate of 1000 ℓ/m^2.min.

Presented in Figure 5.24 is the breakthrough curve for the adsorption cycle of the centre run. This is representative of what was observed in all the runs. The pH dropped from 5.0 at the inlet to ~3.0 for the first few bedvolumes passing through the column. For the first sample the pH was even as low as 2.3, which may be the result of the acid solution still present in the bed. According to mechanism described in the literature review (Section 3.2.2, p.96) the pH should not change during adsorption. It appears from the decreasing pH that the hydrogen ions adsorbed onto the surface were displaced by the base metal species.

Presented in Figure 5.25 are the results for the adsorption cycle of the factorial experiments in terms of the fluoride capacity at a breakthrough point of 10 mg/ℓ fluoride. The capacity of the fluoride at the centre run was determined at 8.65 gF/ℓAA. From the graph it can be seen that the capacity is positively correlated with both temperature and inlet concentration. The average effect of temperature for changing from its low level to its high level, is calculated at 1.41 gF/ℓAA and 0.86 gF/ℓAA for fluoride concentration. Therefore, temperature has a larger influence on the capacity of the fluoride than the initial fluoride concentration.

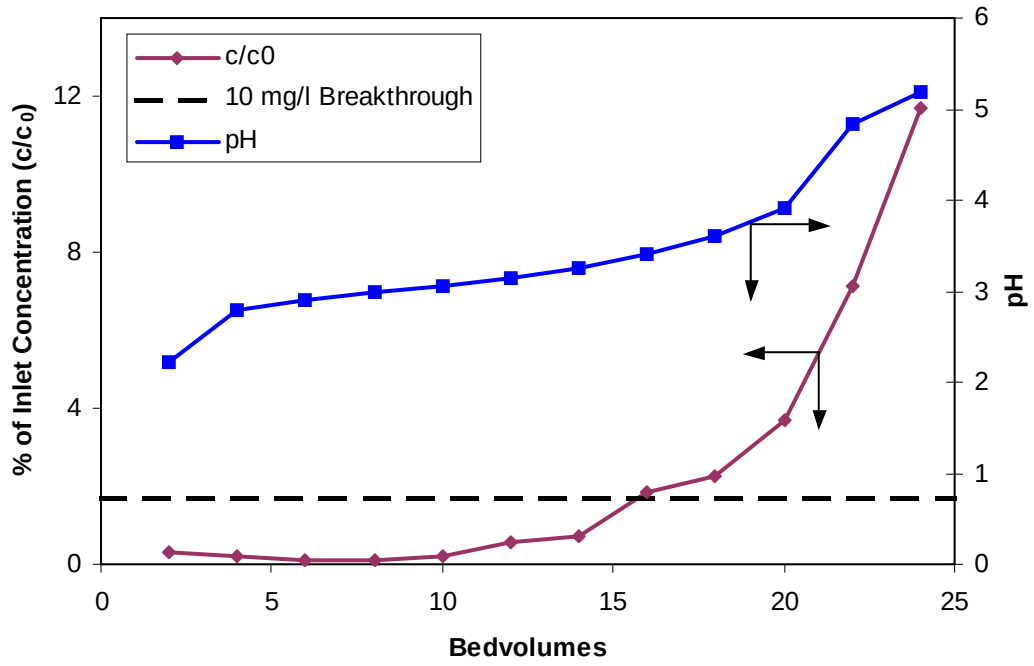

Figure 5.24 Breakthrough curve for the adsorption cycle of the centre run (55 °C, 600 mg/ℓ fluoride).

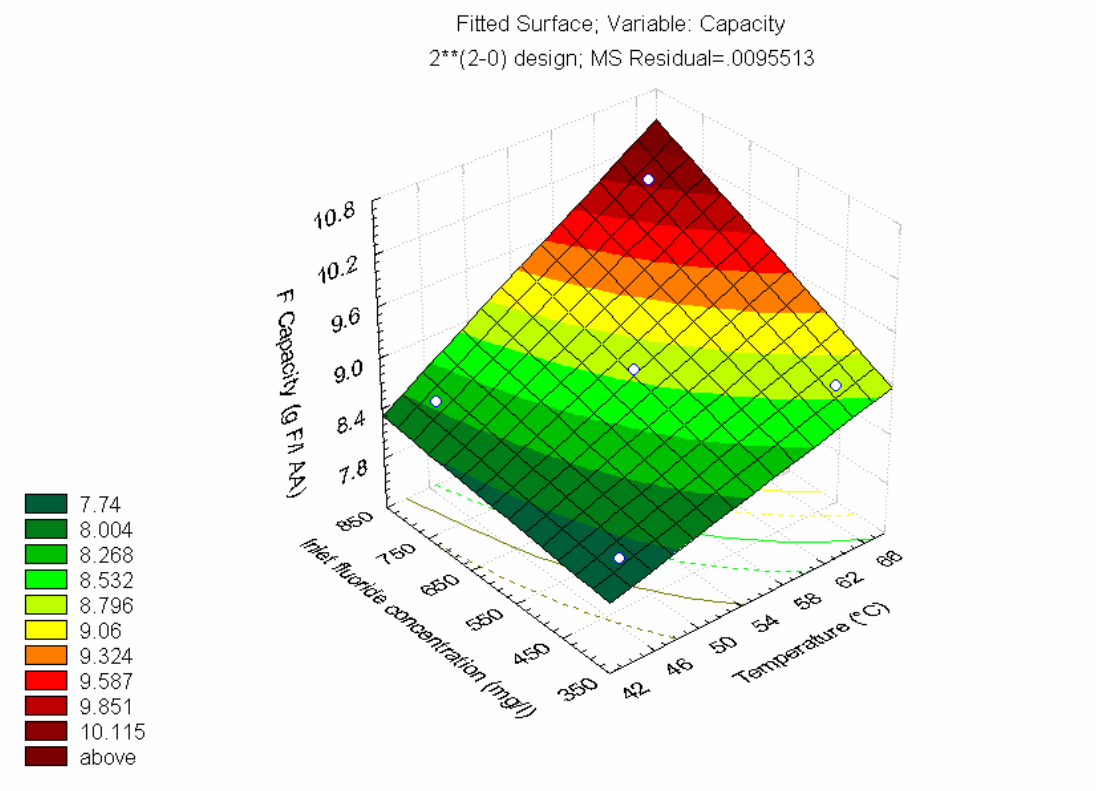

Figure 5.25 Fluoride capacity of the alumina at 10 mg/ℓ breakthrough point.

The saturation point was not reached in the experiments as was seen from the breakthrough curve for the centre run (Figure 5.24). A smaller column was used at the same specific flowrate (1000 ℓ/m^2.min) in an attempt to load the column to its saturation point. This column was also operated at a higher flowrate (4500 ℓ/m^2.min) in a separate experiment to evaluate the effect.

For both curves in Figure 5.26 it can be seen that the saturation point was not reached. It appeared that the system attained a quasi steadystate where the rate of adsorption was in equilibrium with the flowrate. This may be the result of the slow rate of the chemisorption reaction. An exact explanation for this behaviour could not be found. It was not further investigated since a column would not be operated to this point in a practical application. An activated alumina column would rather be loaded till its breakthrough point and then be regenerated. The fact that the curve for the lower flow rate is below the higher flow rate, indicated that more fluoride was loaded for the same amount of solution passed through. Better loading can therefore be attained at the lower flowrate.

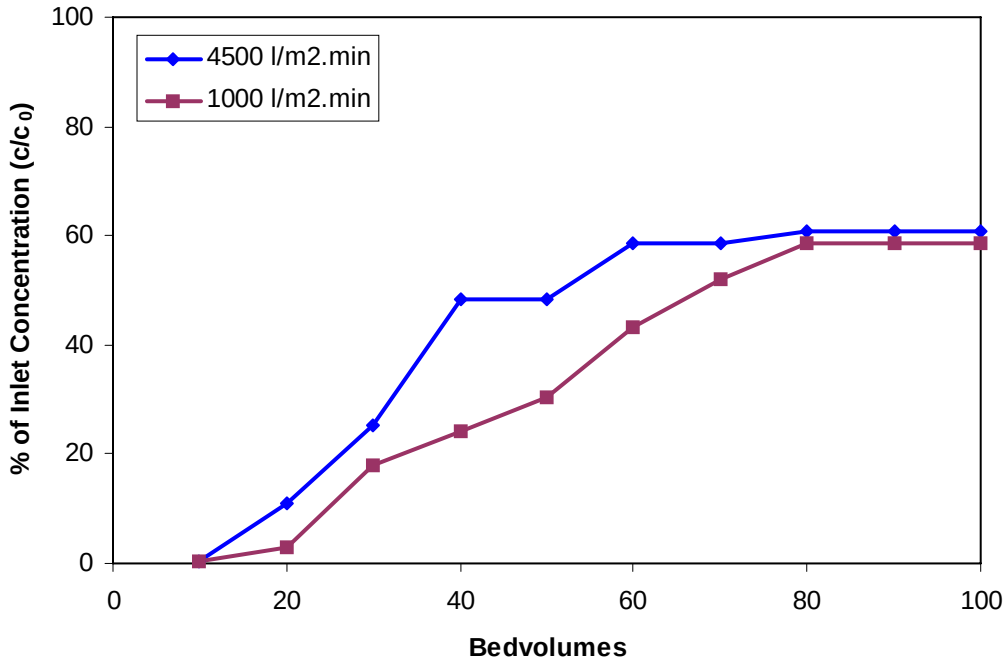

Figure 5.26 Influence of flowrate on the breakthrough curve.

Desorption

For the initial experiments a 0.1% sodium hydroxide solution was used to regenerate the column. The typical regeneration ratio that was obtained at these conditions is illustrated in Figure 5.27. According to the mechanism discussed in the literature review, the amount of hydroxide required to regenerate the column would be double the molar amount of fluoride adsorbed. For the particular run the theoretical regeneration ratio at 40 bedvolumes would have been 75%. In the run only 54% was observed. It is also noticed that there is a lag phase before the fluoride starts to be desorbed.

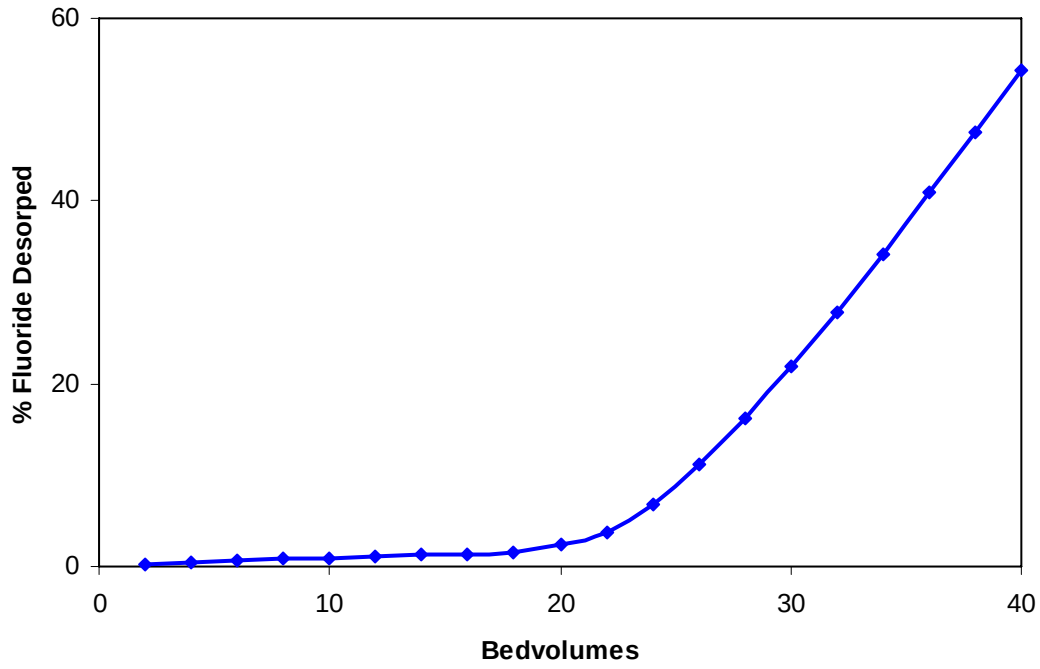

Figure 5.27 Desorption using 0.1% sodium hydroxide solution.

The apparent reason for this lag phase can be seen when inspecting the ionic species in the effluent, and the pH. This is illustrated for the above experiment in Figure 5.28. It is seen for the initial period that the effluent contained a high amount of sulphate ions and the pH was low. A stage was reached where the amount of sulphate ions in the effluent decreased and the pH increased. It was also at this point where the fluoride started to desorb. A possible explanation is that the activated alumina still had a large amount of sulphuric acid and base metal sulphates adsorbed were again the

first to desorb. The desorption of the base metals was evident in a green colour of the effluent from the first two bed volumes. The desorption of the sulphate ions served to reduce the pH to a region where the fluoride is not readily desorped. It is only when the sulphate ions are depleted that the pH increases and the conditions become favourable for the fluoride desorption.

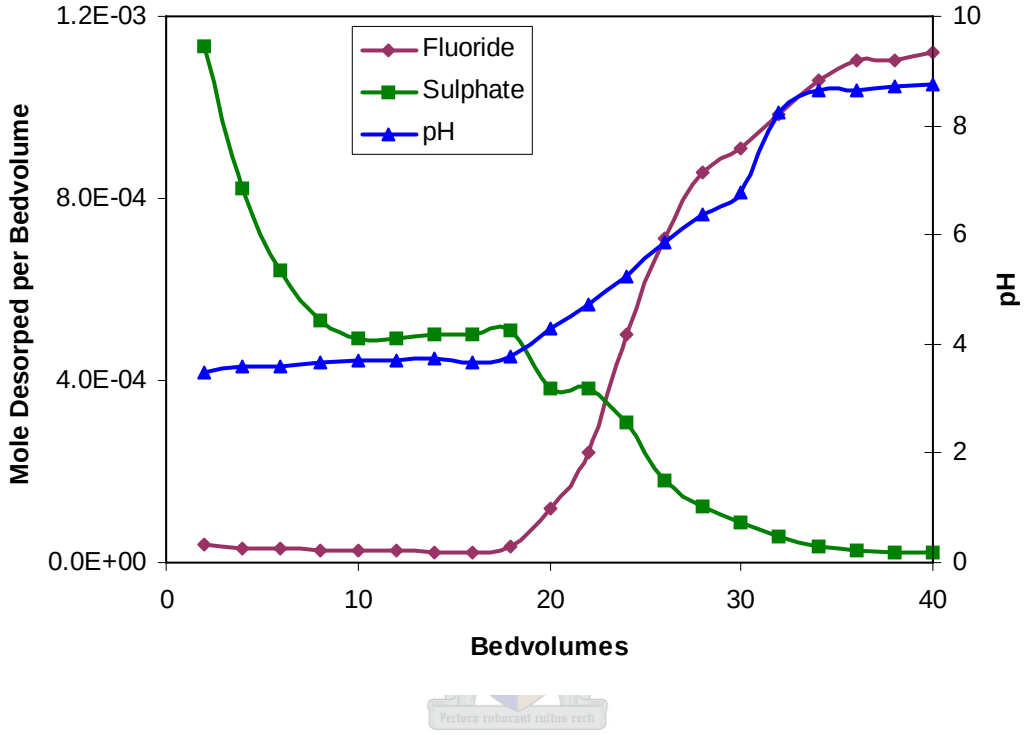

Figure 5.28 Ionic species and pH profile during desorption with 0.1% sodium hydroxide.

The use of the 0.1% sodium hydroxide solution would not be feasible for the practical application of this process. The volume of hydroxide solution required to desorp the bed would be more than double the volume of solution treated, creating an effluent treatment problem. To this end it was decided to test a 1% sodium hydroxide solution. Presented in Figure 5.29 are the desorption profile obtained. It is seen that most of the fluoride is desorped during the first 8 bedvolumes. The corresponding regeneration ratio at this point was 73%.

It was observed for all of the desorption cycles that the initial bedvolume of effluent contained some precipitate. This precipitate analysed to have an aluminium to nickel ratio of 1:3. This raised some concern over the stability of the activated alumina bed.

It was not investigated in this study but would need to be evaluated in the further development of this process.

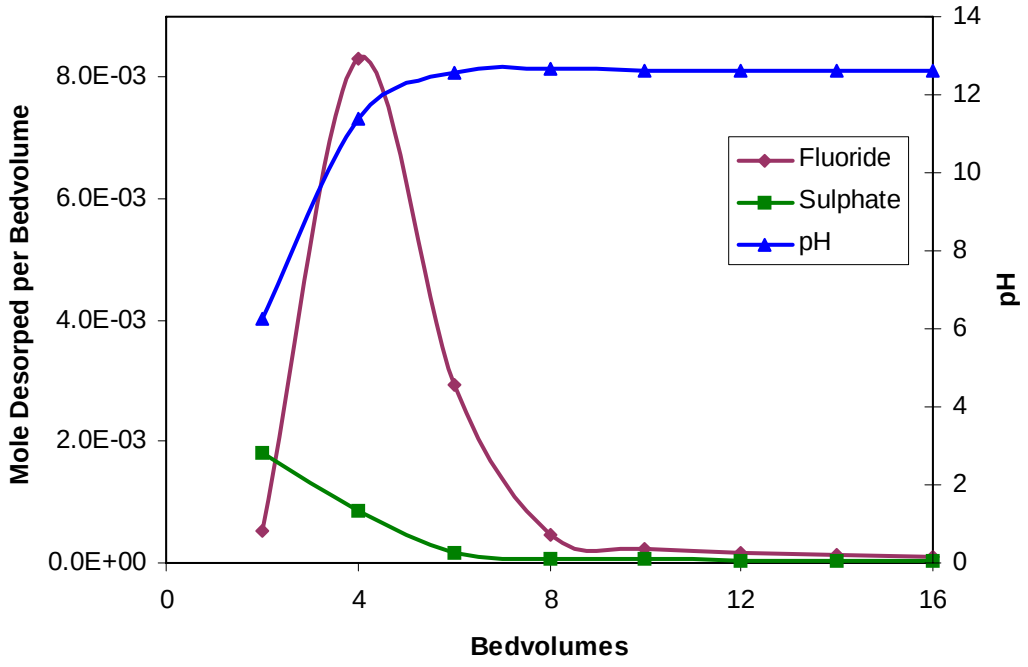

Figure 5.29 Ionic species and pH profile during desorption with 1% sodium hydroxide.

5.4 Summary of Results

Contained within this chapter is a discussion of the experimental observations made in this study. Fluoride precipitation was investigated through batch experiments for its equilibrium and continuous experiments for the effects of residence time and mixing. A similar approach was used for the investigation of activated alumina where batch experiments were used for the isotherm and column tests for the kinetics of the process. The important observations made during the experimental study will be summarised below.

5.4.1 Batch Precipitation

A number of different parameters was evaluated during the batch experiments. From these the following results were obtained:

- Magnesium precipitation dominated over calcium for sub-stoichiometric fluoride additions, where the stoichiomeric addition would be for both calcium and magnesium. The domination is the result of the high magnesium to calcium molar ratio in the feed (10.3:1). Therefore, to remove an appreciable amount of calcium, the fluoride addition should be stoichiometric or in excess. For a 10% excess addition, the amount of calcium and magnesium that was precipitated, were 96% and 98%, respectively.

- Ammonium and hydrogen fluoride were investigated as the soluble fluoride for the precipitation reaction. The use of hydrogen fluoride resulted in the lower completion of the reactions owing to the complexation of the fluoride ions. This would require a larger excess addition of the fluoride. The hydrogen fluoride also adversely affected the pH of the solution, requiring neutralisation with a base other than a calcium base. As a result of the fluoride and the low pH, the solution would be very corrosive. In comparison, the ammonium fluoride would have a no effect on the pH. Ammonium fluoride is therefore preferred.

- It was observed that for a varying magnesium to calcium molar ratio, calcium precipitation dominated for molar ratios up to 3:1 after which magnesium precipitation dominated.

- Temperature appears to have a minimal effect on the precipitation reactions compared to the fluoride addition. Under the conditions investigated an increase of temperature from 45°C to 65°C, only resulted in an increase of 2% for both calcium and magnesium precipitated. The system therefore, appears to be insensitive to temperature.

5.4.2 Continuous Precipitation Experiments

The continuous experiments were used to investigate residence time and the effect of mixing. It was observed that the quality of the precipitate did not vary much for the different parameters. The experiments were conducted at a 10% excess of fluoride for which the amount of calcium and magnesium precipitated was in excess of 94% for

both. The system operated at a solids concentration of 9.6 kg/m^3 dry precipitate. The precipitate had the following characteristics:

- The volume based mean size varied between 16.40 μm to 22.29 μm for the different experiments.

- The particles appeared to be an agglomerated cluster made up of a large number of smaller particles. No distinct crystal faces could be observed and the precipitate appeared to have an amorphous character. The surface was rough, even though it was formed at a low supersaturation ratio for both calcium and magnesium fluoride.

- XRF analysis indicated the precipitate to contain 7500 ppm nickel and 440 ppm cobalt. This is in the same ratio as in the mother liquor and is therefore assumed to be mother liquor inclusions. This means that the precipitate contained 25% by weight of mother liquor, of which most is evaporated during the drying of the precipitate.

- The cake filtration resistance of the precipitate was determined to be 4.0 x 10^9 $m^3/kg.m^2$.

Residence times of 30, 60 and 120 minutes were evaluated. Using the size distribution, the apparent nucleation and growth rate were determined. Both the nucleation rate and crystal growth rate increased with decreasing residence time. The results obtained for the three residence times were similar, indicating that the residence time could be reduced to 30 minutes.

The following results were obtained for the investigation of mixing:

- An increase in macromixing resulted in a decrease of the mean particle size.

- No large difference where observed for the mesomixing of the feed streams. These could not be compared to the control experiment since the micromixing conditions were not the same.

- An increase in micromixing resulted in a decrease in the mean particle size.

- The variations observed for the different parameters were not large and it appears that the system is insensitive to mixing at the parameters investigated.

5.4.3 Activated Alumina Adsorption

From the batch experiments for the activated alumina it was observed that the fluoride is adsorbed at a pH below 8 and desorbed above the pH. The batch experiments were also used in an attempt to fit an adsorption isotherm. A good fit was not obtained for both the Freundlich and Langmuir isotherms, since equilibrium was not attained in the experiments. The results showed the rate of adsorption to be extremely slow as a result of equilibrium not being reached within 24 hours. It appears that the adsortion rate was limited by the chemisorption reaction.

The following results where obtained for the column experiments:

- For the adsorption cycle of the column experiments the influence of temperature and inlet fluoride concentration were evaluated. The column was never operated to the saturation point and the capacity of the column was determined at a fluoride breakthrough concentration of 10 mg/ℓ. For the centre run of the experiments, the capacity was 8.65 gF/ℓAA (gram fluoride per litre activated alumina). The capacity of the alumina appeared to be positively correlated to both temperature and the inlet concentration. Temperature had the biggest effect, calculated at 1.41 gF/ℓAA for changing from 45°C to 65°C.

- A smaller column was used in an attempt to reach the saturation point. The system appeared to attain a quasi steady state where the rate of adsorption was in equilibrium with the flowrate. An explanation could not be determined for

this behaviour and it was not further investigated since a column would not be operated to this point in a practical application.

- A 0.1% sodium hydroxide solution was initially used in the regeneration of the column. It was observed that an excess amount was needed as a result of sulphate species that was adsorbed onto the alumina. Approximately 80 bedvolumes of hydroxide would have been required to regenerate the bed. A 1% sodium hydroxide tested to improve the volume of solution required for regeneration. The regeneration ratio was 73% after 8 bedvolumes and did not increase much in the subsequent bedvolumes.

- The stability of the alumina was not investigated, but there was some indications that the alumina was dissolving.

Chapter 6

The Conceptual Process

Objectives of Chapter 6

- Discuss the design considerations for the fluoride precipitation process.
- Translate the results obtained during the experimental investigation into a conceptual process.

The final objective of this study was the development of a conceptual process for the control of calcium and magnesium. Discussed here is the development of this process from the experimental data, starting with the block flow diagram. Considerations that need to be taken into account will be discussed for each of the steps, after which a conceptual process will be proposed.

6.1 Block Flow Diagram

The conceptual process envisaged thus far consists of three process steps. The first would be the precipitation of the fluorides, followed by solid-liquid separation and then the adsorption of the unreacted fluoride using activated alumina.

In the experimental result it was observed that magnesium dominated the precipitation process as a result of its high molar ratio. It was also shown that it would not be possible to remove more than 20% calcium without precipitating at least 80 % of the magnesium. In most applications the total removal of calcium and magnesium is not required. The control of calcium is usually more important than magnesium owing to the risk of gypsum precipitation. Since the molar ratio of magnesium to calcium is approximately 10 : 1, the precipitation of the magnesium will result in a tenfold increase in the fluoride consumption. For systems that already have tolerable magnesium levels the block flow diagram in Figure 6.1 are proposed.

The concept is to split the leach solution and subject only a portion of it to the fluoride precipitation step. In the fluoride precipitation step the maximum amount of calcium

is precipitated using an excess of fluoride. The precipitate is then subjected to a solid-liquid separation after which the unreacted fluoride could be removed from the solution. The split stream could then be returned to the main stream to lower the overall calcium and magnesium concentrations. The split stream would allow the removal of calcium without first precipitating all of the magnesium. The split ratio will determine the amount of calcium and magnesium to be removed.

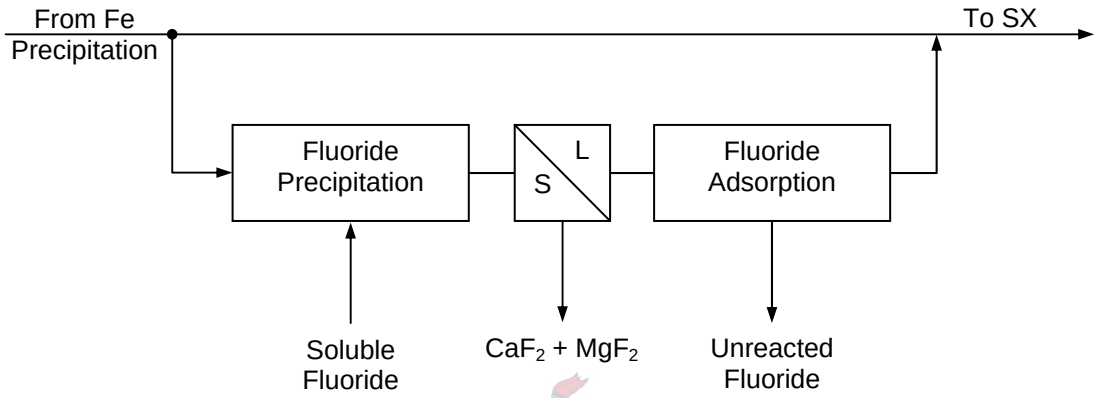

Figure 6.1 Block flow diagram of the conceptual process.

The results of a mass balance for the proposed process is provided in Figure 6.2. The concentrations are for the leach stream after the split stream has been recombined. The mass balance was carried out using the experimental data for a 10% excess addition of fluoride for which 94% and 97% of the calcium and magnesium were precipitated. The results are only for calcium although the same trend was observed for magnesium. The fluoride adsorption step was excluded from the mass balance. The supersaturation ratio provided is relative to the ratio at the outlet of the reactor. It can be seen for most of the split ratios that the relative supersaturation ratio is greater than one, indicating a higher supersaturation than at the outlet. It is therefore, possible that precipitation could occur after the splitstream has been recombined. It is essential to include the fluoride adsorption step to avoid this from happening.

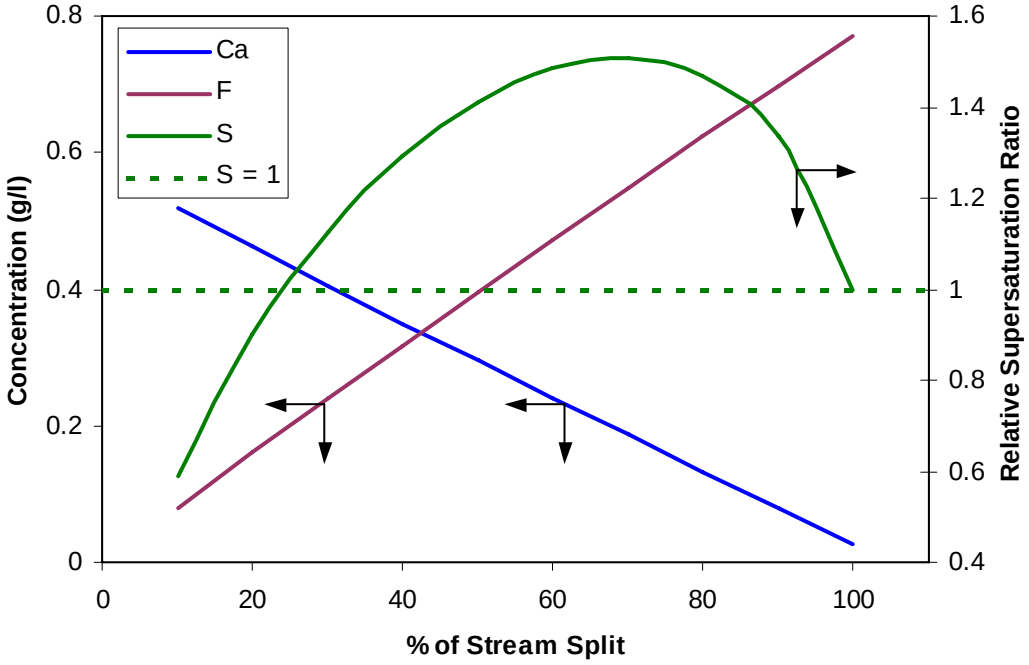

Figure 6.2 Calcium mass balance for the proposed process.

The level to which calcium and magnesium needs to be reduced would depend on the application. For the Nkomati metals plant the calcium should be reduced so that it would not precipitate in the solvent extraction equipment. This is a vague definition for the level of calcium required since it would depend on the operation of the solvent extraction step. The value for the calcium and therefore, the ratio of the split stream could not be fixed. As a result, the process equipment cannot be sized. In the following sections the information would be provided for the sizing of the equipment should the required level of calcium or magnesium be known.

6.2 Precipitation Step

The field of parameters investigated for the precipitation reactor were:

Residence time:	30, 60 and 120 minutes
Circulation time (macromixing time):	55s to 200s
Stirrer intensity (micromixing):	2 to 4 W/kg

At these conditions, a precipitate with relatively constant characteristics are produced. Furthermore, no adverse effects were observed for the mixing of the feed streams.

The system could therefore be scaled-up according to these parameters to produce a precipitate with similar characteristics as was observed in this study.

The precipitation step would be operated at a 10% excess of fluoride using ammonium fluoride. The volume ratio of the fluoride feed stream to the treated stream was selected at 5%. The solubility of the ammonium fluoride would allow this ratio to be reduced down to 2% if required. Other soluble fluorides, which would be accommodated by the overall process, are the base metal fluorides such as cobalt or nickel fluoride.

A greater concern for the scale-up of the process was the formation of scale observed in the continuous experiments. Söhnel and Garside (1992) provide a discussion on the control of scale formation in precipitation processes. They described three possible methods for scale prevention:

- *Chemical methods*: This involves the modification of the solution composition to prevent the formation of scale. This usually involves the addition of an admixture that would inhibit precipitation. This would not be suitable for the current application.

- *Physical methods*: Scale formation could be minimised, by promoting precipitation in the bulk solution. This could be achieved by increasing the crystal concentration, which would act as seed crystals for the precipitating system.

- *Mechanical methods*: Scaling can be limited by the mechanical removal of the encrustations by the addition of inert particles such as sand. The scale would be removed by the abrasive action of the particles.

Of these, the physical method of increasing the crystal concentration of the system would be most appropriate. It is recognised that the system was operated at a low solids concentration, which could be increased without complications. Only if this is not successful should chemical or physical methods be considered.

6.3 Solid-Liquid Separations

Owing to the low solids concentration, the product stream from the precipitation step has to be subjected to a thickening step before the precipitate could be filtered. Part of the thickened stream has to be recycled to the precipitation reactor as seed crystals. Additionally it may be considered to include a classification step such as a cyclone to recycle only the fine particles. There are a number of possibilities surrounding the solid liquid separation step. For the Nkomati metals plant the precipitate product stream could first be thickened and then filtered using the belt filters already available for the leach residue. With this implementation it would be important that the precipitate does not come into contact with the acidic leach solution (pH < 3), which may result in the dissolution of the precipitate to form hydrogen fluoride.

The following properties were observed for the precipitate, which could be used in the design of the filtration system:

Cake filtrtion resistance:	4.0×10^9 $m^3/kg.m^2$
$L_{0.1}$ (size for which 90% particles is larger based on volume)	~3 μm

6.4 Fluoride Adsorption

From the experimental investigation the following results were obtained that can be used in the sizing of the adsorption columns:

Flow rate:	1000 ℓ/m^2.min
Fluoride breakthrough:	10 mg/ℓ
Fluoride Capacity:	8.5 gF/ℓAA

In the experimental study it was proved that activated alumina could successfully adsorb the fluoride from the base metal solution and then be regenerated. During the investigation the following points were identified for future investigation:

- The pH of the solution decreased during the loading cycle, requiring a pH adjustment step afterwards. The acidification of the activated alumina has to

be optimised to ensure that the desorption of sulphuric acid during loading would be a minimum.

- The ratio of the solution treated compared to the volume of the solution required for regeneration was 2 : 1. This value has to be improved for the recycling of the fluoride. The volume ratio should at least be 20 : 1 (5% of the volume of the treated solution). A higher hydroxide concentration could be investigated for this purpose.

- Sodium hydroxide was used for the regeneration of the column. The sodium may not be compatible with overall process and another base such as ammonium hydroxide has to be investigated.

6.5 The Conceptual Process

Given here is a possible implementation for the conceptual process (Figure 6.3). The process consists of a settler (2) with a small recycle loop. The split stream is introduced into the recycle stream after which it is mixed with the soluble fluoride using high intensity mixing equipment (1) such as impinging jets or a venturi mixer. The high intensity mixing is necessary to produce a homogeneous mixture without high localized supersaturations. The flowrate of the recycle stream would be related to the volume of the settler by the circulation time. For this, the experimental values could be used. The recycle (a) flowrate would be much larger than the split stream (b) flowrate which would again be larger than the fluoride feed (c) flowrate.

The purpose of the settler is to provide residence time for crystal growth and serve as the first step in the solid-liquid separation. According to the experimental evaluation, the residence time could be 30 minutes provided that the precipitate does settle in this time. The liquid is withdrawn through two outlets from the settler. Clear liquid is withdrawn from the top through a filtration device such as a candle filter (3) and the slurry is removed from the bottom. The reason for the two outlets is to maintain a higher volume percentage of solids within the settler. The slurry from the bottom is then filtered (4).

Finally the excess fluoride is removed by adsorbing it onto the activated alumina (5) after which it is returned to the mainstream. The activated alumina is regenerated using a base after which it could be recycled.

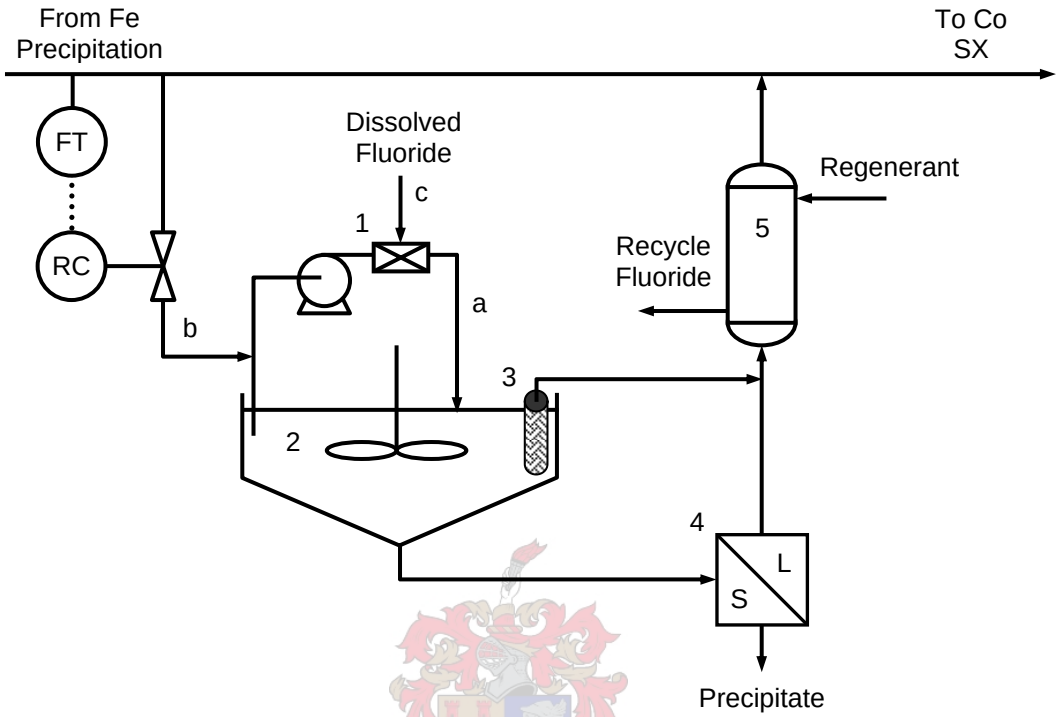

Figure 6.3 Conceptual process for the control of calcium and magnesium.

A provisional patent has been written for this conceptual process to protect the intellectual property of this study. The provisional patent has been registered at the South African Patent Office under the application number 2002/1243. The provisional patent was written at the beginning of this study to cover as much of the results that may come forth from this project. It still has to be rewritten if there is decided to go ahead with the patenting of the proposed process.

6.6 Summary

In this chapter a conceptual process was proposed based on the experimental observations made. This process could be used for the control of calcium and magnesium where maximal removal is not required. The dominance of magnesium precipitation was avoided by subjecting only a portion of the base metal stream to

fluoride precipitation. A 10% excess of fluoride would be added to the split-stream to remove the maximum amount of calcium and magnesium. Thereafter, the precipitate would be removed through a solid-liquid separation step, followed by the adsorption of the unreacted fluoride using activated alumina. The split-stream would then be returned, to lower the overall calcium and magnesium concentration. The block flow diagram was further developed indicating a possible combination of equipment that could be used for the conceptual process.

Chapter 7
Conclusions and Recommendations

Based on the results obtained in this study the following conclusions could be made. This study investigated the control of calcium and magnesium in a base metal sulphate leach solution. From the search of possible methods, it was found that there is no conventional method for the control of these alkaline earth elements. The precipitation of fluorides was selected as a possible method and was experimentally investigated. Additionally, there was looked at methods for removing or possibly recycling the unreacted fluorides after precipitation. Activated alumina was identified as a possible adsorbent for fluoride. The experimental investigation was aimed at the scale-up of the process and therefore, the effects of mixing on the precipitate were also investigated. The fluoride precipitation option was found to be feasible for the control of calcium and magnesium and the unreacted fluoride could be adsorbed using activated alumina. Based on the experimental results, a conceptual process was developed.

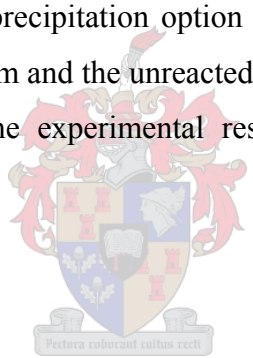

7.1 Conclusions

The main objectives of the study was met in the following ways:

- A survey was carried out of the possible methods for the control of calcium and magnesium, of which the list is summarised in Chapter 2. The methods where discussed with advantages and disadvantages stated. It is recommended that the development of these processes be followed to ensure that the optimum solution is found.

- The feasibility of the fluoride precipitation process was studied in terms of a number of parameters including fluoride addition, identity of the soluble fluoride, magnesium to calcium molar ratio and the effects of temperature. From these parameters it were concluded that both calcium and magnesium could be controlled using a stoichiometric excess of ammonium fluoride. The

precipitation of fluorides was specific for calcium and magnesium and no co-precipitation of the base metals could be detected. For 10% excess, removals of 96.5% calcium and 98.5% magnesium were observed in the batch experiments.

- Activated alumina was experimentally evaluated and it was observed that it does adsorb fluoride to low concentrations from the base metal solution. The fluoride could then be desorbed again by adjusting the pH. The activated alumina was studied in both batch and column experiments. The observed capacity of the activated alumina was 8.65 gF/ℓAA at a 10 mg/ℓ breakthrough level.

- The effects of mixing were investigated as part of the feasibility of the fluoride precipitation process. Mixing was studied on the macro-, meso- and micromixing scale using the three-zone experimental method. For the parameter field investigated, small variations were observed in the characteristics of the precipitate, but these were considered negligible for their implications for the plant scale process.

- Based on the experimental results, a conceptual process was devised whereby only a portion of the leach stream is subjected to the fluoride precipitation process, after which it is returned to lower the overall calcium and magnesium concentrations. This method would reduce the effect of magnesium dominance observed for the precipitation. The fluoride precipitation process consisted of three steps being precipitation itself, the solid-liquid separation and the adsorption of fluoride.

Other than the conclusions on the main objectives, the following specific conclusions could be made:

Precipitation:

- Magnesium fluoride precipitation dominated at a molar ratio 10 : 1 with respect to calcium. As a result, to precipitate an appreciable amount of calcium an excess amount of fluoride was required. The dominance of magnesium was observed for magnesium to calcium molar ratios down to 4 : 1.

- Hydrogen and ammonium fluoride has been evaluated as two soluble fluorides for the precipitation process. A lower completion of the reaction was observed for the hydrogen fluoride, which was also responsible for a lower pH of the solution. The lower completion appears to be the result of the complexation of the fluoride ions. Ammonium fluoride is the preferred soluble fluoride and is also easier to handle.

- It was observed that temperature had the smallest effect on the percentage of calcium and magnesium precipitated compared to the effect of the fluoride addition. The observed change was less than 2% for a temperature increase of 45°C to 65°C.

- The precipitate formed during the continuous experiments appeared to be highly agglomerated and to have an amorphous character. It was analysed to contain 7400 ppm nickel and 440 ppm cobalt. Using the base metals fraction the mother liquor inclusions was estimated to be 25% of the precipitate weight, of which most is evaporated during drying.

- The volume based mean size of the precipitate produced during the continuous experiments were in the range of 15 to 23 μm and had a typical cake filtration resistance of 4.0×10^9 $m^3/kg.m^2$.

- Precipitate with similar characteristics is obtained for the reduction of the residence time from 120 min to 30 min. The latter value could be used for design, as a result of the smaller reactor size. The system was also fairly insensitive for the parameter field used in the investigation of mixing. The

mean particle size decreased for an increase in both macro and micromixing. The mesomixing of the two inlet steams appeared to have a similar effect compared to each other.

Activated Alumina:

- High capacities were observed during the batch experiments that was never realised in the column experiments. This appeared to be the result of the slow kinetics of the adsorption process prohibiting the column to be loaded to its saturation point in a practical application.

- The capacity of the activated alumina at a 10mg/ℓ breakthrough was found to increase with increasing temperature and inlet fluoride concentrations. Of these two parameters, temperature had the largest effect.

- It was observed that an excess amount of sodium hydroxide was needed to desorb the fluoride. The higher consumption appeared to be the result of the desorption of sulphate species.

- The volume of hydroxide solution required for desorption decreased with an increase in hydroxide concentration. The highest concentration that was tested was a 1% sodium hydroxide solution for which the volume was still too high to recycle the whole stream.

7.2 Recommendations

The following recommendations could be made for a continuation study:

- Enough information is provided in this study for a cost estimation to be conducted for the process. If the cost is found to be feasible then it is recommended that this study be continued.

- Different reactor configuration can now be evaluated to find the optimum for precipitation and solid-liquid separation.

- The possibility of reducing the formation of scale by increasing the solids content of the reactor should be investigated.

- The adsorption cycle for activated alumina should be investigated to minimise the reduction of the solution pH.

- The volume of hydroxide solution required for desorption should reduced to allow the recycling of the complete stream containing the unreacted fluoride.

- Sodium may not be compatible with the overall base metals process. Another base such as ammonia should be tested for the desorption cycle.

References

Avmin, 2002. *Avmin Operations Nkomati* [online]. Available from: http://avmin.co.za/operations/nkomati.asp [Accessed 24 March 2002].

Axelrad, B.A., Matson, R.F. and Touro, F.J., 1964. *Method of Inhibiting Dissolution of Calcium Sulphate.* United States patent Number 3,140,915, 6 pages.

Barnes, A.R., 1997. The Selection of a Nickel Smelting Process for the 21st Century, *In: Trends in Base Metals Smelting and Refining*, Randburg, South Africa 24 – 25 April 1997. Johannesburg: The South African Institute of Mining and Metallurgy, 11 pages.

Babjak, J., 1986. *Process for metal recovery by solvent-extraction from $CaSO_4$ containing sulfate solutions*. United States Patent Number 4,610,861, 8 pages.

Bałdyga, J., 1999. *Turbulent mixing and chemical reactions*. New York: Wiley.

Bałdyga, J. and Pohorecki, R., 1995. Turbulent micromixing in chemical reactor – a review. *The Chemical Engineering Journal*, Vol. 58, pp. 183 – 195.

Booster, J.L., Van Sandwijk, A. and Reuter, M.A., 2000. Magnesium removal in the electrolytic zinc industry. *Minerals Engineering*, Vol.13, No.5, pp. 517 – 526.

Boruff, C.S., 1934. Removal of fluorides from drinking water. Industrial and engineering chemistry, Vol. 26, No. 1, pp. 69 – 71.

Burkin, A.R. ed., 1987. *Extractive Metallurgy of Nickel.* Chichester: John Wiley & Sons.

Clifford, D.A., 1990. Ion exchange and inorganic adsorption. *In:* F.W. Pontius, ed. *Water Quality and Treatment*. New York: McGraw-Hill, pp. 561 – 639.

Cole, P.M., 2002. The introduction of solvent-extraction steps during upgrading of a cobalt refinery. *Hydrometallurgy*, Vol. 64, pp. 69 – 77.

Coussement, M., De Schepper, A. and Standaert, R., 1982. Separation of cobalt and nickel in acid solutions. *In:* K. Osseo-Asare and J.D. Miller, eds. *Hydrometallurgy: Research, Development and Plant Practice,* Atlanta, Georgia 6 – 10 March 1983. New York: The Metallurgical Society of AIME, pp. 569 – 585.

CRC Handbook of Physics and Chemistry, 77th edition, 1996. D.R. Lide and H.P.R. Frederikse, eds. Boca Raton: CRC Press.

Creamer, T., 2002. Resources firm prepares for nickel and PGM projects. *Mining Weekly, March 15 – 21,* p. 16.

Dreisinger, D.B., 2001. *Autoclave Processing of Ores and Concentrates*. Short Course, Pretoria 4 – 8 June. University of Pretoria.

Dutrizac J.E., 2002. Calcium sulphate solubility in simulated zinc processing solutions. *Hydrometallurgy*, Vol 65, pp. 109 – 135.

Espencheid, W.F., Heilweil, I.J. and Yan, T.Y., 1978. *Calcite control in an in situ leach operation.* United States Patent Number 4,103,963, 7 pages.

Feather, A., Bouwer, W., Swarts, A. and Nagel, V., 2002. Pilot-plant solvent extraction of cobalt and nickel for AVMIN's Nkomati project. *In:* K.C. Sole, P.M. Cole, J.S. Preston and D.J. Robinson, eds. *ISEC 2002*, Cape Town, South Africa 17 – 21 March 2002 [CD-ROM]. Johannesburg: The South African Institute of Mining and Metallurgy, pp. 946 – 951.

Fitchett, D.E., Tarbell, J.M., 1990. Effect of mixing on the precipitation of barium sulphate in an MSMPR reactor. *AIChE Journal*, Vol. 36, No. 4, pp. 511 – 522.

Garrison, C.M., 1983. How to design and scale mixing pilot-plants. *Chemical Engineering*, Feb. 7, pp. 63 – 70.

Gösele, W. and Kind, M., 1991. Versuche zum Einfluß der Vermischung auf die Qualität eines kontinuierlich gefällten Produktes. Chemie Ingenieur Technik. Vol. 63, Nr. 1, pp. 59 – 62.

Gray, J., Price, M.J. and Fittock, J.E., 1996. Operation of a Cobalt Purification Pilot Plant. In: ISEC '96, Melbourn, Australia, pp. 703 – 708.

Habib, Jr., E.T., 1982. *Process for controlling calcium in a leach operation*. United States Patent Number 4,312,839, 6 pages.

Habashi, F., 1999. *Textbook of Hydrometallurgy*. 2nd edition. Québec City: Métallurgie Extractive Québec.

Hammerbeck, E.C.I. and Schürmann, L.W., 1998. Nickel. *In:* M.G.C. Wilson and C.R. Anhaeusser, eds. *The Mineral Resources of South Africa*. Pretoria: Council for Geoscience, pp. 471 – 482.

Hofirek, Z. and Halton, P., 1990. Production of high quality electrowon nickel at Rustenburg Base Metal Refiners (PTY.) LTD. *In:* P.L. Claessens and G.B. Harris, eds. *Electrometallurgical Plant Practice*, Montreal, Canada 21 – 24 October 1990. New York: Pergamon Press, pp. 233 – 251.

Jeffery, G.H., Bassett, J., Mendham, J. and Denny, R.C., 1991. *Vogel's textbook of quantitative chemical analysis*. 5th edition. Essex: Longman Scientific & Technical.

Jones, D.L., 2000. *Process for the solvent extraction of nickel and cobalt values in the presence of magnesium ions from a solution*. United States Patent Number 6,054,105, 12 pages.

Kanesato, M., Yokoyama, T. and Suzuki, T.M., 1988. Selective adsorption of fluoride ion by La(III)-loaded chelating resin having phosphonomethylamino groups. *Chemistry Letters*, pp. 207 – 210.

Kerfoot, D.G.E., 1991. Nickel. *In:* Elvers, B., Hawkins, S. and Schulz, G., eds. *Ullmann's Encyclopedia of Industrial Chemistry*. Weinheim: VCH Verlagsgesellschaft mbH, pp. 157 – 219.

Kuck, P.H., 2000. Nickel. *U.S. Geological survey minerals yearbook – 2000* [online]. Available from: http://minerals.usgs.gov/minerals/pubs/commodity/nickel/500400.pdf [Accessed 4 October 2002].

Leyva Ramos, R., Ovalle-Turrubiartes, J. and Sanchez-Castillo, M.A. 1999. adsorption of fluoride on aluminum-impregnated carbon. *Carbon*, Vol 37, pp. 609 – 617.

Lounici, H., Addour, L., Belhococine,D., Grib, H., Nicolas, S., Bariou, B. and Mameri, N., 1997. Study of a new technique for fluoride removal from water. *Desalination*, Vol. 114, pp. 241 – 251.

Lounici, H., Adour, L., Belhocine, D., Elmidaoui, A., Bariou, B and Mameri, N., 2001. Novel technique to regenerate activated alumina bed saturated by fluoride ions. *Chemical Engineering Journal*, Vol. 81, pp. 153 – 160.

Mayze, R.S., 2001. Nickel laterite processing in Western Autralia. *In: Copper Cobalt Nickel and Zinc Recovery Conference*, Victoria Falls, Zimbabwe 16 – 18 July 2001. Johannesburg: The South African Institute of Mining and Metallurgy, 12 pages.

Moges, G., Zewge, F., Socher, M., 1996. Preliminary investigation on the defluorination of water using fired clay chips. *Journal of African Earth Science*, Vol. 21, No. 4, pp. 479 – 482.

Møller, H. and Madsen, H.E.L., 1985. Growth kinetics of calcium fluoride in solution. *Journal of Crystal Growth*, Vol. 71, pp. 673 – 681.

Nagel, V. and Feather, A., 2001. The separation of nickel and cobalt from a calcium-saturated bioleach liquor using versatic acid in a synergistic mixture with 4-nonyl pyridine. *In: Copper Cobalt Nickel and Zinc Recovery Conference*, Victoria Falls, Zimbabwe 16 – 18 July 2001. Johannesburg: The South African Institute of Mining and Metallurgy, 17 pages.

Nancollas, G.H., Bochner, R.A., Liolios, E., Shyu, L.J., Yoshikawa, Y., Barone, J.P. and Svrjcek, D., 1982. The kinetics of crystal growth of divalent metal fluorides. *AIChE Symposium Series*, Vol. 78, No. 215, pp. 26 – 36.

Nielsen, A.E., 1955. The kinetics of electrolyte precipitation. *Journal of Colloid Science*, Vol 10, pp. 576 – 586.

Nielsen, A.E., 1984. Electrolyte crystal growth mechanisms. *Journal of Crystal Growth*, Vol. 67, pp. 289 – 310.

Nielsen, A.E. and Toft, J.M., 1984. Electrolyte crystal growth kinetics. *Journal of Crystal Growth*, Vol 67, pp. 278 – 288.

Poggiolini, D., 2001. Decision on R1.8bn South African nickel project by 2002. *Mining Weekly, September 28 – October 4*, p. 6.

Preston, J.S. and Du Preez, A.C., 2000. Separation of nickel and calcium by solvent extraction using carboxylic acids and alkylpyridines. *Hydrometallurgy*, Vol. 58, pp. 239 – 250.

Preston, J.S., 1985. Solvent extraction of metals by carboxylix acids. *Hydrometallurgy*, Vol. 14, pp. 171 – 188.

Raichur, A.M. and Jyoti Basu, M., 2001. Adsorption of fluoride onto mixed rare earth oxides. *Separation and Purification Technology*, Vol 24, pp. 121 – 127.

Ritcey, G.M. and Ashbrook, A.W., 1979. *Solvent-Extraction: Principles and applications to process metallurgy, Part II*. Amsterdam: Elsevier Scientific Publishing Company.

Shyu, L.J. and Nancollas, G.H., 1980. The kinetics of crystallization of calcium fluoride. A new constant composition method. *Croatica Chemica Acta*, Vol 53, No. 2, pp. 281 – 289.

Söhnel, O. and Garside, J., 1992. *Precipitation: Basic Principles and Industrial Applications.* Oxford: Butterworth-Heinemann.

Torbacke, M. and Rasmuson, Å.C., 2001. Influence of different scales of mixing in reaction crystallization. Chemical Engineering Science, Vol. 56, pp. 2459 – 2473.

U.S. Geological Survey, 2002. *Nickel: Statistics and Information* [online]. Available from: http://minerals.usgs.gov/minerals/pubs/commodity/nickel/ [Accessed 4 October 2002].

Van Leeuwen, M.L.J., Bruinsma, O.S.L. and Van Rosmalen, G.M., 1996. Three-zone approach for precipitation of barium sulphate. Journal of Crystal Growth, Vol 166, pp. 1004 – 1008.

Van Peborgh Gooch, J.R., Hounslow, M.J. and Mydlarz, J., 1996. Discriminating between size-enlargement mechanisms. *Transactions of The Institution of Chemical Engineers*, Vol. 74, Part A, pp. 803 – 811.

Van Rosmalen, G.M., Kramer, H.J.M., Lewis, A.E., 2001. *Controlling Precipitation Processes Workshop*. Muldersdrift, 22 – 23 March. University of Cape Town.

Vogel, A.I., 1961. *A text-book of quantitative inorganic analysis including elementary instrumental analysis*. 3rd edition. London: Longmans, Green and Co Ltd.

Pectora roborant cultus recti

Wang, Y. and Reardon, E.J., 2001. Activation and regeneration of a soil sorbent for deflorination of drinking water. *Applied Geochemistry*, Vol. 16, pp. 531 – 539.

Woolfe, J., 1996. The Nkomati Joint Venture – a Nickel Mine in the Making. *Geobulletin*, Vol. 39, No. 1, pp. 5 – 7.

Wren, 2002. *HSR Writeup* [Online]. Available from: http://www.wren.co.za/HSR Writeup.htm [Accessed 30 October 2002].

Yoshikawa, Y. and Nancollas, G.H., 1984. The kinetics of crystallization of group II fluoride salts in aqueous solution. *Journal of Crystal Growth*, Vol. 69, pp. 357 – 361.

Zemsitis, J.F. Jr., Clark, D.M., Rafal, M., Scrivner, N.C., 1986. *Handbook of Aqueous Electrolyte Thermodynamics*. New York: American Institute of Chemical Engineers.

Appendix A

Review of the Processing of Nickel Ores

To avoid creating the obscured view that calcium and magnesium is problematic in all hydrometallurgical base metal processes, an overview of the processing of these ores are required. This discussion will be limited to the system of interest being the processing nickel ore.

A.1 Processing of Nickel Deposits

In 2000 the demand for primary nickel in the Western World was estimated at 1029 Mt, surpassing the previous record of 1004 Mt set in 1999 (Kuck, 2000). Producers continue to add capacity to commission new mines because of the optimistic forecasts for long-term growth in demand for stainless steels and nickel-based batteries. Nickel is primarily sold for first use as refined metal (cathode, powder, briquette, etc.) or ferronickel. This can then be used in the production of a number value added products. The consumption of nickel in the Western World is given in Figure A.1 based on use.

As seen, the largest portion of nickel is consumed by the production of austenitic stainless steel. It is forecasted that this demand will continue to drive the world nickel market for at least another 20 years. The forecasted growth for stainless steel consumption is between 2% and 5% till the year 2007 after which the growth might increase up to 9% (Kuck, 2000). The other large single application of nickel is super alloys (e.g. Inconel 600) and nonferrous alloys (e.g. cupronickel). Both are used because of their corrosion resistance. The aerospace industry is a leading consumer of nickel-base super alloys used for turbine blades, discs and other critical parts of jet engines. Nickel-base super alloys are also used in land based combustion turbines, such as those found at electric power generation stations. The remaining 23% of consumption is divided between alloy steels, rechargeable batteries, catalysts and other chemicals, coinage, foundry products, and electroplating. The principal commercial chemicals are carbonate ($NiCO_3$), chloride ($NiCl_2$), divalent oxide (NiO), and sulphate ($NiSO_4$).

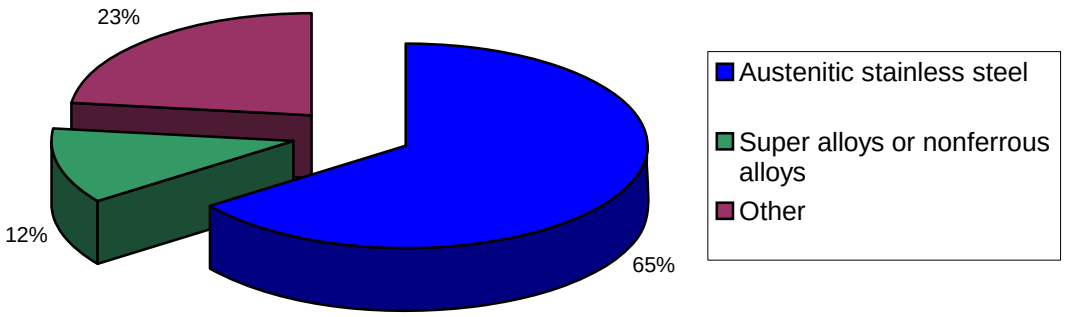

Figure A.1 Consumption of nickel based on use in the Western World (U.S. Geological Survey, 2002)

The bulk of the nickel mined comes from two types of ore deposits being laterites (also referred to as oxide ores) and magmatic sulphides. The principal ore minerals of economic importance are:

- Laterites: nickeliferous limonite [(Fe,Ni)O(OH)] and garnierite (a hydrous nickel silicate)
- Magmatic sulfides: pentlandite [$(Ni,Fe)_9S_8$]

The identified world resources containing 1% Ni or more, is estimated at over 130 Mt of nickel. About 80% of the nickel is in laterite deposits, with only 20% in sulphides. In contrast to this, 60% of the world production of nickel comes from sulphide deposits and only 40% from laterites (Kerfoot, 1991). There are a number of reasons for this imbalance. The nickel content of sulphide ores can be concentrated relatively easily by physical methods such as flotation, while laterite ores must be treated in bulk. Also more numerous and valuable by-product such as precious metals are associated with sulphide ores than with laterites. The only valuable by-product associated with laterites is cobalt. Especially in South Africa, the exploration of sulphide ores is driven by the search for gold and platinum group metals. In these cases the recovery of base metals such as copper and nickel is considered secondary to that of the precious metals. Another reason is that at present, the energy costs of producing nickel from laterite ores using established processes are two to three times

than of sulphide ores. The processing of laterite ores is therefore very sensitive to fuel oil and electricity costs. The energy requirements for producing nickel are given in Table A.1.

Table A.1 Energy requirements to produce nickel (Burkin, 1987).

Process	Typical kWh / (kg Ni)
From sulphide ores containing 1% Ni	
Smelting Process	22
Leaching Process	22
From oxide ores	
2.5% Ni garnierite to matte to metal	57 - 60
2.5% Ni garnierite to 25% FeNi	35 - 42
1.4% Ni mixed ores, Caron process	62 - 84
1.4% Ni laterite, acid process	44 - 57
1.4% Ni laterite, improved acid process (AMAX)	31 - 35

The nickel content of sulphide ores is continually declining and the cost of underground mining is increasing. It is therefore inevitable that laterite ores, which are all relatively uniform in grade and can be surface mined, must support a larger share of the nickel production in future.

To bring the discussion back to calcium and magnesium, the mineralogy of the two types of nickel deposits will now be looked at, followed by the processing of these deposits. The original intention was to give a review of all the process routes available for the processing of nickel ore. This soon proofed to be a too large undertaking if it was to be carried out properly. Luckily it has been done by others (Burkin, 1987 and Kerfoot, 1991) and therefore only a summary would be given here. The intention of the discussion of the processes is not to give a detailed process description but just to highlight the important features of the process route and the behaviour of calcium and magnesium.

A.1.1 Mineralogy of Nickel Deposits

The mineralogy of sulphide and laterite deposits will now be discussed separately.

Sulphide Deposits

The sulphide ores of nickel are derived from liquid magma that ascended from below the earth's crust to form an intrusion, which subsequently solidified on cooling within the pre-existing rock. The magmas that formed the nickel ore usually contained less than 0.3% nickel. During cooling the magma separated into two liquids, a silicate liquid and a heavier sulphide liquid of which the latter usually came to rest in the lower portion of the intrusion. Some of the nickel did not form sulphides and remained in the silicate liquid. The fist silicate that would crystallise is olivine ($9Mg_2SiO_4.Fe_2SiO_4$) followed by the pyroxenes. The pyroxenes include enstatite, $MgSiO_3$; diopside, $CaMg(SiO_3)_2$; jadeite, $NaAl(SiO_3)_2$; spodumene, $LiAl(SiO_3)_2$, etc. The remaining nickel would have preferentially accumulated in the olivine and to a lesser extend in the pyroxenes. Nickel sulphide deposits are therefore associated with large areas of mafic or ultramafic rocks containing nickel in silicates. The sulphide ore bodies can be classified as either massive bodies, containing 90 – 95% sulphide content, or disseminated ore bodies, containing sulphides and silicates in roughly equal proportions.

Nickel sulphide ores consist of nickeliferous pyrrhotite (Fe_7S_8), pentlandite $(Ni,Fe)_9S_8$, and chalcopyrite ($CuFeS_2$). Sulphide ores typically contains 0.4 – 2.0% nickel, 0.2 – 2.0% copper, 10 – 30% iron, and 5 – 20% sulphur. The balance consists of silica, magnesia, alumina and calcium oxide.

Laterite Deposits

Laterite deposits are formed from the weathering of ultra basic rock such as peridotite or serpentine in areas where there are an abundance of rainfall. The major constituent of peridotite rock is olivine, which often contains small amounts of nickel (typically 0.2%) due to the similar ionic radii of iron (0.75 Å), magnesium (0.65 Å) and nickel (0.69 Å). Nickel is therefore able to substitute magnesium and iron in the olivine structure. Serpentine, the second type of rock from which laterite deposits is formed, is an alteration of olivine from which iron has been removed by weathering.

The nickel containing olivine and serpentine were dissolved by acidic surface water containing carbon dioxide. The water, containing dissolved iron, nickel, magnesium and silica, percolated through the rock downwards. Iron is easily oxidised and

precipitated first close to the surface as a hydrated iron oxide, goethite. Most of the cobalt and some of the nickel followed the iron to form a solid solution within the goethite structure. This iron-rich nickeliferous mineral is already enriched with respect to nickel and is referred to as limonitic ore. Limonitic ore is generally uniformed in chemical and mineralogical composition and has poor crystallinity and very fine grain size.

The remaining dissolved nickel, magnesium and silica percolated still deeper into the basic rock. As the dissolved elements penetrated deeper, the pH of the ground water increased due to reactions with the bedrock. This resulted in the precipitation of hydrous nickel-magnesium silicates known as garnierites. The nickel is precipitated in preference to the magnesium resulting in the garnierites being enriched in nickel. This ore has the highest nickel concentrations but is very heterogeneous with respect to chemical and mineralogical composition.

Between the limonite and the garnierite ore occurs a transition zone consisting of various magnesium silicates. The ore in this zone is referred to as serpentine ore. This ore is also very heterogeneous with intermediate nickel, iron, magnesium and silica compositions. The compositions of the three types of ore are given in Table A.2.

Pectora roborant cultus recti

Table A.2 Chemical composition of nickel laterite ores (Burkin, 1987).

Ore	Ni	Fe	MgO	SiO_2
Limonite	0.8 – 1.5	40 – 50	0 – 5	0 – 10
Serpentine	1.5 – 1.8	25 – 40	5 – 15	10 – 30
Garnierite	1.8 – 3.5	10 – 25	15 – 25	30 – 50

A.1.2 Processing of Sulphide Ores

Sulphide ores can be easily and economically upgraded using physical methods such as flotation and magnetic separation. During these beneficiations steps most of the siliceous gangue is rejected from the sulphide concentrate. This can then be processed through a number of routes as indicated in Figure A.2.

The processing of nickeliferous pyrrhotite has been excluded form the diagram since there is little evidence that these processes are still implemented. The nickeliferous

ore was almost exclusively processed by pyrometallurgical methods involving the roasting of the ore. These processes where decommissioned due to unfavourable economics and increasing legislative pressure to reduce sulphur dioxide emissions.

Pyrometallurgical Route

More than 90% of the world's nickel sulphide concentrates are processed to matte using pyrometallurgical methods (Kerfoot, 1991). This is the route that is preferred by precious metals producers. The precious metals are concentrated in the matte, which after leaching of the base metals, provides the feedstock to a precious metals refinery. The matte route involves three steps, being roasting, smelting and converting. During the roasting step, part of the iron is oxidised and the sulphide is driven off as sulphur dioxide. In the following smelting step the roasted product is melted with a siliceous flux to form a matte and a slag phase. The oxidised iron is rejected to the slag, which is then separated from the matte. In the converting step more of the sulphide is oxidised from the matte resulting in more iron being rejected to the slag phase as iron oxide. In modern processes the roasting and smelting has been combined into the flashsmelt step.

The converter matte can be further processed either hydrometallurgically or pyrometallurgically. The continuation of the pyrometallurgical route requires the separation of copper and nickel involving the slow cooling matte separation process whereby a copper sulphide, a nickel sulphide and metallic alloy phase can be formed. These can then be separated by normal beneficiation techniques. The nickel rich fraction can then be roasted to nickel oxide or converted to nickel metal where after it can be further refined by chlorination or carbonylation.

More options exist for the hydrometallurgical treatment of the matte. If the matte has a low copper content the nickel can be directly electrorefined by casting matte anodes. Alternatively one of the following leaching steps can be used:

- Ammoniacal pressure leaching (developed by Sherrit Gordon);
- Atmospheric acid leaching using sulphuric acid (developed by Outokumpu);
- Pressure acid leaching using sulphuric acid (developed by Sherrit Gordon);
- Chloride leaching (independently developed by Falconbridge and Societé Le Nickel).

Kerfoot (1991) gave some guidelines on the selection of the appropriate route for the hydrometallurgical processing of nickel matte. Low copper mattes (>10% Cu) can be treated by ammoniacal pressure leaching, by ferric chloride leaching, or direct electrorefining. Pressure or atmospheric acid leaching, or hydrochloric acid leaching can be used to treat high copper mattes. All of the processes can treat matte at the typical sulphur content of 20 – 23% except for the atmospheric acid leach for which the sulphur content has to be reduced to 6%. The sulphur content can be adjusted during the converting step.

During the hydrometallurgical processing of the converter matte little or no problems are experienced due to calcium and magnesium, even when working in a sulphate medium. Any of the calcium and magnesium present in the ore would report to the slag phase during smelting and converting. If calcium does not enter as a base for pH control, then the concentration of the two elements should be at too low to be problematic.

Direct Hydrometallurgical Route

The only other route for which calcium and magnesium might be problematic would be the direct hydrometallurgical treatment of the ore concentrate. For this route there are two options for leaching the concentrate. The first is the well-known ammonia leaching process developed by Sherrit Gordon. This process was developed as an alternative to smelting in the 1950's. The base metals are extracted in the alkaline medium by the formation of the ammine complexes while the sulphur is oxidised to sulphate. The overall leaching reaction is given in Equation A.1 where M can be Cu, Ni, Co.

$$MS + n\,NH_3 + 2\,O_2 \rightarrow [M(NH_3)_n]^{2+} + SO_4^{2-} \qquad \textbf{Equation A.1}$$

The leaching conditions are 700 kPa air pressure at 70 to 80 °C for 20 to 24 hours (Habashi, 1999). Reactive iron is fixated in the residue as a hydrated oxide together with the pyrite, which does not react. This eliminates the need for an iron control step. The ammonia medium is also ideal for the hydrogen reduction of the base metals

since the ammonia would neutralise any acid formed during the reduction process. From what can be deduced from literature is that calcium and magnesium is not problematic to the Sherrit Gordon process. This can be attributed to the selectivity of the leaching reactions towards base metals and the use of hydrogen reduction to recover them. The second option for the direct hydrometallurgical treatment of sulphide ore concentrates is pressure acid leaching.

Little information has been found in literature on large-scale implementation of the pressure acid leaching option for the processing of nickel sulphide ore concentrates. Although a number of pilot studies have been done on this route, evidence was found of only one process that has been implemented on a commercial scale. The overall reaction for the leaching of the sulphides is given in Equation A.2 where M is Ni, Cu, Co, Fe.

$$MS + H_2SO_4 + \tfrac{1}{2} O_2 \rightarrow MSO_4 + S^0 + H_2O \qquad \textbf{Equation A.2}$$

Although the bulk of the iron is again fixated in the residue by hydrolysis, an iron control step is still required for the pregnant leach solution. The sulphuric acid would also attack the magnesia in the concentrate resulting in the leaching of magnesium into the pregnant leach solution. Part of the elemental sulphur formed can be further oxidised to sulphate according to Equation A.3.

$$S^0 + 1\tfrac{1}{2}O_2 + H_2O \rightarrow H_2SO_4 \qquad \textbf{Equation A.3}$$

The ratio of elemental sulphur to sulphate formed is influenced by the following factors (Dreisinger, 2001):

- Acidity,
- Oxidation-reduction potential,
- Temperature,
- Sulphide mineralogy and
- Presence/concentration of various soluble species like iron.

The conversion of sulphur to sulphate results in the formation of acid that needs to be neutralised. A higher conversion of sulphur would therefore increase the consumption of alkaline to neutralise the acid. Calcium bases like lime is preferred on an economic basis due to the high consumption in these processes. Temperature is one of the major factors influencing the formation of sulphate and accordingly it can be divided into three regimes (Dreisinger, 2001):

- Low temperature (100 to 110 °C), below the melting point of sulphur,
- Intermediate temperature (140 to 160 °C), partial recovery of sulphur as elemental sulphur and
- Elevated temperature (200 to 220 °C), complete oxidation of sulphur to sulphate.

All three of these regimes have been studied on pilot scale by a number of companies. The only commercial implementation found is the HIKO process developed by Outokumpu that came on stream in December 1991. This process operates in the low temperature regime. For this particular process two solvent extraction steps have been introduced to remove calcium and magnesium from the pregnant leach solution.

Calcium and magnesium can cause problems for down stream processes during the pressure acid leaching of sulphide concentrates. Calcium and magnesium would enter the process during leaching, and owing to the use of a calcium base. The concentrations of the two elements would be high enough to be problematic. Additionally, the pressure acid leaching of sulphides results in a sulphate medium for which calcium poses the problem of calcium sulphate precipitation.

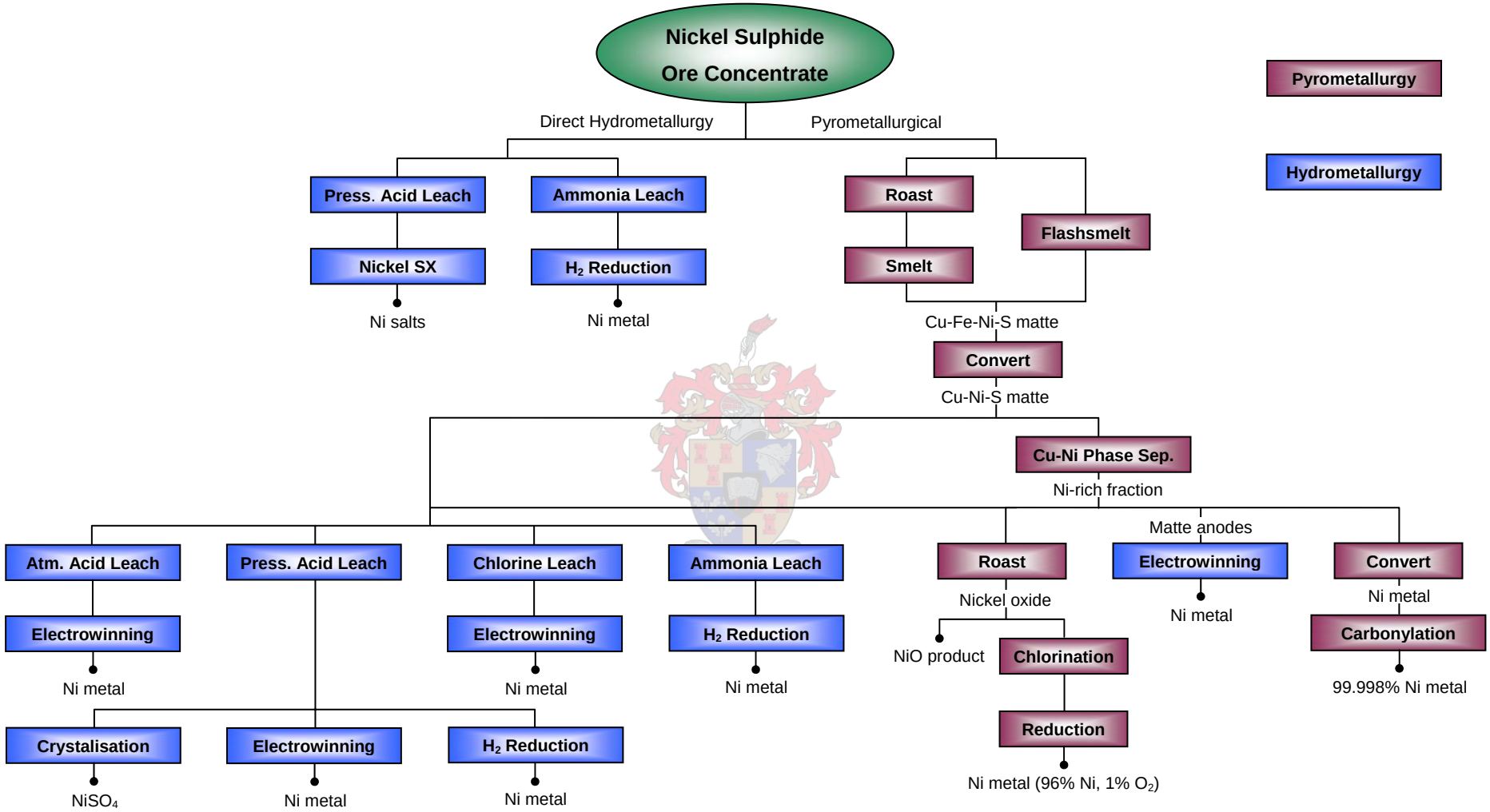

Figure A.2 Routes for the processing of nickel sulphide ore (adapted from Burkin (1987)).

A.1.3 Processing of Laterite Ores

Most laterite deposits contain both the iron rich limonite and the magnesium rich garnierite ore. Selective mining and screening can separate these two types of ore, but the ore is not amenable to further beneficiation by standard ore preparation techniques and must be treated in bulk. Three main routes exist for the treatment of the laterite ores:

- The pure pyrometallurgical treatment of the ore,
- The combined pyro and hydrometallurgical treatment and
- The pure hydrometallurgical treatment of the ore.

These possible routes are summarised in Figure A.3. Garnierite ore, with its higher nickel content (up to 3%) and its lower iron content, is better suited for the production of ferronickel or matte, using pyrometallurgical routes. Limonitic ore, on the other hand, with its lower nickel content (up to 1.5%) and higher iron and cobalt content, is better treated using hydrometallurgical routes. The nickel content of limonitic ore is too low and the iron content too high to be economically treated using pyrometallurgical routes and the high magnesia content of garnierite ore would results in a too high consumption of leaching reagent in hydrometallurgical routes.

Pectora roborant cultus recti

Pyrometallurgical

For the pyrometallurgical processing of laterites, the ore can by subjected to reductive smelting step to produce ferronickel or it can be smelted with a source of sulphur to produce a matte. During ferronickel production the ore is first subjected to a drying step in a kiln to remove the chemical bounded water (typically up to 45%). This also acts as a prereduction step. This is followed by smelting in an electric furnace under reductive conditions. Nickel is a more noble metal than iron and by controlling the reduction potential during smelting would allow the almost complete reduction of nickel while only partially reducing the iron. It is therefore possible to control the iron to nickel ratio of the ferronickel so that it can be directly used for steel making. If the iron content of the ferronickel is too high it can be adjusted during an extra conversion step by oxidising the iron. The ferronickel can also be subjected to a sulphidising step to produce a matte.

Matte smelting of the laterite ore is carried out with similar process equipment as ferronickel production. It is also dried in a kiln after which it is smelted in an electric furnace. The difference is that a sulphur source in the form of elemental sulphur or a sulphide mineral is fed with the ore. Most of the nickel and a large portion of the iron is reduced and sulphidised, to form a low sulphur matte. If required additional iron removal can be carried out in a converting step.

Combined Pyro and Hydrometallurgical

The only process in this route is the Caron process named after its inventor. This process involves four main operations (Burkin et al., 1987):

- Ore drying and grinding,
- Reductive roasting,
- Leaching with ammonical ammonium carbonate solution and
- Metals recovery from solution.

During the ore drying a considerable amount of energy is expended to remove the 30 to 50% moisture from the ore. The second operation involving the reduction of the ore is also energy intensive and combined they account for 60% of the energy requirements of the Caron process. The objective of the reduction operation is to selectively reduce cobalt and nickel to the metallic state without a significant amount of iron following them. The metallics are then leached in the ammoniacal ammonium carbonate solution where the iron is hydrolysed and precipitated as ferric hydroxide. The pregnant leach solution is subjected to a number of purification steps including cobalt recovery after which the nickel is precipitated as a basic nickel carbonate. From this point onwards there exist a few variations for the recovery of nickel. The nickel carbonate can either be calcined to produce nickel oxide as the final product or it can be dissolved again in an ammonium sulphate solution to be precipitated as metallic nickel with hydrogen.

The application of the Caron process is limited to the iron rich limonitic ore. Nickel losses are high for garnierite and serpentine ore due to the nickel being incorporated into the forsterite lattice (Mg_2SiO_4) formed during the roasting of the ore. Dissolution of the magnesium during the leaching of the ore would also result in the loss of ammonia due to the precipitation of magnesium ammonium carbonate.

Hydrometallurgical

The laterite ore is leached under pressure at elevated temperatures of 240 to 260 °C using sulphuric acid. The pressure acid leaching route for laterites is considered to be an improvement over the Caron process since the ore is directly treated hydrometallurgically, avoiding the energy intensive drying and reduction operations. Higher recoveries (> 90%) for both nickel and cobalt can also be obtained with pressure acid leaching compared to the 75 to 80% recovery of nickel and 40 to 50% recovery of cobalt in the Caron process.

The first commercial implementation of the pressure acid leaching of laterites was at Moa Bay in Cuba. At this operation the nickel and cobalt is precipitated as an intermediate product of sulphides to be refined elsewhere. Moa Bay used to be the only plant implementing pressure acid leach of laterites for more than a quarter of a century until the recent interest in this technology for the processing of Australian laterites. Three operations have recently been commissioned in Australia and all of them produce LME (London Metal Exchange) grade metallic nickel by electrowinning or hydrogen precipitation.

The pressure acid leaching of laterites is limited to limonitic ore as a result of the high acid consumption of the magnesia content in garnierite ore. A hydrometallurgical process that was developed to treat both limonitic and garnierite ore was introduced by the AMAX Company. In this process the ore is first split into a limonitic fraction and a garnierite fraction through screening. The limonitic fraction is then pressure acid leached while the garnierite fraction is calcined. The pregnant leach solution is then used to leach the garnierite at atmospheric conditions. The garnierite ore also serves to neutralise the acid from pressure leaching. In the original AMAX process the metal values were also precipitated as sulphides as in the Moa Bay process.

Both calcium and magnesium have the potential to be problematic in the routes involving pressure acid leaching of laterites. The magnesium level could be high owing to the relative high magnesia content of the ore and the sulphuric acid would provide the sulphate medium in which calcium could be problematic.

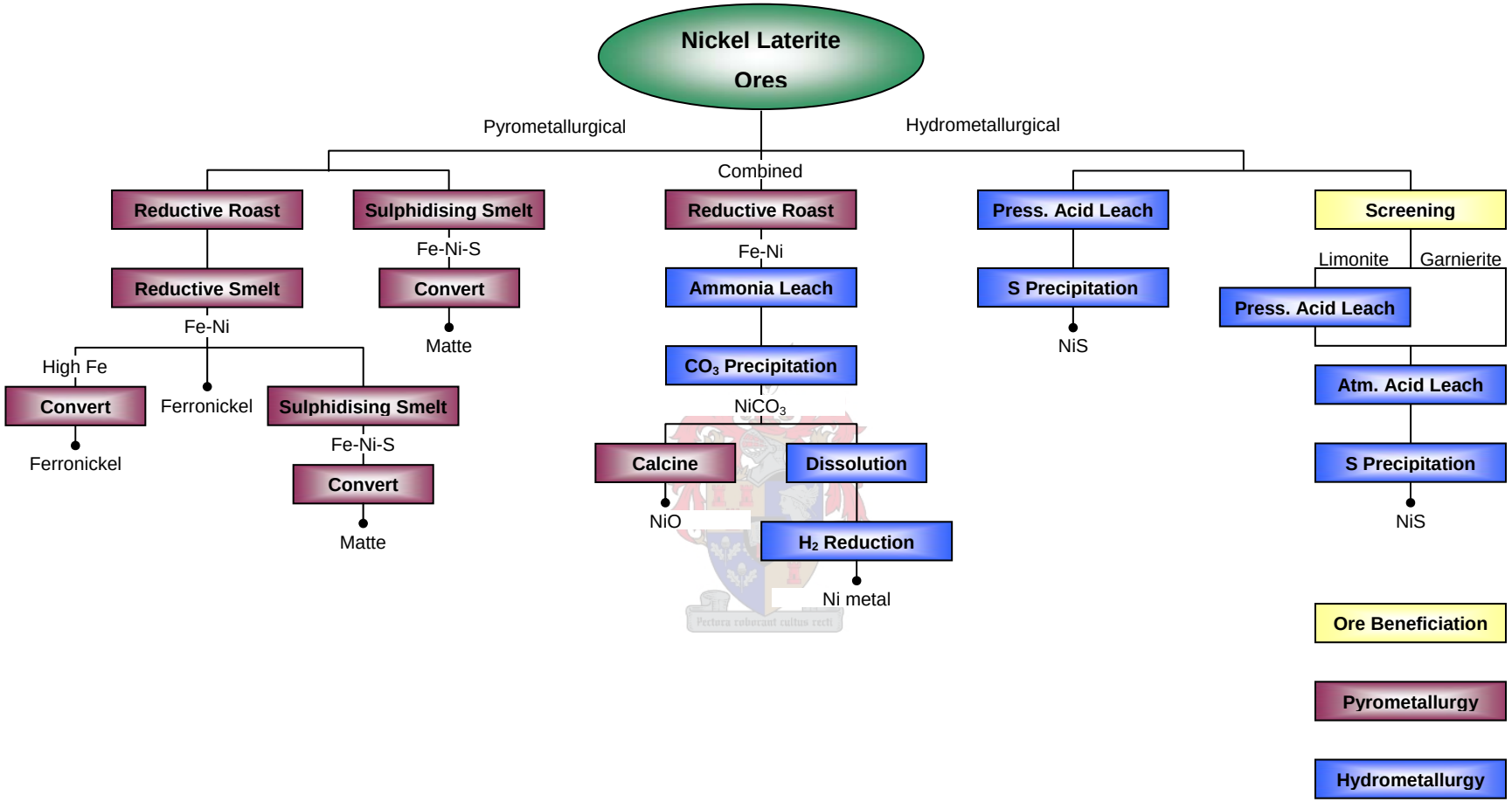

Figure A.3 Routes for processing nickel laterite ore.

A.1.4 Summary of Nickel Ore Processing

In Section A.1.1 nickel deposits were divided into sulphides and laterites. For both of these types of deposits it was shown that the nickel minerals are associated with minerals containing high levels of magnesium. From thereon the processing of sulphide ores and laterite ores was discussed in Section A.1.2 and A.1.3. Pyrometallurgical routes dominate the processing of nickel ores for both ore types. The technologies for hydrometallurgical routes are still fairly young and the most of them were only developed in the latter half of the twentieth century.

The possible routes involving a sulphate medium for which calcium and magnesium can be problematic were identified. For sulphide ores the identified route was the direct hydrometallurgical treatment of ore concentrate using pressure acid leaching. Calcium could also be problematic in the pressure or atmospheric acid leaching of matte if it was introduced as a base into the process. Magnesium would not be a problem in the leaching of matte since it would have been rejected to the slag phase during smelting. For the laterites, the pressure acid leaching route was identified.

To distinguish the systems for what calcium and magnesium is problematic, there have to be looked at the method by which the valuable metals are separated and recovered. In many of the older circuits the base metals was separated and recovered as precipitated sulphides. With sulphide precipitation a separate copper sulphide, a mixed nickel cobalt sulphide (with a Ni:Co molar ratio of approximately 3:1) and a nickel sulphide precipitate could be produced. The intermediate sulphide products were then refined elsewhere. The precipitation of sulphides was an effective general purification step and would have separated the calcium and magnesium from the base metals. Although it is very reagent intensive step for both precipitating the base metals and leaching them again it has been incorporated into modern flowsheets as a single precipitation-and-releach step (Mayze, 2002).

Sulphide precipitation does provide a degree of separation of the base metals, but to produce high purity products, there has to be looked at solvent extraction for both high recovery and selective removal. This is especially true for the separation of cobalt from nickel using Caynex 272 where a separation factor of up to 7000 has been reported (Burkin et al, 1987). It is unfortunate that although a high degree of

separation between the base metals and calcium and magnesium can also be obtained, that the precipitation of calcium may be problematic.

Appendix B

Discussion on Some of the Analytical Methods

B.1 Atomic Absorption Spectrometry

The metal ion concentrations (Ni, Co, Ca, Mg, Mn, Zn) were measured using atomic adsorption spectrometry (Varian SpectrAA 250 Plus). The samples were diluted 100x to fall in the optimum range for the analysis, except for zinc with only needed to be diluted 10x. The samples were diluted with a 10% nitric acid (HNO_3) solution containing 5 g/ℓ lanthanum (La) as a releasing agent. The instrument was set-up to calculate the concentration based on three absorption measurements (each 3 seconds long). Each sample was then analysed three times for which the instrument was recalibrate in between. The standard deviation for the three measurements relative to the average was less than 1% for most of the analysis.

The releasing agent was required to ensure that calcium and magnesium was completely dissociated in the solution. The effect of it can be seen in Table B.1. Given are the measurements with and without lanthanum for a sample made up with known mass of the sulphate salts. Better results were obtained in the presence of lanthanum.

Table B.1 Effect of the releasing agent (1000 mg/ℓ La) on calcium and magnesium.

Element	Calculated (mg/ℓ)	Measured without La (mg/ℓ)	Measured with La (mg/ℓ)
Calcium	5.70	5.89 (+3.3%)	5.59 (-1.9%)
Magnesium	35.8	23.7 (-33.8%)	34.0 (-5.0%)

B.2 Fluoride Ion-Specific Electrode

In the most samples the ratio of the fluoride to the sulphate was too low for it to be analysed using liquid chromatography. The concentration of sulphate would have been too high for the instrument's column if the sample's fluoride concentration were diluted to the measurable range. For these samples the fluoride concentration was measured using a fluoride ion-selective electrode (Radiometer selectrode F1052F)

with a calomel reference electrode (Radiometer REF 401). The instrument used to measure the e.m.f. was a Radiometer PHM 82. It has an accuracy of ± 1mV that equates to ± 4% of the measured concentration.

Interferences from hydroxide ions and complexation for metal ions were eliminated using a *total ionic strength adjustment buffer*, TISAB, at a pH of 5.5. The buffer was prepared according to the method provided by Jeffery et al (1991):

- 57 mℓ of acetic acid, 58 g socium chloride and 4 g cyclohexane diamino-acitic acid (CDTA) was dissolved in 400 mℓ of de-ionised water.

- The temperature of the solution was kept constant by placing the beaker inside a water bath.

- The pH was measured using a glass electrode pH-meter while it was adjusted to 5.5 using a 5M sodium hydroxide solution.

- The solution was then made up to the 1ℓ mark in a graduated flask.

The pH-buffer would avoid the interferences from hydroxide ions while the CDTA would complex with any polyvalent ions that may interact with the fluoride. The samples would also have a constant ionic strength by virtue of the high ionic strength of the TISAB.

The concentration of fluoride was determined from the e.m.f. according to Nernst equation:

$$E_t = k_e + k \cdot Logc_b \qquad \textbf{Equation B.1}$$

Where:

E_t : Measured e.m.f.,

k_e : Electrode constant,

k : Experimental slope,

c_b : Concentration

The calibration of the fluoride electrode at 30°C is given in Figure B.1. Calibrating and measuring the samples at a constant temperature of 30°C in a water bath eliminated the effect of temperature. For easier use Equation B.1 has been transformed into:

$$c_b = 10\exp\left(\frac{1}{k}E_t - \frac{k_e}{k}\right) \qquad \textbf{Equation B.2}$$

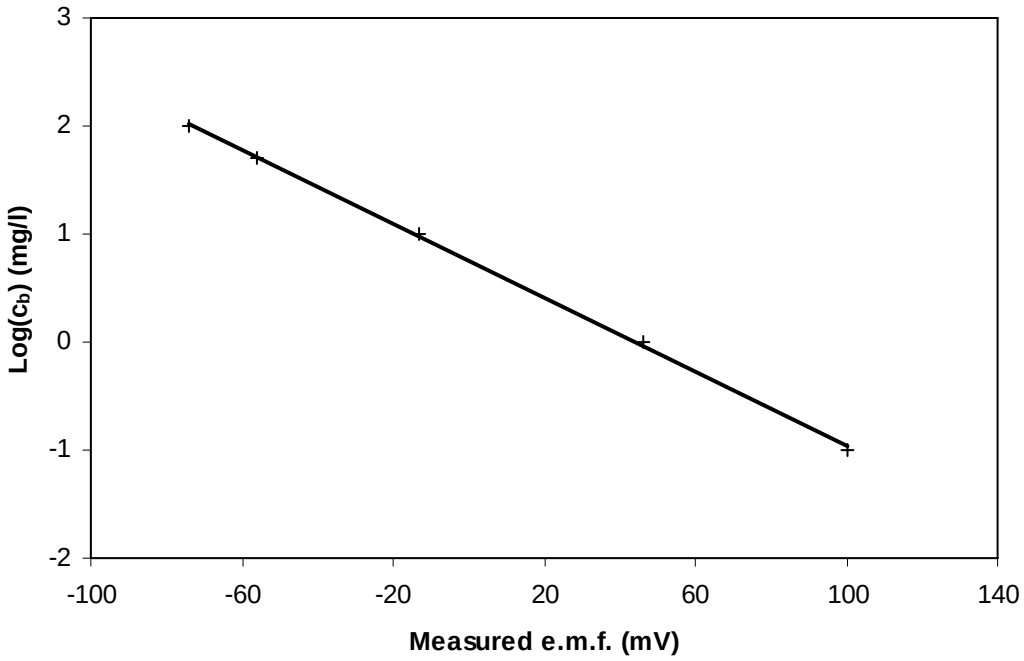

Figure B.1 Calibration of the fluoride electrode at 30°C.

The result from the calibration was the following:

$$c_b = 10\exp(-0.0166E_t + 0.771) \qquad \textbf{Equation B.3}$$

$R^2 = 0.9999$

B.3 Filtration Tests

The aim of the filtration tests was to gather volume filtrate and time data for the calculation of the mass filtration resistance. The experimental set-up for the filtration tests is illustrated in Figure B.2.

The volume data was deduced from a measuring cylinder used to add the sample to the feeding funnel for which the time measurements was taken at the datum provided by the neck of the funnel. The advantage of using the beginning of the funnel neck as a datum was its relative small cross sectional area, providing a much more accurate time versus volume measurements. The funnel also ensured that the filter cake was not disturbed by the addition of new sample.

A volume was provided for the formation of the filter cake. This volume allowed the solution coming from the funnel to spread and form a uniform cake. A 0.45 μm Millipore membrane filter supported by a sinter-glass disc was used to retain the solids. The filtrate was collected in a 1 ℓ flask connected to a vacuum line.

The other properties required for the determination of the mass filtration resistance are the viscosity, mass of precipitate per volume filtrate, filtration area and the applied vacuum. These where determined to be:

Viscosity:	0.00173 Pa.s
Mass precipitate:	10 kg/m^3
Filtration Area:	0.001018 m^2
Vacuum:	88000 Pa

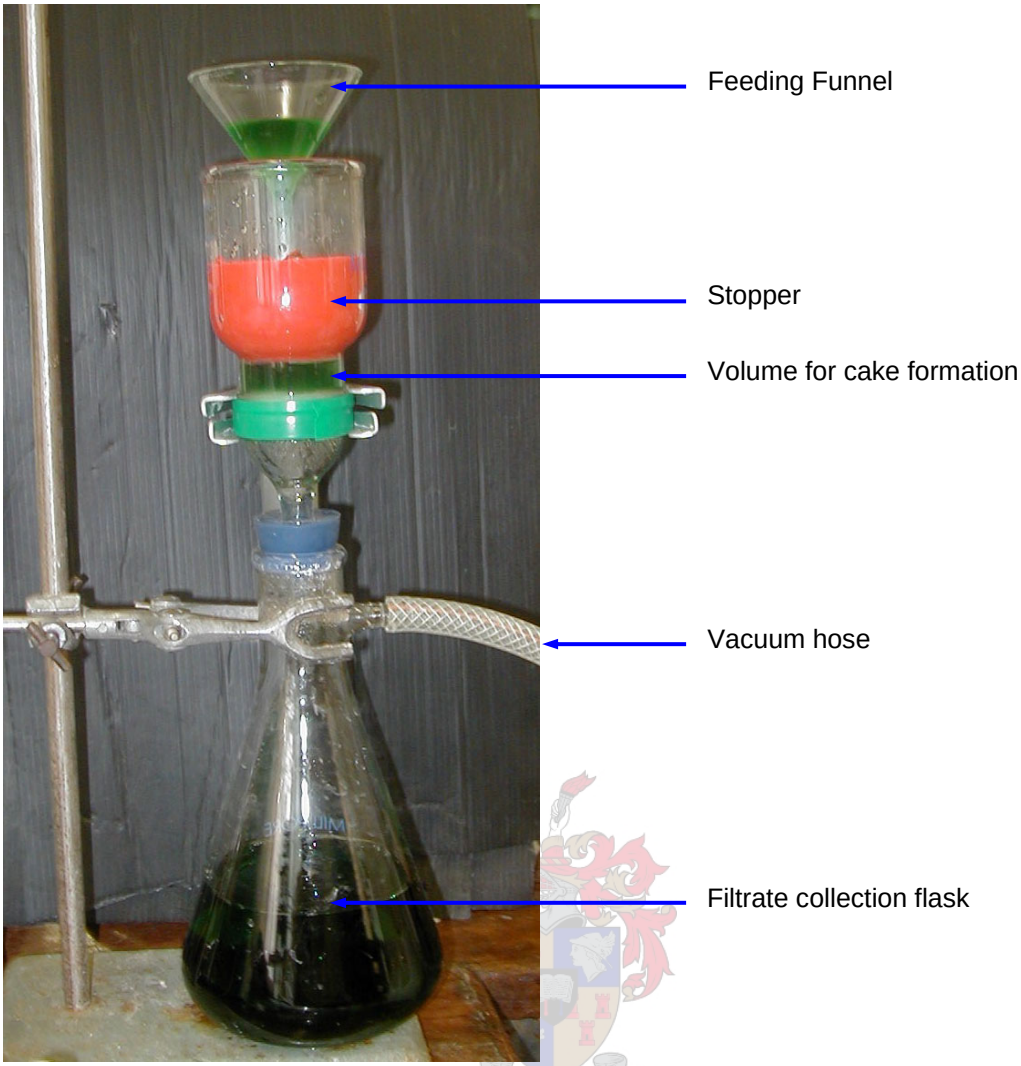

Figure B.2 Filtration tests set-up.

Appendix C

Method of Factorial Design

The method of factorial designed experiments was the appropriate method for the investigation of variables that was seen as external variables using the least amount of experiments. This would allow the comparison of the relative effects of these variables on a selected measure. Provided here is a short discussion on the method used.

Only two variables were investigated at a time for the instances that this method has been applied. The factorial designed experiments would therefore only amount to four experiments without replication. Included in the design was an extra centre run at the conditions that was seen as the normal operating conditions for these variables. For each variable a high and a low level was selected, which was evenly spread around the centre run. Illustrated in Figure C.1 is the experimental design for the above where +1 and –1 denotes the high and low levels.

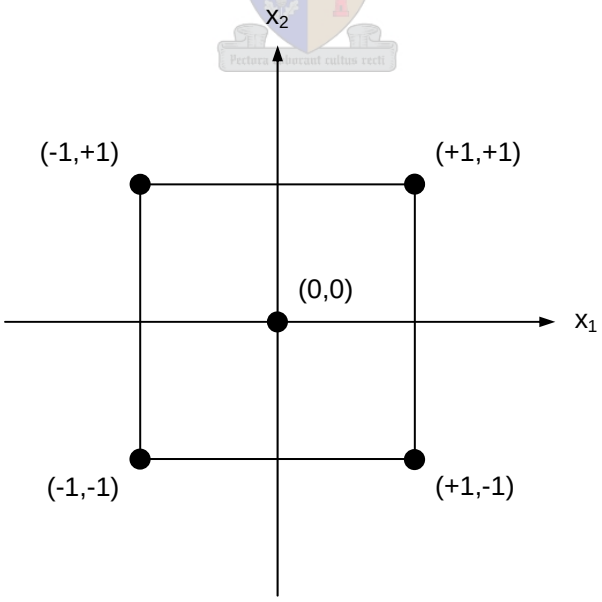

Figure C.1 The 2^2 factorial design with centre run, used in the experimental investigations.

The results obtained were used to calculate the effects of the variables and to see if there is any interaction between them. Let Table C.1 denote the results obtained from the experiments:

Table C.1 Tabulated factorial design.

x_1	x_2	y
-1	-1	$y_{(-1,-1)}$
+1	-1	$y_{(+1,-1)}$
-1	+1	$y_{(-1,+1)}$
+1	+1	$y_{(+1,+1)}$
0	0	$y_{(0,0)}$

The effect of a variable is defined as the difference between the average response at the high level of the variable and the average response at the low level. For x_1 and x_2 the effects are calculated as follows:

$$\text{effect of } x_1 = \frac{\left(y_{(+1,-1)} + y_{(+1,+1)}\right)}{2} - \frac{\left(y_{(-1,-1)} + y_{(-1,+1)}\right)}{2} \qquad \textbf{Equation C.1}$$

$$\text{effect of } x_2 = \frac{\left(y_{(-1,+1)} + y_{(+1,+1)}\right)}{2} - \frac{\left(y_{(-1,-1)} + y_{(+1,-1)}\right)}{2} \qquad \textbf{Equation C.2}$$

Interaction is defined as the dependence of the effect of one variable, on the level of the other. An interaction plot as shown in Figure C.2 and Figure C.3 can easily identify this. Figure C.2 represents a response where there is no interaction between the two variables. This is seen from the lines of the plot being parallel to each other while in Figure C.3 it is not, indicating some interaction.

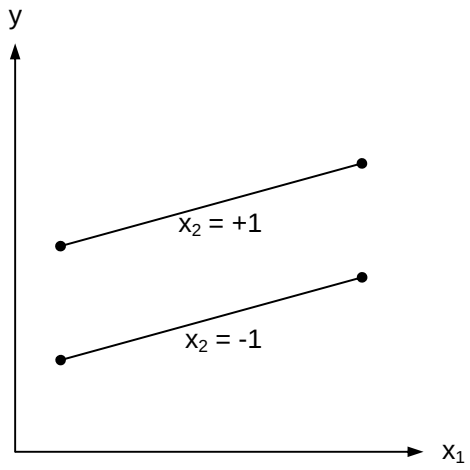

Figure C.2 An interaction plot indicating no interaction between x_1 and x_2.

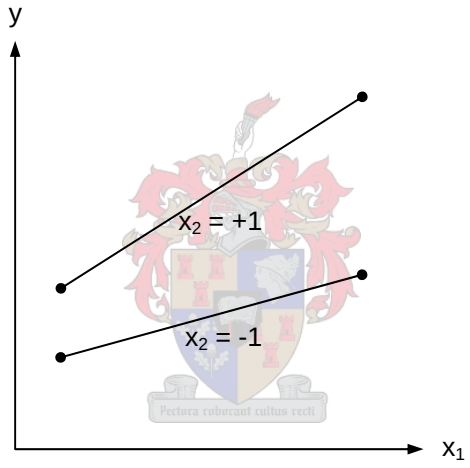

Figure C.3 An interaction plot with interaction between x_1 and x_2.

Statistical software packages such as Statistica can be used to analyse the results obtained. The program would allow the fitting of a surface described by Equation C.3 to the data. The coefficients of each of the single variables (β_1 and β_2) would represent their effect while β_{12} the interaction.

$$y = \beta_0 + \beta_1 x_1 + \beta_2 x_2 + \beta_{12} x_1 x_2 \qquad \textbf{Equation C.3}$$

Appendix D

Photograph Plates

D.1 Experimental Set-up

Figure D.1 Set-up overview.

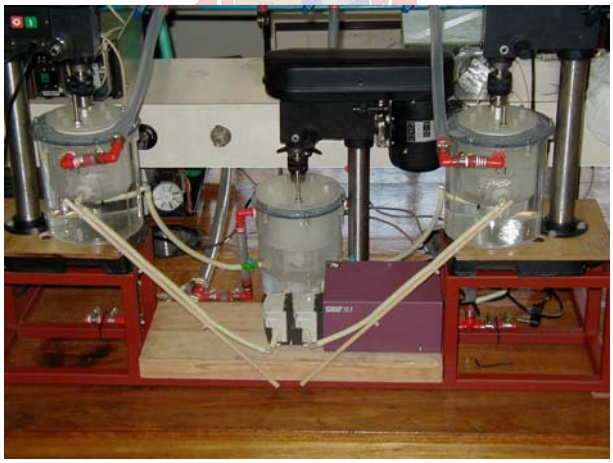

Figure D.2 Closer view of reactors.

Figure D.3 Water bath.

Figure D.4 Overview of the inlet reactor.

Figure D.5 Close view of the bulk reactor.

Figure D.6 Side view of an inlet reactor.

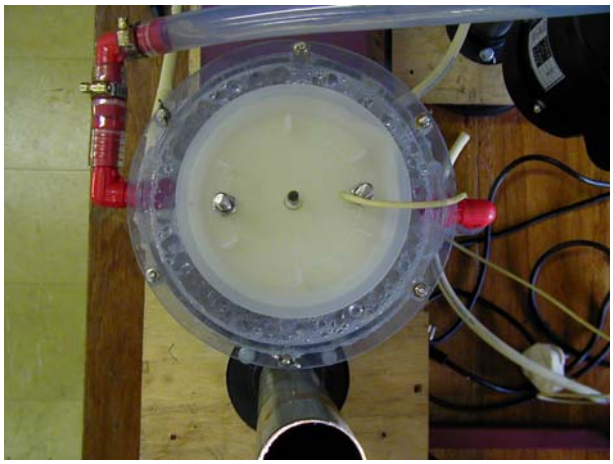

Figure D.7 An inlet reactor from the top.

Figure D.8 An inlet reactor with the internals removed.

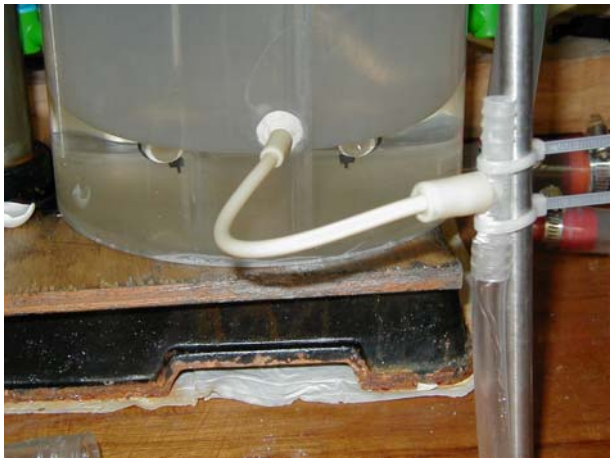

Figure D.9 Product outlet from the bulk reactor.

Figure D.10 Product beaker.

Figure D.11 Close view of the product beaker.

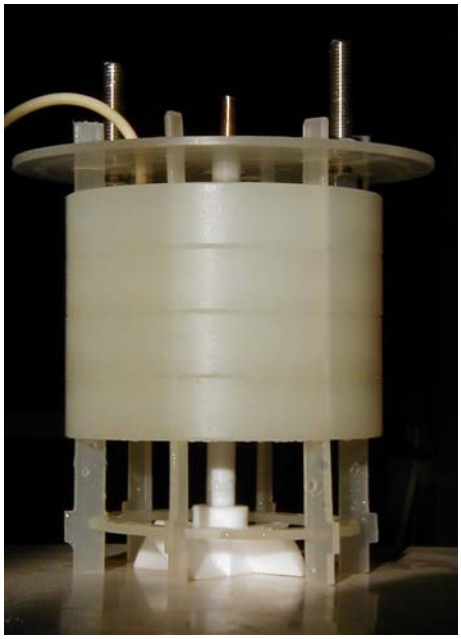

Figure D.12 Inlet reactor internals.

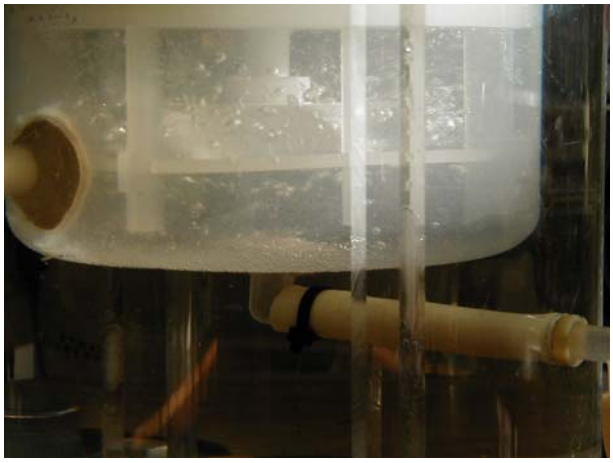

Figure D.13 Close view of the in- and outlets of an inlet reactor.

Figure D.14 Close view of the in- and outlets of the bulk reactor.

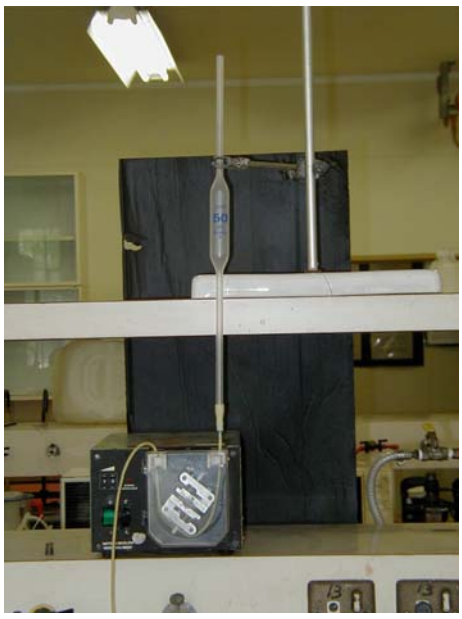

Figure D. 15 Feeding system for the batch experiments.

Figure D.16 Scaling in the Bulk reactor.

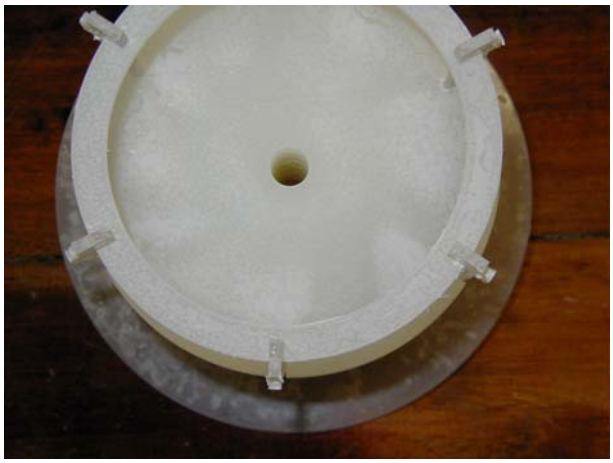

Figure D.17 Scaling on the reactor internals.

Pectora roborant cultus recti

D.2 Column Adsorption Set-up

Figure D.18 Column packed with activated alumina.

Figure D.19 Activated alumina column during the loading cycle.

Figure D.20 Close view of column during loading cycle.

Figure D.21 Activated alumina bed during fluidisation.

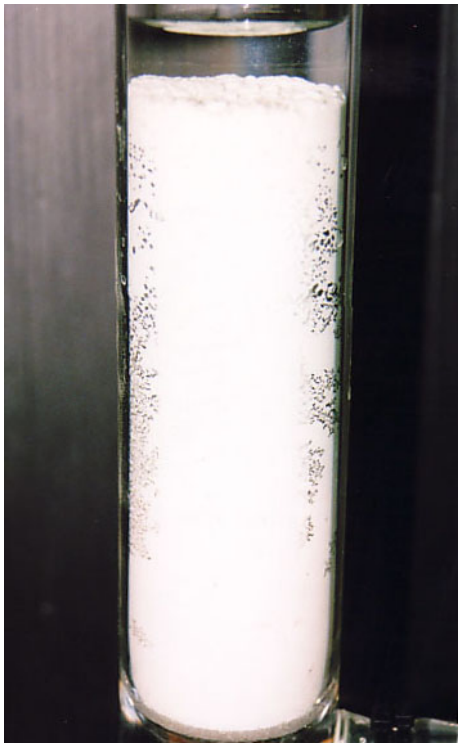

Figure D.22 Close view of column after the desorption cycle.

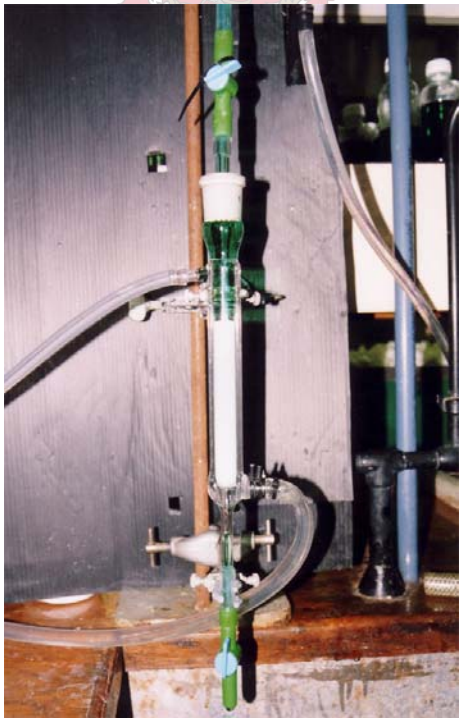

Figure D.23 Small column.

Appendix E

Experimental Results

E.1 Preliminary Batch Precipitation Experiments

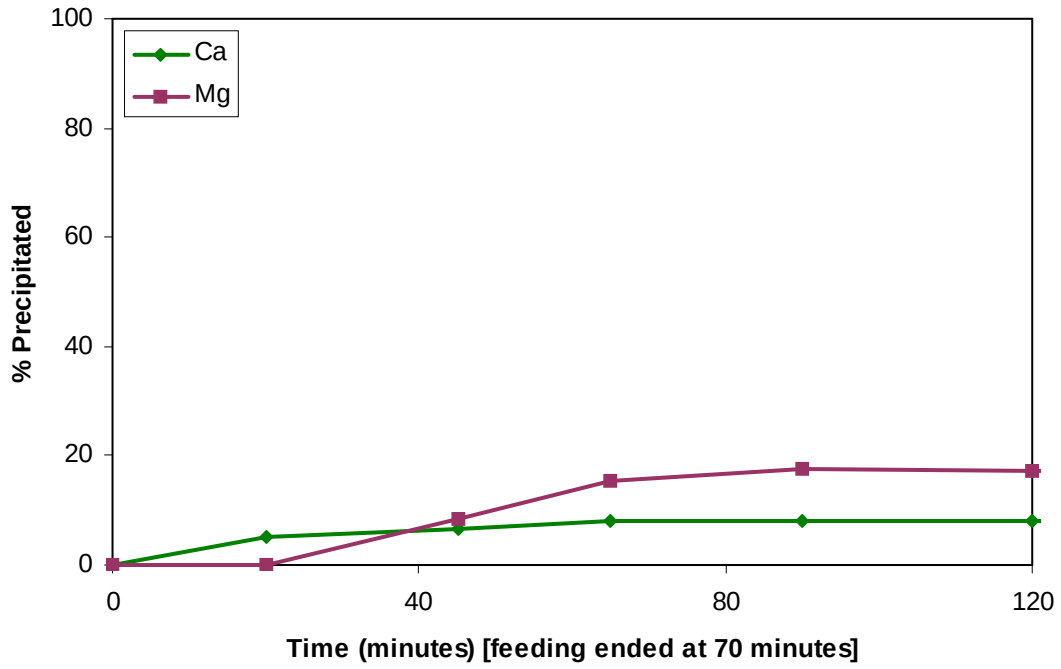

Figure E.1 Initial batch experiment: 20% F-addition.

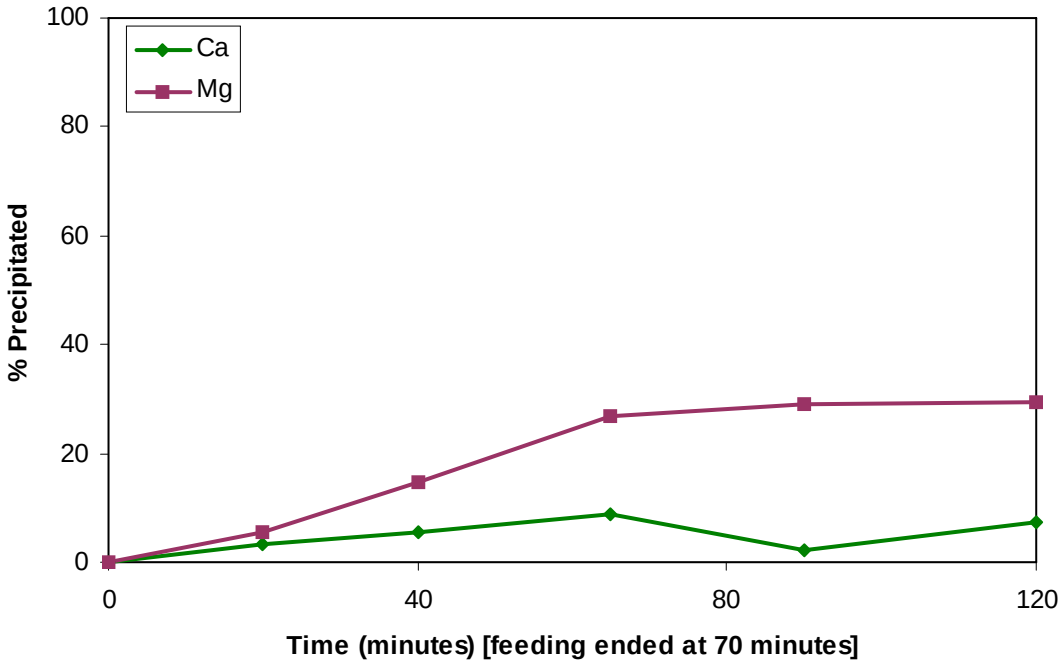

Figure E.2 Initial batch experiment: 25% F-addition.

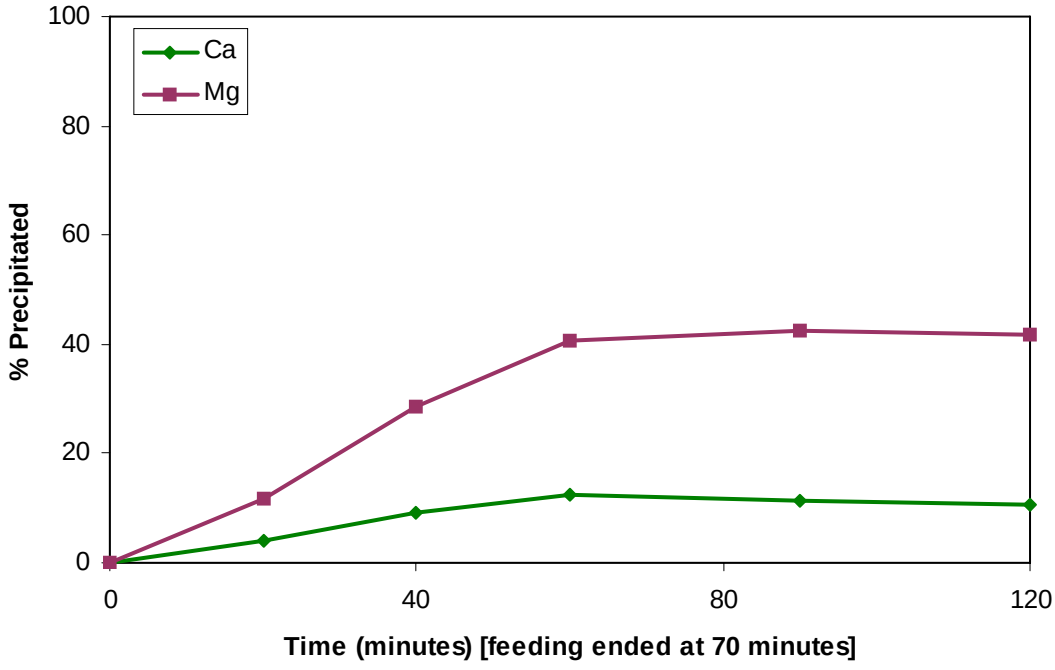

Figure E.3 Initial batch experiment: 45% F-addition.

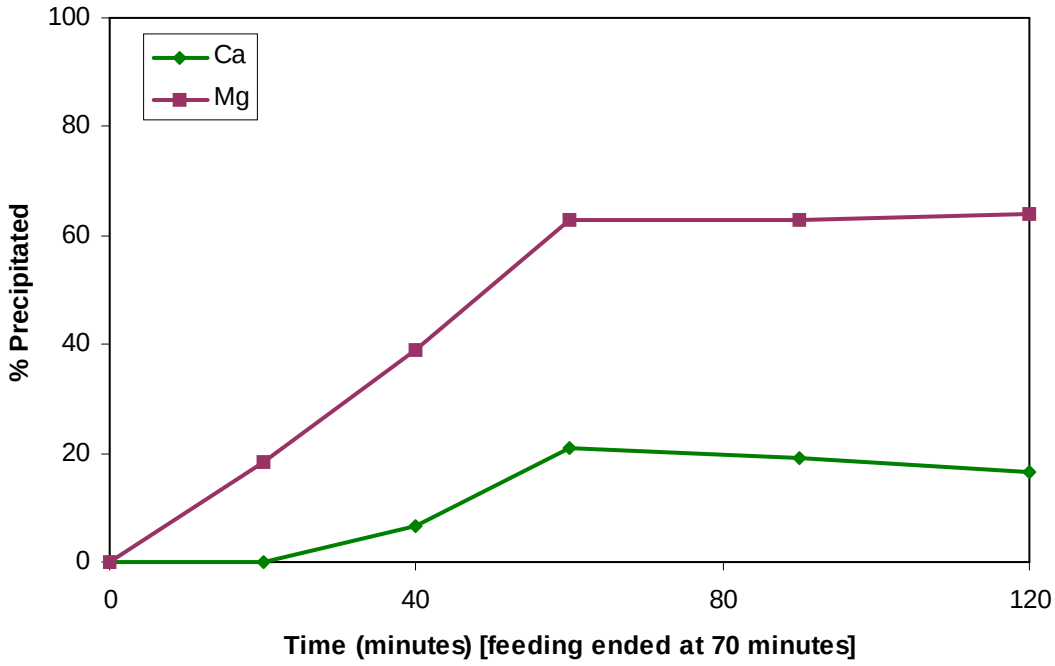

Figure E.4 Initial batch experiment: 75% F-addition.

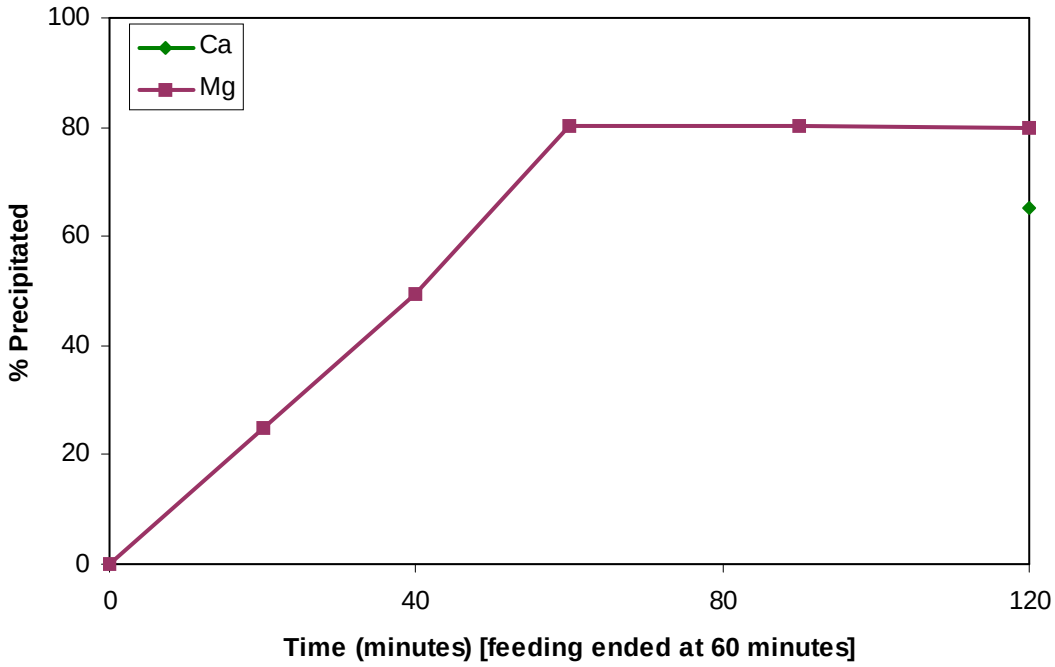

Figure E.5 Initial batch experiment: 100% F-addition.

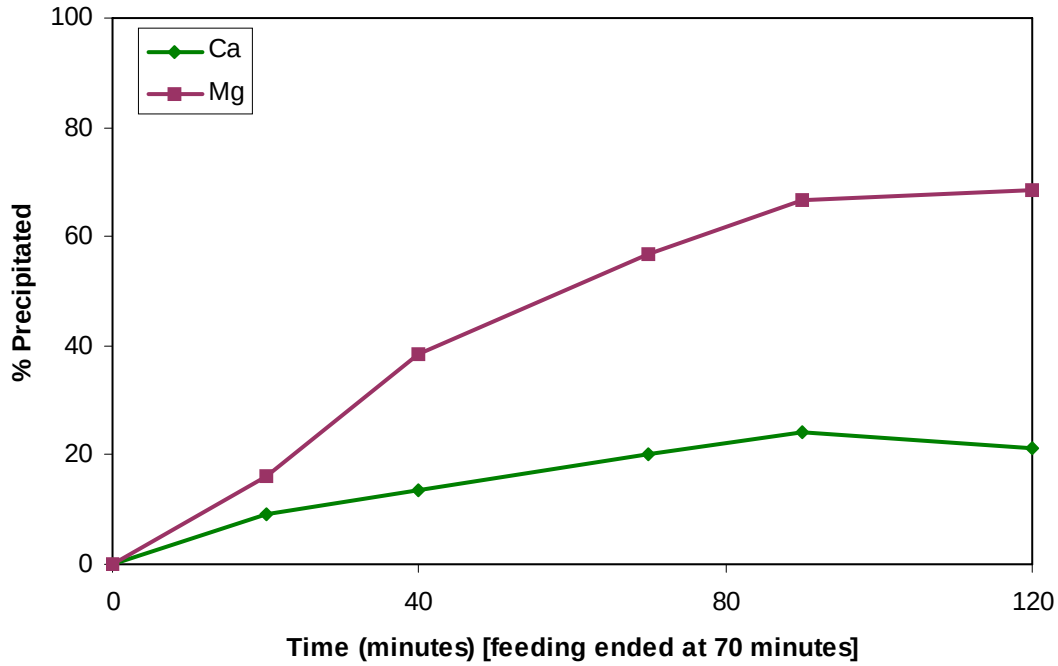

Figure E.6 Initial batch experiment: 100% F-addition as HF.

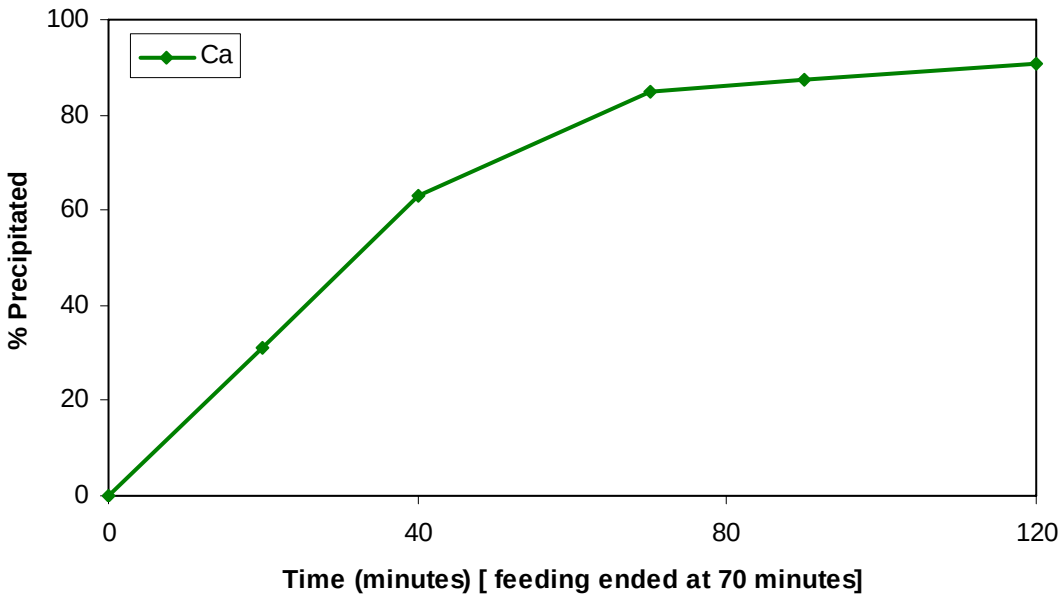

Figure E.7 Initial batch experiment: 100% F-addition with only Ca present.

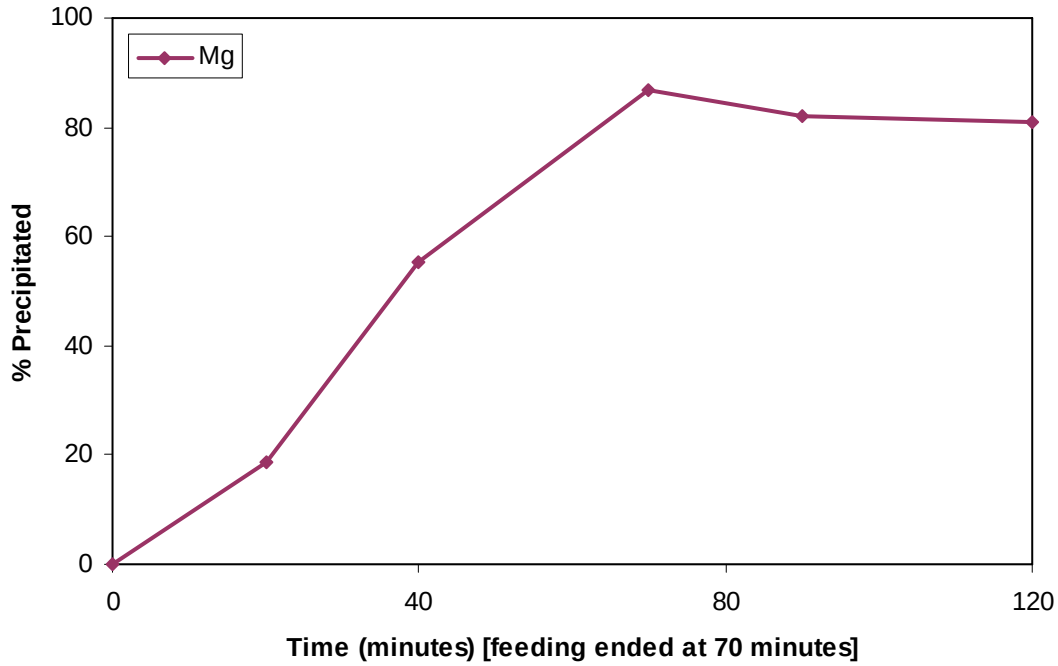

Figure E.8 Initial batch experiment: 100% F-addition with only Mg present.

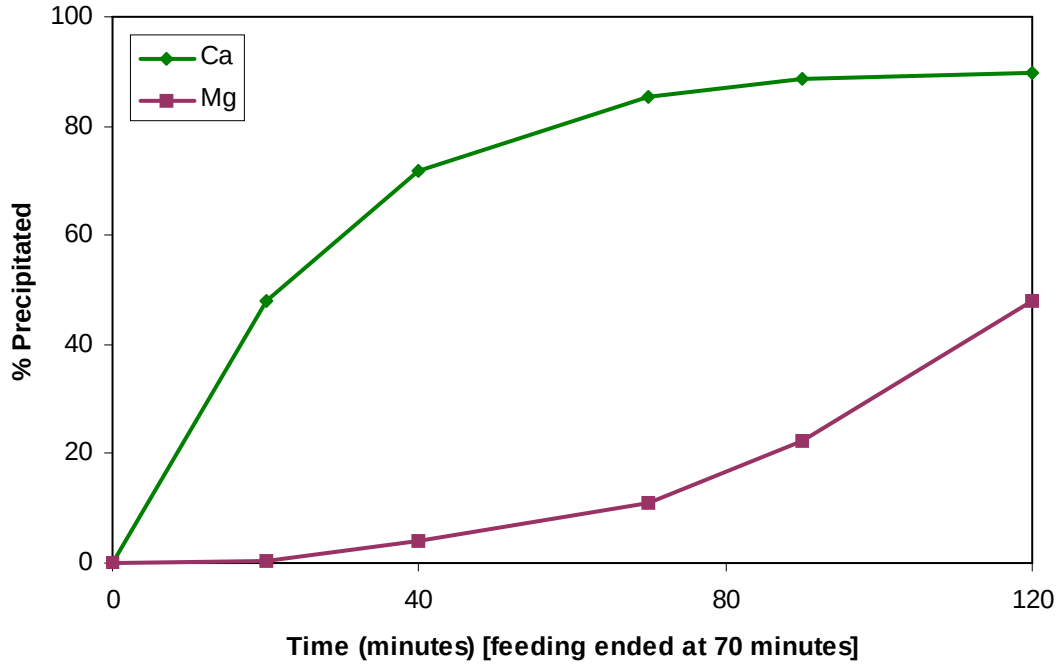

Figure E. 9 Initial batch experiment: 100% F-addition with Mg : Ca = 1 : 1.

E.2 Batch Precipitation Experiments

Table E.1 Fluoride addition results.

Experiment	F-addition	Factor	Concentration (g/ℓ)						% Precipitated	
	%		Ca	Mg	Ni	Co	Mn	Zn	Ca	Mg
Feed	-	1.000	0.556	3.486	31.00	1.72	0.281	0.118	0	0
10% add	10	0.995	0.525	3.045	29.64	1.65	0.268	0.111	0.79	8.28
25% add	25	1.003	0.515	2.538	29.42	1.64	0.269	0.112	2.70	23.56
50% add	50	0.993	0.478	1.625	29.39	1.64	0.270	0.112	9.74	51.05
75% add	75	0.980	0.422	0.759	29.94	1.64	0.266	0.111	20.29	77.13
100% (1) add	100	0.983	0.079	0.159	30.20	1.63	0.266	0.111	85.10	95.20
100% (2) add	100	0.970	0.080	0.152	29.85	1.62	0.264	0.114	84.88	95.43
110% add	110	0.995	0.018	0.048	30.12	1.66	0.263	0.111	96.55	98.56

Table E.2 Results for identity of soluble fluoride.

Experiment	F-addition	Factor	Concentration (g/ℓ)						% Precipitated	
	%		Ca	Mg	Ni	Co	Mn	Zn	Ca	Mg
Feed	-	1.000	0.556	3.486	31.00	1.725	0.281	0.118	0.0	0.0
NH_4F	100	0.970	0.080	0.152	29.85	1.619	0.264	0.114	84.9	95.4
HF	100	0.989	0.373	1.227	29.43	1.634	0.267	0.113	29.5	63.0

Table E.3 Results for the investigation into Mg : Ca.

Experiment	F-addition	Factor	Concentration (g/ℓ)						% Precipitated	
	%		Ca	Mg	Ni	Co	Mn	Zn	Ca	Mg
Feed	-	1.000	0.566	-	32.17	1.741	0.287	0.121	0.0	0.0
Only Ca	100% Ca	1.010	0.033	0.000	30.13	1.687	0.274	0.115	93.9	0.0
1:1	100% Ca	1.018	0.141	0.303	30.16	1.685	0.275	0.114	73.9	5.9
2:1	100% Ca	1.023	0.241	0.598	30.28	1.681	0.275	0.115	55.3	7.2
3:1	100% Ca	1.010	0.307	0.897	30.82	1.669	0.273	0.114	43.2	7.1
4:1	100% Ca	1.022	0.424	1.132	30.84	1.676	0.272	0.114	21.4	11.9
Feed	-	1.000	0.556	3.486	31.00	1.725	0.281	0.118	0.0	0.0
10.3:1	100% Ca	0.996	0.525	3.045	29.64	1.646	0.268	0.111	0.8	8.0
Feed	-	1.000	0.000	3.399	31.14	1.745	0.284	0.120	0.0	0.0
Only Mg	100% Mg	0.991	0.000	0.183	30.03	1.659	0.268	0.114	0.0	94.4

Table E.4 Results for the investigation into fluctuations.

Experiment	F-addition	Factor	Concentration (g/ℓ)						% Precipitated	
	%		Ca	Mg	Ni	Co	Mn	Zn	Ca	Mg
Feed	-	1.000	0.556	3.486	31.00	1.725	0.281	0.118	0.0	0.0
45°C	90	0.992	0.198	0.384	29.39	1.646	0.266	0.113	62.7	88.4
45°C	110	0.992	0.025	0.063	29.68	1.649	0.264	0.113	95.3	98.1
65°C	90	0.979	0.188	0.330	29.60	1.635	0.267	0.112	64.4	90.1
65°C	110	1.002	0.017	0.039	29.92	1.663	0.263	0.111	96.8	98.8
55°C	100	0.984	0.079	0.159	30.20	1.628	0.266	0.111	85.1	95.2
55°C	110	0.995	0.018	0.048	30.12	1.656	0.263	0.111	96.6	98.6

E.3 Continuous Precipitation Experiments

Description: 30 minutes residence time in a single reactor, with the base metal sulphate solution.

Date: 12-10-2002

Residence time: 30 minutes

Sulphate solution: Base metal sulphate solution.

Volume: Reactor A: 0 ml

Reactor B: 1000 ml

Reactor C: 0 ml

Stirrer rate: 520 rpm

Results:

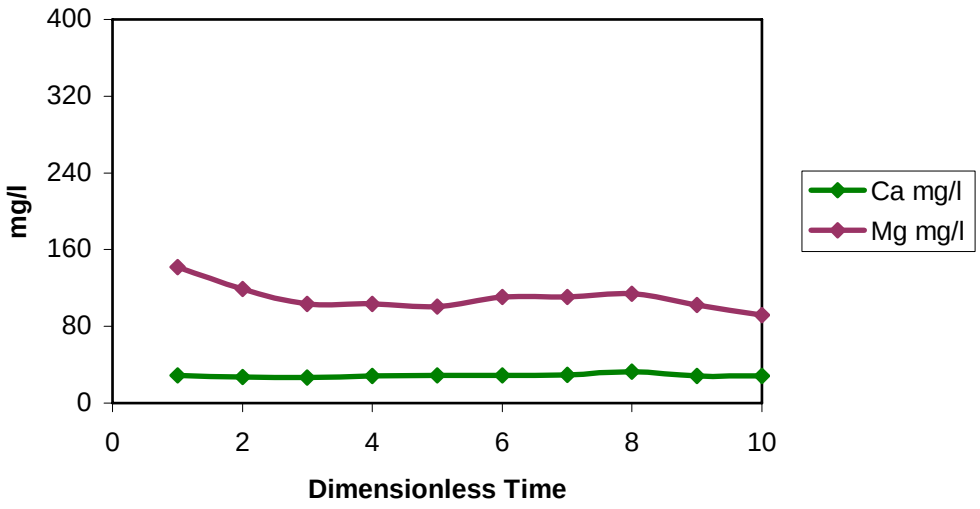

% Ca Precipitated	% Mg Precipitated	Filtration Resistance, $m^3/kg.m^2$	$D_{3,2}$ µm	$D_{4,3}$ µm	Span	Residual Fluoride, mg/ℓ	S_{Ca}	S_{Mg}
94.8	97.2	3.00×10^9	10.4	18.8	1.42	896	1.52	1.94

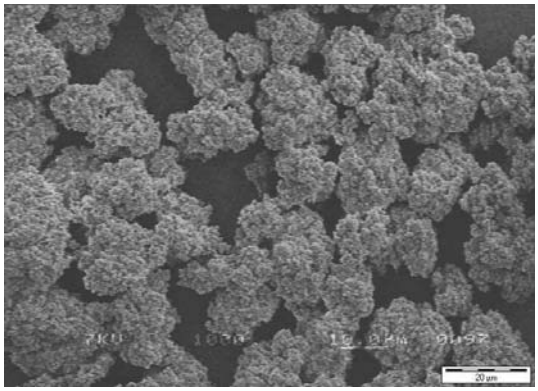

Description: 60 minutes residence time in a single reactor, with the base metal sulphate solution.

Date: 13-10-2002

Residence time: 60 minutes

Sulphate solution: Base metal sulphate solution.

Volume: Reactor A: 0 ml

Reactor B: 1000 ml

Reactor C: 0 ml

Stirrer rate: 520 rpm

Results:

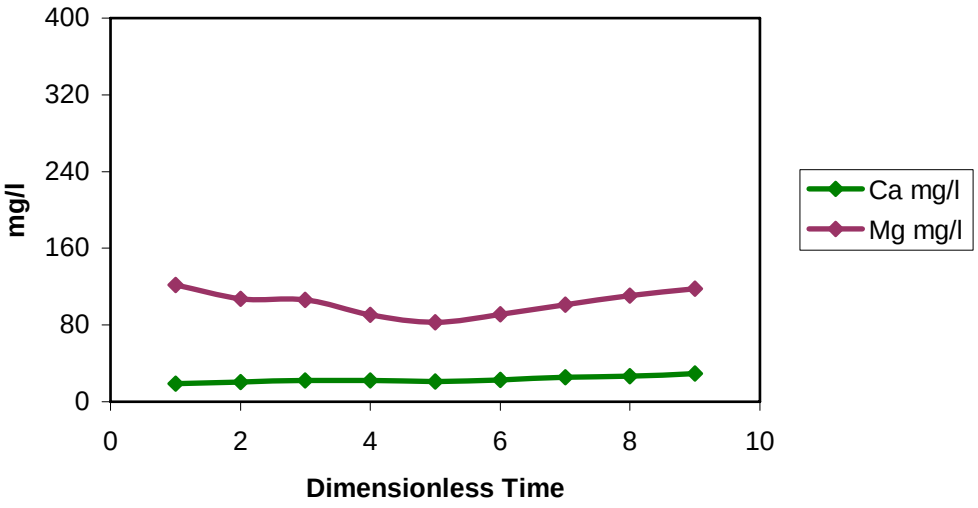

% Ca Precipitated	% Mg Precipitated	Filtration Resistance, $m^3/kg.m^2$	$D_{3,2}$ µm	$D_{4,3}$ µm	Span	Residual Fluoride, mg/ℓ	S_{Ca}	S_{Mg}
94.6	96.5	4.74 x 109	10.1	17.8	1.48	897	1.52	1.94

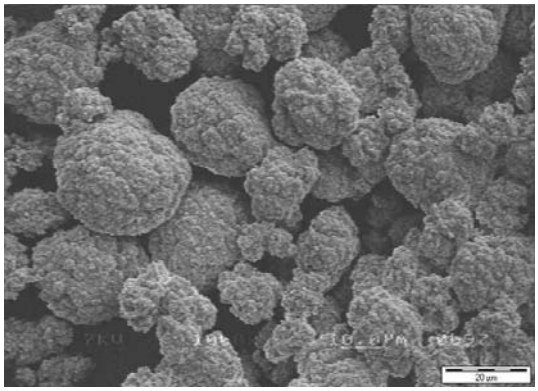

Description: 60 minutes residence time in a single reactor, with the ammonium sulphate solution.

Date: 10-07-2002

Residence time: 60 minutes

Sulphate solution: Ammonium sulphate solution.

Volume: Reactor A: 0 ml

Reactor B: 1000 ml

Reactor C: 0 ml

Stirrer rate: 520 rpm

Results:

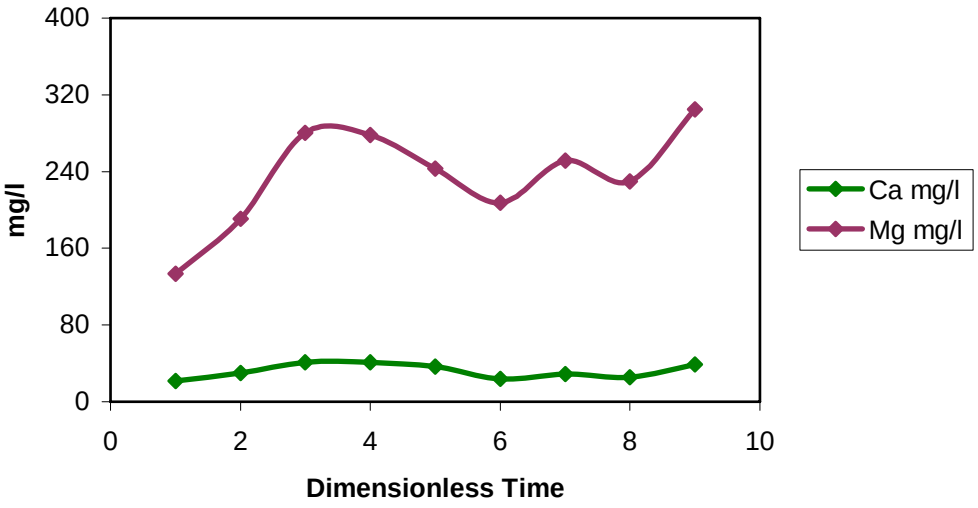

% Ca Precipitated	% Mg Precipitated	Filtration Resistance, $m^3/kg.m^2$	$D_{3,2}$ µm	$D_{4,3}$ µm	Span	Residual Fluoride, mg/ℓ	S_{Ca}	S_{Mg}
93.1	90.9	3.34×10^9	10.3	17.7	1.51	686	1.40	2.23

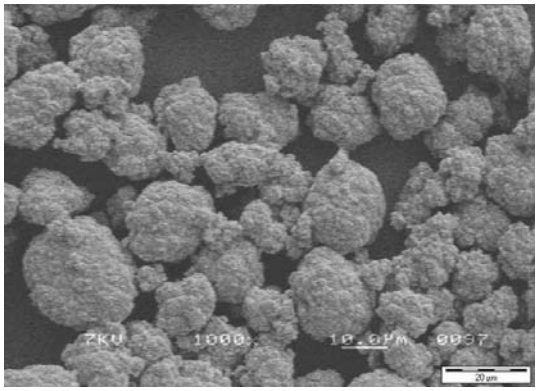

Description: 120 minutes residence time in a single reactor, with the ammonium sulphate solution.

Date: 12-07-2002

Residence time: 120 minutes

Sulphate solution: Ammonium sulphate solution.

Volume: Reactor A: 0 ml

Reactor B: 1000 ml

Reactor C: 0 ml

Stirrer rate: 520 rpm

Results:

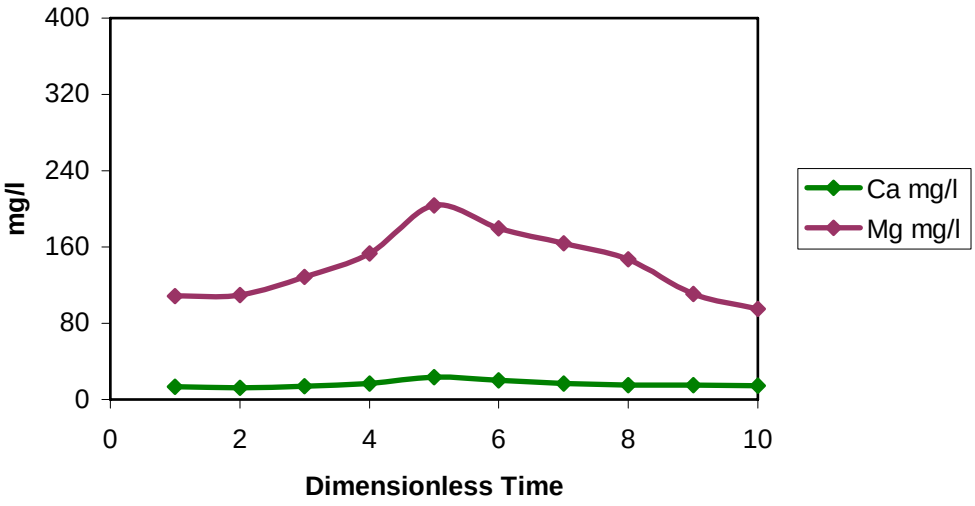

% Ca Precipitated	% Mg Precipitated	Filtration Resistance, $m^3/kg.m^2$	$D_{3,2}$ µm	$D_{4,3}$ µm	Span	Residual Fluoride, mg/ℓ	S_{Ca}	S_{Mg}
97.2	96.8	4.07×10^9	12.0	21.4	1.44	1086	1.38	2.16

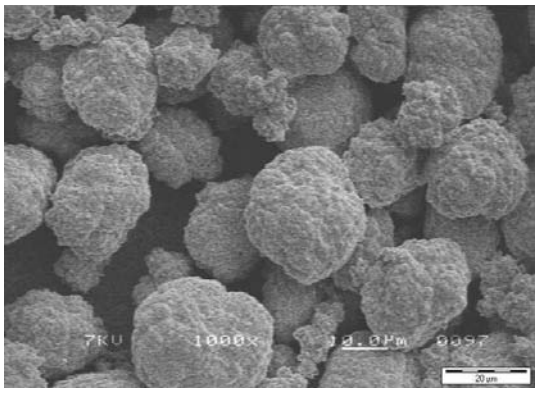

Description: 60 minutes residence time in the three-zone experimental set-up, with the ammonium sulphate solution. This was the control experiment.

Date: 08-08-2002

Residence time: 60 minutes

Sulphate solution: Ammonium sulphate solution.

Volume: Reactor A: 400 ml

Reactor B: 1200 ml

Reactor C: 400 ml

Stirrer rate: 900 rpm

Circulation rate: 1080 ml/min

Results:

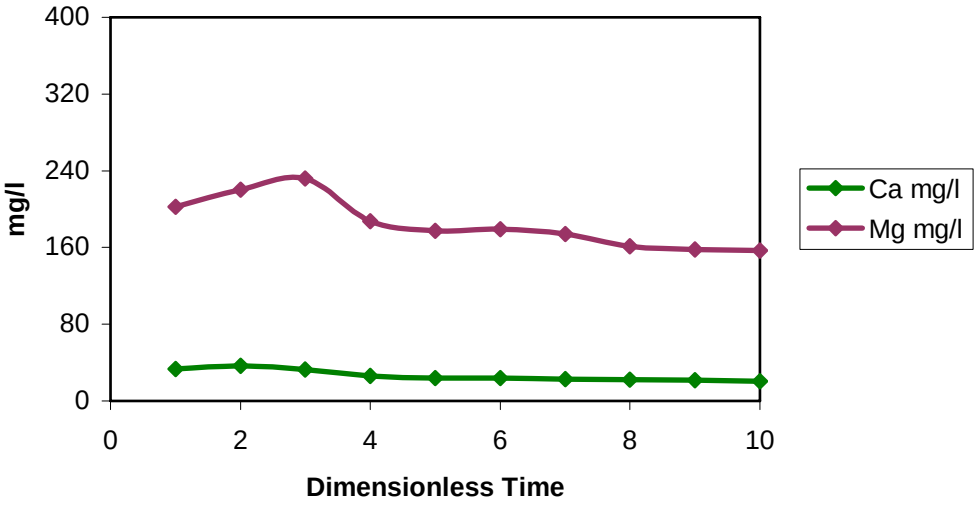

% Ca Precipitated	% Mg Precipitated	Filtration Resistance, $m^3/kg.m^2$	$D_{3,2}$ µm	$D_{4,3}$ µm	Span	Residual Fluoride, mg/ℓ	S_{Ca}	S_{Mg}
96.3	95.4	4.01×10^9	9.2	16.4	1.70	968	1.42	2.24

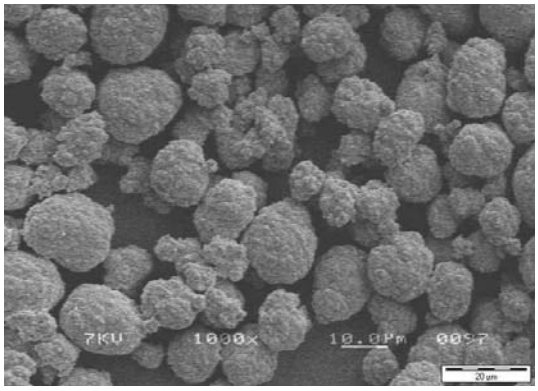

Description: 60 minutes residence time in the three-zone experimental set-up, with the ammonium sulphate solution. Low micromixing.

Date: 20-10-2002

Residence time: 60 minutes

Sulphate solution: Ammonium sulphate solution.

Volume: Reactor A: 400 ml

Reactor B: 1200 ml

Reactor C: 400 ml

Stirrer rate: 520 rpm

Circulation rate: 1080 ml/min

Results:

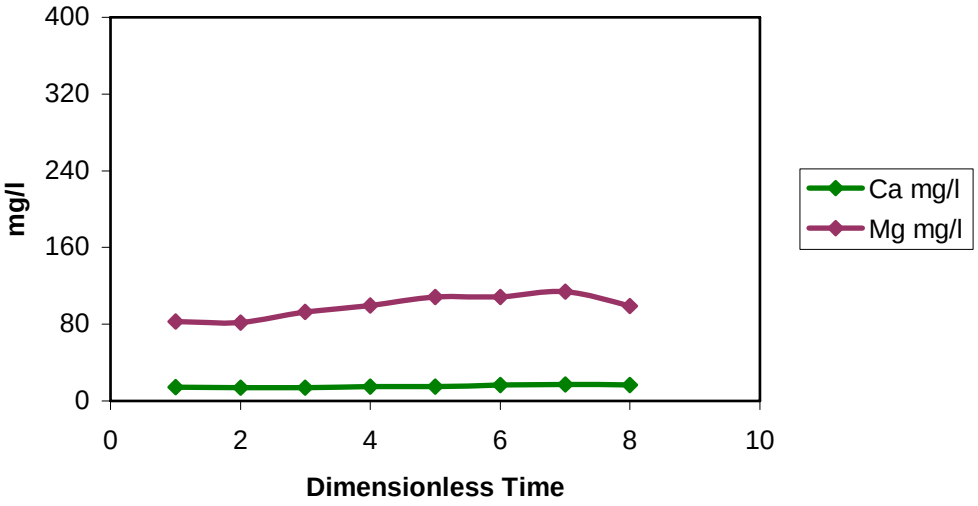

% Ca Precipitated	% Mg Precipitated	Filtration Resistance, $m^3/kg.m^2$	$D_{3,2}$ µm	$D_{4,3}$ µm	Span	Residual Fluoride, mg/ℓ	S_{Ca}	S_{Mg}
96.3	97.2	1.93×10^9	11.2	21.1	1.54	931	1.29	1.88

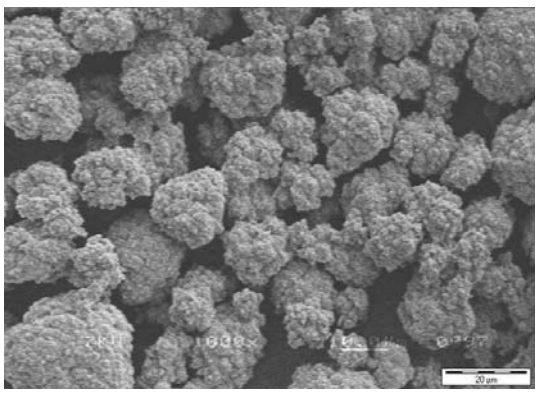

Description: 60 minutes residence time in the three-zone experimental set-up, with the ammonium sulphate solution. High mesomixing of fluoride.

Date: 28-08-2002

Residence time: 60 minutes

Sulphate solution: Ammonium sulphate solution.

Volume: Reactor A: 400 ml

Reactor B: 1600 ml

Reactor C: 0 ml

Stirrer rate: 900 rpm

Circulation rate: 1080 ml/min

Results:

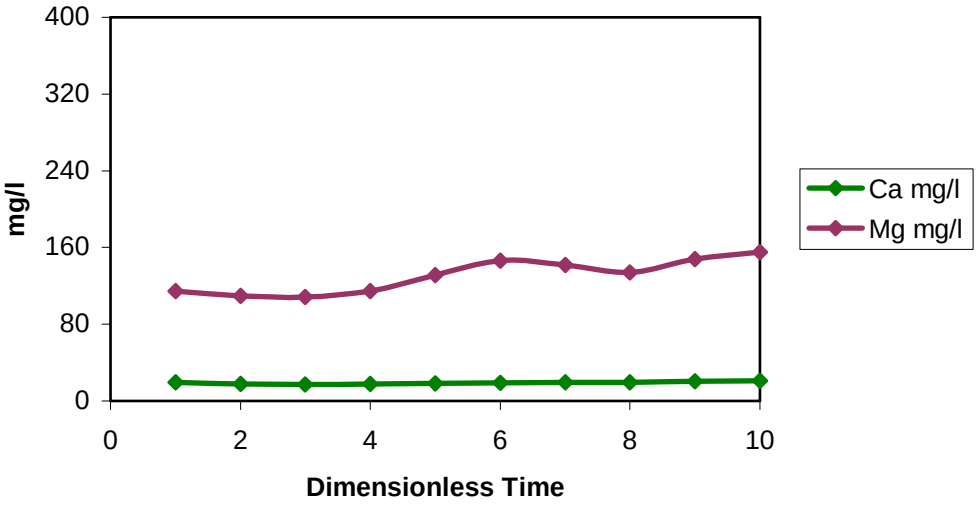

% Ca Precipitated	% Mg Precipitated	Filtration Resistance, $m^3/kg.m^2$	$D_{3,2}$ µm	$D_{4,3}$ µm	Span	Residual Fluoride, mg/ℓ	S_{Ca}	S_{Mg}
96.1	95.3	4.22×10^9	9.4	16.7	1.69	968	1.43	2.24

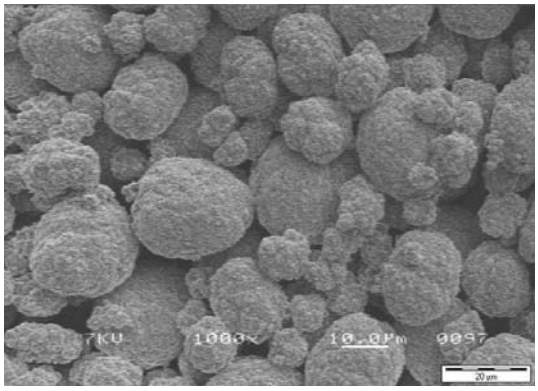

Description: 60 minutes residence time in the three-zone experimental set-up, with the ammonium sulphate solution. High mesomixing of sulphate solution.

Date: 30-08-2002

Residence time: 60 minutes

Sulphate solution: Ammonium sulphate solution.

Volume: Reactor A: 0 ml

Reactor B: 1600 ml

Reactor C: 400 ml

Stirrer rate: 900 rpm

Circulation rate: 1080 ml/min

Results:

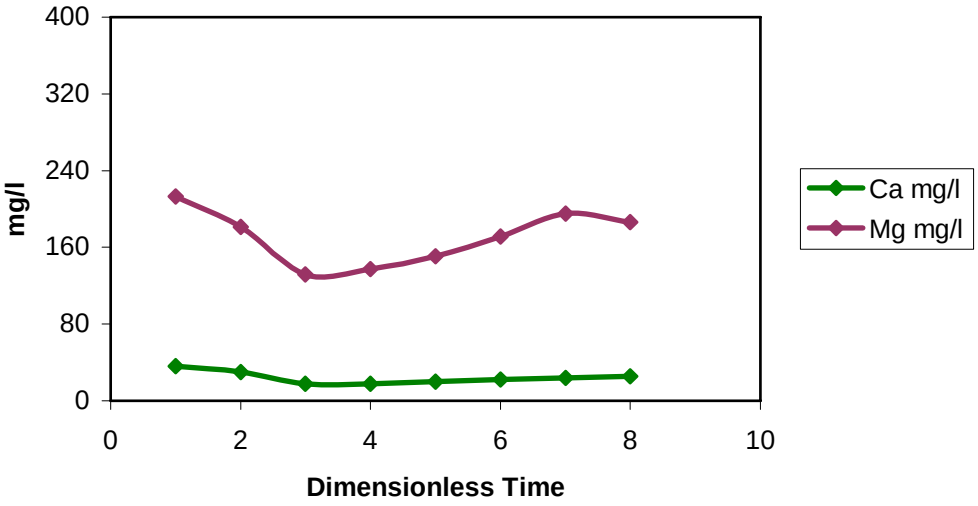

% Ca Precipitated	% Mg Precipitated	Filtration Resistance, $m^3/kg.m^2$	$D_{3,2}$ µm	$D_{4,3}$ µm	Span	Residual Fluoride, mg/ℓ	S_{Ca}	S_{Mg}
95.5	94.57	3.41×10^9	9.9	18.11	1.68	897	1.45	2.26

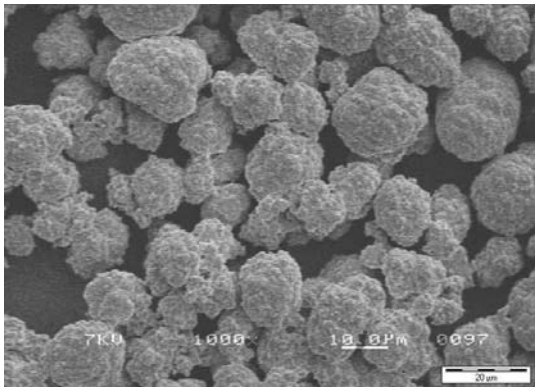

Description: 60 minutes residence time in the three-zone experimental set-up, with the ammonium sulphate solution. Low macromixing.

Date: 05-08-2002

Residence time: 60 minutes

Sulphate solution: Ammonium sulphate solution.

Volume: Reactor A: 400 ml

Reactor B: 1200 ml

Reactor C: 400 ml

Stirrer rate: 900 rpm

Circulation rate: 300 ml/min

Results:

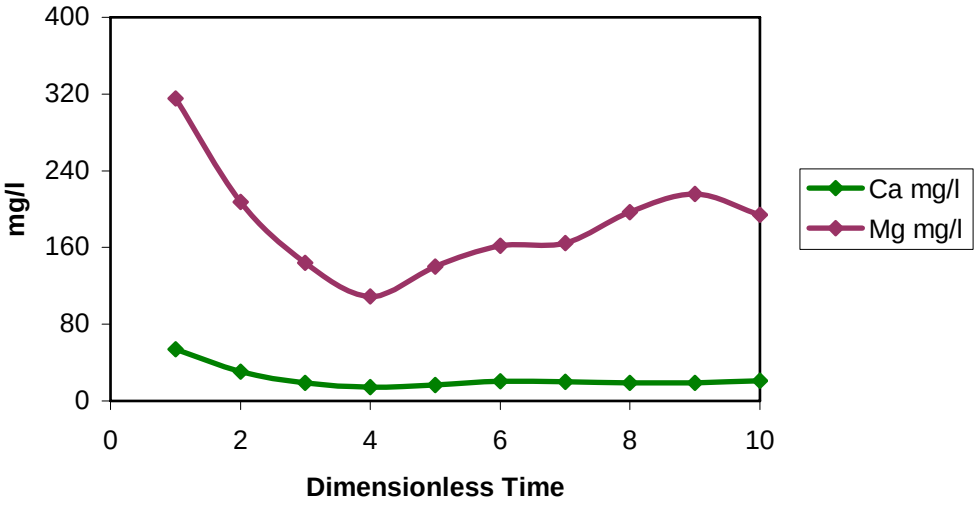

% Ca Precipitated	% Mg Precipitated	Filtration Resistance, $m^3/kg.m^2$	$D_{3,2}$ µm	$D_{4,3}$ µm	Span	Residual Fluoride, mg/ℓ	S_{Ca}	S_{Mg}
96.1	94.2	5.13×10^9	10.5	22.3	1.90	968	1.40	2.35

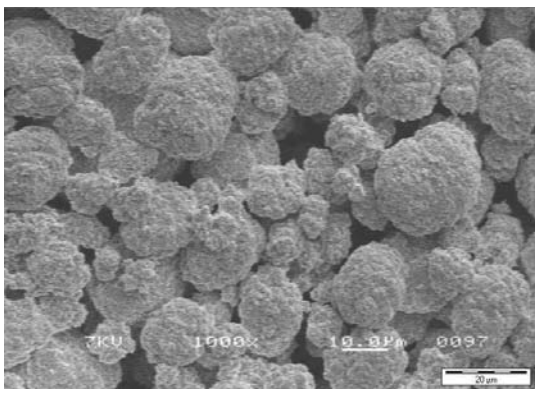

E.4 Batch Adsorption Experiments

Initial		Final			
Activated Alumina, g	Fluoride, mg/l	Contact time, minutes	Fluoride, mg/l	Adsorbed, g	Capacity g F/ ℓ AA
5	2400	1440	1656	0.648	129.5
5	1200	1440	713	0.437	87.4
5	600	2880	154	0.435	86.9
5	600	1440	235	0.358	71.6
5	600	720	295	0.279	55.7
10	600	1440	148	0.440	44.0
10	600	720	217	0.353	35.3
20	600	1440	83	0.502	25.1

E.5 Column Adsorption Experiments

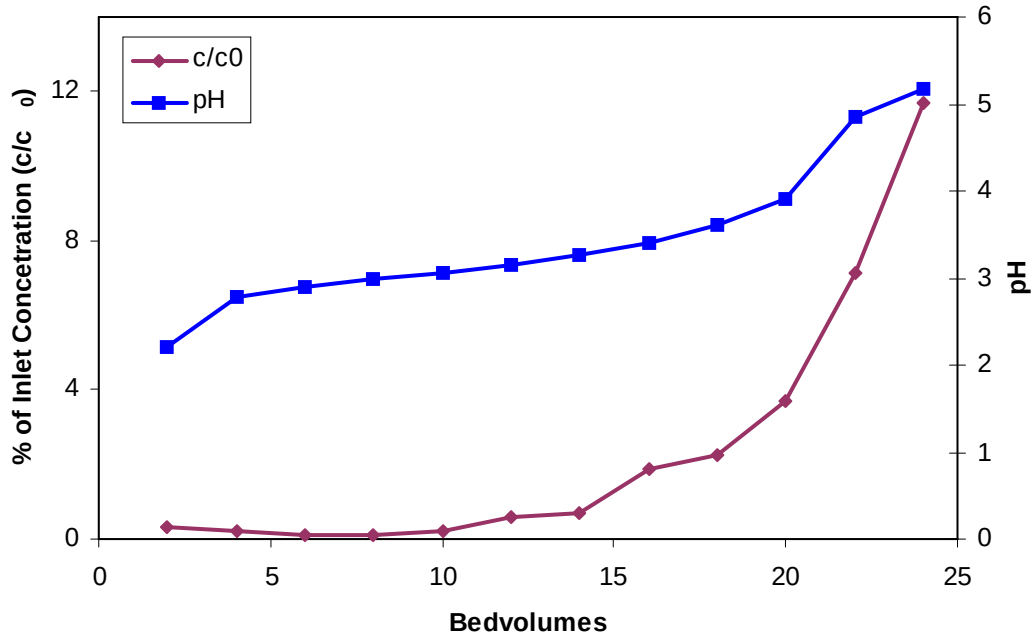

Figure E.10 Adsorption Cycle of centre run (55 °C, 600 mg/l F).

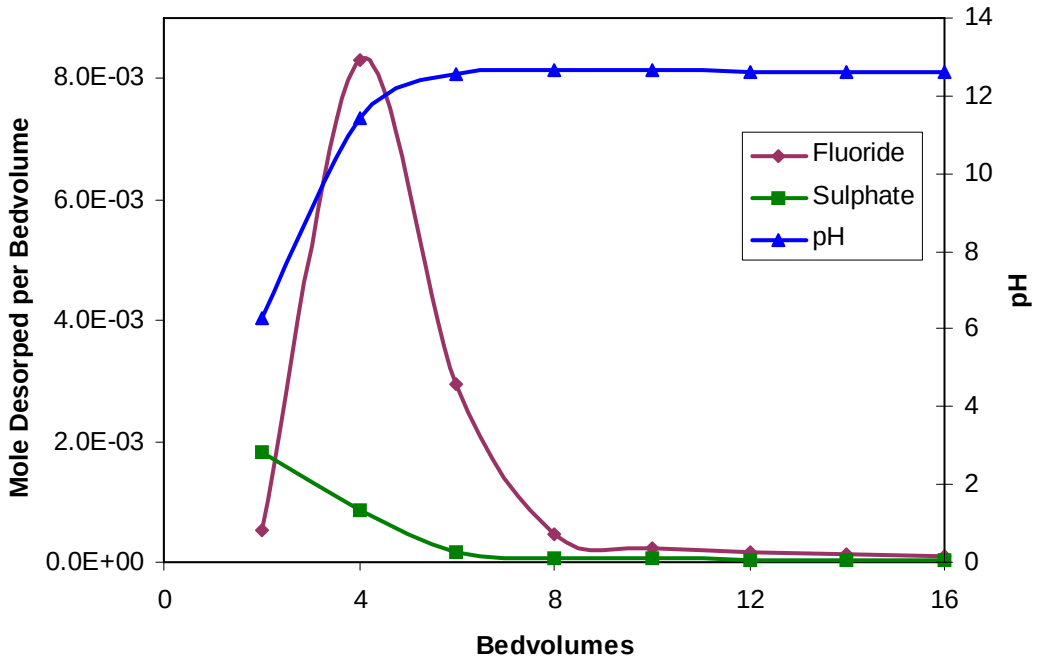

Figure E.11 Desorption cycle of centre run (55 °C, 600 mg/l F).

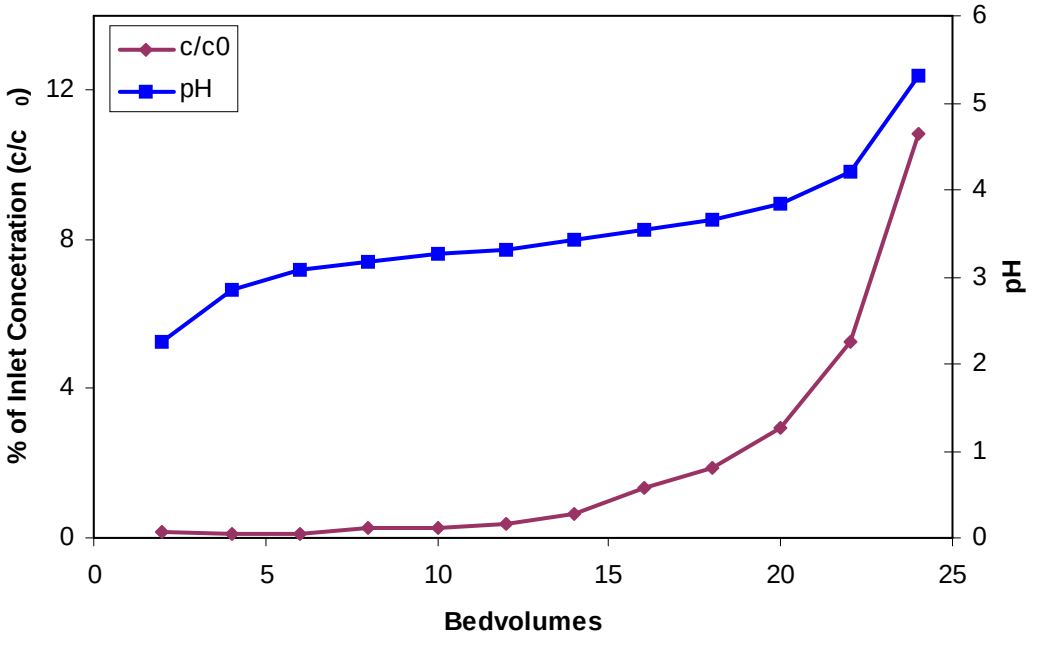

Figure E.12 Adsorption cycle (45 °C, 400 mg/l F)

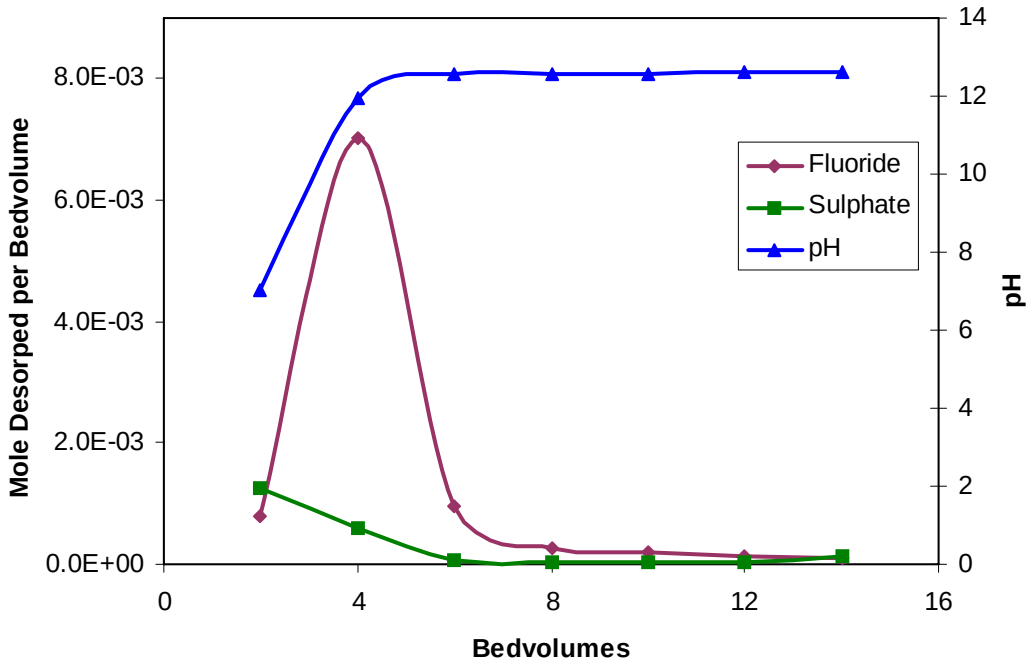

Figure E.13 Desorption cycle (45 °C, 400 mg/l F).

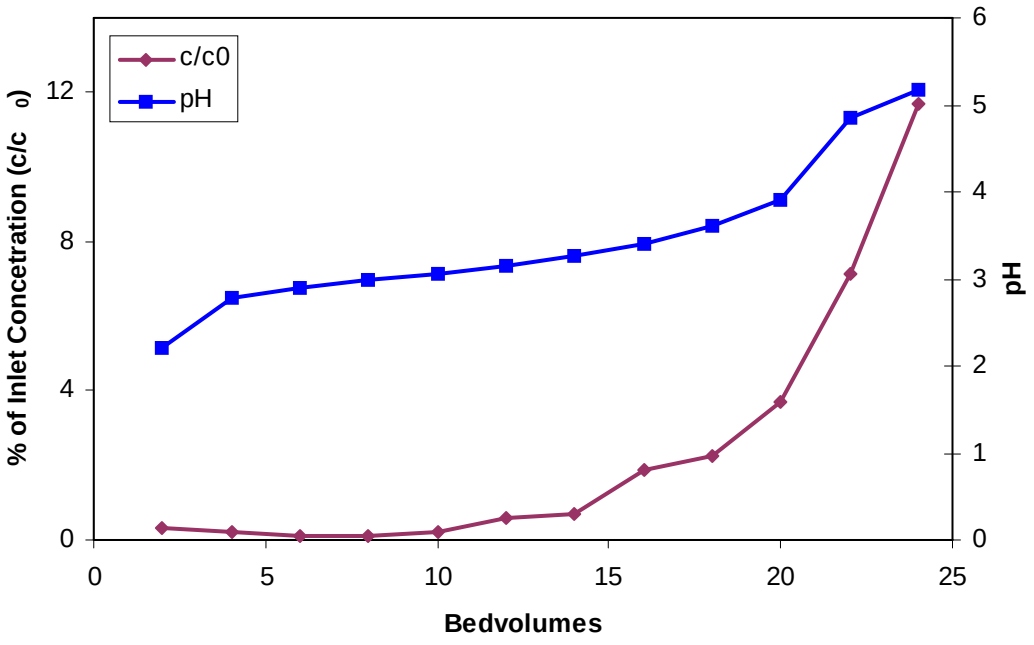

Figure E.14 Adsorption cycle (45 °C, 800 mg/l F)

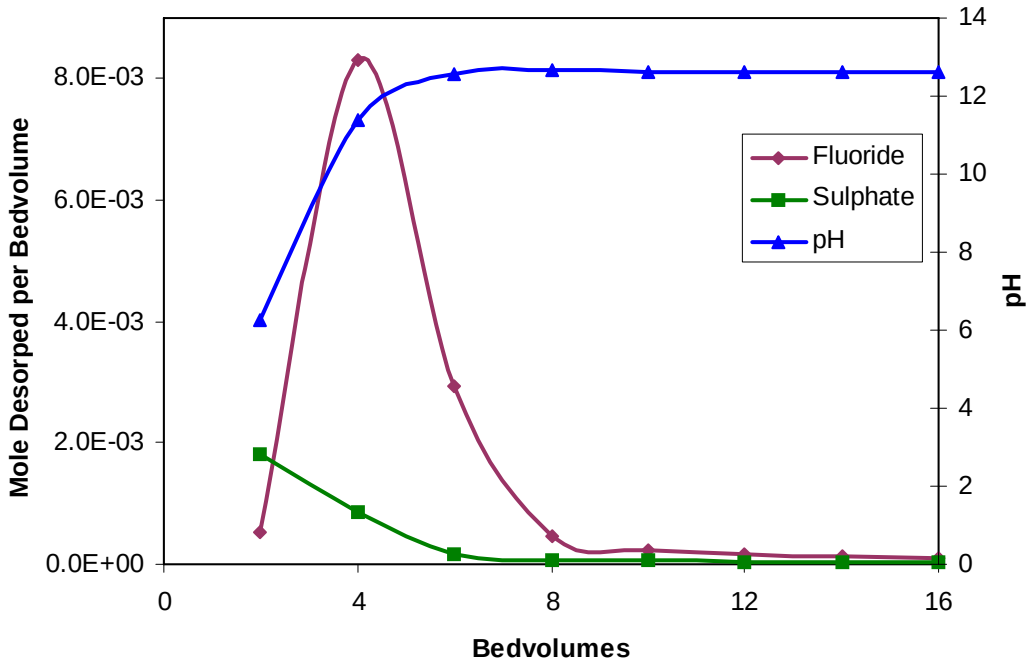

Figure E.15 Desorption cycle (45 °C, 800 mg/l F).

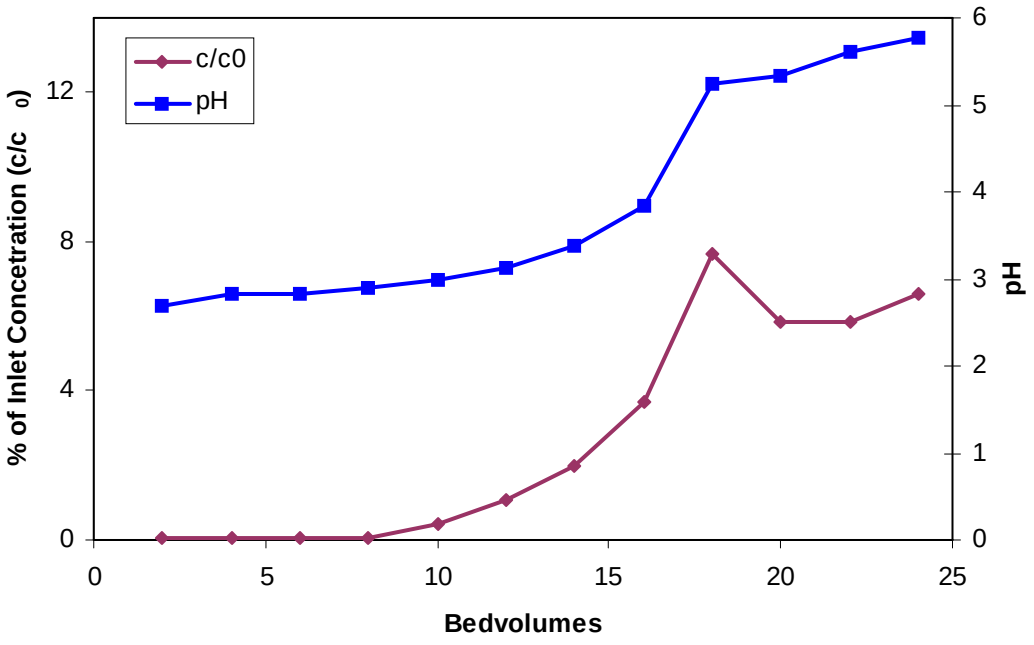

Figure E.16 Adsorption cycle (65 °C, 400 mg/l F)

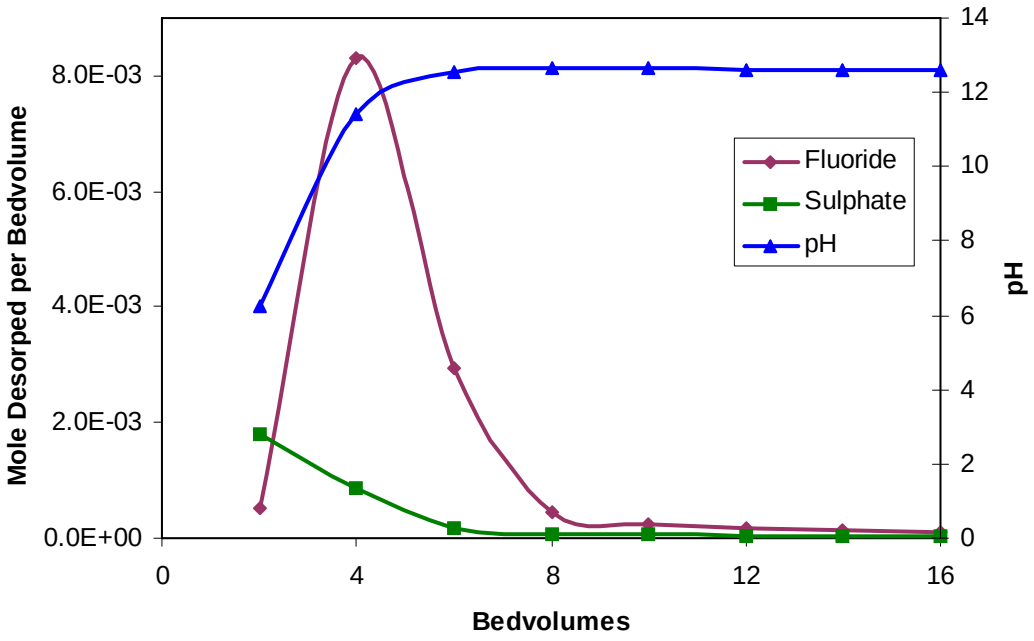

Figure E.17 Desorption cycle (65 °C, 400 mg/l F).

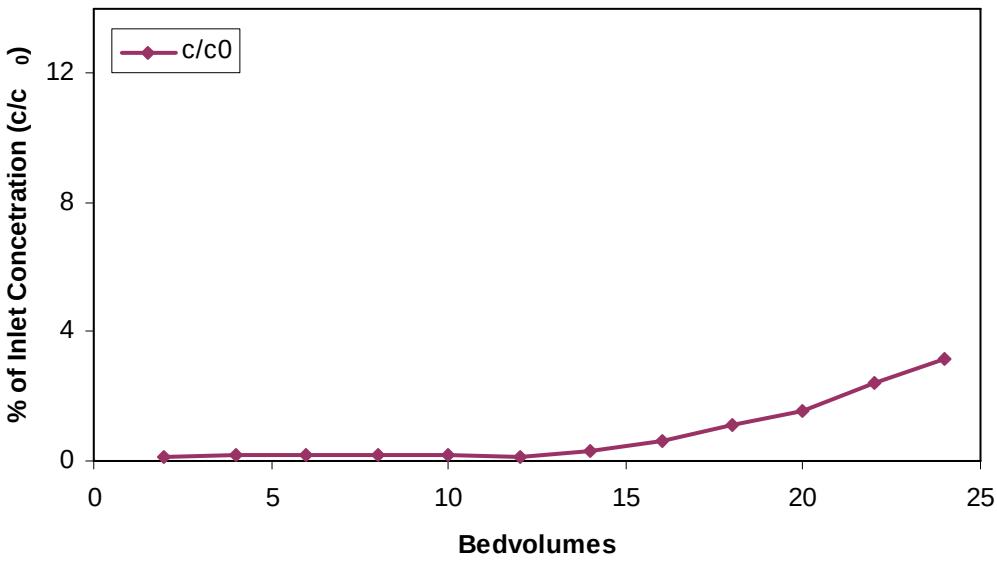

Figure E.18 Adsorption cycle (65 °C, 800 mg/l F)

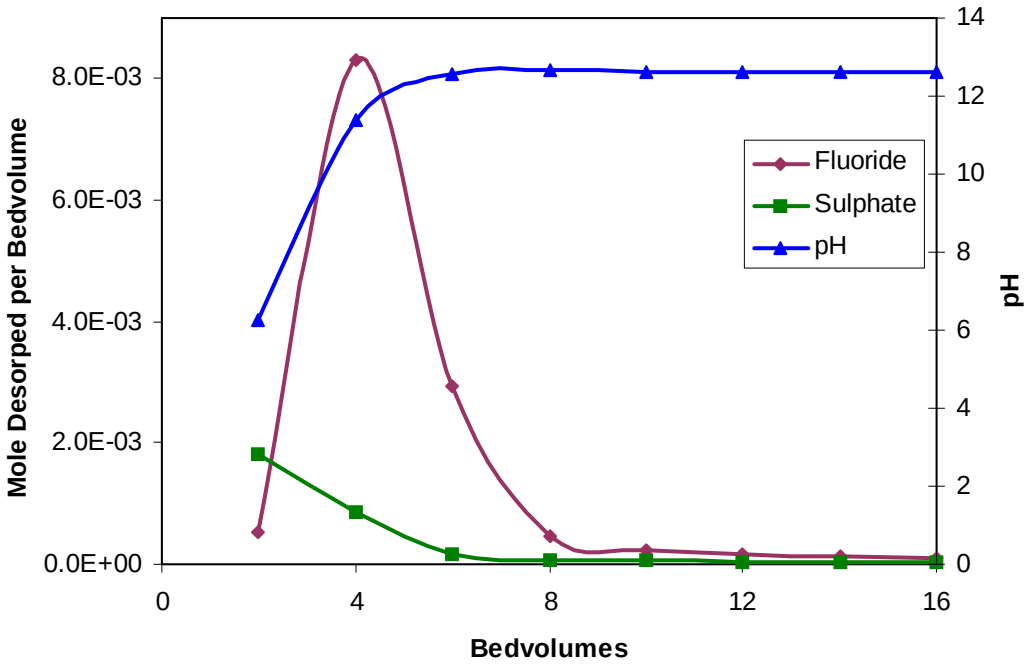

Figure E.19 Desorption cycle (65 °C, 800 mg/l F).

Nomenclature

Symbols

a	Activity	
$a_{\pm}$	Mean activity	
A	Constant for the linearised filtration equation	s/m^3
A_F	Filtration area	m^2
A_T	Total surface area	m^2/m^3
b_L	Constant for the Langmuir isotherm	mole/ℓ or g/ℓ
b_F	Constant for the Freunlich isotherm	g/kg
B	Constant for the linearised filtration equation	s/m^6
B_0	Secondary nucleation rate	$\#/(m^3.s)$
B_S	Constant for the BCF rate equation	
c	Molar concentration	mole/ℓ
c_c	Concentration in the crystal	mole/ℓ or g/ℓ
c_b	Concentration in the bulk liquid	mole/ℓ or g/ℓ
c_E	Equilibrium concentration	mole/ℓ or g/ℓ
c_0	Initial or inlet concentration	mole/ℓ or g/ℓ
C_S	Constant for the BCF rate equation	
d	Interplanar distance in the crystal lattice	m
D	Diffusion coefficient	
G	Exponent for the simplified growth rate equation	
G_F	Mass of precipitate per volume filtrate	kg/m^3
ΔG	Change in gibbs free energy	J/mole
J	Nucleation rate	$\#/(m^3.s)$
k	Boltzman constant	J/unit.K
k_a	Area shape factor of a particle	
k_D	Constant for diffusion controlled rate law	$kg/m^2.s$
k_{eff}	Impurity effective distribution coefficient	
k_g	Simplified growth rate equation	m/s
k_N	Constant in power law for secondary nucleation	

k_P	Constant for the polynuclear rate law	m/s
k_S	Constant for the parabolic rate law	m/s
k_R	Constant for the rough growth rate law	m/s
k_v	Volume shape factor of a particle	
K_P	Constant for the polynuclear rate law	
K_s	Solubility product	
K_{sp}	Thermodynamic solubility product	
l	Constant in power law for secondary nucleation	
L	Crystal or particle size	m
L_T	Total length of crystals	m/m^3
m	Constant in power law for secondary nucleation	
m_a	Mass of molecules adsorbed	g
m_d	Mass of molecules desorbed	g
m_j	Moment of the number density distribution	m^j/m^3
m(L)	Mass density distribution	$kg/m.m^3$
M	Molecular mass	g/mole
M_T	Crystal mass of slurry	kg/m^3
M(L)	Mass distribution	kg/m^3
n	Constant in power law for secondary nucleation	
n_F	Constant for the Freundlich isotherm	
n(L)	Number density distribution	$\#/m.m^3$
$\dot{n}$	Rate of the number of moles deposited	$mole/s.m^3$
N	Number of atoms or solute units	
N_A	Avogadro number	units/mole
N_T	Total number of particles per unit volume	$\#/m^3$
N(L)	Cumulative oversize number distribution	$\#/m^3$
pH_{50}	pH value at which 50% of a metal is extracted	pH units
P	Pressure	Pa
r	Radius of cluster, Crystal size	m
$\dot{r}$	Linear growth rate	m/s
R	Molar universal gas constant	J/mole.K
R_m	Resistance of filter media	$1/m^3$
$R_{d:a}$	Regeneration ratio	
S	Supersaturation ratio	

Sc	Schmidt number	
t	Time	s
t_g	Time for nucleus to grow to a detectable size	s
t_i	Time for the formation of the critical nucleus	s
t_{ind}	Induction period	s
T	Absolute Temperature	K
$\dot{v}$	Volumetric flowrate	m^3/s or ℓ/s
V_E	Volume of effluent	m^3
V_F	Volume of filtrate	m^3
V_m	Molar volume: $V_m = M/(\rho.N_A)$	m^3/unit
V_R	Volume of MSMPR reactor	m^3
V_{total}	Total volume of reactor system	m^3
V_T	Total volume of crystals	m^3/m^3
X	Equilibrium loading during adsorption	g/kg
X_m	Loading for monolayer coverage	g/kg
X_p	Capacity of bed at breakthrough	g/kg
X_s	Capacity of bed at saturation	g/kg

Greek Symbols

α_F	Mass filtration resistance	$m^3/m^2.kg$
β	Shape factor for polynuclear rate equation	
δ	Boundary layer thickness	m
Δ	Difference	
ε	Energy dissipation	W/kg
ϕ	Reaction affinity	J/mole; J/unit
γ	Interfacial free energy	J/m^2
$\gamma_\pm$	Mean activity coefficient	
η	Kinematic viscosity $\eta = \mu_v/\rho$	m^2/s
λ_B	Batchelor concentration microscale	m
λ_K	Kolmogorov length scale of turbulence	m
μ_v	Viscosity	Pa.s
ν	Number of ions into which a molecule dissociates	

Θ	Wetting angle	
ρ	Density	kg/m^3
σ	Relative supersaturation ratio	
τ	Mean residence time in reactor	s
τ_C	Macromixing time	s
τ_D	Turbulent diffusion time for mesomixing	s
τ_E	Engulfment time for micromixing	s
τ_{Gcr}	Crystal growth characteristic time	s
τ_N	Nucleation characteristic time	s
τ_R	Chemical reaction characteristic time	s
τ_S	Inertial convective time for mesomixing	s
Ω	Pre-exponential variable for nucleation rate	
ξ	Activity coefficient ratio	
ψ_{AC}	Ratio of flowrates	
ψ_V	Ratio of inlet zones to bulk zone	
ψ_F	Ratio of exchange flowrate to feeding flowrate	

Superscripts

Me – Ni	Difference in value for a metal, Me, and nickel
0	Standard state
*	Related to critical nucleus
+	Value related to cation
-	Value related to anion

Subscripts

c	Concentrations in molarities
D	Diffusion controlled
R	Rough growth controlled
S	Screw dislocation controlled
P	Polynuclear controlled
eq.	Equilibrium state
hetero	heterogeneous
homo	homogeneous

surface	Value relate to surface of solute cluster
volume	Value relate to volume of solute cluster